The Design and Synthesis of Chemical Probes for Non-BET Bromodomains

PhD Thesis

Michael A. Clegg

December 2019

GlaxoSmithKline R&D, Gunnels Wood Road, Stevenage, SG1 2NY (UK)

Department of Pure and Applied Chemistry, University of Strathclyde, 295 Cathedral Street, Thomas Graham Building, Glasgow, G1 1XL (UK)

Declaration

This thesis is the result of the author's original research. It has been composed by the author and has not been previously submitted for examination which has led to the award of a degree.

The copyright of this thesis belongs to the author under the terms of the United Kingdom Copyrights Acts as qualified by University of Strathclyde Regulation 3.50. Due acknowledgement must always be made of the use of any material contained in, or derived from, this thesis.

Signed: Date:

Acknowledgements

Abbreviations

Å	Angstrom
A	Adenine
Ac	Acetyl
ALDH1A1	Aldehyde dehydrogenase 1 family member A1
Alpha	Amplified luminescent proximity homogeneous assay
AML	Acute myeloid leukemia
AMP	Artificial membrane permeability
APP	Amyloid precursor protein
AR	Androgen receptor
Ar	Aromatic group
Arg	Arginine
Asn	Asparagine
Asp	Aspartic Acid
ATAD2	ATPase family, AAA domain containing protein 2
ATAD2B	ATPase family, AAA domain containing protein 2B
ATPase	Adenosine triphosphatase
Aq.	Aqueous
BAZ2A	Bromodomain adjacent to zinc finger domain protein 2A
BAZ2B	Bromodomain adjacent to zinc finger domain protein 2B
BAZ1B	Bromodomain adjacent to zinc finger domain, 1B
BC	Breast cancer
BCP	Bromodomain containing protein
BD	Bromodomain
BET	Bromodomain and extra terminal domain
Boc	*N-tert*-Butoxycarbonyl
Bn	Benzyl
BRD1	Bromodomain containing protein 1
BRD2	Bromodomain containing protein 2
BRD2(1)	Bromodomain 1 of bromodomain containing protein 2
BRD2(2)	Bromodomain 2 of bromodomain containing protein 2
BRD3	Bromodomain containing protein 3
BRD3(1)	Bromodomain 1 of bromodomain containing protein 3
BRD3(2)	Bromodomain 2 of bromodomain containing protein 3
BRD4	Bromodomain containing protein 4
BRD4(1)	Bromodomain 1 of bromodomain containing protein 4
BRD4(2)	Bromodomain 2 of bromodomain containing protein 4
BRD7	Bromodomain containing protein 7
BRD8	Bromodomain containing protein 8
BRD9	Bromodomain containing protein 9
BRDT	Bromodomain testis-specific protein
BRDT(1)	Bromodomain 1 of bromodomain testis-specific protein
BRDT(2)	Bromodomain 2 of bromodomain testis-specific protein
BRET	Bioluminescence resonance energy transfer
BRPF1	Bromodomain and PHD Finger Containing protein 1
BRPF2	Bromodomain and PHD Finger Containing protein 2
BRPF3	Bromodomain and PHD Finger Containing protein 3
Bu	Butyl

*t*Bu	Tertiary-butyl
B3LYP	Becke, 3-parameter, Lee-Yang-Parr
C	Cytosine
CAD	Charged aerosol detection
CECR2	Cat eye syndrome chromosome region, candidate 2
CHI	Chromatographic hydrophobicity index
CLND	Chemiluminescent nitrogen detection
CNS	Central nervous system
CREBBP	CREB-binding protein
CRPC	Castration resistant prostate cancer
CS	Conformational search
CTK	C-terminal kinase domain
DBU	1,8-Diazabicyclo[5.4.0]undec-7-ene
DCM	Dichloromethane
DFT	Density functional theory
DHP	Dihydropyran
DIPEA	*N,N*-Diisopropylethylamine
DLBCL	Diffuse large B-cell lymphoma
DMF	*N,N*-Dimethylformamide
DMSO	Dimethylsulfoxide
DNA	Deoxyribonucleic acid
DSF	Differential scanning fluorimetry
DUF	Domain of unknown function
EP300	E1A binding protein p300
EPL1	Enhancer of polycomb-like
Et	Ethyl
ET	Extra terminal
eq.	Equivalent
FALZ	Bromodomain PHD finger transcription factor
FBS	Fetal Bovine Serum
FF	Force field
FOXP3	Forkhead box P3
FRAP	Fluorescence recovery after photobleaching
FRET	Forster (fluorescence) resonance energy transfer
G	Guanine
GCN5L2	General control non-depressible 5
Gln	Glutamine
Glu	Glutamic acid
GNAT	GCN5-related *N*-acetyltransferases
GPCR	G-protein-coupled receptor
GSK	GlaxoSmithKline
h	Hour(s)
HAT	Histone acetyltransferase
HATU	*N,N,N′,N′*-Tetramethyl-O-(1H-benzotriazol-1-yl)uronium hexafluorophosphate
HBA	Hydrogen-bond acceptor
HBD	Hydrogen-bond donor
HC	Hepatocellular carcinoma
HDAC	Histone deacetylase

HIV	Human immunodeficiency virus
HMBC	Heteronuclear multiple-bond correlation spectroscopy
HPLC	High performance liquid chromatography
HPV	Human papillomavirus
HRMS	High resolution mass spectrometry
H2A	Histone 2A
H2B	Histone 2B
H3	Histone 3
H4	Histone 4
IC_{50}	Concentration at 50% inhibition
Ile	Isoleucine
IPA	Isopropyl alcohol
ITC	Isothermal titration calorimetry
KAc	Acetyl-lysine
K_a	Acid dissociation constant
K_D	Dissociation constant
LCMS	Liquid chromatography mass spectrometry
LE	Ligand efficiency
LEE	Lipophilic ligand efficiency
Leu	Leucine
Lys	Lysine
M	Molar, moles/decimetre^3
MDAP	Mass directed autopreparation
MDCK	Madin-Darby canine kidney
MDR1	Multidrug resistance gene 1
Me	Methyl
Met	Methionine
µg	Microgram
µM	Micromolar
min	Minute
mmol	Millimole
mRNA	Messenger ribonucleic acid
MS	Mass spectrometry
m/z	Mass/charge ratio
N.A.	Not available
NaHMDS	Sodium bis(trimethylsilyl)amide
NBS	*N*-Bromosuccinimide
NHL	Non-Hodgkin's lymphoma
nM	Nanomolar
NMM	*N*-Methylmorpholine
NMR	Nuclear magnetic resonance
NTK	N-terminal kinase domain
NTD	N-terminal domain
PAMPA	Parallel artificial membrane permeability assay
PARP	Poly ADP ribose polymerase
PB1(2)	Bromodomain 2 of protein polybromo-1
PB1(5)	Bromodomain 5 of protein polybromo-1
PBS	Phosphate-buffered saline
PCAF	P300/CREBBP-associated factor

PDB	Protein data bank
PEG	Poly-ethylene glycol
Ph	Phenyl
PHD	Plant homeodomain
Phe	Phenylalanine
PK	Pharmacokinetic
Pr	Propyl
Pro	Proline
PROTAC	Proteolysis targeting chimera
PTM	Post-translational modification
PWWP	Pro-Trp-Trp-Pro
QM	Quantum mechanics
RNA	Ribonucleic acid
ROESY	Rotating-frame nuclear Overhauser effect spectroscopy
RPM	Revolutions per minute
RPMI	Roswell Park Memorial Institute
rt	Room temperature
R_t	Retention time
SAR	Structure activity relationship
SGC	Structural Genomics Consortium
SMARCA2	SWI/SNF-related matrix-associated actin-dependant regulator of chromatin subfamily A member 2
SMARCA4	SWI/SNF-related matrix-associated actin-dependant regulator of chromatin subfamily A member 4
Sol.	Solubility
SPMB	Screening profiling and mechanistic biology
T	Thymine
$t_{1/2}$	Half-life
TAF1	TBP associated factor 1
TAF1(1)	Bromodomain 1 of TBP associated factor 1
TAF1(2)	Bromodomain 2 of TBP associated factor 1
TAF1L	TBP associated factor 1 like
TAF1L(1)	Bromodomain 1 of TBP associated factor 1 like
TAF1L(2)	Bromodomain 2 of TBP associated factor 1 like
TBAB	Tetra-*n*-butyl ammonium bromide
TBP	TATA-binding protein
TFA	Trifluoroacetic acid
THF	Tetrahydrofuran
TFIID	Transcription Factor IID
THIQ	Tetrahydroisoquinoline
Thr	Threonine
THQ	Tetrahydroquinoline
T_m	Melting temperature
TMEDA	Tetramethylethylenediamine
TNBC	Triple negative breast cancer
TR-FRET	Time-resolved Forster (fluorescence) resonance energy transfer
TRIM24	Tripartite motif-containing 24
TRIM33	Tripartite motif-containing 33
tRNA	Transfer ribonucleic acid

Trp	Tryptophan
Tyr	Tyrosine
Val	Valine
vs.	Versus
WDR9(2)	Bromodomain 2 of WD repeat 9
wt	Weight
w/v	Weight by volume

x

Abstract

This thesis describes the design and synthesis of chemical probes for non-BET bromodomains.

Studies have shown that inhibition of the BET bromodomains leads to profound activity in immuno-inflammation and oncology disease settings, with several BET bromodomain inhibitors entering the clinic. The validation of this new target class has led to a surge of interest in the remaining 53 non-BET bromodomains. Whilst the majority of non-BET bromodomains have been implicated in disease pathways, the biological role they play in mediating disease states is unknown. To help delineate the function of the non-BET bromodomains in disease, and establish their potential as therapeutic targets, academia and industry have begun developing chemical probes for their preclinical target validation.

A chemical probe for the TAF1/TAF1L bromodomains was designed from a naphthyridinone scaffold. Statistical analysis was used to establish a relationship between permeability and pKa and, in turn, guide the optimization of permeability on the series. The developed probe molecule shows excellent potency (TAF1(2) pK_D = 9.1), selectivity over the BET bromodomains (1000-fold) and other non-BET bromodomains where tested (≥50-fold), improved permeability (62 nm/s), and represents a novel chemotype for TAF1/TAF1L inhibitors. From here, the concept of conserved water interactions was explored in an attempt to further increase non-BET bromodomain selectivity for TAF1(2).

A BRD7/9 template was then selected to explore the concept of bromodomain selectivity through conserved water interactions more extensively. A novel butyl acetylated Lys methyl mimetic motif was discovered and utilized to produce a selective BRD7/9 chemical probe with accompanying negative control. The broader applicability of the butyl motif was then demonstrated across a variety of scaffolds to enhance selectivity for BRD7/9 in a predictable manner.

1. Introduction

1.1 DNA Structure and Function

Found inside the nucleus of almost all living cells, deoxyribonucleic acid (DNA) contains the genetic blueprint to synthesize the proteins a cell requires to grow, function and reproduce. As a result, DNA is often referred to as the information molecule, and is essential to life as we know it.

Although DNA was first discovered in 1869 by Miescher,[1] it wasn't until 1953 that the three-dimensional structure of DNA was first investigated by Wilkins and Franklin using X-ray diffraction.[2,3] The characteristic diffraction pattern observed suggested that DNA was comprised of two chains, assembled in a regular helical structure. Utilizing this discovery, Watson and Crick would go on to confirm the structure of DNA, work which would eventually earn them the Nobel Prize in Medicine, and give rise to the current understanding of DNA.[4]

DNA consists of two polynucleotide chains, with each covalently linked nucleotide containing a phosphate group, a deoxyribose sugar, and one of four nitrogenous bases, namely thymine (T), cytosine (C), guanine (G) and adenine (A) (**Figure 1.01**). Together these four bases form two complementary base pairings, A always with T and G always with C, which interact *via* hydrogen bonds, tethering the two polynucleotide strands together in a double helix structure (**Figure 1.02**).[5,6,7]
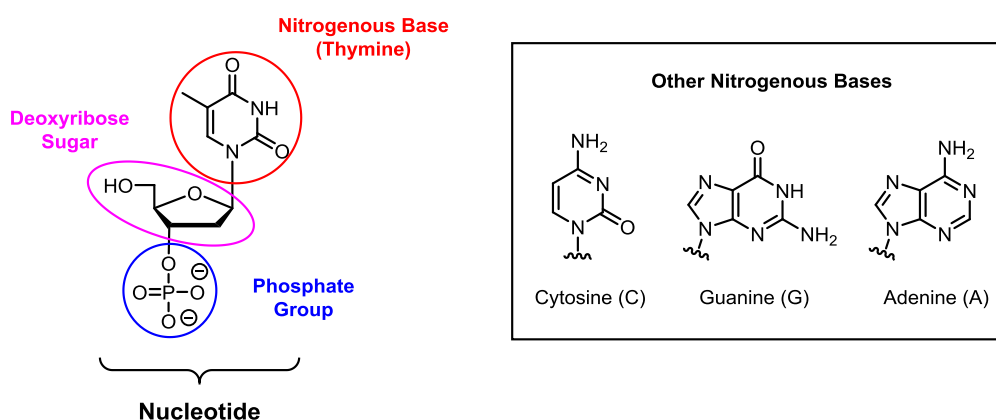
Figure 1.01: An example thymine nucleotide highlighting the phosphate group (circled in blue), the deoxyribose sugar (circled in pink) and the nitrogenous base (circled in red).
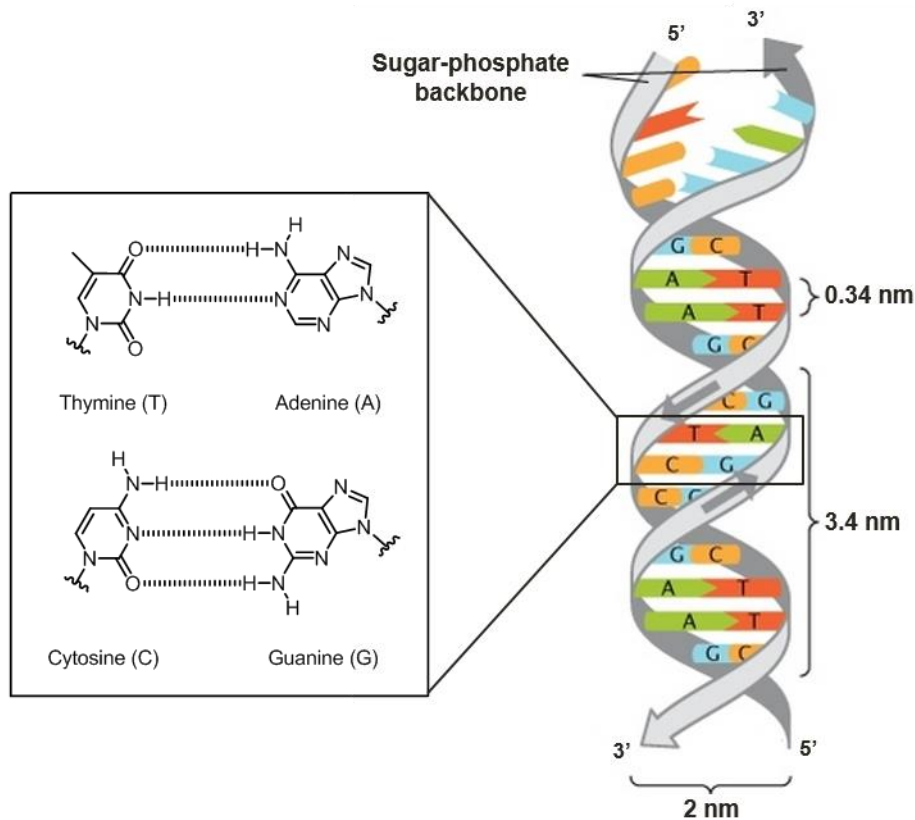
Figure 1.02: The DNA double helix structure highlighting the sugar-phosphate backbone and complementary base pairs. Figure adapted with permission.[8]

Whilst the majority of DNA found in living cells adopts the structure outlined above, termed B-DNA, factors such as water content,[9] base composition, and species of counter ion,[10,11] can all give rise to additional helical forms, most notably the right-handed A-DNA and left-handed Z-DNA helices (**Figure 1.03**).[12–14] Additionally, higher-order DNA structures have also been discovered, including three-stranded helical structures such as H-DNA,[7] and four-stranded helical structures such as G-quadruplexes and iMotifs (**Figure 1.03**).[15]

A-DNA **B-DNA** **Z-DNA**

H-DNA **G-Quadruplex** **iMotif**
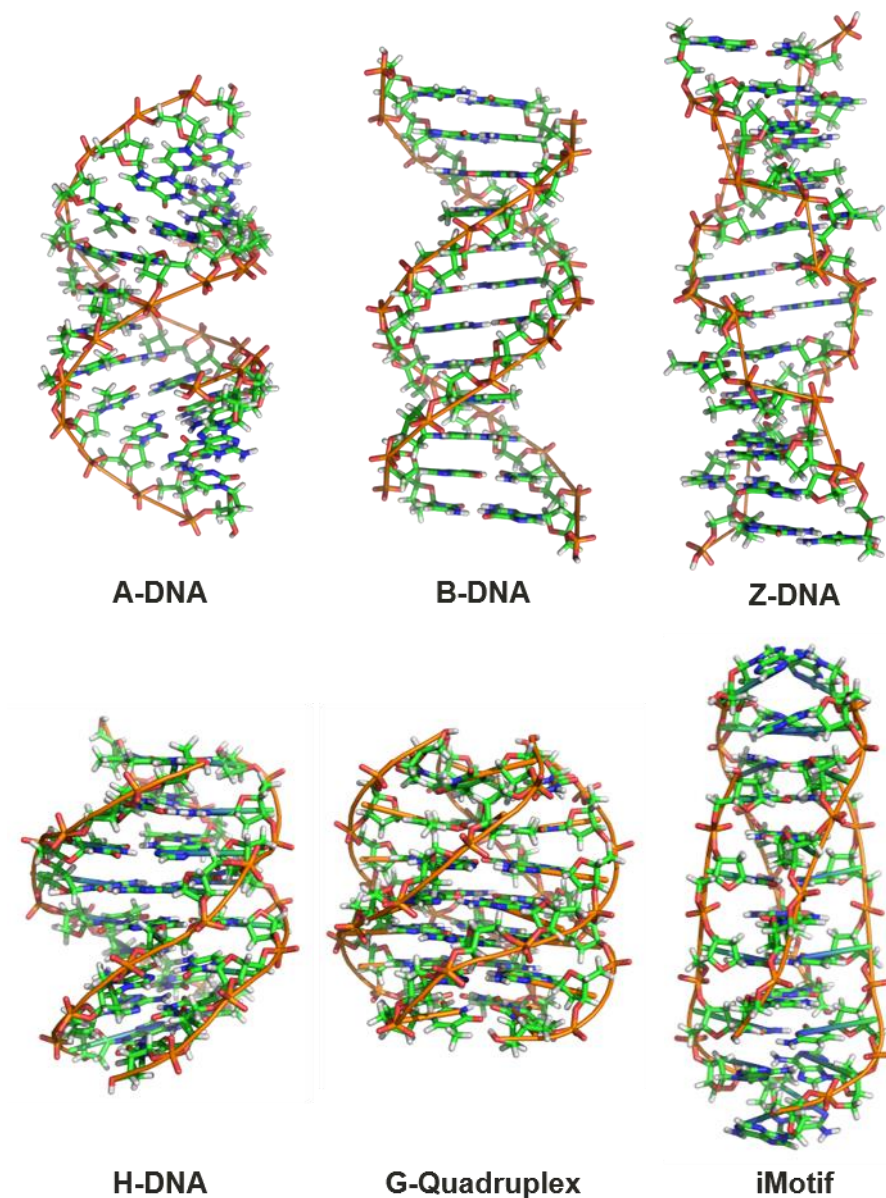
Figure 1.03: Helical structures of A-DNA, B-DNA, Z-DNA (reproduced under the GFDL license),[16] H-DNA (PDB: 1D3X), G-quadruplex (PDB: 139D) and iMotif (PDB: 1YBL) structures.

Although DNA possesses the genetic code required for protein biosynthesis, DNA itself does not function as the direct template. Instead, a complementary strand of ribonucleic acid (RNA), specifically messenger RNA (mRNA), is synthesized *via* a process known as transcription.

Transcription commences with the disruption of the hydrogen bonds between the nitrogenous bases and the partial unraveling of DNA, generating a sense (coding) and antisense (template) strand. Utilizing the antisense strand as a template, a complementary strand of mRNA is then synthesized by RNA polymerase (**Figure 1.04**).[17] Once complete, the DNA strands wind back into the double helix structure and the complementary strand of mRNA leaves the nucleus.
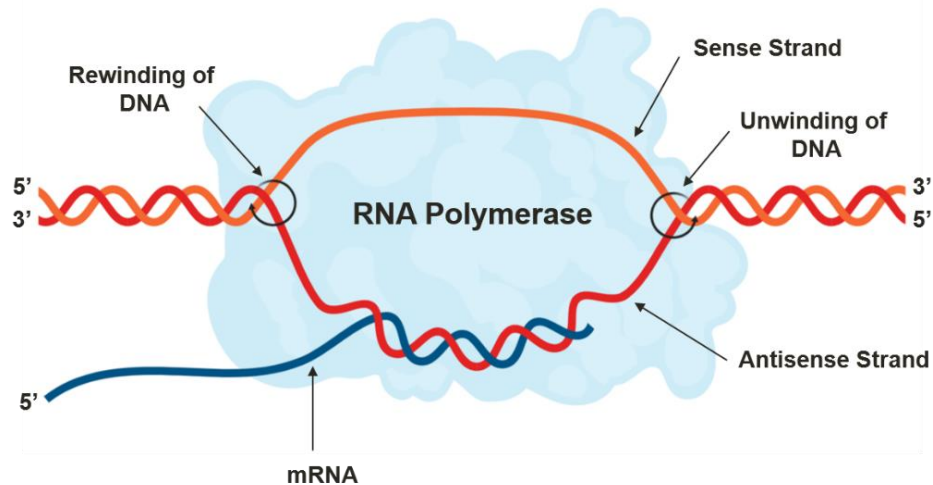
Figure 1.04: Diagram of the transcription process.

Although similar in structure, RNA differs from DNA in a few important ways: 1) RNA is single stranded; 2) the sugar component of RNA is a ribose unit; and 3) the nitrogenous base thymine is replaced by the unmethylated analogue uracil (U) (**Figure 1.05**).
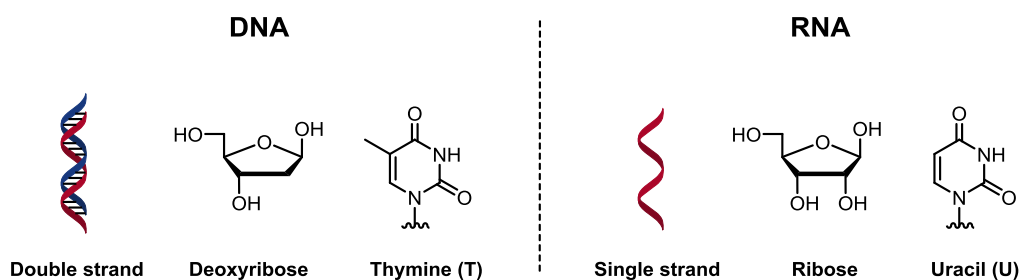
Figure 1.05: Three key differences between DNA and RNA.

Once in the cytoplasm, the mRNA strand migrates to a ribosome protein where translation, the next stage of protein biosynthesis, can take place (**Figure 1.06**). mRNA sequences of three bases, known as codons, correspond to individual amino acids and signal to the ribosome where to start and end the protein synthesis (e.g. GUC = Val and UAA = stop). At the ribosome, mRNA codons bind to complementary anticodons found on another form of RNA known as transfer RNA (tRNA). Each molecule of tRNA carries a specific amino acid which in turn is incorporated into the growing protein chain by the ribosome.[18]
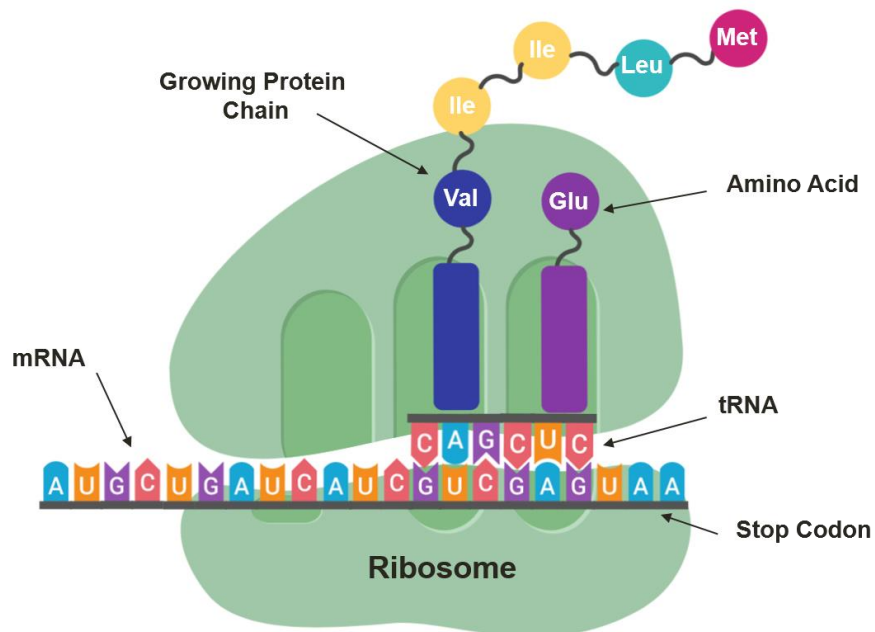
Figure 1.06: Diagram of the translation process.

This two-step process outlines the central dogma of molecular biology, a concept which describes the flow of genetic information from DNA through to functional proteins (**Figure 1.07**).[19] More specifically, the central dogma of molecular biology acts as a framework to describe the possible transfers of genetic information between DNA, RNA and proteins. These transfers can be split into three classes: 1) general transfers (solid arrows), those that occur in all cells; 2) special transfers (dashed arrows), transfers that are known to occur but only in very specific cases; and 3) transfers that are believed not to occur, such as protein to DNA or protein to RNA.
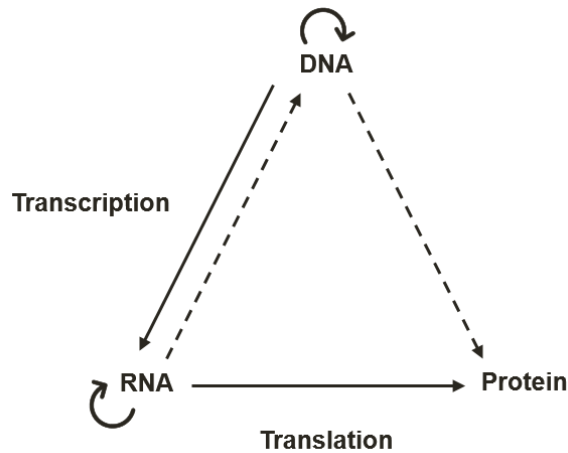
Figure 1.07: Central dogma of molecular biology summarizing the various possible transfers of genetic information. Solid arrows indicate general transfers that occur in all cells whilst dashed arrows indicate special transfers that are known to occur in very specific cases.

1.2 Epigenetics

Through the completion of the human genome sequence, it has been estimated that the human genome contains 20,000-25,000 protein coding genes.[20] Comparing this number to the vast array of phenotypes displayed in human development suggests that genetic sequencing can only be partly responsible. One theorized explanation for the remaining diversity is epigenetics, literally meaning "above genetics".[21,22]

Epigenetics is defined as the study of heritable changes in gene expression without alteration of the underlying DNA sequence.[23] Instead, epigenetic modifications work by disrupting the structure of chromatin and thus modulating the accessibility of DNA towards transcription. The two major categories of epigenetic modifications are alterations to DNA itself, such as DNA methylation,[24] and post translational modifications of histone tails, such as histone methylation,[25] acetylation,[26] ubiquitination,[27] phosphoration,[28] sumoylation[29] and ribosylation.[30] To fully understand these modifications and their distinct functional consequences, the structure and function of histones and chromatin must first be explained.

1.2.1 Histone Structure and Function

The average human cell contains ~3 billion base pairs of DNA, each of which is ~3.4 Å in length. This equates to a staggering ~2 m of DNA, all of which is packaged into

a 6 µm nucleus. To achieve this, DNA is wrapped around a series of proteins known as histones. The negatively charged phosphate backbone present in DNA is attracted to the positively charged Lys and Arg residues found in histones, which together account for ~25% of all histone residues.[31] More specifically, DNA is wrapped around an octamer of core histone proteins (two H3-H4 dimers surrounded by two H2A-H2B dimers)[32] to form structural sub units called nucleosomes, with each nucleosome containing ~147 base pairs of DNA. Nucleosomes in turn coil up to form the DNA protein complex known as chromatin, which is condensed even further to form chromosomes (**Figure 1.08**).[33,34]
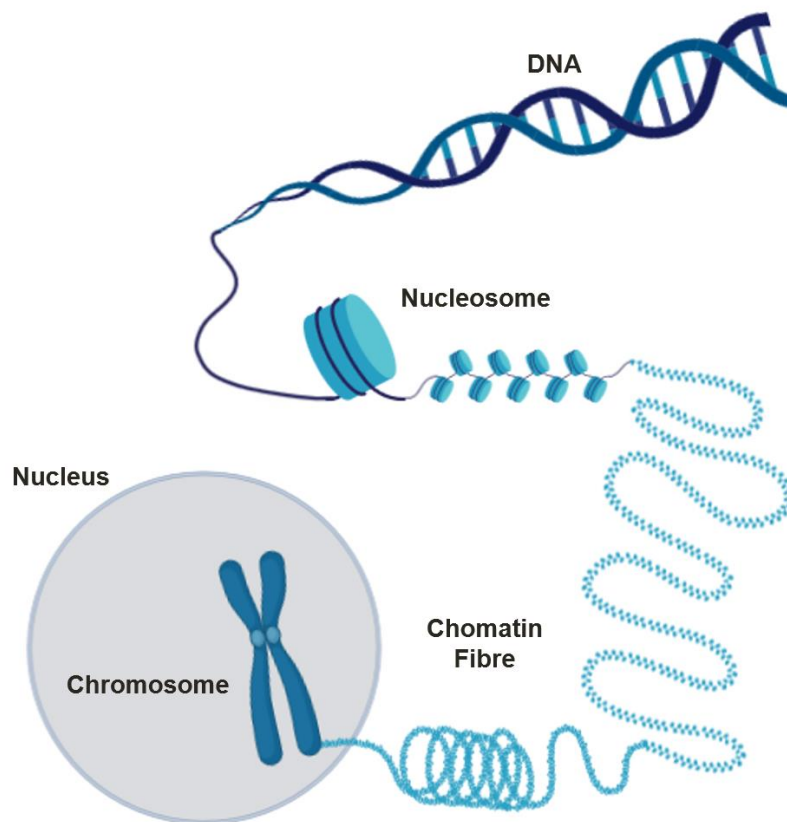
Figure 1.08: The packaging of DNA into nucleosomes which in turn form chromatin fibre and chromosomes.

Each core histone protein can be viewed as two separate domains; a globular domain, responsible for mediating histone-histone interactions within the octamer, and organizing the wrapping of DNA into two super helical turns;[35] and a 20-37 residue N-terminal domain which protrudes out into the nuclear lumen (**Figure 1.09**). The latter

are known as histone 'tails', and form the focal point for several of the aforementioned post translational modifications.[36]
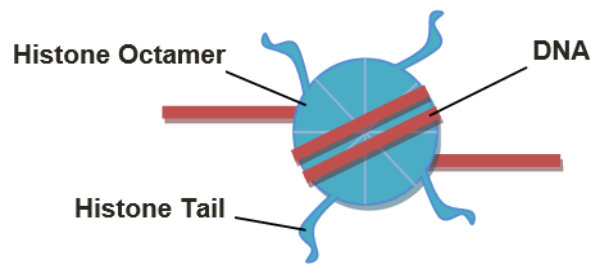
Figure 1.09: Structure of a nucleosome highlighting the histone octamer, the protruding N-terminal tails, and the two turns of DNA.

1.2.2 Epigenetic Modifications

The structure of chromatin, and thus the accessibility of DNA to transcriptional machinery, is controlled by epigenetic modifications. Epigenetic modifications are facilitated by proteins which can be split into the following three classes; 'writers' which catalyze the introduction of chemical groups to histones and DNA; 'erasers' which catalyze the removal of these chemical groups; and 'readers' which recognize and bind to these specific chemical groups (**Figure 1.10**). Together epigenetic 'writers' and 'erasers' produce a sequence of site specific modifications known as the 'epigenetic code'.[37]
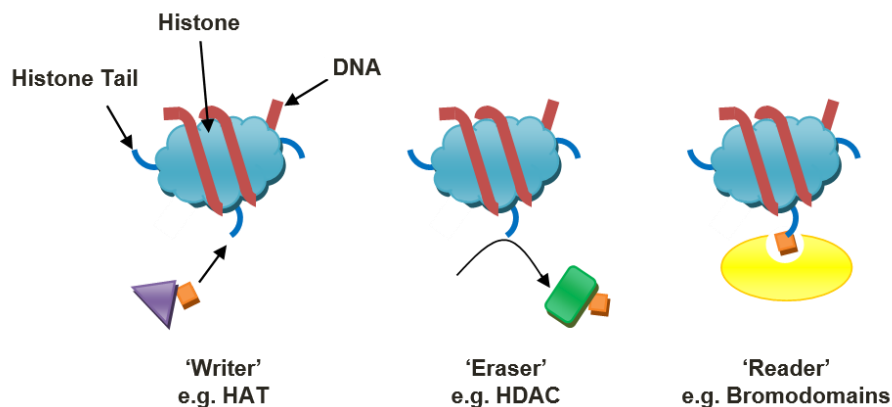
Figure 1.10: Epigenetic 'writers' (left) introduce chemical groups, 'erasers' (centre) remove chemical groups, and 'readers' (right) recognize chemical groups. HAT, histone acetyl transferase; HDAC, histone deacetylase.

1.2.2.1 Histone Acetylation

Histone acetylation is a fundamental example of a post-translational modification and involves the transfer of an acetyl group from acetyl-CoA to the amino groups of Lys residues found on the N-terminal tails of histones. This modification is facilitated by two classes of enzymes, histone acetyl transferases (HATs) and histone deacetylases (HDACs), which competitively catalyze the introduction and removal of acetyl groups respectively. An example of the proposed mechanism employed by GCN5-related *N*-acetyltransferases (GNAT), a family of HATs, to facilitate this transformation is shown in **Figure 1.11**.[38] Initially, a ternary complex is formed between both substrates (acetyl-CoA and histone) and the GNAT enzyme. A conserved Glu residue then activates a water molecule for the removal of a proton from the Lys amine group, mediating nucleophilic attack on the carbonyl group of acetyl-CoA (**Figure 1.11 left**). Elimination of the resulting tertiary intermediate (**Figure 1.11 centre**) and proton transfer completes the transfer of the acetyl group (**Figure 1.11 right**).
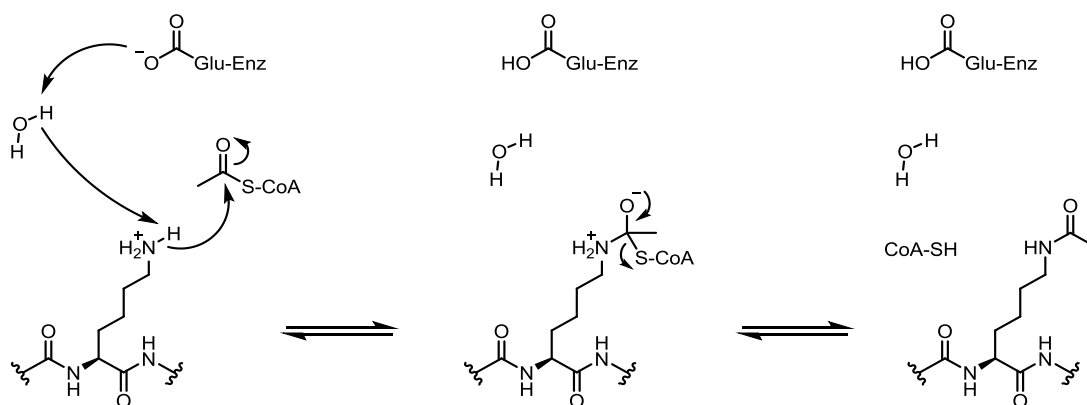
Figure 1.11: Mechanism for Lys acetylation from acetyl-CoA catalyzed by a GNAT.

Upon introduction of the acetyl group the positive charge of the Lys tail is neutralized (**Figure 1.12**), reducing the attraction between the histone proteins and the negatively charged DNA phosphate backbone. Consequently, the DNA is held less tightly in a more relaxed form of chromatin (euchromatin), allowing RNA polymerase and transcription factors to bind more readily, often leading to an increase in gene expression. Conversely, deacetylation of histones reestablishes the attraction

between DNA and histones restoring chromatin to its compact structure (heterochromatin) and often gene suppression. As a result, histone acetylation/deacetylation allows for the structure of chromatin, and thus gene expression, to be regulated.[39–41]

= Histone
= DNA
= Histone Tail
= Acetylated Lys
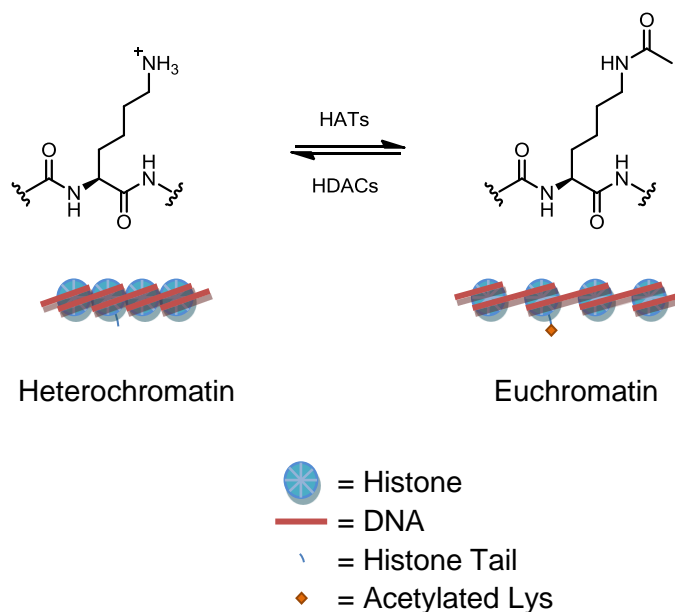
Figure 1.12: Schematic of Lys acetylation and its effect on chromatin structure.

1.3 Bromodomain Structure and Function

Bromodomains, named after the *Drosophila* gene *brahma* where they were first identified,[42,43] are a collection of epigenetic reader domains that, more specifically, bind selectively to acetylated Lys residues. In total there have been 61 different bromodomain protein modules identified spanning across 46 diverse human proteins. That is to say, some bromodomain containing proteins (BCPs) contain multiple bromodomains. In such cases, the bromodomain in question is denoted in brackets after the protein (e.g. BRD4 bromodomain 1 = BRD4(1) and BRD4 bromodomain 2 = BRD4(2)).

In 1999 the first three-dimensional structure of a bromodomain was elucidated *via* the NMR studies of BCP p300/CBP-associated factor (PCAF). The bromodomain of PCAF was shown to possess a unique left-handed bundle of four antiparallel alpha helices (αZ, αA, αB, and αC) connected by two flexible loop regions (ZA and BC), which together form the hydrophobic pocket for acetylated Lys binding.[44] Since then,

the structures of 41 of the 61 unique bromodomains have been solved *via* X-ray crystallography (including at least one from each subgroup),[45] confirming the originally reported structure and allowing for a full analysis of the hydrophobic pocket.

Within the hydrophobic pocket of each typical human bromodomain (48/61) are two conserved amino acid residues (Asn and Tyr) which form a direct hydrogen bond and a water mediated hydrogen bond to the acetylated Lys residue respectively (**Figure 1.13**). The water molecule involved in the latter interaction is one of four highly conserved water molecules located in the binding site of bromodomains.
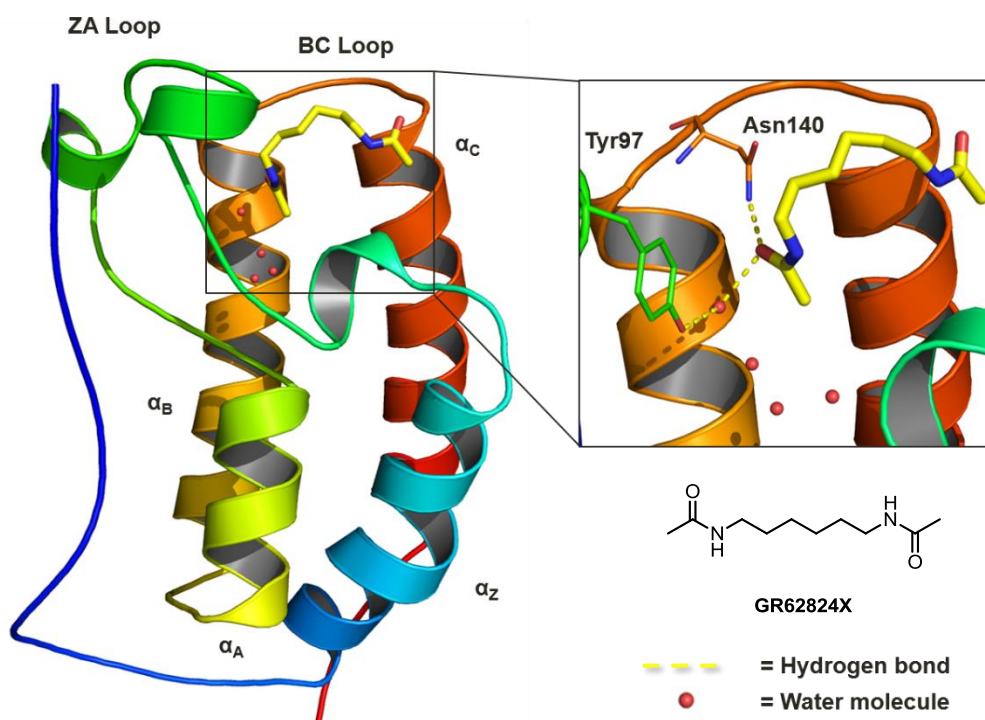
Figure 1.13: GSK internal X-ray crystal structure of BRD4(1) and GR62824X (shown in yellow), an acetyl Lys mimetic, highlighting the conserved structure of bromodomains, the hydrogen bond interaction between the carbonyl group of acetylated Lys and Asn140, the water mediated interaction to Tyr97 and the conserved water network.

Also contained within the acetyl Lys binding site is a three residue hydrophobic 'shelf' (named after the WPF shelf present in the bromodomain and extra terminal (BET) family bromodomains),[46] a hydrophobic 'gatekeeper residue' (located at the start of the αC helix)[47] and the ZA channel, which collectively help define the structure of the pocket (**Figure 1.14**).[48]
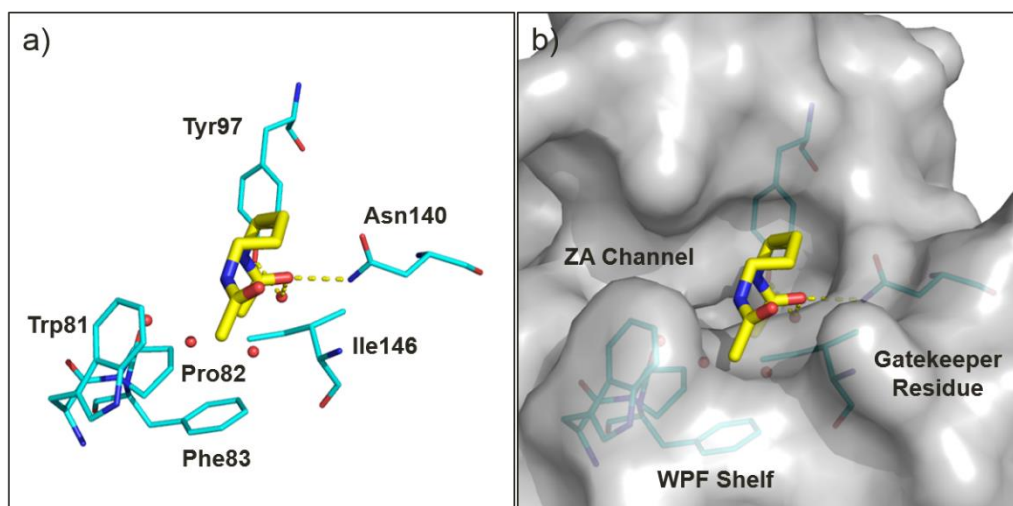
Figure 1.14: a) GSK internal X-ray crystal structure of GR62824X (shown in yellow) bound to BRD4(1) highlighting the conserved Asn and Tyr residues, the WPF shelf (Trp81, Pro82 and Phe83) and gatekeeper (Ile146) residues; and b) X-ray crystal structure of GR62824X (shown in yellow) bound to BRD4(1) highlighting the protein surface, the WPF shelf, the ZA channel and the gate keeper residue.

Despite this conserved structure, a great deal of diversity has been shown between the loop regions and surfaces of bromodomains, resulting in hydrophobic pockets that differ greatly in size, shape and charge, and thus suggesting that selective inhibitors can be produced for individual bromodomains. Bromodomains have subsequently been categorized into eight subfamily groups based on their genetic homology (**Figure 1.15**),[49] and can be categorized further into typical (79% of human bromodomains), as discussed above, and atypical (21%), where the conserved Asn residue is mutated for a Tyr, Thr or Asp.[50] This mutation has made targeting atypical bromodomains more challenging due to a less well-defined binding pocket, and more complex interactions within the binding pocket.
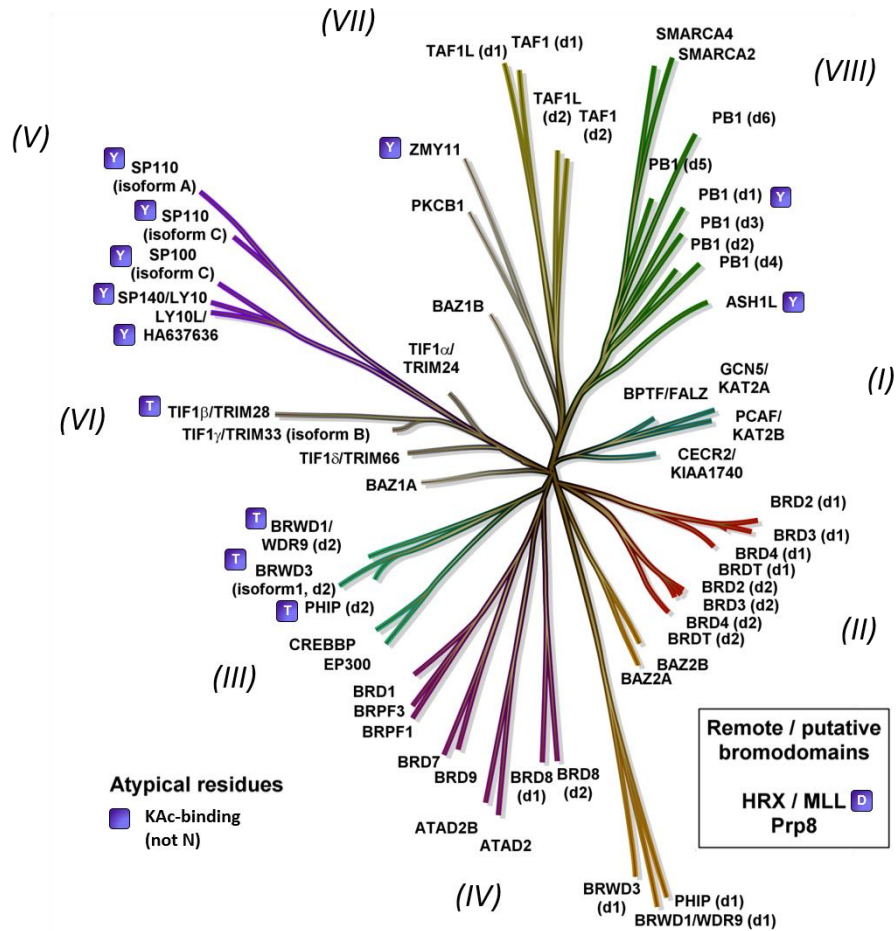
Figure 1.15: Human bromodomain phylogenetic tree, highlighting the eight subfamilies and the atypical bromodomains. The letter indicates what residue replaces the conserved Asn. Figure adapted with permission.[51]

1.4 Target Validation

There are two main causes of molecule-related clinical attrition, firstly drugs are not efficacious enough, and secondly they aren't safe; both of which can be the result of poor target validation.[52,53] Target validation is one of the early stages of a drug discovery program and, if done effectively, can help prevent late stage failures of drug discovery and development programs.

Before embarking on a drug discovery program, it is vital that the biological target is validated to ensure that it is directly involved in the disease in question and its biological role is well defined. Target validation can be accomplished in a number of ways, most commonly through gene knockout and gene knockdown,[54] or through the use of small tool molecules known as chemical probes.[55]

1.4.1 Chemical Probes

A chemical probe is a tool molecule that selectively binds to a target protein and is used to elucidate its biological function.[56,57] This provides an invaluable link between chemical biology and drug discovery, ensuring confident and accurate target validation is achieved before commencing a drug discovery program.[58,59]

A classic example of target validation through the use of chemical probes are the BET subfamily of bromodomains. I-BET762 (**1.001**)[60] and (+)-JQ-1 (**1.002**)[61] were identified in 2010 by two separate groups as potent and highly selective inhibitors of the BET bromodomains (**Figure 1.16**). Upon discovery, the structures and properties of both probes (and their structurally related negative control compounds) were made available for the scientific community. In doing so the biological function of this family of bromodomains and the role they play in a number of diseases was vigorously interrogated, ultimately accelerating bromodomain drug discovery. As of 2019, there are currently 15 BET bromodomain clinical candidates (including **1.001**) spanning 14 different companies (**Table 1.01**), underpinning both **1.001** and **1.002** as extremely successful and effective chemical probes.[62–64] The structures of these potential therapeutics, where disclosed, is shown in **Figure 1.17**.

I-BET762
1.001

(+)-JQ-1
1.002
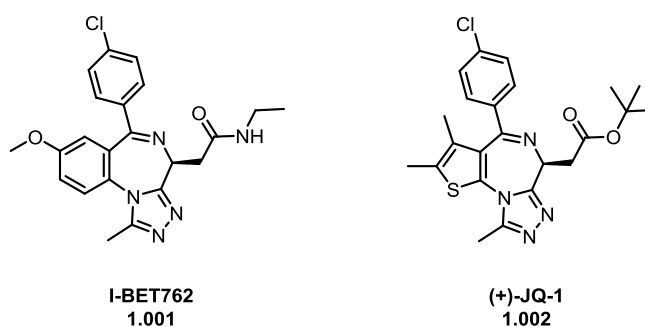
Figure 1.16: Structures of 1.001 and 1.002.

BET Inhibitor	Company	Disease Indication	Clinical Trial	Phase
GSK525762/	GlaxoSmithKline	Refractory hematologic malignancies	NCT01943851	II
(I-BET762)		NUT midline carcinoma (& other cancers)	NCT01587703	I
		Combination with Enzalutamide, CRPC	NCT03925428	I
		Combination with Fulvestrant, BC	NCT02964507	II
		NUT midline carcinoma	NCT04116359	I/II
ABBV-744	AbbVie	Advanced CRPC and AML	NCT03360006	I
Apabetalone	Resverlogix	Pulmonary arterial hypertension	NCT03655704	I
		End-stage renal disease	NCT03160430	II
		Fabry disease	NCT03228940	II
		Coronary artery disease	NCT02586155	III
AZD-5153	AstraZeneca	Relapsed or refractory solid tumours	NCT03205176	I
		Relapsed or refractory NHL		
BI-894999	Boehringer Ingelheim	Advanced malignancies	NCT02516553	I
BMS-986158	Bristol-Myers Squibb	Select advance solid tumours	NCT02419417	II
		Pediatric cancer	NCT03936465	I
CC-90010	Celgene	Advanced solid tumours/NHL	NCT03220347	I
		Astrocytoma/glioblastoma	NCT04047303	I
CPI-0610	Constellation	Myelofibrosis	NCT02158858	II
INCB-057643	Incyte	Advanced solid tumours	NCT02959437	II
INCB-059872	Incyte	Ewing sarcoma	NCT03514407	I
		Advanced malignancies	NCT02712905	II
		Overlap syndromes	NCT04061421	II
MK-8628	Merck	Hematological malignancies	NCT02698189	I
PLX-51107	Plexxikon	Combination with Azacitidine, AML	NCT04022785	I
RO6870810	Roche	Combination with Ventoclax, DLBCL	NCT03255096	I
		Advanced multiple myeloma	NCT03068351	I
SF1126	SignalRX	Combination with Nivolumab, HC	NCT03059147	I
ZEN-3694	Zenith	Combination with Talazoparib, TNBC	NCT03901469	II
		Combination with Enzalutamide, CRPC	NCT02711956	II

Table 1.01: Summary of BET inhibitors currently active in clinical trials on clinicaltrials.gov as of October 2019.[65] **CRPC, castration resistant prostate cancer; BC, breast cancer; AML, acute myeloid leukemia; NHL, non-Hodgkin's lymphoma; DLBCL, diffuse large B-cell lymphoma; TNBC, triple negative breast cancer; HC, hepatocellular carcinoma.**
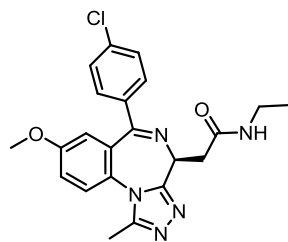
I-BET762
1.001
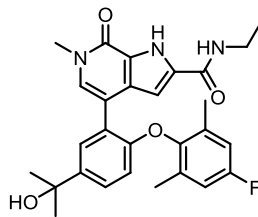
ABBV-744
1.003
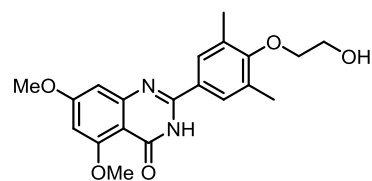
Apabetalone
1.004
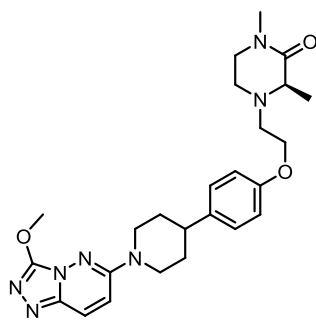
AZD5153
1.005
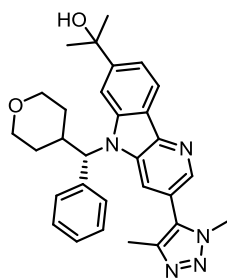
BMS-986158
1.006
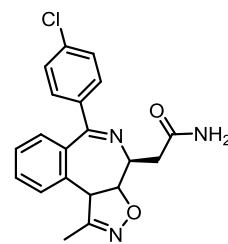
CPI 0610
1.007
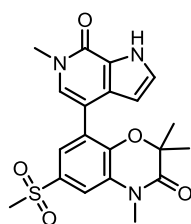
INCB-057643
1.008
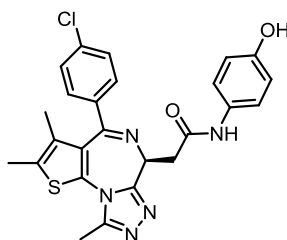
MK-8628
1.009
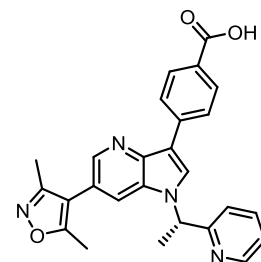
PLX-51107
1.010
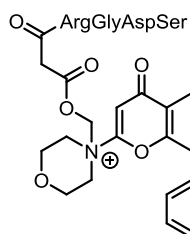
SF1126
1.011

Figure 1.17: Disclosed structures of BET inhibitors currently in active clinical trials.

Unfortunately, under-characterization has led to a number of potentially unsuitable chemical probes, many of which are still being used today, producing suspect results and compromising attempts at target validation. An ongoing example of this, reviewed by Nelson *et al.*,[66] is turmeric the "golden spice". Most commonly found in cooking, turmeric, the powdered rhizome of *Curcuma longa*, has long been used as a traditional Asian medicine to treat a wealth of ailments. These include, but are not limited to, chicken pox, small pox, insect bites, and cancers.[67] Turmeric has been heavily investigated for drug discovery, focusing in particular on a group of linear diarylheptanoids (**Figure 1.18**), the suspected active constituents of turmeric, known as curcuminoids (~1-6% of turmeric by dry weight).
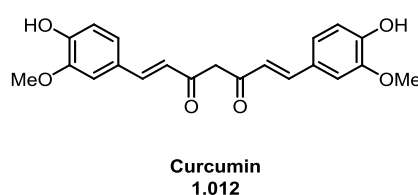
Curcumin
1.012

Figure 1.18: Structure of the keto form of curcumin, an example of a linear diaryl heptanoid.

More specifically, curcumin (**1.012**) has been used as a natural product-based drug lead in thousands of studies, ultimately resulting in numerous assay hits across several disease areas. The origin of these hits, however, is thought not to be due to specific drug-like interactions between the molecule and protein, but instead due to the pan-assay interference properties displayed by curcumin.[68,69] The two enones present in curcumin have been shown to covalently modify proteins unspecifically, leading to false positive assay hits.[70] Additionally, the monomethylated catechol groups have been shown to interfere with membranes, disrupting the response of membrane receptors; to chelate metals, sequestering metal ions that inactivate proteins; and to be redox active, producing reactive species which in turn can activate or inactivate different proteins.[71,72] Despite showing poor potency, little to no selectivity and displaying the aforementioned properties associated with pan-assay interference compounds (PAINS), these hits were heavily pursued as drug leads developing candidates for over 120 clinical trials. To this date not a single curcumin compound has made it to drug maturity, highlighting the damage that poor or misunderstood probes can cause.[66]

In order to prevent the identification and use of ineffective chemical probes, a collection of expert medicinal chemists and chemical biologists across academia and industry have come together to provide guidelines for what is required of an effective chemical probe.

In particular, Bunnage *et al.* have outlined some key guidelines that should be satisfied: 1) the probe must be able to reach the site of action at pharmacologically relevant concentrations; 2) the probe must display *in vitro* evidence of target engagement and selectivity; 3) the probe must provide sufficient data to assign phenotypic results to an original structure or a well characterized derivative; and 4) the probe must provide cellular activity data to answer a hypothesis on the role of the target.[73] Elaborating on these four principles has helped establish a set of requirements that a chemical probe should aim to fulfill (outlined in **Figure 1.19**).[73]
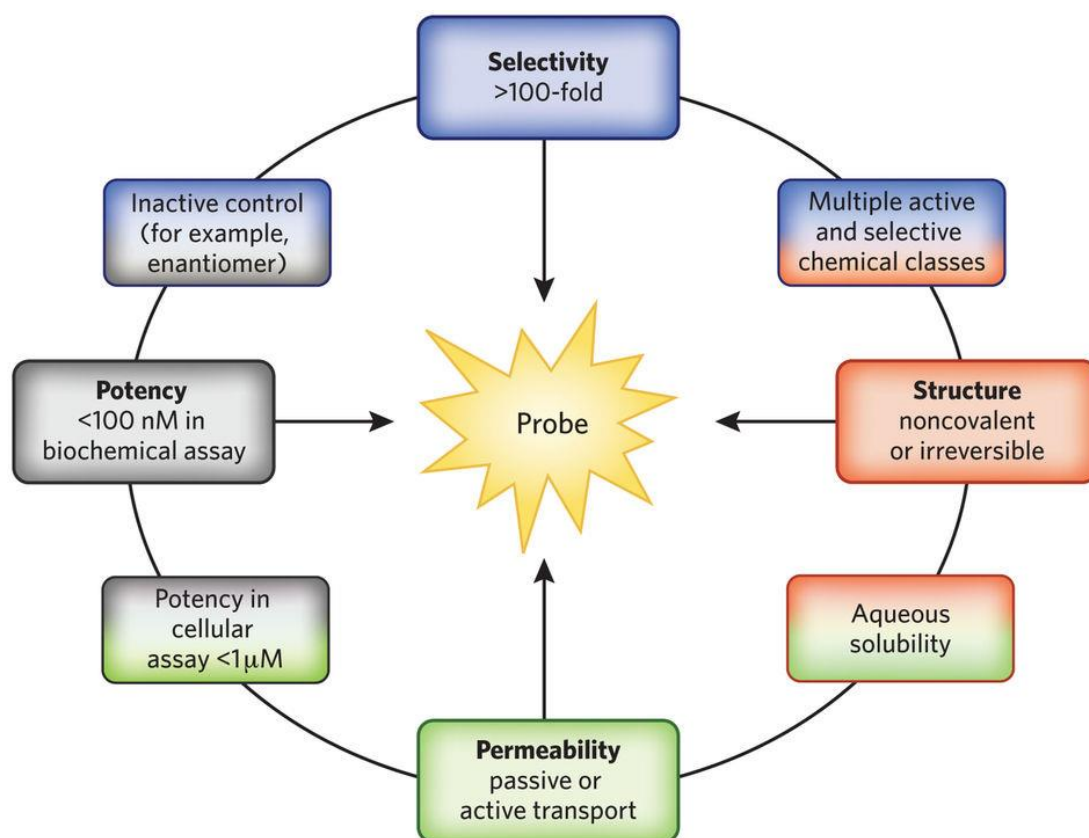
Figure 1.19: An outline of the criteria an ideal chemical probe should aim to fulfill. Figure reproduced with permission.[73]

Key to demonstrating exposure at the site of action is cellular permeability. Cellular permeability is essential for assigning a phenotypic response to intracellular target engagement and is crucial for ruling out false negatives caused by a lack of cell penetration. Artificial membrane permeability (AMP) assays (e.g. AMP or PAMPA),[74] absorption and transporter assays (e.g. Caco-2 or MDCK cell permeability assays),[75] and intracellular concentration assays can all provide insight into a compounds ability to reach a cellular target.[76,77] Similarly, partition and distribution coefficients (e.g. ClogP, CLogD, ChromLogD) provide an indication of a compound's lipophilicity, a well-known contributing factor to a compounds permeability.[78,79] LogP, LogD and ChromLogD are calculated using the equations shown in **Figure 1.20**. In the case of ChromLogD, a chromatographic hydrophobicity index (CHI) value is used to facilitate the high throughput measurement.[80]

$$LogP_{pH} = \left(\frac{[solute]_{octanol}^{un-ionized}}{[solute]_{water}^{un-ionized}} \right)$$

$$LogD_{pH} = \left(\frac{[solute]_{octanol}^{un-ionized} + [solute]_{octanol}^{ionized}}{[solute]_{water}^{un-ionized} + [solute]_{octanol}^{ionized}} \right)$$

$$ChromLogD_{pH} = \left(CHI_{pH} \times 0.0857 \right) - 2$$

Figure 1.20: Equations for calculating partition/distribution coefficients.

Aqueous solubility should also be considered when assessing a probe's ability to reach the designated target. As chemical probes are likely to be administered as a solution, kinetic solubility is usually sufficient and can be measured in a high-throughput manner *via* charged aerosol detection (CAD) or chemiluminescent nitrogen detection (CLND) assays.[81–83]

The potency of the probe for the desired target provides evidence of target engagement and, along with detailed SAR, is essential in establishing a relationship between target engagement and phenotypic response. As a result, a chemical probe should display *in vitro* potency at less than 100 nM (pIC$_{50}$ or pK$_D$ ≥7). Potency is typically measured *via* ligand binding assays utilizing a fluorescence detection

method. A popular example is time-resolved Förster (fluorescence) resonance energy transfer (TR-FRET) which measures the energy transferred between donor fluorophore and acceptor fluorophore molecules, positioned on the protein of interest and a known binding partner, when in close proximity.[84,85] As the compound is dosed, one half of the donor-acceptor couple is displaced, giving rise to IC_{50} values as an indicator of potency. Other methods include amplified luminescent proximity homogeneous assay screen (AlphaScreen),[86] a proximity based assay where chemiluminescence is measured instead of fluorescence; isothermal titration calorimetry (ITC), where the heat absorbed/released during ligand binding is measured to calculate association constants (K_a);[87] and differential scanning fluorimetry (DSF), where ligand binding causes a destabilization of the protein and thus an increase in melting temperature (T_m).[88] It should be noted that whilst T_m is a valid indicator of protein binding, the magnitude of T_m shift observed during DSF varies from protein to protein, and as such, quantitative comparisons should be treated with caution. The efficiency which a ligand binds to a given protein can also be quantified for the ligand's size (ligand efficiency, LE) and lipophilicity (lipophilic ligand efficiency, LLE) using the equations shown in **Figure 1.21**.[89,90]

$$LE = \frac{pIC_{50} \times 1.4}{Number\ of\ heavy\ atoms}$$

$$LLE = pIC_{50} - CLogP$$

Figure 1.21: Equations used for calculating LE and LLE.

Although useful in driving the optimization of potency and selectivity, biochemical assays provide limited information on a chemical probe's ability to function within a cellular context. Consequently, chemical probes should also show cellular target engagement at <1 μM to confirm a probe's ability to reach the site of action. Some common techniques include Nanoluciferase-bioluminescence resonance energy transfer (NanoBRET),[91] and fluorescence recovery after photo bleaching (FRAP).[92]

The selectivity of a probe is equally important for assignment of an observed phenotype to engagement of the desired target, and not to an uncharacterized off-

target. Consequently, a chemical probe should display selectivity against other subfamily proteins (>100-fold), other protein families (>30-fold), and be profiled against other pharmacologically relevant off-targets where possible. Despite strict selectivity criteria, the likelihood of unknown off-targets is still high. Consequently, it is advised that a probe is accompanied by a structurally similar negative control, ideally in the form of an inactive enantiomer, to provide further evidence for the 'true' on and off-targets of the probe.

A final consideration when designing chemical probes is the importance of structural diversity. Multiple inhibitors of differing chemotypes provides a greater confidence in the experimental outcome, a reduced probability of finding common off-targets and a greater conviction that observed phenotypes are due to target engagement.

Although an ideal chemical probe should satisfy all these criteria, this is often not possible, and caution should be taken not to be overly restrictive with these guidelines as there is a risk innovation can be stifled in exchange for a "fit-for-purpose" approach. Instead, the caveats and limitations of the chemical probe in question should be properly understood and its application considered accordingly.[93]

1.4.2 Non-BET Bromodomain Chemical Probes

The success of chemical probes in the validation and understanding of the BET bromodomains as potential therapeutic targets, and the development of new pharmaceutical candidates across a range of disease areas, has led to a growing interest in non-BET BCPs, the majority of which by comparison are drastically less well understood.

Unlike the relatively simple BET BCPs (two tandem bromodomains and an extra terminal domain), non-BET BCPs are often more complicated, possessing several other protein domains (**Figure 1.22**). As such, the ability to inhibit individual domains selectively using chemical probes is particularly valuable in elucidating the biological role each domain plays within diseases, a feat not possible with other target validation techniques, such as gene knockout and knockdown, where the synthesis of the entire protein is reduced or prevented.
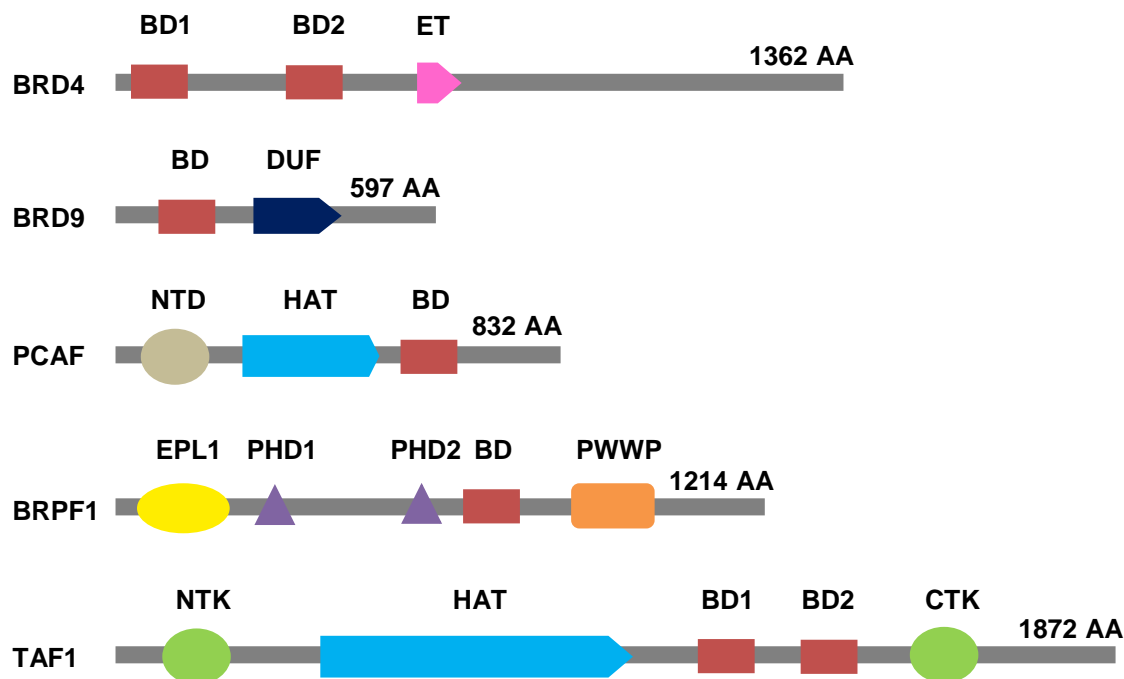
Figure 1.22: Schematic diagram of BCPs BRD4, BRD9, PCAF, BRPF1 and TAF1. Organization and location of the individual domains is indicated by the relative positions of each shape. Bromodomains are shown in red. BD, bromodomain; ET, extra terminal; DUF, domain of unknown function; NTD, N-terminal domain; HAT, histone acetyl transferase; EPL1, enhancer of polycomb-like 1; PHD, plant homeodomain; PWWP, Pro-Trp-Trp-Pro; NTK, N-terminal kinase; CTK, C-terminal kinase.

To further understand non-BET BCPs and the role their bromodomains can play in disease, academia and industry have begun developing non-BET bromodomain chemical probes. As the field has progressed, the quality of non-BET bromodomain chemical probes, and the variety of chemotypes included, has advanced dramatically, reflecting the awareness and uptake of the guidelines discussed in **Section 1.4.1**. The advancements made within this field has been exemplified by CREBBP inhibitor CCS1477, the first non-BET bromodomain inhibitor to enter clinical trials.[94] The structure of CCS1477 is currently undisclosed, however, several posters have been presented supporting the clinical testing of CCS1477 for the down regulation of androgen receptor (AR) and MYC, and the treatment of haematological cancers.[95]

The field of non-BET chemical probes was comprehensively reviewed in March 2016,[58] and more recently in January 2019.[96] A selection of compounds from the most

recent review are discussed below, highlighting GSK's recent contributions to the field. Emphasis was placed on each compound's fulfillment of the aforementioned probe criteria, highlighting the advances that have been made in potency, bromodomain selectivity and negative control development. For clarity, all bromodomain inhibitors have been drawn (where possible) with the acetylated Lys mimetic in the top-left or bottom-left corner and, when available, a crystal structure of the inhibitor bound to the target protein has been included. All existing TAF1/TAF1L and BRD7/9 inhibitors are discussed in their relevant sections (**Section 2.2** and **Section 3.2**, respectively).

1.4.2.1 PCAF/GCN5L2 Chemical Probe: GSK4027

PCAF and general control non-depressible 5 (GCN5L2) are two HAT proteins that have been linked with diseases spanning across a diverse range of therapeutic areas, including oncology,[97–99] neuro-degeneration,[100,101] HIV infection,[102–104] and inflammation pathways. Despite being mutually exclusive proteins, the highly homologous amino acid sequence shared between them (~73%), and their bromodomains in particular, suggests targeting one selectively over the other is challenging.

By the end of 2015, the PCAF/GCN5L2 chemical tool landscape was limited, with only one PCAF/GCN5L2 inhibitor having been disclosed. Moreover, the reported inhibitor possessed micromolar potency (pIC_{50} = 5.8), thus requiring further optimization. During the past three years, multiple PCAF/GCN5L2 inhibitors and chemical probes have been disclosed across patents and peer reviewed literature.[105–109]

In 2016, researchers at GSK published GSK4027 (**1.014**) as a selective and potent PCAF/GCN5L2 chemical probe (**Figure 1.23**).[108] Starting from a screening of ~30000 known and potential acetyl Lys mimetic-containing compounds, an initial pyridazinone scaffold, demonstrating moderate potency (pIC_{50} = 4.8) and good ligand efficiency (0.37), was optimized by iterative SAR to develop compound **1.014**. X-ray crystallography was used to drive the optimization of hit compound **1.013** and to identify several hydrogen bond interactions between **1.014** and the bromodomain of PCAF (**Figure 1.24**). These included the expected hydrogen bond and water-mediated hydrogen bond to Asn808 and Tyr765, respectively. More interesting was

the observation that the halogen group was acting as the methyl mimetic, and not the expected *N*-methyl group, and the identification of Glu761 as a key acidic residue found in the PCAF/GCN5L2 ZA channel, absent in BET bromodomains, from which high BET selectivity was achieved. Utilizing a TR-FRET assay, **1.014** demonstrated good potency against PCAF (pIC_{50} = 7.4) and >1000-fold selectivity over the BET subfamily (BRD4(1) pIC_{50} <4.3). The selectivity of **1.014** was further investigated *via* the DiscoverX BROMO*scan* panel, demonstrating ≥18000-fold selectivity over the BET family of bromodomains and ≥70-fold selectivity over the other remaining bromodomains. This excludes the highly homologous GCN5L2 where equipotency was displayed. Additionally, **1.014** showed selectivity over a collection of pharmacologically relevant off-targets *via* a cross screening panel of 53 biochemical and phenotypic assays, showing no activity pIC_{50} >5.5. Compound **1.014** showed good permeability (500 nm/s) and aqueous solubility (149 µg/mL) and demonstrated cellular target engagement of PCAF (pIC_{50} = 7.2) in a NanoBRET assay, providing convincing evidence to support its ability to reach the target site. Importantly, compound **1.014** was also accompanied by GSK4028 (**1.015**) an enantiomeric negative control (PCAF pIC_{50} = 4.9), providing greater confidence in the target validation achieved through the use of **1.014**.

1.013
PCAF pIC_{50} = 4.8
BRD4(1) pIC_{50} = 4.8

GSK4027
1.014
PCAF pIC_{50} = 7.4
BRD4(1) pIC_{50} < 4.3

GSK4028
1.015
PCAF pIC_{50} = 4.9
BRD4(1) pIC_{50} < 4.3

Figure 1.23: Structures of PCAF/GCN5L2 chemical probe 1.014, accompanying negative control 1.015 and initial hit compound 1.013. pIC_{50} values refer to potency in a TR-FRET assay.
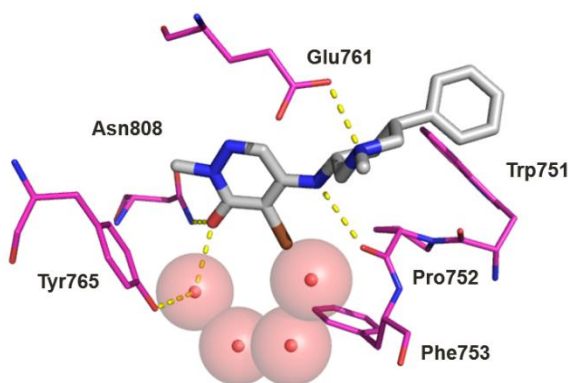
Figure 1.24: a) Crystal structure (PDB: 5MLJ) of 1.014 (grey) bound to human bromodomain GCN5L2 (purple).

1.4.2.2 ATAD2/ATAD2B Chemical Probe: GSK8814

Adenosine triphosphatase (ATPase) family AAA domain containing protein 2 (ATAD2) and ATPase family AAA domain containing protein 2B (ATAD2B) are chromatin remodelling proteins which consist of an AAA ATPase domain and a highly homologous (76% consistent amino acid sequence) bromodomain. Both bromodomains have been strongly linked with a diverse range of cancers including lung,[110] liver,[111] prostate and breast,[112,113] hence the desire for ATAD2/ATAD2B chemical probes for further target validation.[114,115]

GSK have reported the first ATAD2/2B chemical probe, GSK8814 (**1.017**) (**Figure 1.25** & **1.26**), optimized from their previously reported ATAD2 inhibitor (**1.016**).[116,117] Of note was the substitution of the sulfone group for the less polar -CF_2 bioisostere which provided a needed increase in permeability. Secondly, 1,3-interactions on the piperidine ring were utilized to destabilize the axial conformation favoured for BRD4(1) binding, thus improving selectivity over the BET subfamily. Compound **1.017** demonstrated potency for ATAD2/2B (ATAD2/2B pIC_{50} = 7.3/7.7) with selectivity over the BET family (>1000-fold) and other non-BET bromodomains (100-fold). Cellular target engagement of **1.017** with ATAD2 (pIC_{50} = 5.7) was demonstrated using a NanoBRET assay and was reflected in the solubility (>439 µM) and permeability (190 nm/s) of **1.017**. Moreover, **1.017** was screened against an internal GSK panel of 40 pharmacological off-targets and was inactive at the concentrations tested. The enantiomer of **1.017**, known as GSK8815 (**1.018**), displayed a reduced potency for

ATAD2/2B (pIC_{50} = 5.5/5.5) and provides an enantiomeric negative control for phenotypic screening.

1.016
ATAD2 pIC_{50} = 7.2
ATAD2B pIC_{50} = N.A.
BRD4(1) pIC_{50} = 5.4

GSK8814
1.017
ATAD2 pIC_{50} = 7.3
ATAD2B pIC_{50} = 7.7
BRD4(1) pIC_{50} < 4.5

GSK8815
1.018
ATAD2 pIC_{50} = 5.5
ATAD2B pIC_{50} = 5.5
BRD4(1) pIC_{50} < 4.4
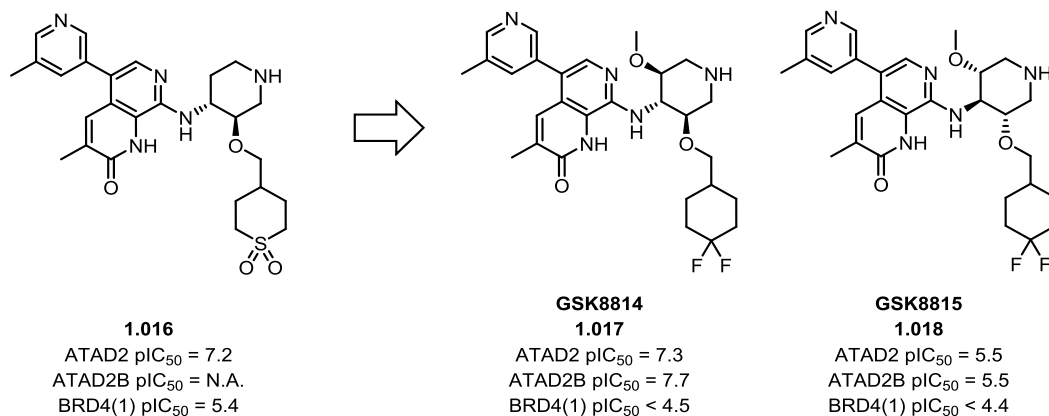
Figure 1.25: Structure of ATAD2/ATAD2B chemical probe 1.017, accompanying negative control 1.018, starting point 1.016. pIC_{50} values refer to potency in a TR-FRET assay.
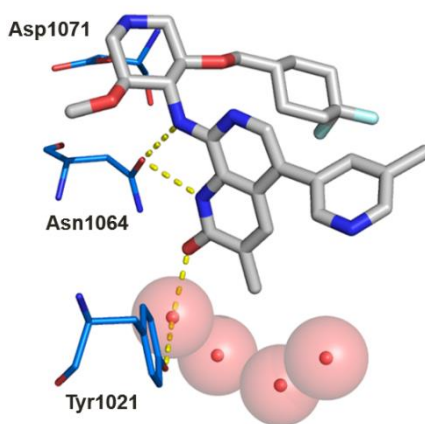
Figure 1.26: Crystal structure (PDB: 5LJ0) of 1.017 (grey) bound to human bromodomain ATAD2 (blue).

1.4.2.3 BRPF1/2/3 Chemical Probe: GSK6853

The bromodomain and PHD finger-containing protein family (BRPF1/2/3) are a group of paralogs found within HAT complexes which have been predicted to play a critical role in acute myeloid leukemia.[118,119] BRPF1/2/3 are some of the more extensively studied bromodomains which is reflected in their sophisticated portfolio of chemical probes. Recently, efforts have focused around diversifying the chemotypes present in BRPF1/2/3 inhibitors[120,121] and improving selectivity between the BRPF paralogs.

One of the more recent additions to the BRPF1/2/3 chemical probe tool box is GSK6853 (**1.020**), a potent and highly selective BRPF1 bromodomain inhibitor optimized from the previously reported GSK5959 (**1.019**) (**Figure 1.27**).[122] In optimizing **1.019** to **1.020**, GSK improved kinetic solubility from 8 µg/mL to 140 µg/mL, and consequently improved its applicability to *in vivo* experiments.[123] This was achieved through the introduction of a basic nitrogen at the 4-position of the piperidine ring, improving the compounds physicochemical properties whilst in turn forming a hydrogen bond to the carbonyl group of Asn651 to maintain potency, as predicted by X-ray crystallography (**Figure 1.28**). Further interrogation of the crystal structure presented the 2-position of the piperidine ring as a vector towards Pro658, one of only a few residues not conserved between the BRPF family, where a favourable interaction with a methyl group was harnessed for improved BRPF1 potency (pIC_{50} = 8.1) and BRPF subfamily selectivity (≥1000-fold). Moreover, **1.020** retained its high selectivity over the BET bromodomains (>1600-fold), as measured by TR-FRET assay, and was selective (>2000-fold) against a further 26 non-BET bromodomains in the DiscoverX BROMO*scan* panel. Additionally, **1.020** displayed selectivity (500-fold) against a cross screen panel of 48 pharmacologically relevant off targets including kinases, ion channels, GPCRs, enzymes, transporters and a nuclear receptor. The cellular activity of **1.020** was then demonstrated using a NanoBRET assay where potent inhibition (BRPF1 pIC_{50} = 7.7) was displayed. Furthermore, **1.020** also possesses suitable PK for *in vivo* mouse studies following intraperitoneal delivery and is accompanied by a structurally related negative control GSK9311 (**1.021**).

GSK5959
1.019
BRPF1/2/3 pIC$_{50}$ = 7.1/5.2/4.5
BRD4(1) pIC$_{50}$ = <4.3
CLND = 8 µg/mL

GSK6853
1.020
BRPF1/2/3 pIC$_{50}$ = 8.1/5.1/4.8
BRD4(1) pIC$_{50}$ = 4.7
CLND = 140 µg/mL

GSK9311
1.021
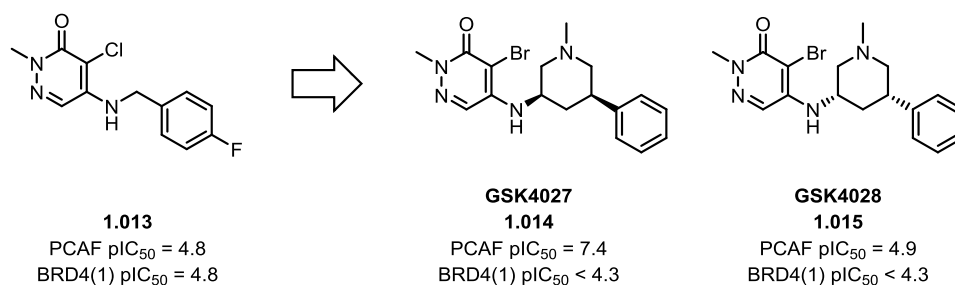BRPF1/2/3 pIC$_{50}$ = 6.0/4.3/4.9
BRD4(1) pIC$_{50}$ < 4.3
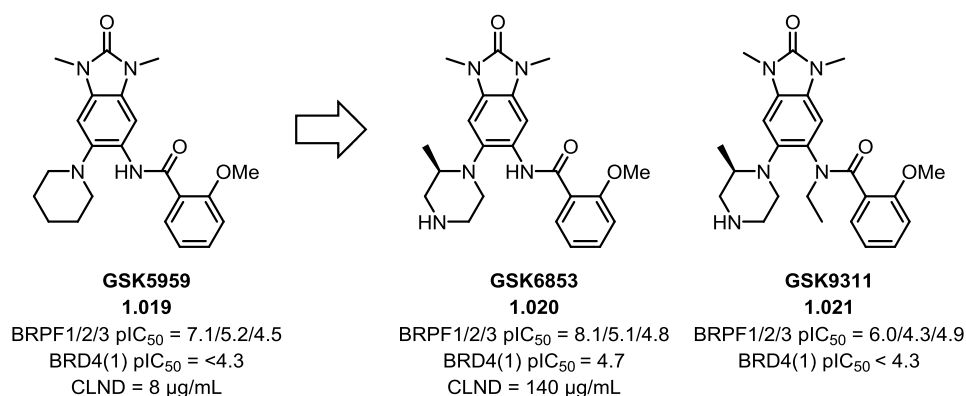
Figure 1.27: Structures of BRPF1 chemical probe 1.020, accompanying negative control 1.021 and initial hit compound 1.019. pIC$_{50}$ values refer to potency within a TR-FRET assay.
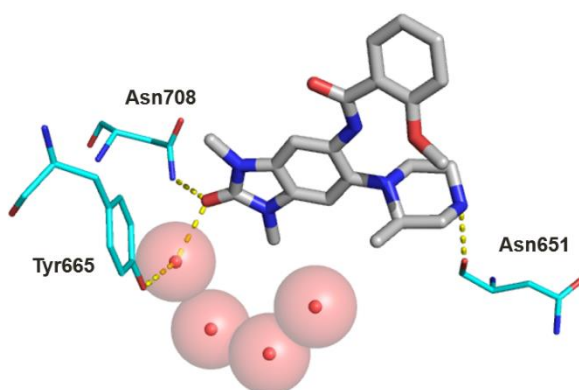
Figure 1.28: Crystal structure (PDB: 5G4R) of 1.020 (grey) bound to human bromodomain BRPF1 (cyan).

1.4.3 Non-BET Bromodomain PROTACs

The generation of high-quality chemical probes, and the structural information typically obtained during their development, has also facilitated the evolution of more sophisticated bifunctional chemical biology tools. These include bivalent inhibitors, photoaffinity probes and biotinylated derivatives. Access to such molecules can provide additional information into the validation of biological targets and, through the use of complementary techniques such as Chem-seq, map the interactions between small molecules and the human genome.[124,125]

An area of particular interest has been the development of bifunctional molecules known as proteolysis targeting chimeras (PROTACs). Fundamentally, PROTACs

work by combining two protein-binding regions, one region which binds to the target protein and another which binds to an E3 ligase. The bivalent binding of PROTACs brings the target protein and an E3 ligase into close proximity, facilitating ubiquitination of the target protein and ultimately degradation *via* the proteasome (**Figure 1.29**).[126]
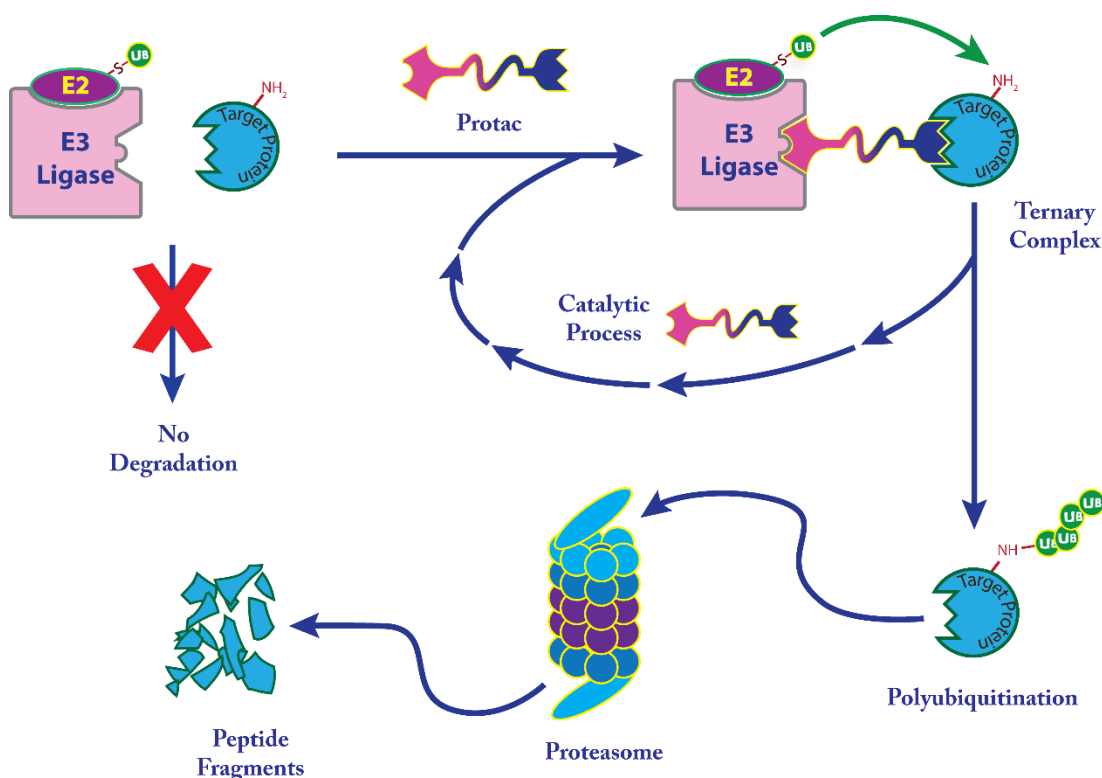
Figure 1.29: Schematic of protein degradation as facilitated by PROTACs. Figure reproduced with permission.[126]

Whilst PROTACs have been used in the past to effectively degrade a variety of proteins, such as kinases,[127,128] transcription factors[129,130] and even BET bromodomains,[131] the design of non-BET bromodomain PROTACs is relatively underexplored.[132,133] A recent example in this area is discussed below.

GSK have disclosed the first bifunctional PCAF/GCN5L2 PROTAC, GSK699 (**1.022**), utilizing **1.014** as the PCAF/GCN5L2 binding component (**Figure 1.30**).[134] X-ray crystallography was used to identify the 4-position of the pendant phenyl ring as a suitable, solvent exposed vector, for an E3 ligase binder to be attached. A thalidomide derivative was chosen as a ligand for the cereblon E3 ligase complex and was

appended to **1.014** *via* a rigidified linker. Like PCAF/GCN5L2 inhibitor **1.014**, binding to PCAF/GCN5L2 is dependent on the stereochemistry across the piperidine ring. As a result, only the (*R*,*R*) enantiomer (**1.022**) showed potent PCAF/GCN5L2 degradation (pDC_{50} = 9.0 and 8.6 respectively). For comparison, GSK702 with (*S*,*S*) stereochemistry only showed 35% PCAF degradation at 100 nM and provides a useful negative control against any potential phenotype mediated by the cereblon binding portion of **1.022**. Whereas PCAF/GCN5L2 bromodomain inhibition with **1.014** was shown to be ineffective in replicating the anti-inflammatory phenotype demonstrated by gene knockdown, PCAF/GCN5L2 degradation with **1.022** was successful in reducing the production of multiple inflammatory cytokines such as IL-6 and IL-10, thus presenting PCAF/GCN5L2 degradation as a new anti-inflammatory therapeutic avenue and highlighting the potential of the PROTAC approach. Compounds **1.022** and **1.023** demonstrate the importance for high quality chemical probes in the development of more sophisticated tool molecules, and again highlights the benefit to designing accompanying negative controls.

GSK4027
1.014
PCAF pIC$_{50}$ = 7.4
BRD4(1) pIC$_{50}$ < 4.3

GSK699
1.022
PCAF pDC$_{50}$ = 9.0
GCN5 pDC$_{50}$ = 8.6

GSK4028
1.015
PCAF pIC$_{50}$ = 4.9
BRD4(1) pIC$_{50}$ < 4.3

GSK702
1.023
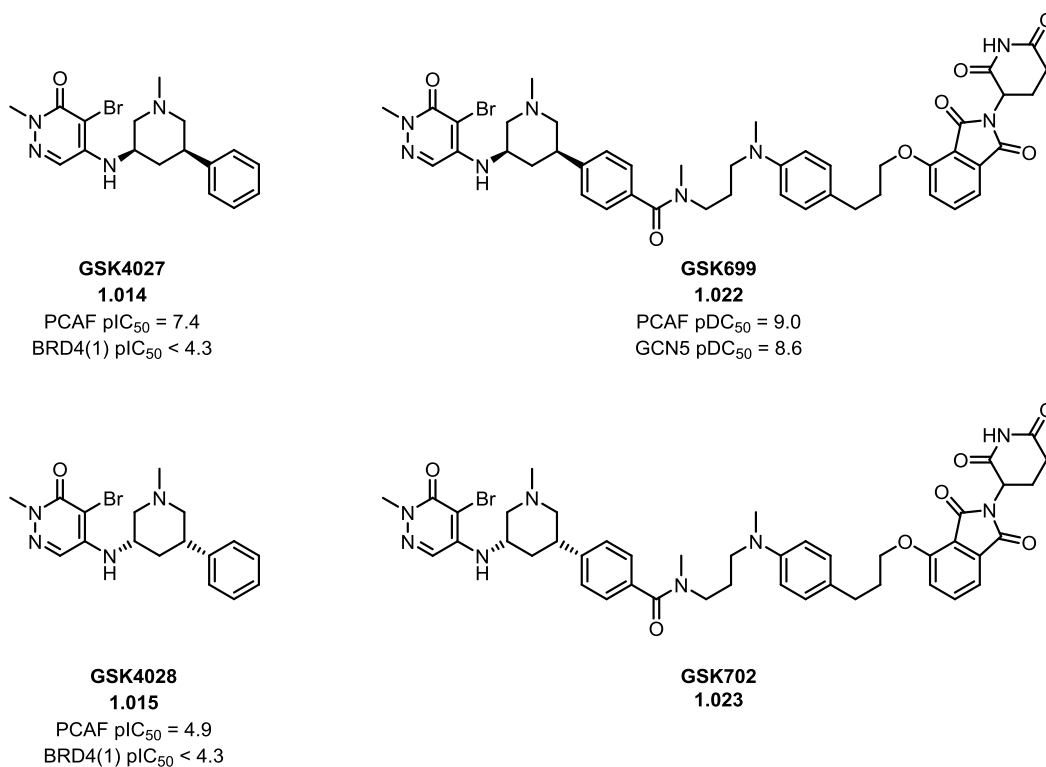
Figure 1.30: Structure of PCAF/GCN5L2 inhibitor 1.014, PROTAC 1.022 and their corresponding negative control compounds 1.015 and 1.023. pIC$_{50}$ values refer to potency in a TR-FRET assay. pDC$_{50}$ values refer to degradation as measured by western blot.

1.4.4 Summary

In recent years the bromodomain chemical probe research field has become dramatically more advanced and more precisely defined. As a result, the non-BET bromodomain chemical tool portfolio has flourished, with more potent, selective and *in vivo* capable tool molecules being developed. Additionally, we are beginning to see more negative controls being developed and a more diverse range of chemotype inhibitors. Similarly, the development of more sophisticated bifunctional chemical tools, such as PROTACs, will hopefully allow for more extensive target validation of the non-BET BCPs.

Despite these advances, several non-BET bromodomains remain insufficiently researched, with many still lacking sufficiently characterized chemical probes and chemically diverse inhibitor portfolios.

1.5 Aims

The aim of this PhD research was to design effective chemical probes for non-BET bromodomain target validation, focusing primarily on bromodomains lacking sufficiently characterized chemical probes, and chemically undiverse tool boxes. Using the guidelines outlined in **Section 1.4.1**, and taking inspiration from Bunnage *et al.*,[73] the following criteria were considered for any probe developed:

1. $pIC_{50} \geq 7$ against the target bromodomain, as determined by a biochemical assay.
2. ≥100-fold selectivity over the BET-bromodomain family (using BRD4(1) as a representative example) for which a strong biological phenotype is known. From GSK's own experience, a minimum of 100-fold selectivity is required for adequate biological interpretation.
3. ≥30-fold selectivity over other non-BET bromodomain families.
4. ≥30-fold selectivity over other pharmacologically relevant off-targets.
5. Suitable solubility and permeability to ensure exposure at target site.
6. Cellular activity at <1 µM concentrations.
7. Be the product of iterative SAR exploration.
8. Be accompanied by a structurally related negative control.
9. Expand the structural diversity of any existing chemical probe tool box.

Additionally, as selectivity is heavily scrutinized in the development of chemical probes, and therefore methodology to obtain selectivity for a target in a predictable and facile manner would be extremely powerful, this work focussed (where possible) on the implementation of conserved water interactions for bromodomain selectivity and their broader applicability.

2. Designing a Chemical Probe for TAF1

2.1 Identifying TAF1 as a Therapeutic Target

As mentioned in **Section 1.1**, RNA polymerase catalyzes the transcription of DNA into mRNA. Before transcription commences, a preinitiation complex forms consisting of the RNAP-II subunit and the general transcription factors TFIIA, TFIIB, TFIID, TFIIE, TFIIF and TFIIH.[135] TFIID in particular plays a key role in this complex acting as a scaffold for the coordination of the remaining transcription factors, alignment of RNA polymerase with DNA, and the binding to DNA.[6, 24]

TFIID consists of several subunits including the TATA binding protein (TBP), responsible for binding to DNA, and a collection of TBP associated factors (TAFs), the largest of which is known as TAF1. Structurally TAF1 is comprised of 1872 amino acids and consists of two kinase domains (an N-terminal and a C-terminal), a HAT domain, and two tandem bromodomains (BD1 and BD2) (**Figure 2.01**), which together show a 66% sequence similarity across their acetylated Lys binding pockets (**Table 2.01**). BD1 and BD2 of TAF1 will be referred to as TAF1(1) and TAF1(2), respectively, throughout this work.

Figure 2.01: Schematic diagram of TAF1, highlighting the N-terminal and C-terminal kinases (NTK and CTK), the HAT domain, and the two tandem bromodomains (BD1 and BD2).

TAF1(1)	TAF1(2)	Comment
Tyr1403	Trp1526	WPF motif
Pro1404	Pro1527	WPF motif
Phe1405	Phe1528	WPF motif
His1406	His1529	ZA channel
Thr1407	His1530	ZA channel
Pro1408	Pro1531	ZA channel
Val1409	Val1532	ZA channel
Asn1410	Asn1533	ZA loop
Ala1411	Lys1534	ZA loop
Lys1412	Lys1535	ZA loop
Val1413	Phe1536	ZA loop
Val1414	Val1537	ZA loop
Tyr1417	Tyr1540	Water-binding Tyr
Tyr1418	Tyr1541	
Ile1421	Ile1544	
Ile1452	Ile1575	
Asn1455	Asn1578	
Ser1456	Ser1579	
Tyr1459	Tyr1582	Conserved Tyr
Asn1460	Asn1583	Conserved Asn
His1464	Ser1587	
Ser1465	Gln1588	
Leu1466	Tyr1589	Gatekeeper
Thr1467	Thr1590	
Ile1469	Thr1592	
Ser1470	Ala1593	

Table 2.01: The amino acid sequence for the acetyl Lys binding pockets found in TAF1(1) and TAF1(2) highlighting sequence similarity. Identical residues shown in green, different residues shown in red and similar residues shown in orange.[136]

One difference of note between the binding pockets of TAF1(1) and TAF1(2) is the 'gatekeeper' residue, Leu1466 and Tyr1589, respectively (**Figure 2.02**). The large difference in size for these two residues provides very different steric constraints for the binding pocket, including varied accessibility to the WPF shelf motif, which could potentially be exploited to bias selectivity for one bromodomain over the other. Additionally, the gatekeeper residues themselves could be targeted for selective interactions, for example π-stacking with Tyr1589.[137]
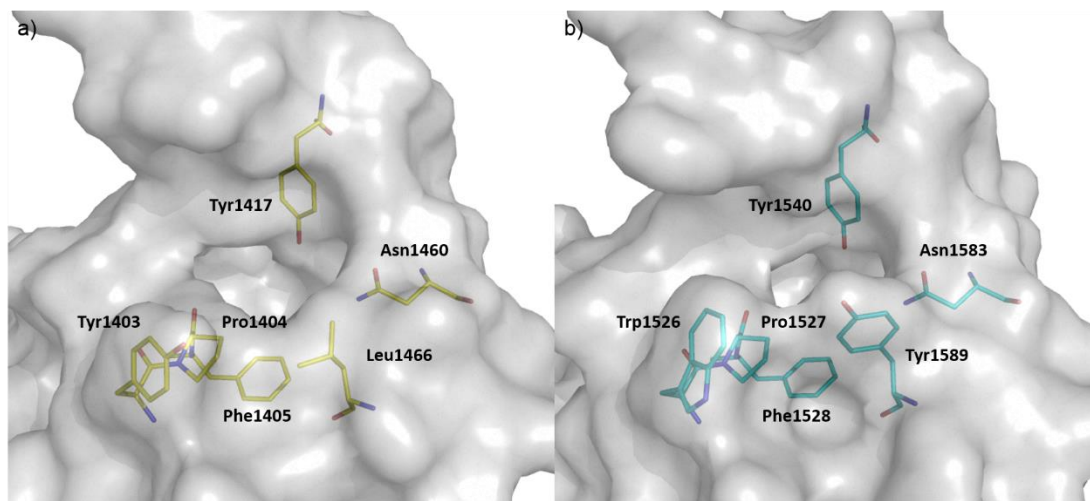
Figure 2.02: X-ray crystal structures of a) apo-TAF1(1) bromodomain (PDB: 1EQF) and b) apo-TAF1(2) bromodomain (GSK internal X-ray crystal structure) highlighting the different residues.

Belonging to bromodomain subfamily VII, TAF1 is highly homologous (95% amino acid homology)[138] to TATA binding protein associated factor 1 like (TAF1L), possessing almost identical acetylated Lys binding sites: the BD1 domains differ by a single amino acid whilst the BD2 domains are identical (**Table 2.02**). As one might expect from their homologous nature, TAF1 and TAF1L are thought to function interchangeably.[139]

TAF1(1)	TAF1L(1)		TAF1(2)	TAF1L(2)	Comment
Tyr1403	His1422		Trp1526	Trp1545	WPF motif
Pro1404	Pro1423		Pro1527	Pro1546	WPF motif
Phe1405	Phe1424		Phe1528	Phe1547	WPF motif
His1406	His1425		His1529	His1548	ZA channel
Thr1407	Thr1426		His1530	His1549	ZA channel
Pro1408	Pro1427		Pro1531	Pro1550	ZA channel
Val1409	Val1428		Val1532	Val1551	ZA channel
Asn1410	Asn1429		Asn1533	Asn1552	ZA loop
Ala1411	Ala1430		Lys1534	Lys1553	ZA loop
Lys1412	Lys1431		Lys1535	Lys1554	ZA loop
Val1413	Val1432		Phe1536	Phe1555	ZA loop
Val1414	Val1433		Val1537	Val1556	ZA loop
Tyr1417	Tyr1436		Tyr1540	Tyr1559	Water-binding Tyr
Tyr1418	Tyr1437		Tyr1541	Tyr1560	
Ile1421	Ile1439		Ile1544	Ile1563	
Ile1452	Ile1440		Ile1575	Ile1594	
Asn1455	Asn1471		Asn1578	Asn1597	
Ser1456	Ser1475		Ser1579	Ser1598	
Tyr1459	Tyr1478		Tyr1582	Tyr1601	Conserved Tyr
Asn1460	Asn1479		Asn1583	Asn1602	Conserved Asn
His1464	His1483		Ser1587	Ser1606	
Ser1465	Ser1484		Gln1588	Gln1607	
Leu1466	Leu1485		Tyr1589	Tyr1608	Gatekeeper
Thr1467	Thr1486		Thr1590	Thr1609	
Ile1469	Ile1488		Thr1592	Thr1611	
Ser1470	Ser1489		Ala1593	Ala1612	

Table 2.02: The amino acid sequence for the acetyl Lys binding pockets found in BD1 and BD2 of TAF1 and TAF1L highlighting sequence similarity. Identical residues are shown in green and different residues are shown in red.[136,140]

Like many BCPs, TAF1 and TAF1L are believed to be associated with a number of diseases, primarily spanning oncology[138,141,142,143] and neurology.[144–148] More specifically, TAF1 and TAF1L have been shown to interact with a transcription factor protein of the human papilloma virus (HPV-E2), and lead to an increased activation of E2 protein and thus HPV, the principal etiological factor in the development of cervical cancer.[141] Similarly, overexpression of TAF1 and TAF1L have been shown to increase androgen receptor activity several fold, resulting in the progression of prostate cancer,[142] whilst it has also been proposed that TAF1 and TAF1L mutations might play a role in tumorigenesis of colorectal and gastric cancers.[138]

Mutations in TAF1 and TAF1L have been shown to contribute to the phenotypes displayed across multiple neurodegenerative X-linked syndromes, including intellectual disability, global development delay, facial dysmorphology and general hypotonia.[144] It has also been reported that reduced expression of TAF1 is linked to X-linked dystonia parkinsonism, a movement disorder found in people of Philippine descent.[145–148] Whilst the involvement of TAF1 and TAF1L within such diseases has been established, the biological role of these proteins and their bromodomains in modulating healthy/disease states is less clear. More robust target validation is therefore required before TAF1 and TAF1L can be considered as therapeutic targets, and as such both are in need of high-quality chemical tools to probe their various domains. Currently there are no known selective TAF1/TAF1L kinase or HAT inhibitors, although it is understood that TAF7 (a separate sub unit of TFIID) acts as a dissociable TAF1 HAT inhibitor in transcription regulation.[149] Instead, attempts to better understand TAF1 and TAF1L's applicability as druggable targets have focused around TAF1/TAF1L bromodomain inhibitors.

2.2 Current TAF1/TAF1L Bromodomain Inhibitors

A number of groups have attempted to develop selective TAF1/TAF1L bromodomain inhibitors. In this section these inhibitors shall be discussed, along with their advantages, disadvantages and ability to function as a chemical probe.

Whilst investigating BRD4 inhibitors, the Research Center for Molecular Medicine discovered a selection of small molecules that mimic BRD4 inhibition without binding to the target.[150] One of these small molecules, CeMMEC13 (**2.001**, **Figure 2.03**), was shown to inhibit TAF1(2) (pIC_{50} = 5.7) with selectivity against the BET subfamily (<20% inhibition against BRD4(1) at 10 µM). Compound **2.001** also displayed selectivity over other non-BET bromodomains tested (<60% inhibition against BRD9, CREBBP and EP300 at 10 µM). In addition, **2.001** was also shown to stimulate red-fluorescent protein within REDS3 cells, confirming cellular penetration. CeMMEC15 (**2.002**) was developed as a negative control for **2.001**, although the two compounds are structurally quite different, and consequently may not share the same off-targets. In addition, compound **2.001** would benefit from further selectivity characterization, in particular against the remaining non-BET bromodomains. Continuation of this research has led to the release of a patent disclosing further TAF1 inhibitors.[151]

Although limited data is provided for the molecules, the most potent inhibitor (TAF1(2) pIC_{50} = 7.3) has been included for reference (**2.003**), and shows an increase in potency from **2.001**.

CeMMEC13
2.001
TAF1(2) pIC_{50} = 5.7

CeMMEC15
2.002
TAF1(2) pIC_{50} < 4.7
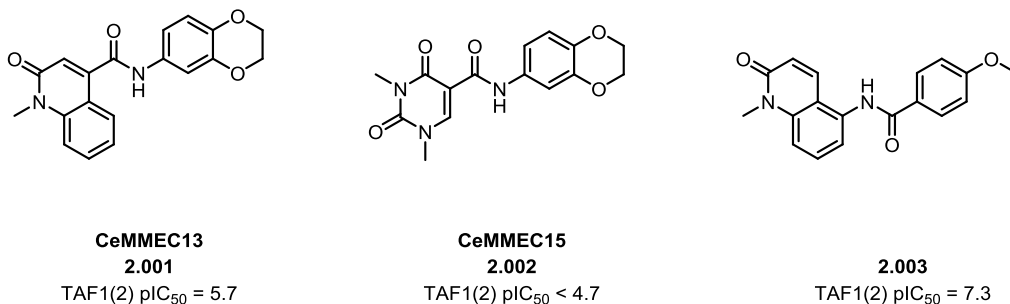
2.003
TAF1(2) pIC_{50} = 7.3

Figure 2.03: TAF1(2) inhibitor CeMMEC13, negative control CeMMEC15 and patented TAF1(2) inhibitor 2.003. pIC_{50} values refer to activity in a Cisbio EPIgeneous binding assay.

A series of TAF1 inhibitors have also been discovered by collaborative work between Genentech and Constellation Pharmaceuticals (**Figure 2.04**) and disclosed in a recent patent.[152] 208 compounds, based around the patented Markush structure (**2.004**), were synthesized and tested for potency against both bromodomains of TAF1. Two compounds, the most selective TAF1(2) compound (**2.005**) and the most potent pan-TAF1 compound (**2.006**), have been included for reference. Compound **2.005** displayed potency for TAF1(2) (pIC_{50} = 7.2) and was selective over TAF1(1) (pIC_{50} <4.7). By contrast, compound **2.006** displayed potency towards both bromodomains of TAF1 (TAF1(1)/TAF1(2) pIC_{50} = 7.1/7.7). It is currently unknown whether selective TAF1(2) inhibition or pan-TAF1 inhibition is preferred, however, having access to inhibitors of each type will help elucidate this information. Currently, no information on these compound's selectivity, solubility, permeability or cellular target engagement has been disclosed.

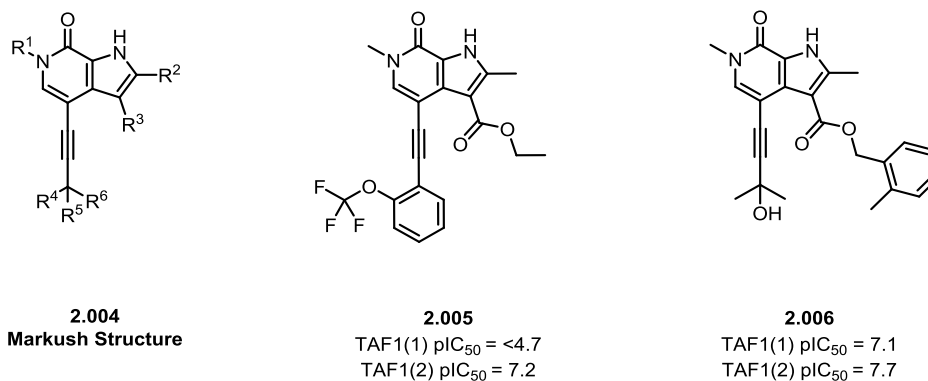| 2.004	2.005	2.006
Markush Structure	TAF1(1) pIC_{50} = <4.7	TAF1(1) pIC_{50} = 7.1
	TAF1(2) pIC_{50} = 7.2	TAF1(2) pIC_{50} = 7.7

Figure 2.04: Patented Markush structure 2.004, TAF1(2) inhibitor 2.005 and pan-TAF1 inhibitor 2.006. pIC_{50} values refer to activity in TR-FRET assays.

Collaborative work between Bayer and the SGC developing BRPF2 inhibitors has led to the identification of BAY-299 (**2.008**), a potent and selective triple inhibitor of BRPF2 and TAF1/TAF1L (**Figure 2.05** & **Figure 2.06**).[153] An initial HTS of ~3.5 million compounds resulted in potent (BRPF2 pIC_{50} = 6.3) hit compound **2.007**, selected for displaying selectivity over BRD4 (BRD4(1) pIC_{50} = 4.9). Optimization of potency, solubility, *in vitro* DMPK and selectivity resulted in **2.008**, with a key interaction between a carbonyl group and Ser592 providing the desired BRPF2 selectivity. Compound **2.008** was shown to engage BRPF2 (BRPF2 pIC_{50} = 7.2) selectively over BRPF1 (BRPF1 pIC_{50} = 5.5) and BRPF3 (BRPF3 pIC_{50} = 5.3) as measured by a TR-FRET assay. Compound **2.008** also demonstrated selectivity over the BET subfamily (BRD4 pIC_{50} = 4.8), >300 kinases (<50% inhibition in all cases at 10 µM) and against a LeadProfilingScreen containing 68 pharmacologically relevant targets (<25% inhibition in all cases at 10 µM). Selectivity was also demonstrated against 32 bromodomains in an AlphaScreen excluding CREBBP where at 100 nM modest CREBBP potency was shown (CREBBP pIC_{50} = 5.8). Compound **2.008** demonstrated permeability (Caco-2 cell P_{app} = 163 nm/s) and was shown to successfully engage BRPF2 (pIC_{50} = 6.3) within a NanoBRET assay, despite poor solubility (10 µg/mL). During this investigation activity was also observed for TAF1(2). Although this wasn't optimized, substantial potency for TAF1(2) was shown in both TR-FRET (pIC_{50} = 8.1) and NanoBRET assays (pIC_{50} = 6.0). A structurally similar negative control, BAY-364 (**2.009**), was also developed and showed reduced potency at both BRPF2 (pIC_{50} <4.7) and TAF1 (pIC_{50} = 4.9). **2.008**'s inability to selectively inhibit TAF1/TAF1L without

BRPF1 inhibition creates difficulty in assigning any observed phenotype to a specific bromodomain, and thus limits its application as a chemical probe to that of a triple probe. Additionally, only moderate selectivity (17-fold) over CREBBP may also limit its application.

2.007
BRPF1/2/3 pIC$_{50}$ = < 4.8/6.3/N.A.
TAF1(2) pIC$_{50}$ = N.A.
BRD4(1) pIC$_{50}$ < 4.9

BAY-299
2.008
BRPF1/2/3 pIC$_{50}$ = 5.5/7.2/5.3
TAF1(2) pIC$_{50}$ = 8.1
BRD4(1) pIC$_{50}$ = 4.8

BAY-364
2.009
BRPF1/2/3 pIC$_{50}$ < 4.7/< 4.7/< 4.7
TAF1(2) pIC$_{50}$ = 4.9
BRD4(1) pIC$_{50}$ < 4.7
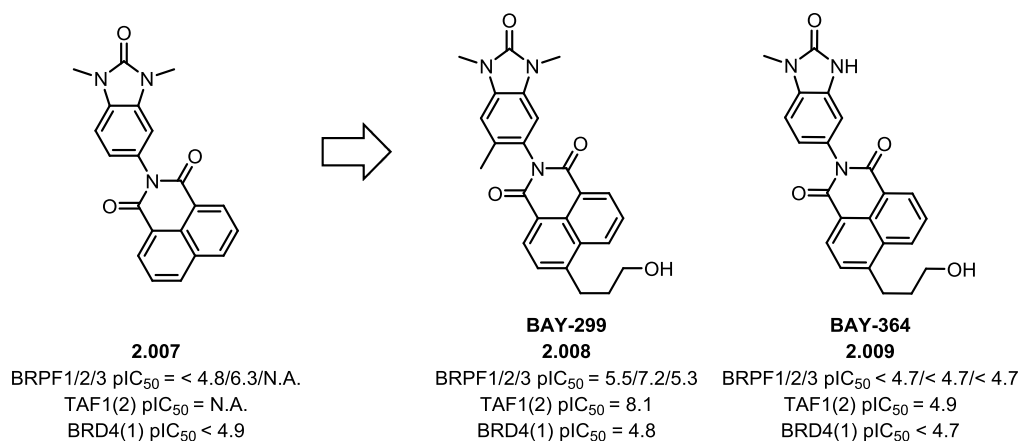
Figure 2.05: Triple inhibitor BAY-299 (2.008), negative control BAY-364 (2.009) and initial hit compound 2.007. pIC$_{50}$ values refer to activity in TR-FRET assays.
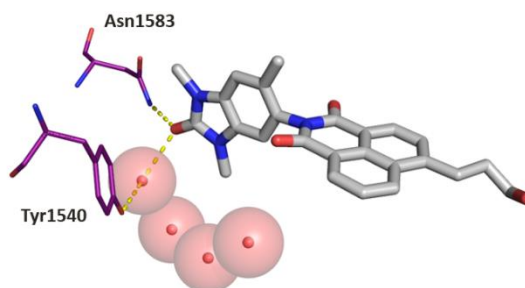
Figure 2.06: Crystal structure (PDB: 5MG2) of TAF1/TAF1L inhibitor 2.008 (grey) bound to TAF1(2) (purple).

Whilst investigating the use of fluorous-tagged multicomponent reactions for the synthesis of BET inhibitors, Bradner *et al.* developed lead compound UMB-32 (**2.010**), as a BRD4(1) inhibitor molecule (**Figure 2.07**).[154] Compound **2.010** displayed good selectivity for the BET bromodomains, with the exception of TAF1(2) (pK$_D$ = 6.3). Good intrinsic cell permeability is associated with the chemical series, although no

permeability or solubility data is provided for compound **2.010**. Cellular activity against BRD4 (pEC_{50} = 6.1) was reported *via* increased cell proliferation of a BRD4-dependent cell line, again suggesting good permeability. Consequently, **2.010** has been suggested for application as a BRD4 and TAF1/TAF1L triple probe. Insufficient TAF1 potency, a lack of selectivity (in particular over the BET family), unknown activity against pharmacologically relevant off-targets, absence of a structurally similar negative control, unknown solubility and unknown cellular activity against TAF1 limit its application as a TAF1/TAF1L probe.
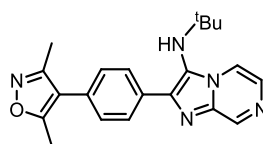
UMB-32
2.010
BRD4(1) pK_D = 7.1
TAF1(2) pK_D = 6.3

Figure 2.07: BRD4(1) and TAF1/TAF1L triple probe UMB-32. pK_D values refer to activity in the DiscoverX BROMO*scan* assay.

Exploiting the tandem nature of the bromodomains in TAF1, Frye *et al.* have reported the first examples of bivalent TAF1 inhibitors (**Figure 2.08**).[155] Starting from the bromosporine derived ligand UNC4493, three bivalent TAF1 inhibitors were developed, each containing two UNC4993 monomers connected *via* PEG linkers. The most potent bivalent inhibitor, **2.012c**, was shown to have a marginally enhanced potency (TAF1 pK_D = 7.1) compared to the monovalent inhibitor **2.011** (TAF1 pK_D = 6.5), possibly attributable to the bivalent nature of the inhibitor. The bromodomain promiscuity of bromosporine-related ligands raises doubt over the selectivity of the inhibitors, in particular over the dual bromodomain BET subfamily. Unfortunately, no selectivity data for the inhibitors is reported, nor for the monovalent inhibitor **2.011**. Additionally, no permeability or solubility data is provided, or evidence of cellular target engagement. Absence of the above data highlights the caveats to using these bivalent inhibitors in target validation, however, further characterization could provide access to target validation of both TAF1 bromodomains.

UCN4493
2.011
TAF1 pK_D = 6.5

2.012a, n = 4, TAF1 pK_D = 6.8
2.012b, n = 17, TAF1 pK_D = 6.9
2.012c, n = 29, TAF1 pK_D = 7.1
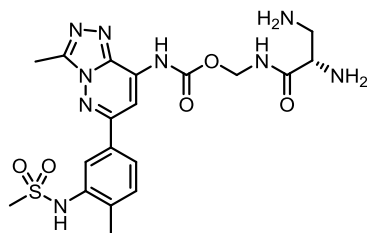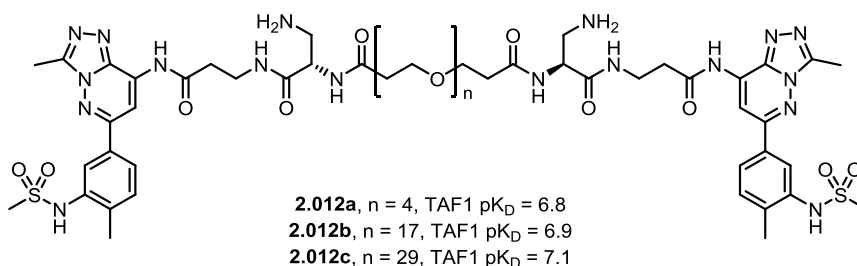
Figure 2.08: Structure of monovalent inhibitor UCN4493 and bivalent TAF1 inhibitors 2.012a-c. pK_D values refer to activity within an ITC assay.

Genentech and Constellation Pharmaceuticals have reported selective CECR2, BRD9 and TAF1(2) bromodomain inhibitors, where selectivity can be attributed to bromodomain specific interactions with the conserved water network found within the binding pocket of each bromodomain.[156] Starting from the *N*-methyl pyrrolopyridone **2.013**, Crawford *et al*. substituted the *N*-methyl group for a selection of small hydrophobic substituents. The introduction of hydrophobic substituents was shown to disrupt the water network present in bromodomains in one of two ways: direct displacement and rearrangement, as is the case for TAF1; or induction of a narrow hydrophobic channel, demonstrated by CECR2 and BRD9. As shown in **Table 2.03** large variations in selectivity were achieved for the different substituents tested.[156]
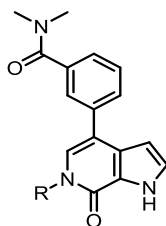
R =	Me			
	2.013	**2.014**	**2.015**	**2.016**
BRD4(1) pIC$_{50}$	7.0	5.2	6.3	5.6
BRD4(2) pIC$_{50}$	7.2	5.8	5.9	5.3
CREBBP pIC$_{50}$	6.3	<4.7	<4.7	<4.7
BRPF1 pIC$_{50}$	5.8	<4.7	<4.7	<4.7
BRD9 pIC$_{50}$	6.6	6.5	6.8	5.9
TAF1(1) pIC$_{50}$	5.4	<4.7	<4.7	5.0
TAF1(2) pIC$_{50}$	7.2	6.1	6.4	7.3
CECR2 pIC$_{50}$	6.6	6.8	5.2	5.3

Table 2.03: Variation in potency for several bromodomains upon variation of
***N*-substituent. Reproduced with permission.**[156]

Substitution of the *N*-methyl group of hit molecule **2.013** for a 1-butene group (**2.016**) dramatically reduced the potency for BRD4, BRD9, BRPF1, CREBBP and CECR2, whilst maintaining submicromolar potency for TAF1(2) (pIC$_{50}$ = 7.3) (**Figure 2.09**). Compound **2.016** was then subjected to iterative structure-based drug design efforts leading to GNE-371 (**2.017**, **Figure 2.09** and **2.10**).[157] Introduction of a morpholine group to the benzamide provided an optimal occupancy of the lipophilic-shelf region and an accompanying boost in TAF1(2) potency. Additionally, substitution off the benzamide ring was utilized to induce disfavourable protein surface interactions within BRD4(1), thus reducing BRD4(1) potency and improving BET selectivity. Compound **2.017** displayed potency for TAF1(2) *via* TR-FRET (pIC$_{50}$ = 8.0) and BROMO*scan* (pIC$_{50}$ = 9.0) assays, and selectivity over the BET family (2000-fold). Furthermore, **2.017** was screened against 37 additional bromodomains *via* the BROMO*scan* panel where ≥1000-fold selectivity was observed excluding TAF1L(2) where equipotency was observed. Similarly, **2.017** appeared selective against a 35-kinase panel (<17% inhibition observed at 1 µM). Finally, cellular target engagement was demonstrated using a NanoBRET assay where submicromolar potency (pIC$_{50}$ = 7.4) was observed.

Unfortunately, compound **2.017** isn't accompanied by a negative control but does show major progress in the development of TAF1/TAF1L chemical probes.

2.013
TAF1(2) pIC$_{50}$ = 7.2
BRD4(1) pIC$_{50}$ = 7.0
Non-BET selectivity = 4-fold

2.016
TAF1(2) pIC$_{50}$ = 7.3
BRD4(1) pIC$_{50}$ = 5.6
Non-BET selectivity = 25-fold

GNE-371
2.017
TAF1(2) pIC$_{50}$ = 8.0
BRD4(1) pIC$_{50}$ < 4.7
Non-BET selectivity >1000-fold
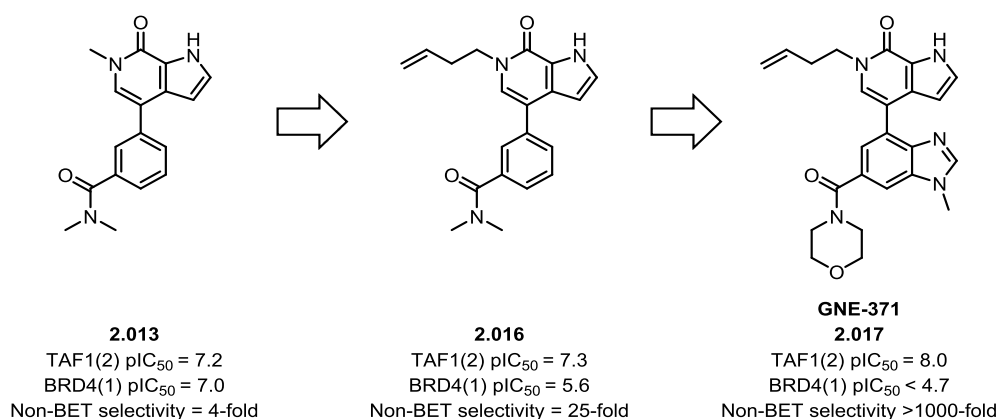
Figure 2.09: Structure of TAF1(2) chemical probe 2.017, start point 2.013 and intermediate 2.016. pIC$_{50}$ values refer to activity in a TR-FRET assay.
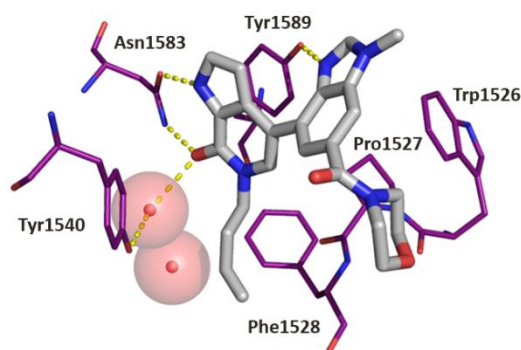
Figure 2.10: Crystal structure (PDB:6DF7) of TAF1/TAF1L inhibitor 2.017 (grey) bound to TAF1(2) (purple) highlighting the displacement of two conserved water molecules.

Finally, Remillard *et al.* have disclosed TAF1 biased bromodomain inhibitor **2.019**,[158] optimized from a polo-like kinase 1 (PLK1) inhibitor scaffold with reported TAF1 and BRD4(1) activity (**Figure 2.11**).[159,160] Potent and selective PLK1 inhibitor BI-2536 (**2.018**) was selected as a start point and was subjected to multiple SAR investigations. Removal of the hinge-binding motif, embedded in the aminopyrimidine ring, reduced activity for PLK1 whilst the butenyl KAc mimetic was employed to gain selectivity over BRD4(1). Compound **2.019** showed potency for TAF1(2) (pIC$_{50}$ 7.1)

and selectivity over BRD4(1) (120-fold) within an AlphaScreen assay. Unfortunately, no further selectivity profiling was provided for **2.019**, nor any evidence to support its ability to reach the active site. Compound **2.019** does, however, offer a new chemotype for future TAF1(2) chemical probe development.

BI-2536
2.018
TAF1(2) pIC_{50} = 6.8
BRD4(1) pIC_{50} = 6.8

2.019
TAF1(2) pIC_{50} = 7.1
BRD4(1) pIC_{50} < 5.0
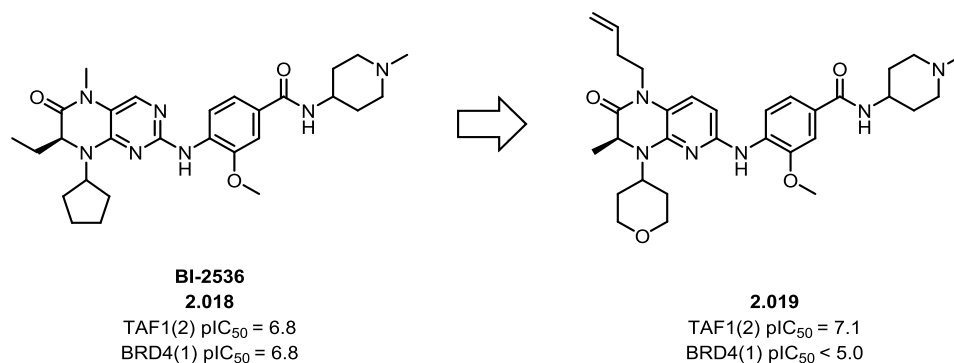
Figure 2.11: Structure of TAF1(2) inhibitor 2.019 and start point 2.018. pIC_{50} values refer to activity in an AlphaScreen assay.

Despite the growing number of TAF1/TAF1L inhibitors, there are none that fit all the requirements for an effective chemical probe (**Table 2.04**) discussed in **Section 1.4.1**. A lack of characterization, in particular regarding selectivity, and the absence of negative controls for the most promising TAF1/TAF1L inhibitors, suggests further TAF1/TAF1L inhibitor development is required to achieve adequate TAF1/TAF1L target validation.

Compound	TAF1 potency	Selective against BET bromodomains	Selective against other bromodomain families	Selective against pharmacological off-targets	Solubility	Permeability	Cellular activity <1 μM	Accompanying negative control
2.001	✗	✓	✓	✗	✗	✗	✓	✓
2.005	✓	✗	✗	✗	✗	✗	✗	✗
2.008	✓	✓	✗	✓	✗	✗	✓	✓
2.010	✗	✗	✗	✗	✗	✗	✓	✗
2.017	✓	✓	✓	✓	✓	✓	✓	✗
2.019	✓	✓	✗	✗	✗	✗	✗	✗

Table 2.04: Summary of the current TAF1 inhibitors and whether they fulfill the requirements of a chemical probe discussed in Section 1.4.1. (Tick signifies passing the requirement, cross signifies failure or the information not being disclosed).

2.3 Aims

To help elucidate the biological function of TAF1/TAF1L in modulating healthy/disease states, the aim was to design a novel and effective chemical probe that fulfilled the criteria outlined in **Section 1.5** and reproduced below:

1. $pIC_{50} \geq 7$ against TAF1(2), as determined by a biochemical assay.
2. ≥100-fold selectivity over the BET bromodomain family (using BRD4(1) as a representative example) for which a strong biological phenotype is known.
3. ≥30-fold selectivity over other non-BET bromodomain families. (Due to the highly homologous nature of the TAF1 and TAF1L acetylated Lys binding sites, selectivity over TAF1L was neither expected nor targeted).
4. ≥30-fold selectivity over other pharmacologically relevant off-targets.
5. Suitable solubility and permeability to ensure exposure at target site.
6. Cellular activity at <1 µM concentrations.
7. Be the product of iterative SAR exploration.
8. Be accompanied by a structurally related negative control.
9. Expand the structural diversity of TAF1/TAF1L chemical probes.

Ideally, selective probes (and structurally similar negative control compounds) would be identified for TAF1(1), TAF1(2) and pan-TAF1. However, priority was placed on designing a TAF1(2) chemical probe for which a TR-FRET assay was already available. Currently there is no TAF1(1) assay available within GSK, nor is there one available at DiscoverX. Consequently, TAF1(1) potency was not measured and it was assumed that compounds displayed no selectivity between TAF1(1) and TAF1(2).

2.4 Identifying Compound 2.021 as a Start Point

The development of a novel chemical probe for TAF1 began from compound **2.021**, developed by Natalie Theodoulou as part of her PhD studies (**Figure 2.12**).[161] Compound **2.021** was developed from compound **2.020**, an initial hit from a systematic cross-screening strategy. The previous work in the development of **2.021** from initial hit compound **2.020** is summarized below.

In total, 946 compounds (with a known or hypothetical acetylated Lys binding mimetic) were screened against TAF1(2) using a TR-FRET assay, resulting in the selection of naphthyridinone **2.020** for further profiling.

Compound **2.020** was originally designed and synthesized with the intention of functioning as an ATAD2 chemical probe, and shares the same naphthyridinone chemotype as published ATAD2 inhibitors (see **Section 1.4.2.2** for further details).[116,162] Despite this, compound **2.020** displayed nanomolar potency for TAF1(2) (pIC_{50} = 8.1), good selectivity over ATAD2 (80-fold) and BRD4(1) (80-fold), and presented a new chemotype for TAF1(2) chemical probe development (**Figure 2.12**).
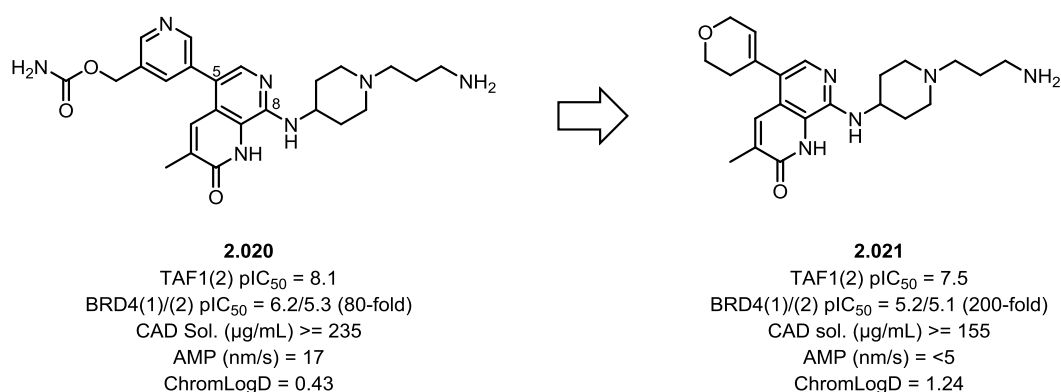

2.020
TAF1(2) pIC_{50} = 8.1
BRD4(1)/(2) pIC_{50} = 6.2/5.3 (80-fold)
CAD Sol. (µg/mL) >= 235
AMP (nm/s) = 17
ChromLogD = 0.43

2.021
TAF1(2) pIC_{50} = 7.5
BRD4(1)/(2) pIC_{50} = 5.2/5.1 (200-fold)
CAD sol. (µg/mL) >= 155
AMP (nm/s) = <5
ChromLogD = 1.24

Figure 2.12: Hit molecule 2.020 and lead compound 2.021. CAD solubility, AMP and ChromLogD measurements were all performed at pH$_{7.4}$.

In silico docking of **2.020** into TAF1(2) (**Figure 2.13a**) was utilized to quickly identify the pyridinone moiety (**Figure 2.13b** circled in red) as the acetylated Lys mimetic, with the carbonyl group forming a direct hydrogen bond to Asn1583 and a water-mediated interaction with Tyr1540. Additional hydrogen bond interactions between the pyridinone NH and the amine NH (**Figure 2.13b** circled in blue) to the carbonyl group of Asn1583 were also identified, completing a tridentate interaction to the conserved Asn. As such these groups were maintained and left unchanged. The remaining areas of compound **2.020** were then individually analyzed for potential SAR investigations. The key findings from these SAR investigations will now be discussed in turn.
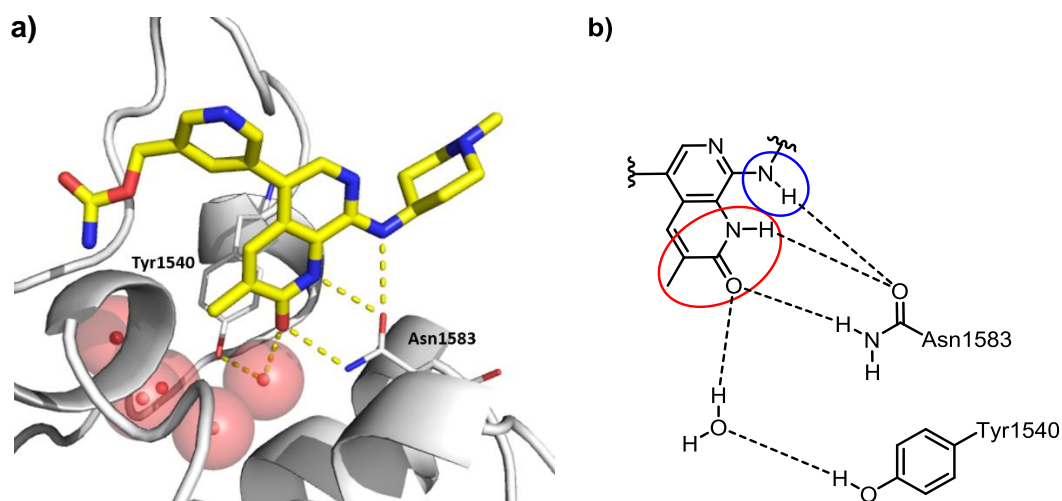
a)

b)

Figure 2.13: a) *In silico* **docking of 2.020 into TAF1(2) highlighting the key interactions to Asn1583 and Tyr1540; and b) schematic of the key interactions between the naphthyridinone scaffold and Asn1583 and Tyr1540 during TAF1(2) binding. Docking performed by Dr. Paul Bamborough.**

2.4.1 SAR at the 5-Position

Although at times throughout optimization the 5-position was considered as a vector for improving selectivity and potency, SAR investigations were primarily focused around improving the physicochemical properties of **2.020**. The two main breakthroughs in this regard are discussed below, although alternative pyridyl substitution patterns, all carbon analogues, bicyclic rings and 5-membered heterocycles were also investigated in this position.

SAR was initially focused around reducing the polarity of compound **2.020** *via* removal of the carbamate group, which was thought to be contributing to the poor permeability (17 nm/s) and low ChromLogD (0.43) (**Table 2.05**). Truncation of the carbamate group to give hydroxy compound **2.022** was accompanied by an equal reduction in potency at both TAF1(2) and BRD4(1) with marginal effect on permeability and ChromLogD. Substitution of the carbamate group for a methyl group (**2.023**), however, showed only a minor further reduction in potency for both TAF1(2) and BRD4(1) resulting in an overall increase in LE, whilst maintaining selectivity over the BET subfamily (60-fold). Although permeability remained low, the desired reduction in polarity was reflected in an increased ChromLogD. In an attempt to reduce the planarity of the compound and therefore improve solubility, saturated and partially saturated ring systems were

investigated as alternatives for the pyridyl unit. Completely saturated ring systems (cyclohexane **2.024** and tetrahydropyran **2.025**) showed a general decrease in TAF1(2) potency with more negligible effect on BRD4(1). A reintroduction of unsaturation at the 5-position linker in the form of compound **2.021** did, however, maintain high potency for TAF1(2) and showed an improvement in selectivity and solubility as desired.
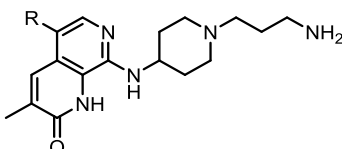
Entry	Compound	R =	TAF1(2) pIC$_{50}$ (LE)	BRD4(1) pIC$_{50}$	CAD Solubility (μg/mL)	AMP (nm/s)	ChromLogD
1	**2.020**		8.1 (0.33)	6.2 (×79)	>=235	17	0.43
2	**2.022**		7.5 (0.33)	5.6 (×79)	56	8	0.23
3	**2.023**		7.3 (0.33)	5.6 (×50)	>=95	11	1.24
4	**2.024**		6.2 (0.29)	4.9 (×20)	27	<10	3.12
5	**2.025**		6.4 (0.30)	4.8 (×40)	102	<10	0.82
6	**2.026**		6.3 (0.30)	5.4 (×8)	41*	<10	3.23
7	**2.021**		7.5 (0.35)	5.2 (×200)	>=155	<5	1.24

Table 2.05: 5-Position SAR table. Selectivity for TAF1(2) against the given protein is shown in brackets underneath potency values. *CLND solubility. Solubility, AMP and ChromLogD measurements were all performed at pH$_{7.4}$.

2.4.2 SAR at the 8-Position

The propylamine group at the 8-position was initially thought to be pointing out into solvent, as predicted by computational modeling. X-ray crystallography of **2.022**, however, revealed a key salt bridge interaction between the propylamine nitrogen and an Asp residue (Asp1539). This interaction was identified as crucial for TAF1(2) potency and selectivity over the BET bromodomains and was therefore maintained (**Figure 2.14**).
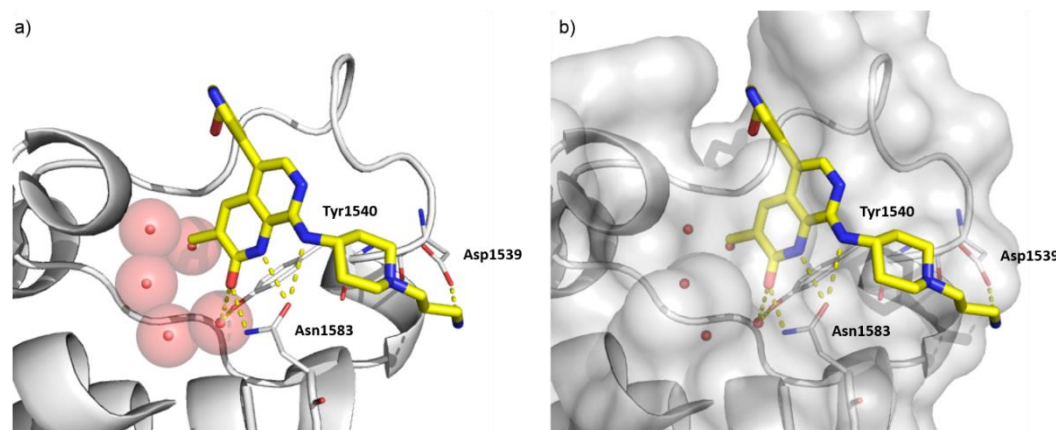

Figure 2.14: a) GSK internal X-ray crystal structure of 2.022 bound to TAF1(2) highlighting the key interactions with Asn1583, Tyr1540 and Asp1539; and b) GSK internal X-ray crystal structure of 2.022 bound to TAF1(2) highlighting the surface of the binding pocket.

Compound **2.021** possessed a range of promising properties for use as a TAF1/TAF1L chemical probe. These included good potency for TAF1(2) ($pIC_{50} = 7.5$), good selectivity against the BET bromodomains (200-fold) and good solubility (>=155 µg/mL). As a result, compound **2.021** was selected as a suitable start point for the development of a TAF1/TAF1L chemical probe.

Although selective over the BET subfamily of bromodomains, **2.021**'s selectivity against other non-BET bromodomains was unknown, and, in the absence of a structurally related negative control, would make phenotypic responses difficult to assign. To confirm the previous results, and further investigate the non-BET bromodomain selectivity, compound **2.021** was first resynthesized.

2.5 Resynthesis of Lead Compound 2.021

Resynthesis of lead compound **2.021** began from naphthyridinone **2.027**, an in house intermediate, which in turn could be synthesized in five steps from commercially available aminopyridine **2.028** (**Scheme 2.01**).[162]
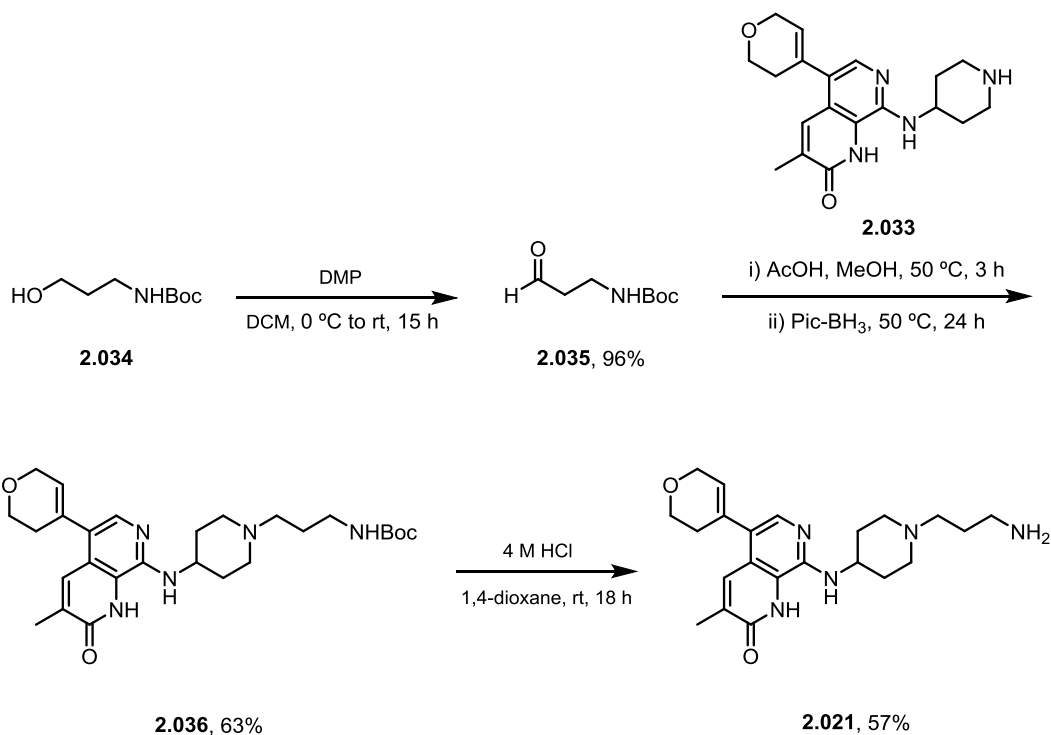

2.021

2.027
35 g in house at GSK
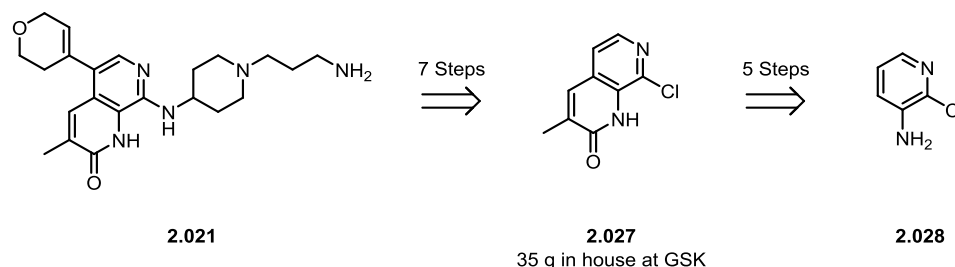
2.028

Scheme 2.01: Retrosynthetic analysis of lead compound 2.021 from in house naphthyridinone 2.027 and commercially available aminopyridine 2.028.

To prevent a poor yield for the subsequent Buchwald-Hartwig coupling, naphthyridinone **2.027** was first benzylated using benzyl bromide and potassium carbonate at room temperature, producing *O*-benzyl ether **2.029** in 84% yield (**Scheme 2.02**). Improved yields had previously been reported using this protecting group strategy with speculation that in the absence of this benzyl group the Pd catalyst coordinates to the pyridinone moiety, preventing oxidative addition and initiation of the catalytic cycle.[162] Once benzylated, compound **2.029** underwent a Buchwald-Hartwig amination using $Pd_2(dba)_3$ and BrettPhos catalyst system, introducing the protected piperidine ring in 72% yield. The electron-rich amino-piperidine group then directed an electrophilic bromination using NBS to the 5-position, producing **2.031** in 99% yield. A Suzuki coupling was then performed using the complementary boronic acid, $Pd(OAc)_2$, cataCXium A, potassium carbonate, and heating at 100 ºC for 1-1.5 hours. As expected, this introduced the dihydropyran (DHP) ring at the 5-position in good yield (86%). Finally, a global deprotection of the benzyl and Boc protecting groups was performed by heating **2.032** in refluxing TFA, delivering intermediate **2.033** in 95% yield.
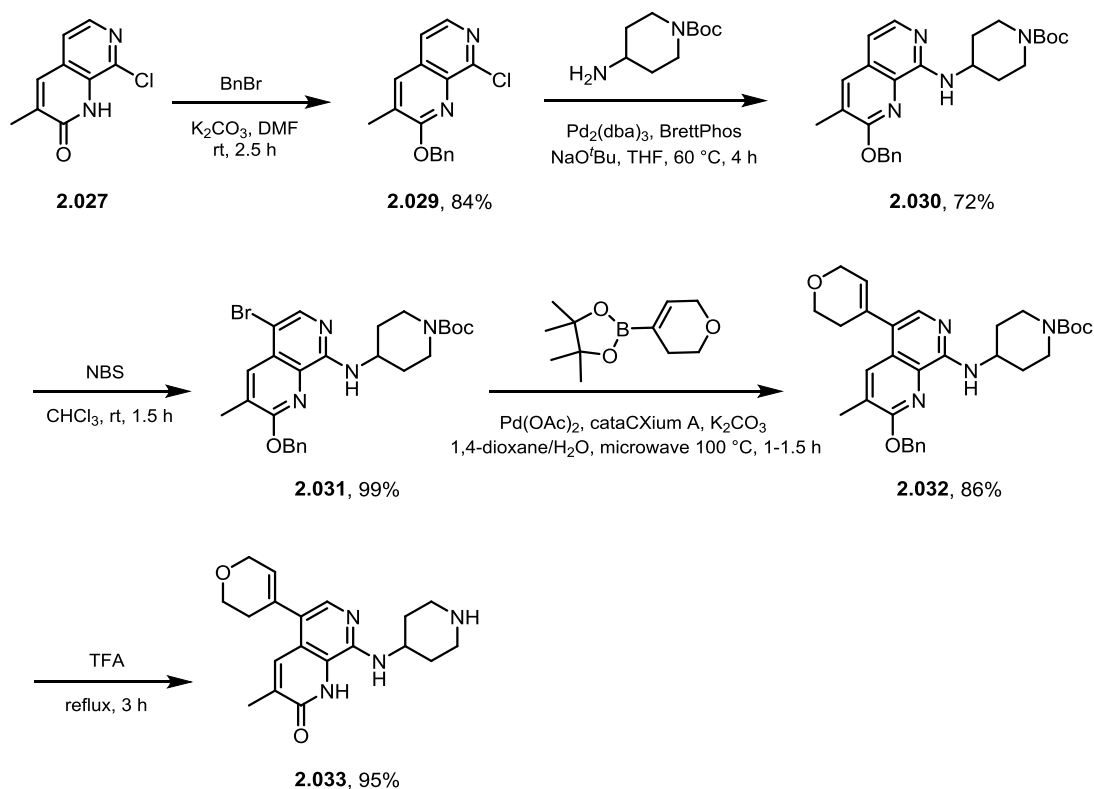
Scheme 2.02: Reaction scheme to synthesize common intermediate 2.033 from available starting material 2.027.

To append the desired propylamine chain, the commercially available 3-(Boc-amino)-1-propanol (**2.034**) was first oxidized using Dess-Martin periodinane to yield the corresponding aldehyde (**2.035**) in 96% yield (**Scheme 2.03**). After premixing **2.035** and **2.033** at 50 °C in the presence of acetic acid and methanol to preform the iminium ion, reductive amination was performed at 50 °C using picoline borane, yielding the protected lead compound **2.036** in 63% yield. Finally, **2.036** was deprotected using 4 M HCl in 1,4-dioxane solution to give **2.021** in 57% yield.

Scheme 2.03: Reaction scheme to synthesize lead compound 2.021 from commercially available 2.034.

Once resynthesized, **2.021**'s physicochemical properties were reanalyzed, confirming the original findings of good kinetic solubility (>=155 µg/mL) and poor permeability (<5 nm/s). **2.021**'s potency and selectivity for TAF1/TAF1L was then investigated using two assays. Firstly, **2.021** was screened at 10 µM against the DiscoverX BROMO*scan* panel of 32 bromodomains, providing insight into broader bromodomain selectivity and identifying any major bromodomain off-targets (**Figure 2.15**). At 10 µM **2.021** showed activity against a wide range of bromodomains with BRD2(1), ATAD2B, BAZ2B, BRD9 and CECR2 showing ≥99% inhibition at 10 µM (**Table 2.06**).
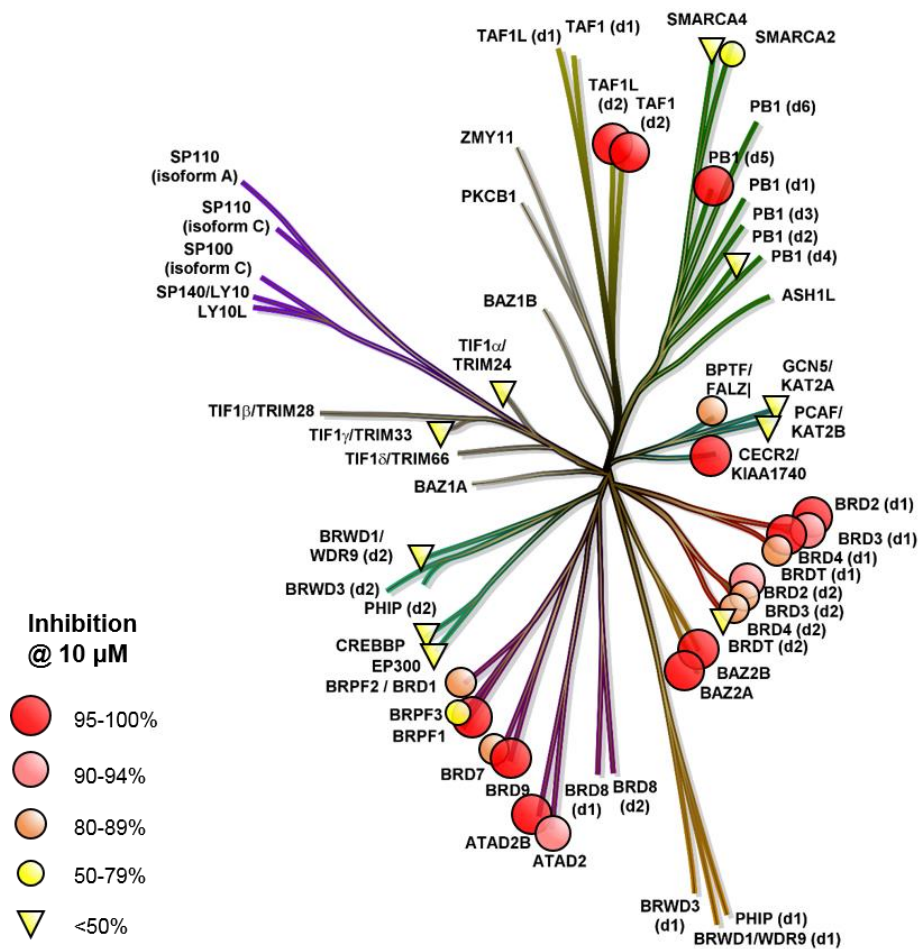
Figure 2.15: Phylogenetic tree inhibition plot generated for 2.021's 10 µM single-shot DiscoverX BROMO*scan* data (data shown in Table 2.06).

Compound Number	ATAD2A	ATAD2B	BAZ2A	BAZ2B	BRD1	BRD2(1)	BRD2(2)	BRD3(1)	BRD3(2)	BRD4(1)	BRD4(2)	BRD7	BRD9	BRDT(1)	BRDT(2)	BRPF1
2.021	94	99	97	100	88	99	92	93	85	97	88	88	100	82	49	96

Compound Number	BRPF3	CECR2	CREBBP	EP300	FALZ	GCN5L2	PB1(2)	PB1(5)	PCAF	SMARCA2	SMARCA4	TAF1(2)	TAF1L(2)	TRIM24	TRIM33	WDR9(2)
2.021	57	99	49	48	89	9	22	98	13	55	40	99	96	21	0	24

Table 2.06: Percentage inhibition of bromodomains tested at 10 µM (DiscoverX BROMO*scan* assay) for compound 2.021.

Consequently, potency against TAF1(2), a representative BET bromodomain (BRD4(1)), ATAD2B, BAZ2B, BRD9 and CECR2 was characterized further across a number of different concentrations using a quantitative polymerase chain reaction (qPCR) assay, providing access to 11-point dose response curves, from which accurate pK_Ds were calculated (**Table 2.07**). Pleasingly, **2.021** demonstrated sub-nanomolar potency for TAF1(2) ($pK_D = 9.4$) and selectivity over the bromodomains tested (>5000-fold over BRD4(1) and >100-fold over other bromodomains) (**Figure 2.16**). The large difference in observed TAF1(2) potency between the internal TR-FRET and BROMO*scan* assays may be due to the use of a different detection system, alternate protein constructs or the sample preparation methods.

Compound Number	Bromodomain pK_D						
	TAF1(2)	BRD4(1)	ATAD2B	BAZ2B	BRD9	CECR2	CREBBP
2.021	9.4	5.7	6.4	7.2	6.4	6.0	5.3

Table 2.07: pK_D values for compound 2.021 against a selection of bromodomains, calculated from 11-point dose response curves as measured by DiscoverX qPCR assays.
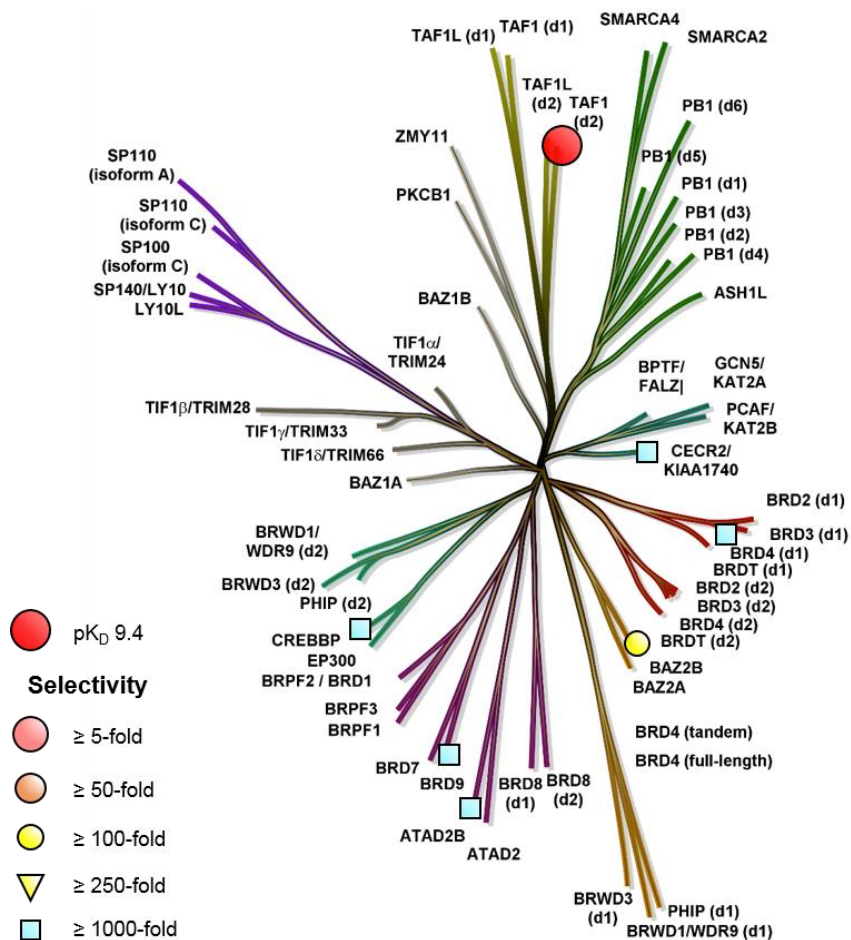
Figure 2.16: Phylogenetic tree inhibition plot generated for 2.021's full curve data. Selectivity determined from the difference between TAF1(2) and the relative bromodomain pK_D values.

Such a dramatic improvement in selectivity when moving from the 10 µM BROMO*scan* assay to the 11-point dose response curves, highlights the danger of over interpreting selectivity data at high concentrations and provides evidence for the possibility of selective compounds appearing promiscuous at 10 µM. Three example dose response curves are shown in **Figure 2.17**, demonstrating how three compounds can appear equipotent at a single concentration, but possess very different potencies.
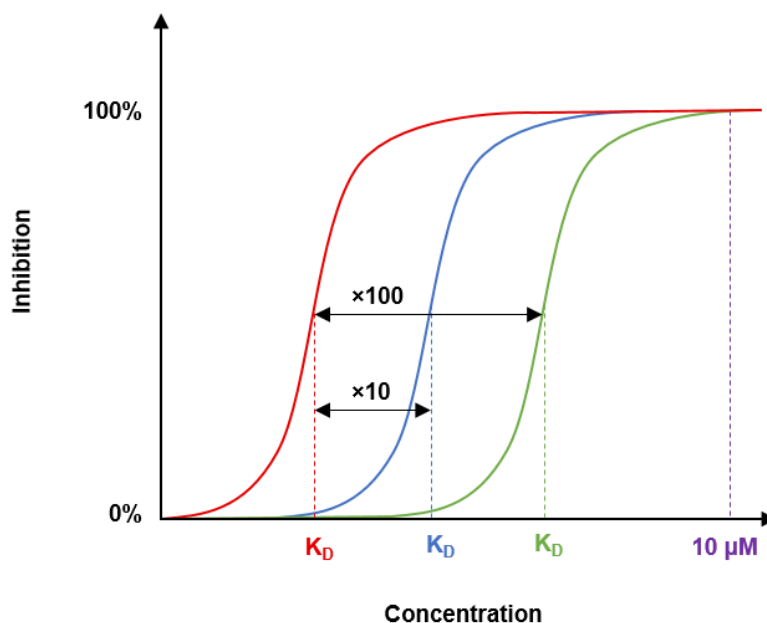
Figure 2.17: Three example dose response curves demonstrating the possibility for three different K$_D$s (and therefore selectivity) despite showing equipotency at a single concentration (10 µM).

Due to the importance of selectivity in the applicability of chemical probes, broader bromodomain selectivity was investigated throughout this project. As discussed above, 10 µM single-shot screening was first used to identify any potential bromodomain off-target activity and follow up 11-point dose response curves used to quantify TAF1(2) potency, BRD4(1) potency, and for the most promising compounds, any bromodomain off-targets displaying ≥95% inhibition at 10 µM.

Despite having demonstrated TAF1(2) potency, broad bromodomain selectivity and kinetic aqueous solubility, **2.021**'s poor permeability (AMP <5 nm/s) and unknown cellular activity raised doubts over its ability to reach the site of action, one of the requirements outlined for a chemical probe (**Section 1.4.1**).

2.6 Improving the Permeability of Compound 2.021

To address these caveats, attention was shifted to improving the permeability of **2.021** whilst maintaining potency and selectivity for TAF1(2). At the outset of this work, a TAF1 cellular target engagement assay was unavailable, so focus was placed on permeability as the appropriate property to modulate as a surrogate for predicted cellular activity. The permeability was monitored using an AMP assay, where passive diffusion through a lipid infused artificial membrane, separating a donor and receiver well, is measured.

2.6.1 Design Hypothesis 1: Reduced Hydrogen Bond Donors

It is well reported that there is a correlation between poor permeability and a large number of hydrogen bond donors (HBDs).[163] Consequently, it was initially hypothesized that an increase in permeability could be obtained by reducing the number of HBDs present in **2.021**. Compounds **2.037** and **2.038** were designed to test this hypothesis (**Table 2.08**). Additionally, it was hypothesized that alkylation of the propylamine nitrogen could probe the observed interaction to Asp1539 (found on the surface of TAF1(2)) (**Section 2.4.2**, **Figure 2.14**) and the potential of the propylamine nitrogen as a handle for bifunctional TAF1/TAF1L chemical tools.
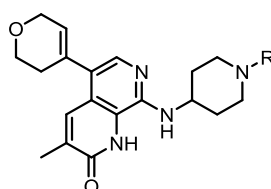

Entry	Compound	R =	HBDs
1	**2.021**		4
2	**2.037**		3
3	**2.038**		2

Table 2.08: Alkylated target compounds 2.037 and 2.038, highlighting the reduction in number of HBDs.

2.6.1.1 Alkylated Compounds: Synthesis

Due to the multiple nucleophilic nitrogens present in **2.021**, it was hypothesized that a chemoselective alkylation would not be possible. As such, it was decided to introduce the propylamine chain prealkylated *via* the corresponding amide, which in turn could be reduced to the desired amines *via* a borane reduction (**Scheme 2.04**). Similarly, due to concerns over the stability of the double bond present in the DHP group to the amide reduction conditions, it was decided to introduce the DHP group after amide reduction. Compound **2.041** was therefore identified as a common intermediate from which both target molecules could be synthesized *via* late stage derivatization.

2.037, R = H
2.038, R = Me

2.039, R = Boc
2.040, R = Me
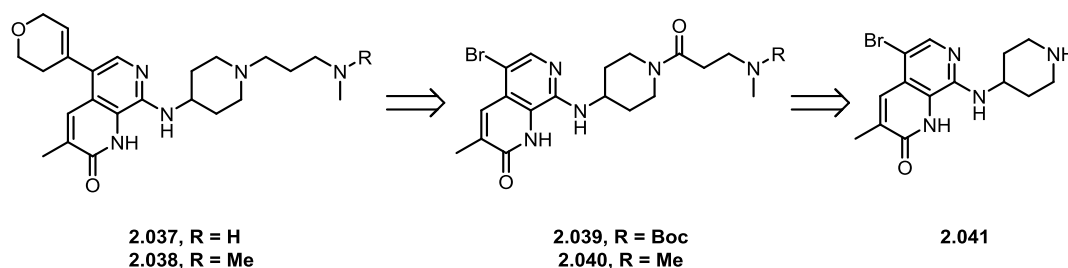
2.041

Scheme 2.04: Retrosynthetic analysis of target compounds 2.037 and 2.038 from intermediate 2.041.

Intermediate **2.041** (**Scheme 2.05**) was synthesized in 95% yield *via* a global deprotection of intermediate **2.031** under refluxing TFA conditions.

2.031

TFA
reflux, 18 h

2.041, 95%
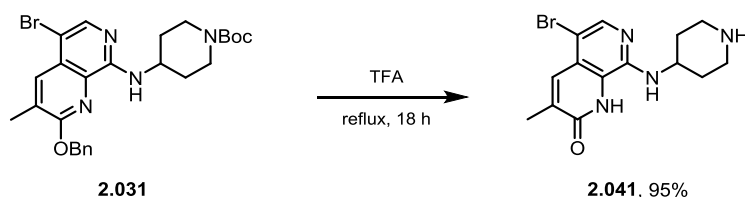
**Scheme 2.05: Reaction scheme to synthesize intermediate 2.041 from 2.031.**

Once intermediate **2.041** was obtained, a HATU promoted amide coupling with *N*-Boc-*N*-methyl-β-alanine delivered **2.039** in 71% yield (**Scheme 2.06**). Compound

2.039 was then reduced to the corresponding amine using 1 M BH$_3$·THF complex at room temperature. To avoid Boc deprotection the resulting boron adducts were cleaved in a neutral methanol solution over 96 hours, yielding desired amine **2.042** in 66% yield. A subsequent Suzuki cross-coupling delivered **2.043** in 61% yield. Finally, Boc deprotection using 4 M HCl in 1,4-dioxane solution provided target compound **2.037** in 64% yield.
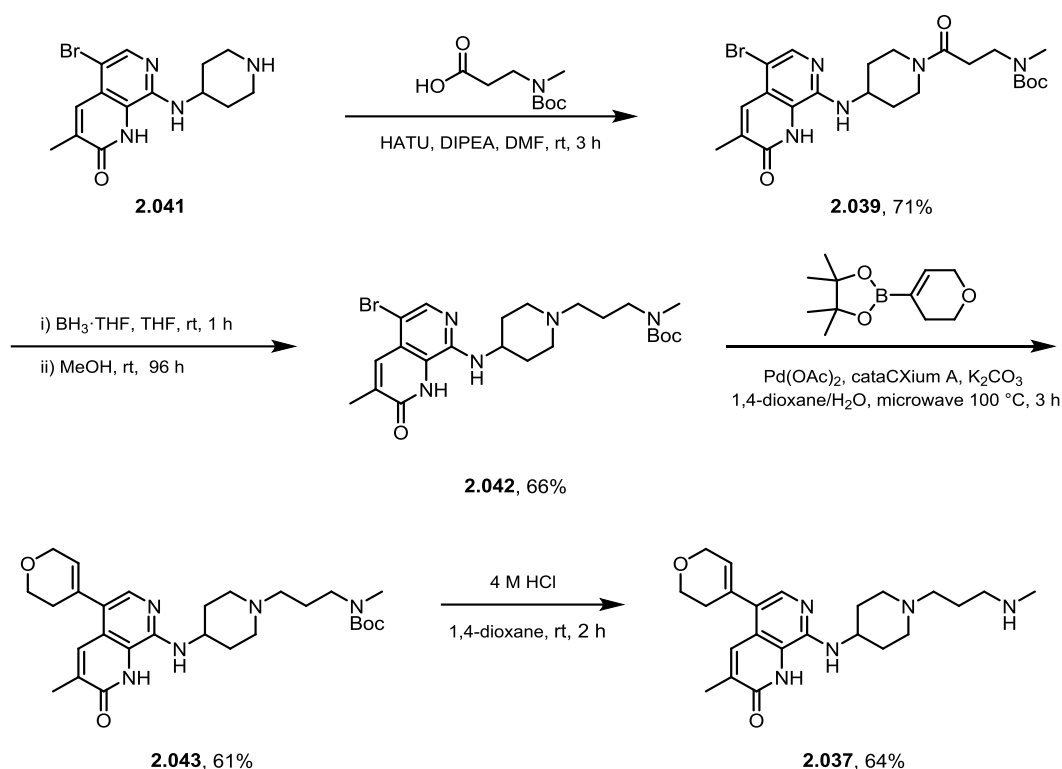
Scheme 2.06: Synthesis of monomethylated compound 2.037.

Synthesis of **2.038** was then attempted *via* a similar synthetic route. A HATU-promoted amide coupling between intermediate **2.041** and *N,N*-dimethyl-β-alanine delivered the desired amide **2.040** in 28% yield (**Scheme 2.07**). The amide reduction was then attempted using 1 M BH$_3$·THF but showed no conversion to the desired product *via* LCMS. Increased temperatures and alternative reducing agents, including solutions of LiAlH$_4$ and Red-Al, were also trialed but similarly showed no conversion to the desired product.
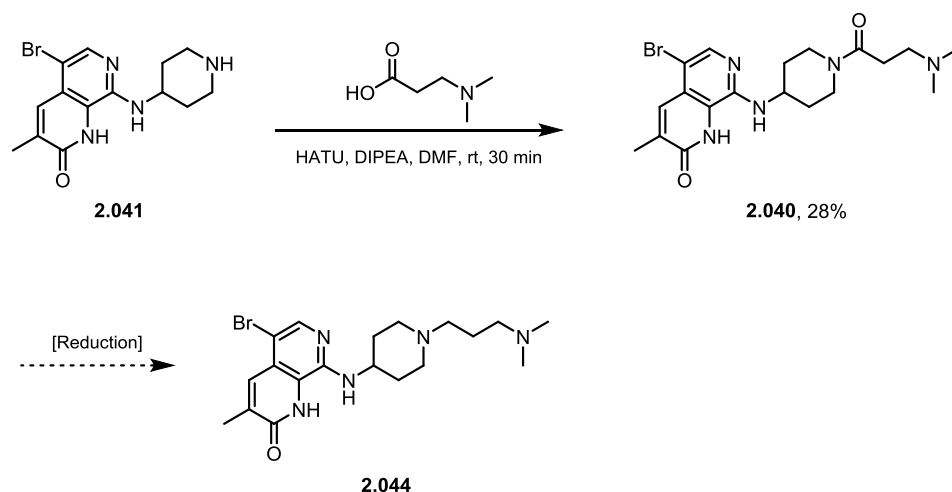
Scheme 2.07: Failed synthesis of dimethylated compound 2.038 *via* the amide reduction pathway.

To overcome this issue, a new route was designed to introduce the dimethylpropylamine chain *via* an aza-Michael addition, utilizing dolomite (a naturally occurring mineral) as a recyclable heterogeneous basic catalyst.[164] The aza-Michael addition between **2.041** and dimethylacrylamide yielded the desired amide (**2.045**) in 91% yield (**Scheme 2.08**). Compound **2.045** was then reduced to the corresponding amine **2.046** in 22% yield utilizing 1 M BH$_3$·THF complex solution. A subsequent Suzuki cross-coupling under standard conditions delivered dimethylated target compound **2.038** in 30% yield.
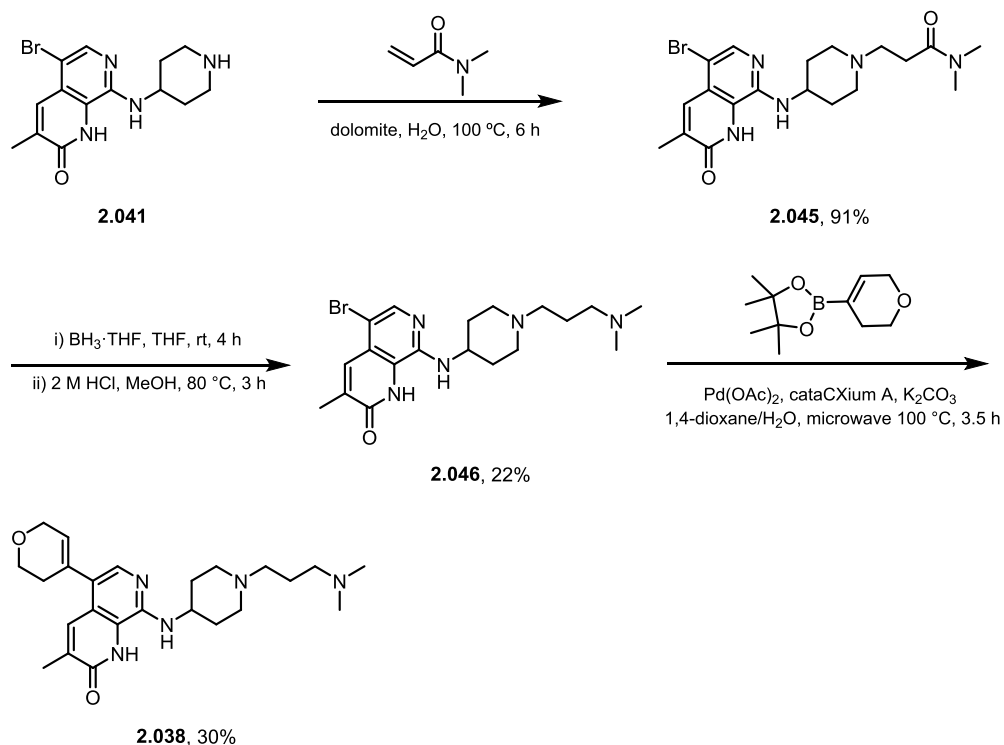
Scheme 2.08: Synthesis of dimethylated compound 2.038.

2.6.1.2 Alkylated Compounds: Results and Discussion

Once synthesized, **2.037** and **2.038** were screened *via* DiscoverX against TAF1(2) and BRD4(1) and their physicochemical properties measured (**Table 2.09**). Unfortunately, mono- and dimethylation of the propylamine nitrogen showed no improvement in AMP although an increase in solubility and ChromLogD was observed for both compounds. TAF1(2) potency was maintained for monomethylated compound **2.037** and only a slight reduction in TAF1(2) potency was observed for dimethylated compound **2.038**. As a result, this design hypothesis was abandoned, and attempts were made to further understand how the permeability of the series could be improved.

Entry	Compound	R =	TAF1(2) pK$_D$	BRD4(1) pK$_D$	AMP (nm/s)	CAD Solubility (µg/mL)	ChromLogD
1	**2.021**		9.4	5.7 (×5000)	<5	>=155	1.24
2	**2.037**		9.7	6.1 (×4000)	<6.5	>=216	1.37
3	**2.038**		8.9	5.7 (×1600)	<10	>=160	1.50

Table 2.09: Physicochemical properties and potency profile for compounds 2.021, 2.037 and 2.038. Selectivity for TAF1(2) against the given protein is shown in brackets underneath potency values. CAD solubility, AMP and ChromLogD measurements were all performed at pH$_{7.4}$.

2.6.2 Regression Modelling

An *in silico* predictive permeability model was first investigated in an attempt to help guide the design of target compounds with improved permeability. A sample of 571 naphthyridinone core-containing compounds (investigated during GSK's ATAD2 chemical probe work),[116,117,162] for which known AMP values were available, were tested using the predictive permeability models available to GSK. Unfortunately, a poor correlation between predicted permeability and measured AMP was observed (the most promising shown in **Figure 2.18**), suggesting predictive permeability models were not suitable for the series.
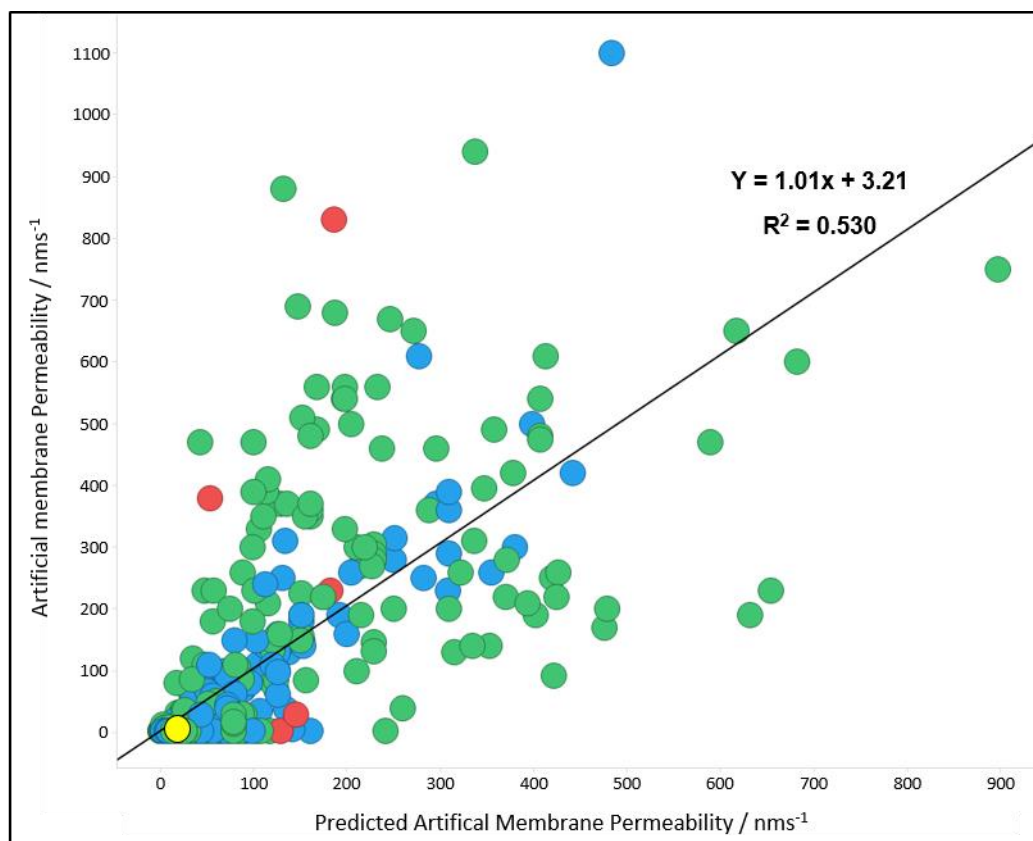
Figure 2.18: Plot of predicted AMP vs measured AMP, highlighting 2.021 in yellow. Coloured by number of aromatic ring (blue = 2, green = 3, red = 4).

In the absence of a predictive permeability model, attention was instead turned to statistical analysis. A regression model analysis was performed, using TIBCO Spotfire software, on the aforementioned internal library of 571 naphthyridinone core containing compounds for which AMP data was available. From this analysis it was possible to estimate the relationships between permeability and a selection of variables, as well as the relative importance of each variable on permeability. As shown in **Figure 2.19**, hydrogen bond acceptors (HBA), the pK_a/pK_aH of the most basic subunit (pka_mb) and number of aromatic rings (aring) showed the largest importance in affecting permeability and were therefore considered for initial investigations. It should be noted that the model only detected oxygen atoms as HBAs, and although not an accurate representation of the number of HBA, was still a valid variable to explore.
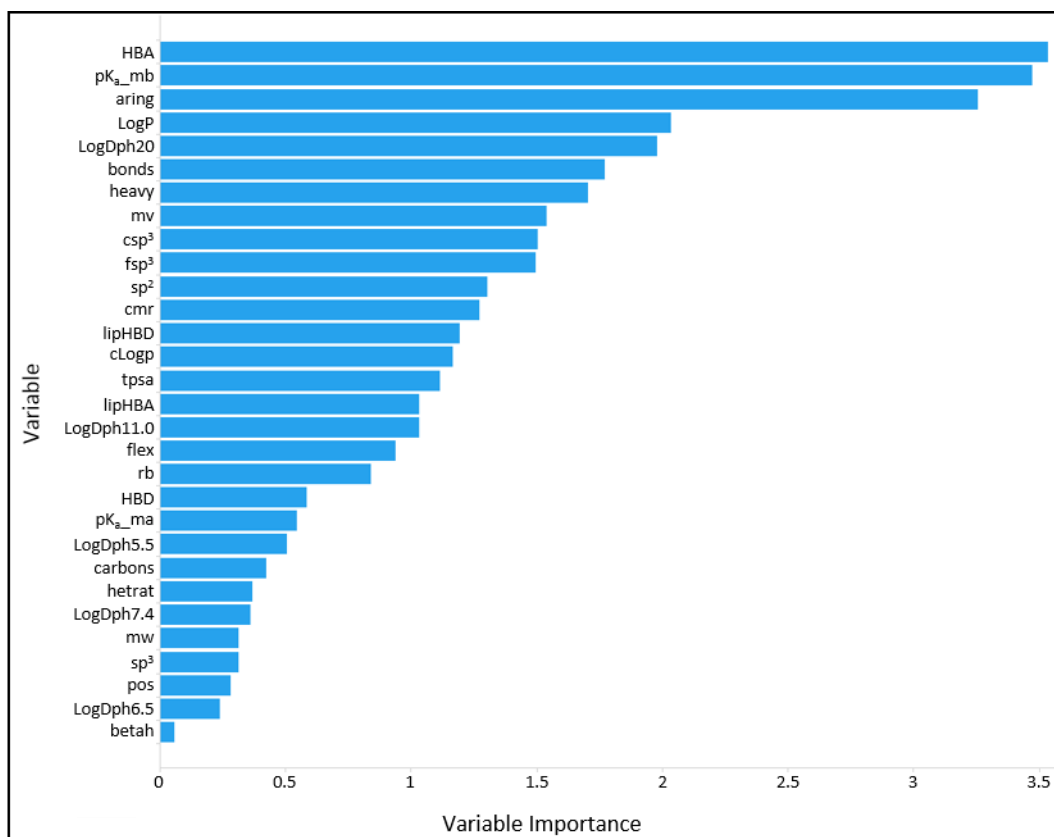
Figure 2.19: Plot of variable vs variable importance. See Appendix Table 5.01 for key.

Further analysis of each variable identified a clear drop in permeability for compounds containing >5 oxygen atoms (**Figure 2.20**), and a correlation between basicity and low permeability (**Figure 2.21**). From here constraints were applied to the variables (oxygen atoms <5, a reduced pK_a/pK_aH) to provide an outline as to what was required to achieve good permeability when designing future compounds. The number of aromatic rings was disregarded due to no clear correlation (**Figure 2.22**).

Figure 2.20: Plot of AMP vs number of oxygen atoms, highlighting lead compound 2.021 in yellow.
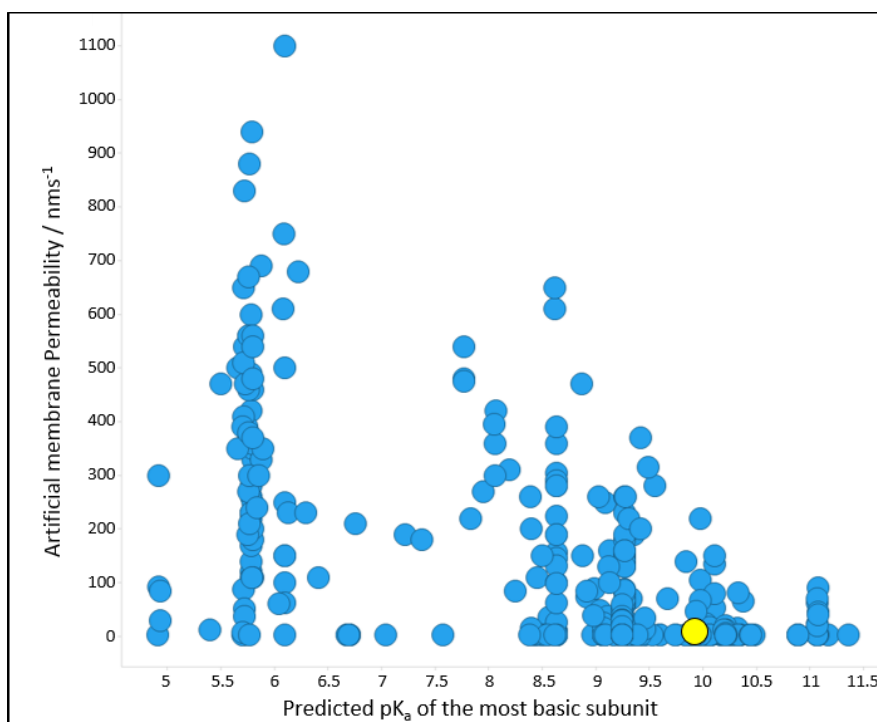
Figure 2.21: Plot of AMP vs predicted pK_a_mb highlighting lead compound 2.021 in yellow. Predicted pKa_mb calculated using ChemAxon software.[165]

Figure 2.22: Plot of AMP vs number of aromatic rings highlighting lead compound 2.021 in yellow.

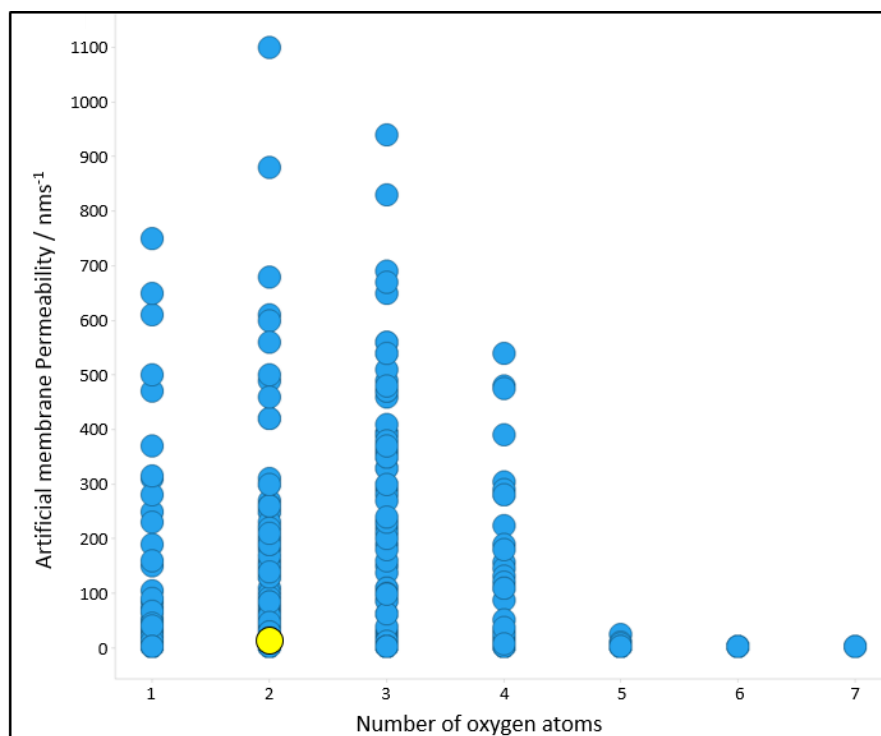As compound **2.021** only contained two oxygen atoms, and therefore fulfilled the constraint of <5, emphasis was placed on reducing the pK_a of the most basic subunits of **2.021**.

2.6.3 Design Hypothesis 2: Reducing Basicity

The pK_a of a molecule has a strong influence on the molecule's permeability, solubility, lipophilicity and protein binding,[166] which in turn modulates pharmacokinetic properties such as absorption, distribution, metabolism and excretion.[167] Consequently, pK_a lowering strategies have been utilized in the literature several times and thus posed as an attractive design hypothesis.[168,169] An example is discussed below and shown in **Figure 2.23**.

β-Site amyloid precursor protein cleaving enzyme 1 (BACE1) inhibitor **2.047** was developed for the potential treatment of Alzheimer's disease.[170,171] However, poor permeability (P_{app} = 13 nm/s) and a high efflux ratio (ER) (ER = 24) in an MDR1-

MDCK cell line, resulted in poor exposure in the brain (C_b = 0.04 µM after 4 hours) of APP51/16 mice following 60 µmol/kg oral dosing. Consequently, a pK_a lowering strategy was utilized to reduce the basicity of the ethanolamine moiety of **2.047** (pK_a ~ 8.5), to which a high ER and poor permeability were attributed. Introduction of a spirocyclopropane moiety at the benzylic carbon adjacent to the ethanolamine group yielded **2.048**, a compound with reduced pK_a (7.3), improved passive permeability (P_{app} = 40 nm/s) and a reduced ER value (3.5), demonstrated by an increased concentration in the brain (C_b = 0.32 µM after 4 hours).

2.047
pK_a ~ 8.5
P_{app} = 13 nm/s
ER = 24
C_b = 0.04 µM

2.048
pK_a = 7.3
P_{app} = 40 nm/s
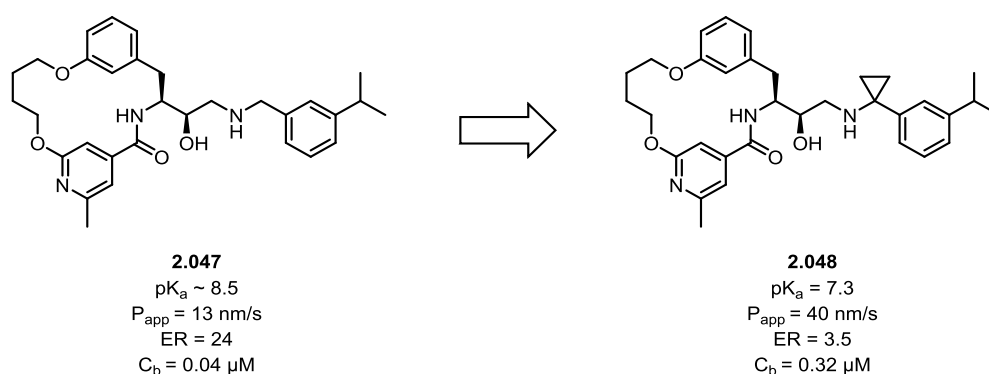ER = 3.5
C_b = 0.32 µM

Figure 2.23: BACE1 inhibitors 2.047 and 2.048, highlighting the use of a pK_a lowering strategy to improve permeability.

The piperidine and propylamine nitrogens were identified as the most basic regions of **2.021** and thus were targeted to reduce the pK_a through the introduction of electron-withdrawing groups. Amide compounds **2.049** and **2.050** (**Table 2.10**) were targeted first to investigate how the complete removal of basicity from each nitrogen would affect permeability and protein binding.
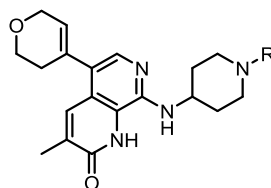
Entry	Compound	R =	Predicted pK$_a$ (most basic)
1	**2.021**		9.91
2	**2.049**		9.12
3	**2.050**		8.81

Table 2.10: Lead compound 2.021 and target compounds 2.049 and 2.050, highlighting the predicted reduced basicities. Predicted pK$_a$ values were calculated using ChemAxon software.[165]
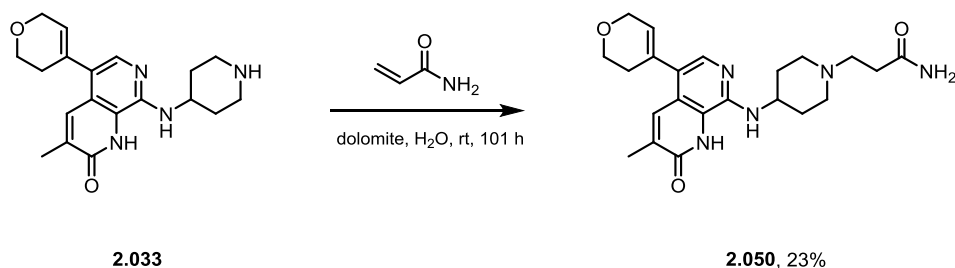
2.6.3.1 Amide Compounds 2.049 and 2.050: Synthesis

Tertiary amide compound **2.049** was synthesized first, starting with a HATU promoted amide coupling with commercially available *N*-Boc-β-alanine and key intermediate **2.033** (**Scheme 2.09**). **2.051** was worked up before undergoing Boc deprotection under standard conditions. Purification *via* MDAP delivered target compound **2.049** in 18% yield over the two steps.

2.033

HATU, DIPEA, DMF, rt, 6.5 h

2.051

4 M HCl

1,4-dioxane, rt, 2 h

2.049, 18% (over two steps)
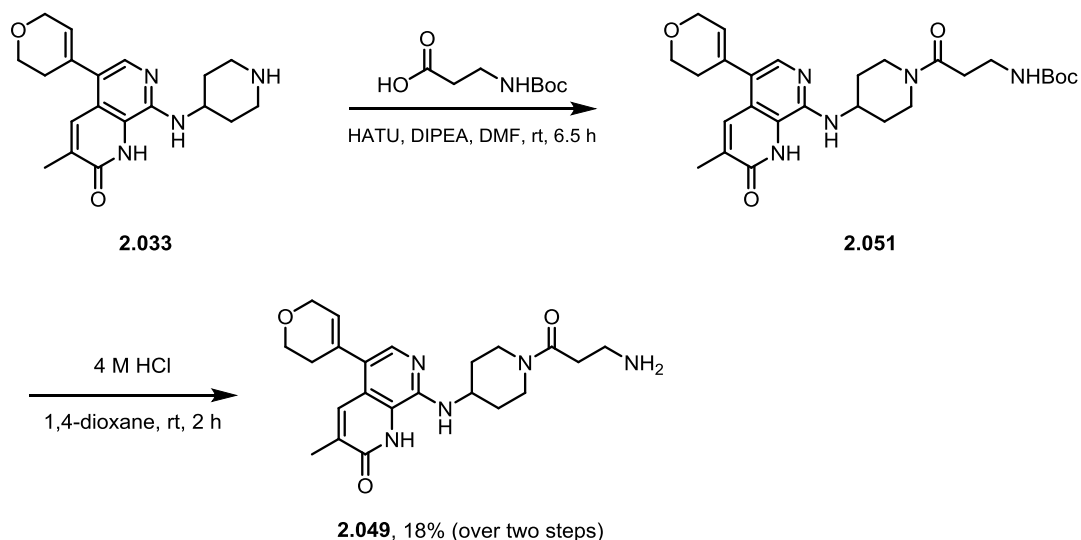
**Scheme 2.09: Synthesis of tertiary amide compound 2.049.**

Primary amide compound **2.050** was synthesized in 23% yield *via* an aza-Michael addition between **2.033** and acrylamide (**Scheme 2.10**), utilizing dolomite as a recyclable heterogeneous basic catalyst. Compound **2.050**'s poor solubility in water gave rise to a long reaction time and poor conversion to the desired product. This could have potentially been reduced *via* heating (see **Section 2.6.1.2 Scheme 2.08**) but this was not investigated.

2.033   **2.050**, 23%

Scheme 2.10: Synthesis of primary amide compound 2.050.

2.6.3.2 Amide Compounds 2.049 and 2.050: Results and Discussion

Once synthesized, **2.049** and **2.050** were screened *via* DiscoverX against TAF1(2) and BRD4(1) and their physicochemical properties measured (**Table 2.11**). The free base of compound **2.049** was observed to be insoluble in DMSO over prolonged periods of time preventing testing in biochemical assays. To circumvent this issue, the hydrochloride salt (**2.049·HCl**) was prepared (**Scheme 2.11**) which showed much improved solubility. To prevent formation of the free base, purification was carried out after the amide coupling step.
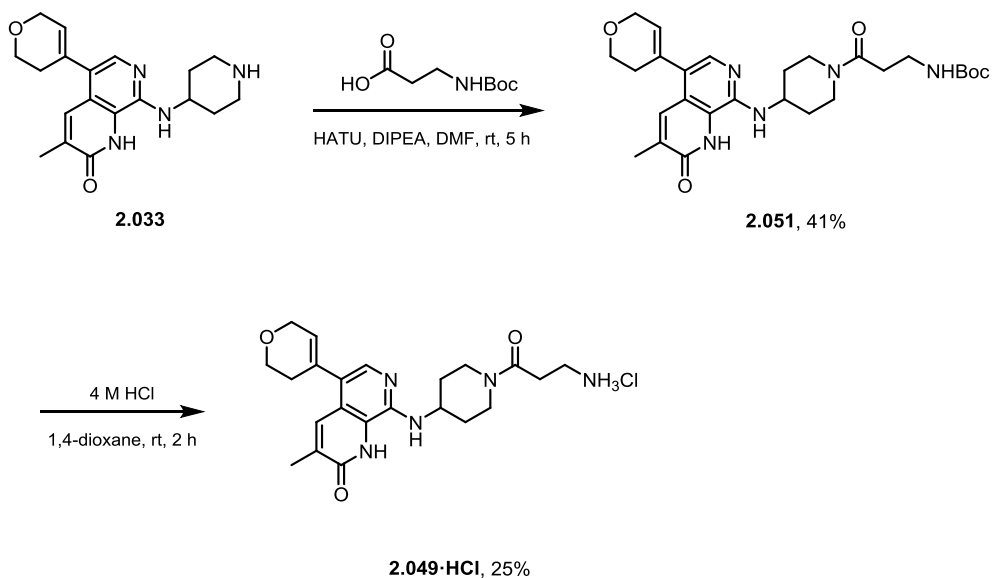
**Scheme 2.11: Synthesis of HCl salt compound 2.049·HCl.**

Unfortunately, conversion of the piperidine amine and propylamine to the corresponding amides (**2.049·HCl** and **2.050**) showed no effect on AMP. Compound **2.049·HCl** retained high TAF1(2) potency, BET selectivity and solubility, suggesting that the basicity of the piperidine nitrogen was not crucial for TAF1(2) activity. By contrast, conversion of the propylamine to the corresponding amide (**2.050**) (and thus removing all substantial basicity from the nitrogen) showed a dramatic drop in TAF1(2) potency, further supporting the significance of the interaction with Asp1539 (**Section 2.4.2**, **Figure 2.14**).

Entry	Compound	R =	TAF1(2) pK$_D$	BRD4(1) pK$_D$	AMP (nm/s)	CAD Solubility (µg/mL)	ChromLogD
1	**2.049·HCl**		8.9	6.1 (×630)	<3	>=386	1.27
2	**2.050**		6.5	<5.0 (≥×32)	<7	>=199	1.38

Table 2.11: Physicochemical properties and potency profile for compounds 2.049·HCl and 2.050. Selectivity for TAF1(2) against the given protein is shown in brackets underneath potency values. CAD solubility, AMP and ChromLogD measurements were all performed at pH$_{7.4}$.

It was therefore hypothesized that the basicity of both nitrogens would need to be reduced simultaneously to improve permeability, with care taken not to reduce the basicity of the terminal nitrogen too far as to jeopardise the vital interaction with Asp1539. Racemic monofluorinated compounds **2.052** and **2.053** were therefore targeted (**Table 2.12**).
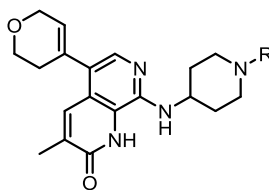
Entry	Compound	R =	Predicted pK$_a$ (most basic)
1	**2.021**	NH_2	9.91
2	**2.052**	NH_2, F	8.60
3	**2.053**	O, NH_2, F	7.80

Table 2.12: Lead compound 2.021 and target compounds 2.052 and 2.053, highlighting the predicted reduced basicities. Predicted pK$_a$ values were calculated using ChemAxon software.[165]
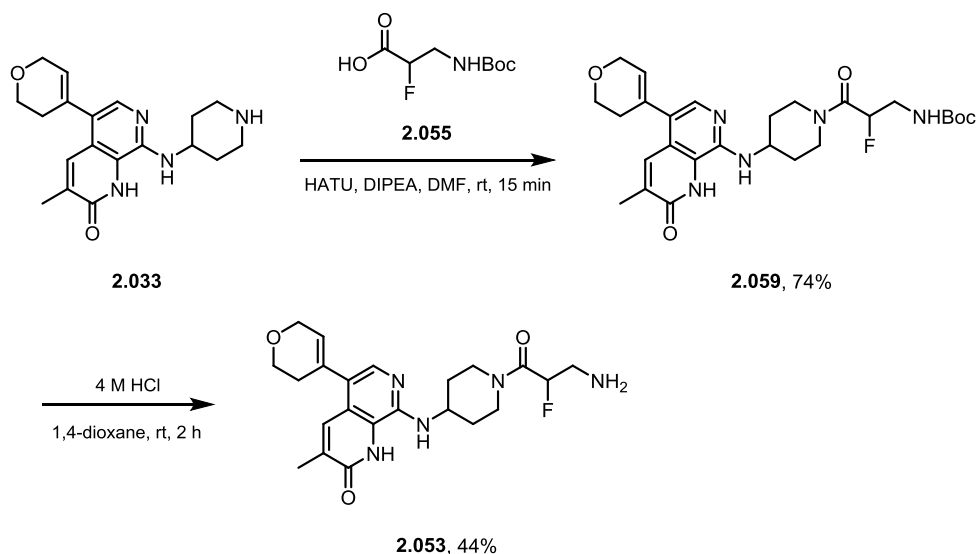
2.6.3.3 Monofluorinated Compounds: Synthesis

Synthesis of fluorinated amine compound **2.052** began from commercially available 3-amino-2-fluoropropanoic acid hydrochloride (**2.054**, **Scheme 2.12**) which was Boc protected in 94% yield using Boc anhydride and sodium hydroxide. As discussed in **Section 2.6.1.1**, it was decided to introduce the DHP group after amide reduction to avoid any unwanted reactivity. A HATU promoted amide coupling between **2.055** and **2.041** delivered intermediate **2.056** in 43% yield. Amide reduction using the preferred BH$_3$·THF complex conditions was unsuccessful, resulting in other amide reduction conditions being trialled. LiAlH$_4$ was shown to reduce the amide bond successfully, however, upon work up *via* the Fieser method,[172] the majority of desired product remained coordinated to the aluminium salts visible by LCMS when leached with methanol. Consequently, the reaction was repeated and worked up using Rochelle's salt to completely dissolve the aluminium salts, delivering the desired amine **2.057** in 28% yield. The reduced yield observed for the reduction was attributed to the use of a harsher reducing agent, leading to a more convoluted reaction profile and a poorer yield. A subsequent Suzuki reaction under standard conditions produced **2.058** in 50% yield, which was then followed by a Boc deprotection using 4 M HCl in 1,4-dioxane, yielding racemic target compound **2.052** in 52% yield.
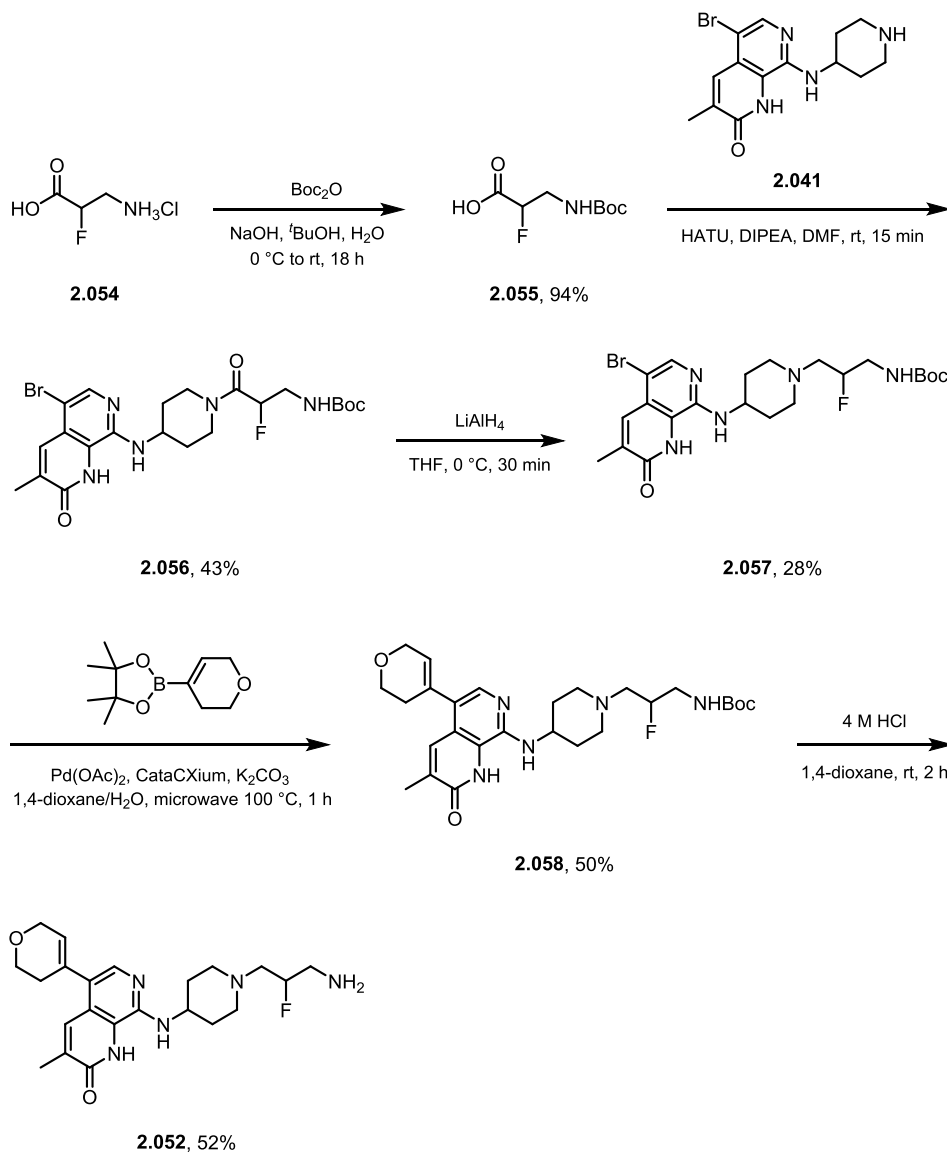
Scheme 2.12: Synthesis of monofluorinated compound 2.052.

Monofluorinated amide compound **2.053** was synthesized from key intermediate **2.033**, starting with a HATU promoted amide coupling to Boc-protected carboxylic acid **2.055** (**Scheme 2.13**). Boc deprotection under standard conditions yielded racemic target compound **2.053** in 44% yield.

Scheme 2.13: Synthesis of monofluorinated compound 2.053.

2.6.3.4 Monofluorinated Compounds: Results and Discussion

Once synthesized **2.052** and **2.053** were screened *via* DiscoverX against TAF1(2) and BRD4(1) and their physicochemical properties measured (**Table 2.13**). Introduction of a fluorine atom also showed no improvement in AMP. Pleasingly, both compounds **2.052** and **2.053** remained potent at TAF1(2), showed high BET selectivity and solubility, and a boost in lipophilicity as measured *via* ChromLogD. Interestingly, an increase in potency was observed for compound **2.053** (TAF1(2) pK_D = 9.7), which appeared over half a log unit more potent than its amine counterpart **2.052** (TAF1(2) pK_D = 9.0).

Entry	Compound	R =	TAF1(2) pK_D	BRD4(1) pK_D	AMP (nm/s)	CAD Solubility (µg/mL)	ChromLogD
1	**2.052**		9.0	<5.3 (≥×5000)	<10	>=175	1.61
2	**2.053**		9.7	6.2 (×3200)	<7	146	1.73

Table 2.13: Physicochemical properties and potency profile for compounds 2.052 and 2.053. Selectivity for TAF1(2) against the given protein is shown in brackets underneath potency values. CAD solubility, AMP and ChromLogD measurements were all performed at pH$_{7.4}$.

The partial double bond character of amides, caused by donation from the nitrogen lone pair into the carbonyl group *via* resonance (**Figure 2.24a**), is well understood, and known to increase sp^2 character and reduce rotational flexibility. Similarly, large barriers to rotation (~8.0 kcal/mol) have been reported for α-fluoroamides, in which the C-F bond favours adopting a conformation *anti* to the carbonyl group and *syn* to the N-H bond (**Figure 2.24b**).[173] It was therefore hypothesized that the amide and fluorine groups rigidified the propylamine chain, locking the chain into the desired conformation to facilitate the interaction to Asp1539 (**Section 2.4.2**, **Figure 2.14**) and leading to an increase in potency.
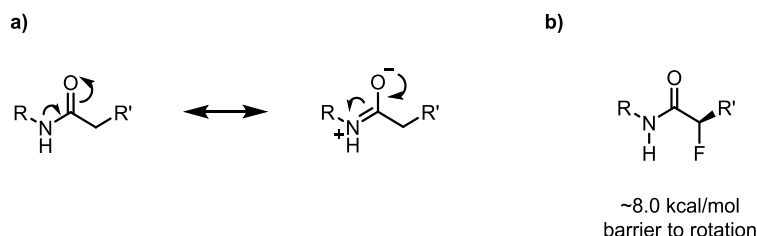

Figure 2.24: a) The two predominant amide resonance forms responsible for the partial double bond character of the C-N bond and thus restricted rotation; and b) the preferred conformation adopted by α-fluoroamides highlighting the barrier to rotation.[173]

To test the accuracy of the predicted pK_a model, the most basic pK_a of compounds **2.052** and **2.053** were measured (pK_a = 8.57 and 7.5, respectively) and agreed well with the predicted values (predicted pK_a = 8.60 and 7.80, respectively), supporting the use of the model for future design iterations.

Introduction of a fluorine between the piperidine and propylamine nitrogens (**2.052** and **2.053**) demonstrated that TAF1(2) potency could still be maintained with a reduced basicity but failed to yield the desired improvement in AMP. It was hypothesized that introduction of an additional fluorine atom would further reduce the basicity of the piperidine and propylamine nitrogen to produce permeable compounds. Consequently, the difluorinated derivatives (**2.060** and **2.061**) were targeted to test the hypothesis (**Table 2.14**).
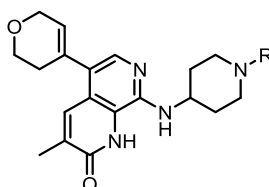

Entry	Compound	R =	Predicted pK_a (most basic)
1	**2.021**		9.91
2	**2.060**		7.29
3	**2.061**		6.54

Table 2.14: Lead compound 2.021 and target compounds 2.060 and 2.061, highlighting the predicted reduced basicities. Predicted pK_a values were calculated using ChemAxon software.[165]

2.6.3.5 Difluorinated Compounds: Synthesis

Synthesis of difluorinated amine compound **2.060** began with Boc protection of amino acid **2.062** using Boc anhydride and sodium hydroxide (**Scheme 2.14**). Compound **2.063** was then coupled to key intermediate **2.041** *via* a HATU promoted amide formation in 36% yield. An amide reduction using $BH_3 \cdot THF$ complex was successful and the boron adducts liberated under acidic conditions. As might be expected, the

Boc group was also removed under the acidic conditions yielding intermediate **2.065** in 88% yield. Finally, a Suzuki coupling under standard conditions yielded target compound **2.060** in 18% yield. This poor yield was attributed to the free amine coordinating to the Pd and interfering with the catalytic cycle. This could potentially have been avoided *via* a prolonged neutral work up for the amide reduction step, thus maintaining the Boc group, which in turn could have been removed after the Suzuki-coupling.
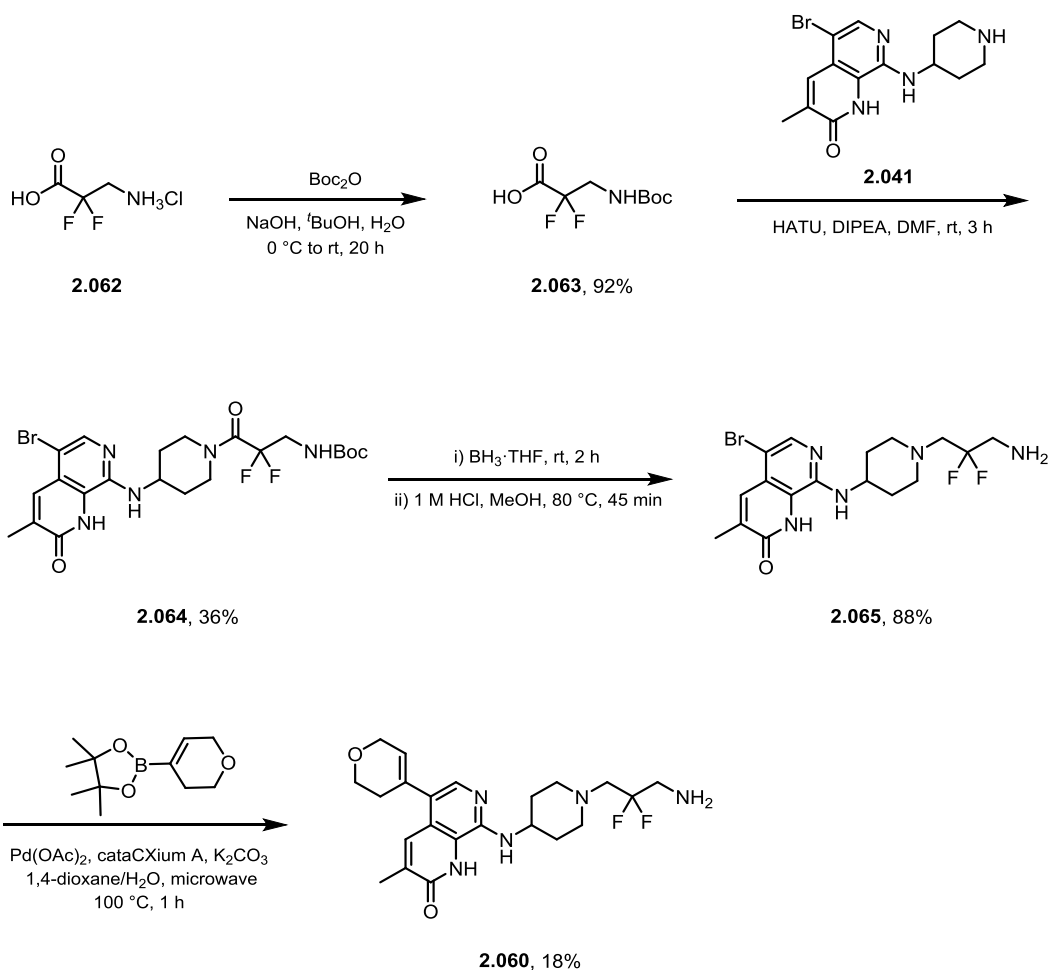
Scheme 2.14: Synthesis of difluorinated compound 2.060.

Difluorinated amide compound **2.061** was synthesized *via* the same route as monofluorinated amide compound **2.053**. A HATU promoted amide coupling between key intermediate **2.033** and Boc-protected carboxylic acid **2.063** yielded compound

2.066 in 26% yield (**Scheme 2.15**). Boc deprotection under standard conditions yielded target compound **2.061** in 40% yield.
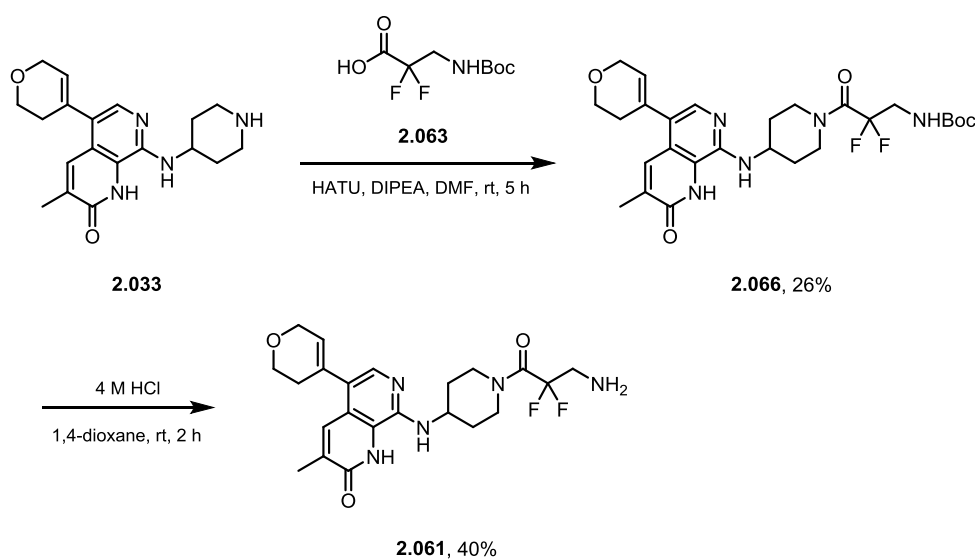
Scheme 2.15: Synthesis of difluorinated compound 2.061.

2.6.3.6 Difluorinated Compounds: Results and Discussion

Once synthesized **2.060** and **2.061** were screened *via* DiscoverX against TAF1(2) and BRD4(1) and their physicochemical properties measured (**Table 2.15**). Pleasingly, incorporation of a second geminal fluorine atom further reduced the basicity of the propylamine nitrogen and provided the desired increase in AMP, and the first permeable compounds of the series. Difluoro amine compound **2.060** demonstrated high permeability in the AMP assay (220 nm/s) and maintained high solubility. Unfortunately, the reduction in basicity and dramatic improvement in AMP was accompanied by a reduction in TAF1(2) potency ($pK_D = 7.3$) for **2.060**, suggesting that the interaction with Asp1539 had been compromised. Despite the reduction in potency, compound **2.060** maintained the desired selectivity over the BET bromodomains (≥100-fold). Compound **2.061** also showed an increase in permeability (62 nm/s) and, interestingly, maintained TAF1(2) potency ($pK_D = 9.1$) and high BET selectivity (≥6300-fold).

80
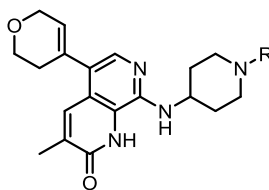
Entry	Compound	R =	TAF1(2) pK$_D$	BRD4(1) pK$_D$	AMP (nm/s)	CAD Solubility (µg/mL)	ChromLogD
1	**2.060**		7.3	<5.3 (≥×100)	220	>=196	2.92
2	**2.061**		9.1	<5.3 (≥×6300)	62	24	2.73

Table 2.15: Physicochemical properties and potency profile for compounds 2.060 and 2.061. Selectivity for TAF1(2) against the given protein is shown in brackets underneath potency values. CAD solubility, AMP and ChromLogD measurements were all performed at pH$_{7.4}$.

As discussed in **Section 2.5.3.4**, it was hypothesized that the increased rigidity of the propyl chain helped lock the group into the desired conformation to facilitate the interaction to Asp1539, thus providing a greater TAF1(2) potency. To investigate this further, both **2.060** and **2.061** were docked into the TAF1(2) bromodomain, which suggested a drastic switch in conformation of the difluoropropylamine chain (**Figure 2.25a** & **b**). The fluorine atoms of compound **2.060** were shown to be adopting a gauche-gauche conformation relative to the piperidine nitrogen atom, optimizing hyperconjugation into the C-F σ* orbitals (**Figure 2.26**). This phenomenon[174,175] (and its effect on chain rigidity)[176,177] is well understood for vicinal fluorides and has also been reported for other electron-withdrawing atoms such as oxygen and nitrogen.[178]

Introduction of the amide group was shown to invert the propylamine chain forcing the fluorine atoms away from the protein surface (**Figure 2.25c** & **d**) to adopt a conformation where one fluorine sits *anti* to the carbonyl group (as discussed in **Section 2.6.3.4**). It is therefore hypothesized that relieving this clash with the protein surface also provided an increase in TAF1(2) potency.
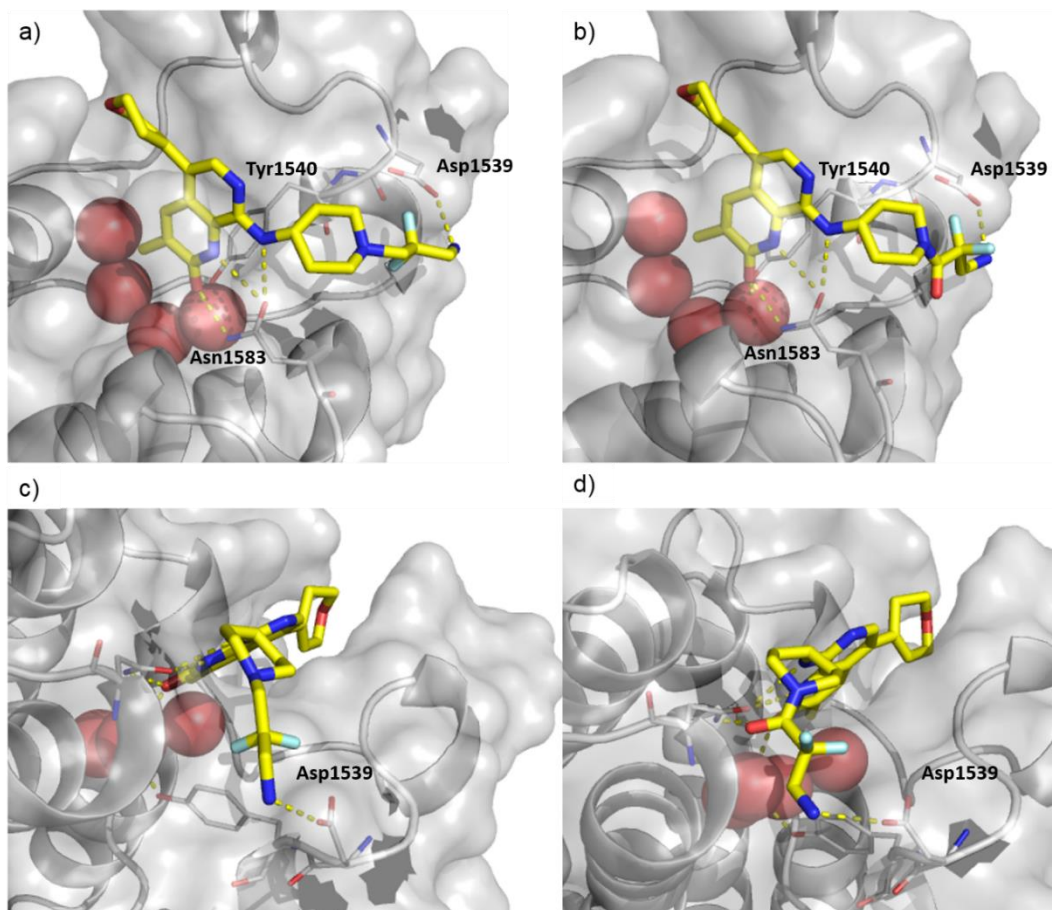
Figure 2.25: a) Docking of compound 2.060 bound to TAF1(2) highlighting the key interactions with Asn1583, Tyr1540 and Asp1539; b) docking of compound 2.061 bound to TAF1(2) highlighting the key interactions with Asn1583, Tyr1540 and Asp1539; c) docking of compound 2.060 bound to TAF1(2) highlighting the conformation of the difluoro chain; and d) docking of compound 2.061 bound to TAF1(2) highlighting the conformation of the difluoro chain.
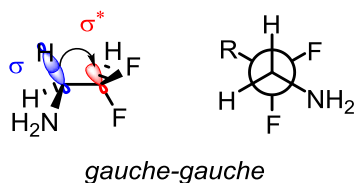

gauche-gauche

Figure 2.26: The gauche-gauche conformation adopted by the difluoropropylamine chain, highlighting the hyperconjugation from C-H σ-orbital into C-F σ*-orbital.

To further validate the predictive pK_a model, the most basic pK_a of **2.061** was measured (pK_a = 6.44) and agreed well with the predicted pK_a (predicted pK_a = 6.54).

Following the success of the difluoro compounds and their improved permeability, two new target compounds (**2.067** and **2.068**) were identified (**Table 2.16**) to further investigate the effect of reduced pK_a on permeability. Due to the apparent dependence of TAF1(2) potency on the basicity of the propylamine nitrogen, attention was shifted to reducing the basicity of the amino piperidine nitrogens. It was hypothesized that introduction of electron-withdrawing groups between the two nitrogens would reduce the pK_a of both amino piperidine nitrogens, and thus improve permeability.
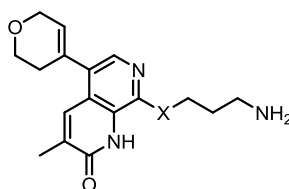
Entry	Compound	X =	Predicted pK_a (most basic)
1	**2.067**		9.87
2	**2.068**		9.87

Table 2.16: Target compounds 2.067 and 2.068, highlighting the predicted reduced basicities. Predicted pK_a values were calculated using ChemAxon software.[165]

Due to the well-established preference for fluorine groups to sit axially in 3-fluoro piperidines,[179,180] where dipole-dipole interaction is maximized (**Figure 2.27**), the single desired *syn*-diastereomer for favouring this interaction was synthesized, thus preventing any entropic costs caused by conformational rearrangement, and avoiding any resulting loss of potency.
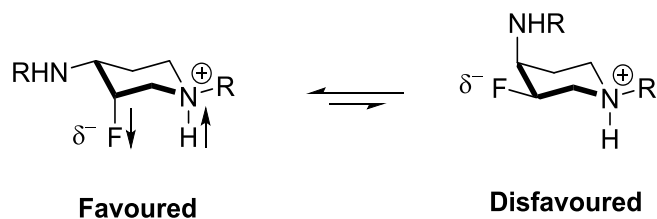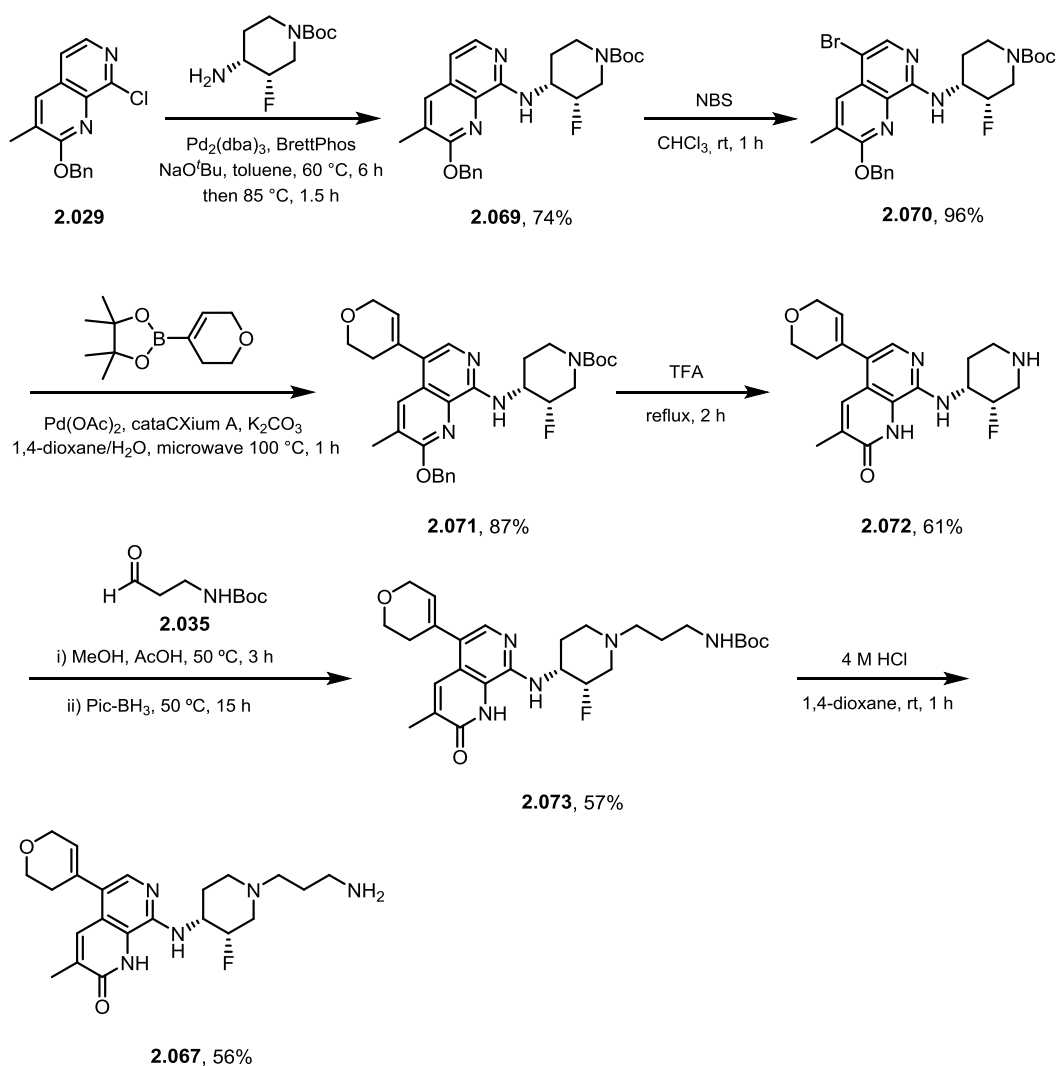
**Figure 2.27: Preferred axial conformation of 3-fluoro-piperidines.**

2.6.3.7 Fluoropiperidine Compounds: Synthesis

Synthesis of fluoropiperidine compound **2.067** began from early intermediate **2.029** (**Scheme 2.16**). The desired fluoropiperidine ring was installed *via* a Buchwald-Hartwig amination using the commercially available *tert*-butyl (3*S*,4*R*)-4-amino-3-fluoropiperidine-1-carboxylate, yielding **2.069** in 74%. The same catalyst was used as before with a solvent switch from THF to toluene providing a greater conversion. Bromination of **2.069** with NBS gave intermediate **2.070** in 96% yield, which in turn underwent a Suzuki-coupling with the desired boronic ester to yield **2.071** in 87% yield. Deprotection of the benzyl and Boc protecting groups was then achieved using TFA to yield intermediate **2.072** in 61%. Reductive amination under standard conditions gave compound **2.073** in 57% yield and a subsequent Boc deprotection yielded final compound **2.067** in 56%. The e.e. of compound **2.067** was not determined, however, compound **2.067** was confirmed as non-racemic *via* optical rotation showing a positive $[\alpha_D]^{23}$ (c = 10 mg/mL, MeOH): +8°.

Scheme 2.16: Synthesis of fluoropiperidine compound 2.067.

A similar set of reactions were then utilized to synthesize difluoropiperidine compound **2.068**, again starting from early intermediate **2.029**. A Buchwald-Hartwig amination with *tert*-butyl 4-amino-3,3-difluoropiperidine-1-carboxylate produced intermediate **2.074** in 85% yield (**Scheme 2.17**). Toluene was again preferred over THF but, due to the more electron deficient amine, required heating to higher temperatures for effective conversions. Bromination of **2.074** with NBS gave intermediate **2.075** in 92% yield which then underwent a Suzuki-coupling to deliver **2.076** in 82% yield. A global deprotection using TFA gave intermediate **2.077** in 79% yield, which then underwent reductive amination with **2.035** to give compound **2.078** in 56% yield. Finally, compound **2.078** was Boc deprotected to yield compound **2.068** in 40% yield.
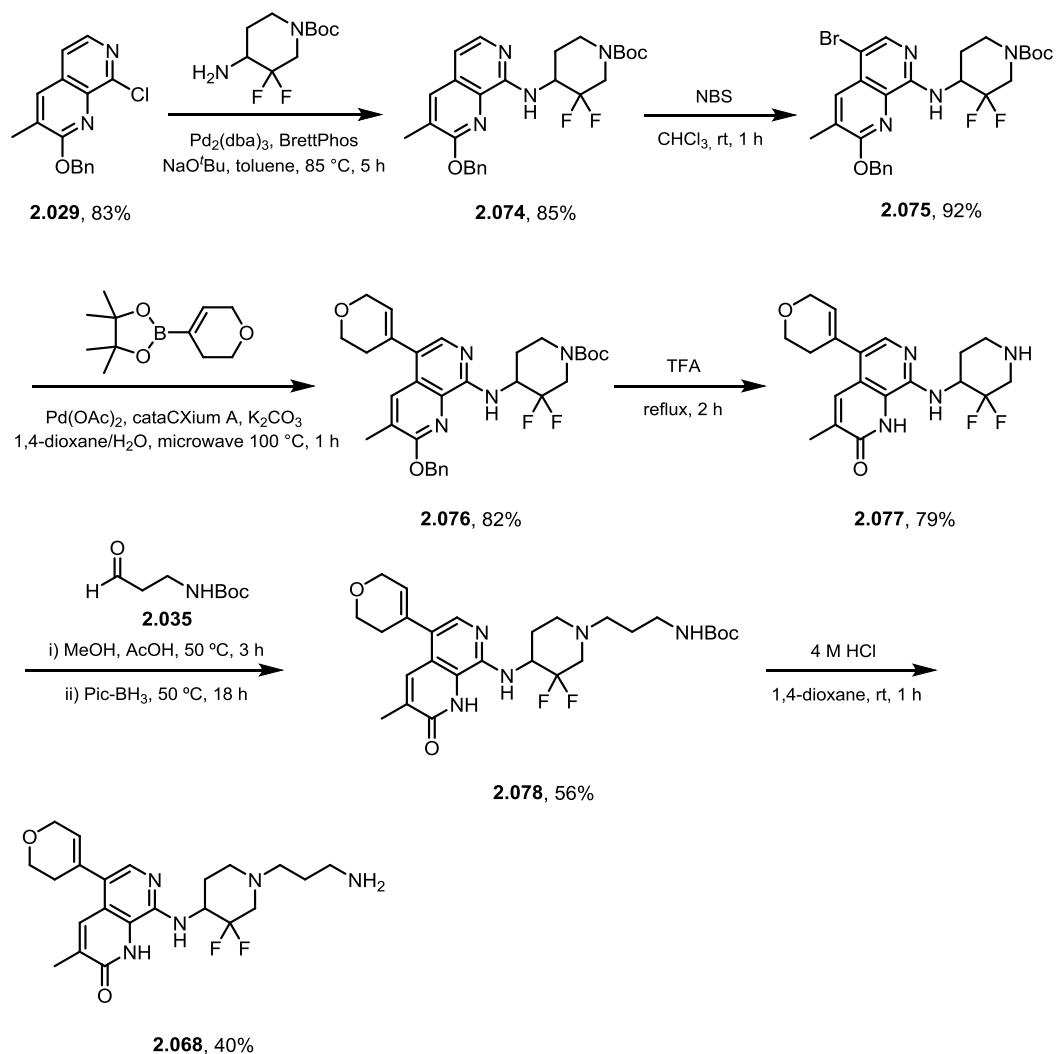
Scheme 2.17: Synthesis of difluoropiperidine compound 2.068.

2.6.3.8 Fluoropiperidine Compounds: Results and Discussion

Once synthesized **2.067** and **2.068** were screened *via* DiscoverX against TAF1(2) and BRD4(1) and their physicochemical properties measured (**Table 2.17**). Shifting the basicity reducing focus from the propylamine chain to the piperidine ring was successful in producing potent and selective compounds for TAF1(2) but failed to induce any measurable permeability in the AMP assay.
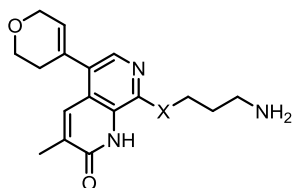
Entry	Compound	R =	TAF1(2) pK$_D$	BRD4(1) pK$_D$	AMP (nm/s)	CAD Solubility (µg/mL)	ChromLogD
1	**2.067**		9.2	5.6 (×3900)	<5	141	1.49
2	**2.068**		8.5	5.3 (×1600)	<10	>=106	1.75

Table 2.17: Physicochemical properties and potency profile for compounds 2.067 and 2.068. Selectivity for TAF1(2) against the given protein is shown in brackets underneath potency values. CAD solubility, AMP and ChromLogD measurements were all performed at pH$_{7.4}$.

2.6.4 Intracellular Concentration

With little information gained from the AMP assay, uncertainty remained over the potential of the series to engage the cellular target. As a result, compounds **2.021**, **2.060**, **2.061**, **2.067** and **2.068** were screened in an intracellular concentration assay to help provide insight into their behaviour within cells (**Table 2.18**).[76,77] The assay provided access to two key pieces of data: pΔC, a measure of the influx/efflux ratio of the compound to the cell; and % fraction unbound, the percentage of compound that is unbound within the cell and available for target binding.[181] An outline of the assay and how each piece of data is acquired is shown below (**Figure 2.28**).

HeLa cells are first incubated with the desired compound and allowed to equilibrate. Once equilibrium has been reached the cells are separated from the media and the cell membranes ruptured using a detergent. LCMS-MS is then used to quantify the ratio of compound in the cellular solution and the media. This provides access to the pΔC values which can be interpreted as follows: a value of 0 represents a highly permeable compound which can enter and leave the cell at equal rate; a value <-1 represents an impermeable compound; and >1 represents accumulation of the compound within the cell.

Separately, HeLa cells are lysed *via* homogenization, physically rupturing the cell membrane. The lysed cells are then treated with compound and allowed to dialyze through a semipermeable membrane. Unbound compound will diffuse through the membrane whilst compound undergoing non-specific binding to cellular components will remain in the initial compartment. LCMS-MS is then used to quantify the concentration of compound in each compartment which can then be used to calculate the % fraction unbound.
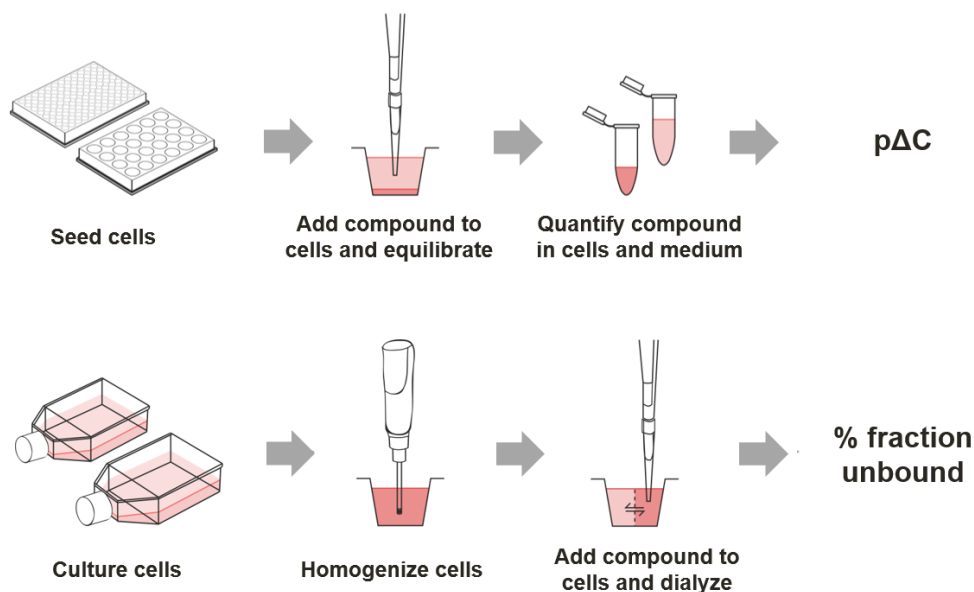

Figure 2.28: Schematic of the intracellular concentration assay workflow.

Despite some compounds reporting poor AMP, all compounds tested reported an approximately equivalent influx/efflux ratio or accumulation within the cell, suggesting good cellular permeability. Of note were the difluoropropylamine compounds **2.060** and **2.061** with high AMP which showed good permeability or accumulation within the cell. Interestingly, fluoropiperidine compounds **2.067** and **2.068** both showed good permeability within the assay, contradicting the AMP results obtained, and high levels of unbound compound (30 and 60% respectively). By contrast, **2.021** was shown to be highly bound within cells with only 11% of the compound available to interact with a given target. Similarly, both difluoropropylamine derivatives (**2.060** and **2.061**) showed low fractions unbound (6 and 9% respectively).
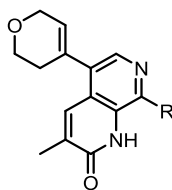
Entry	Compound	R =	AMP (nm/s)	pΔC	Fraction Unbound
1	**2.021**		<10	0.55	11%
2	**2.060**		220	1.02	6%
3	**2.061**		62	0.65	9%
4	**2.067**		<5	0.11	30%
5	**2.068**		<10	-0.16	60%

Table 2.18: Intracellular concentration assay data table.

Despite the low percentage fraction unbound, compound **2.061** was selected for further profiling having demonstrated permeability in both the AMP and intracellular concentration assays.

2.7 Compound 2.061, a Chemical Probe for the TAF1/TAF1L Bromodomains

2.7.1 Selectivity Profiling
Compound **2.061** was then screened against the DiscoverX BROMO*scan* panel at 10 μM to provide an insight into non-BET bromodomain selectivity (**Figure 2.29** & **Table 2.19**).
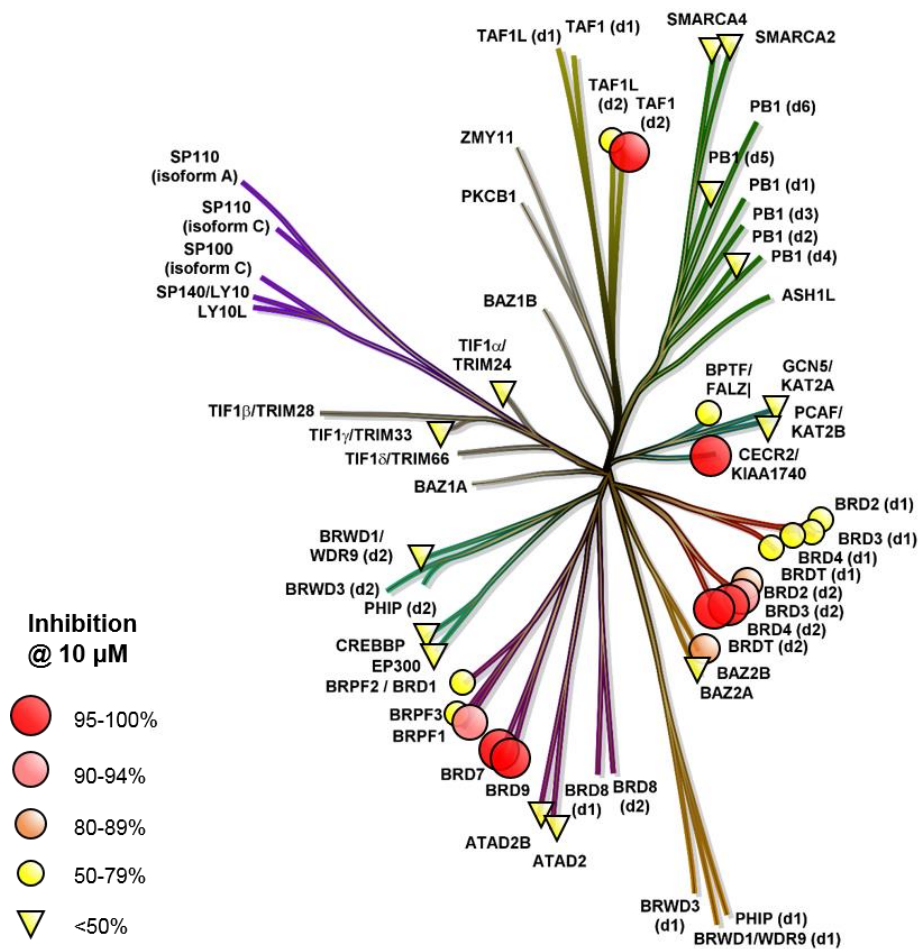
Figure 2.29: Phylogenetic tree inhibition plot generated for 2.061's 10 µM single-shot DiscoverX BROMO*scan* (data shown in Table 2.19).

Compound Number	ATAD2A	ATAD2B	BAZ2A	BAZ2B	BRD1	BRD2(1)	BRD2(2)	BRD3(1)	BRD3(2)	BRD4(1)	BRD4(2)	BRD7	BRD9	BRDT(1)	BRDT(2)	BRPF1
2.061	24	33	32	85	61	63	83	67	92	73	99	97	100	54	98	94

Compound Number	BRPF3	CECR2	CREBBP	EP300	FALZ	GCN5L2	PB1(2)	PB1(5)	PCAF	SMARCA2	SMARCA4	TAF1(2)	TAF1L(2)	TRIM24	TRIM33	WDR9(2)
2.061	53	95	0	44	78	34	0	0	34	0	0	100	74	2	0	23

Table 2.19: Percentage inhibition of bromodomains tested at 10 µM (DiscoverX BROMO*scan* assay) for compound 2.061.

At 10 µM **2.061** appeared selective over a number of BET and non-BET bromodomains. High levels of inhibition were, however, observed against BAZ2B, BRD7/9, BRPF1, CECR2 and the second bromodomain of the BET bromodomain containing proteins (e.g. BRD4(2)). Consequently, 11-point dose response curves, from which pK$_D$s were calculated, were measured for these bromodomains to investigate selectivity (**Figure 2.30** and **Table 2.20**).
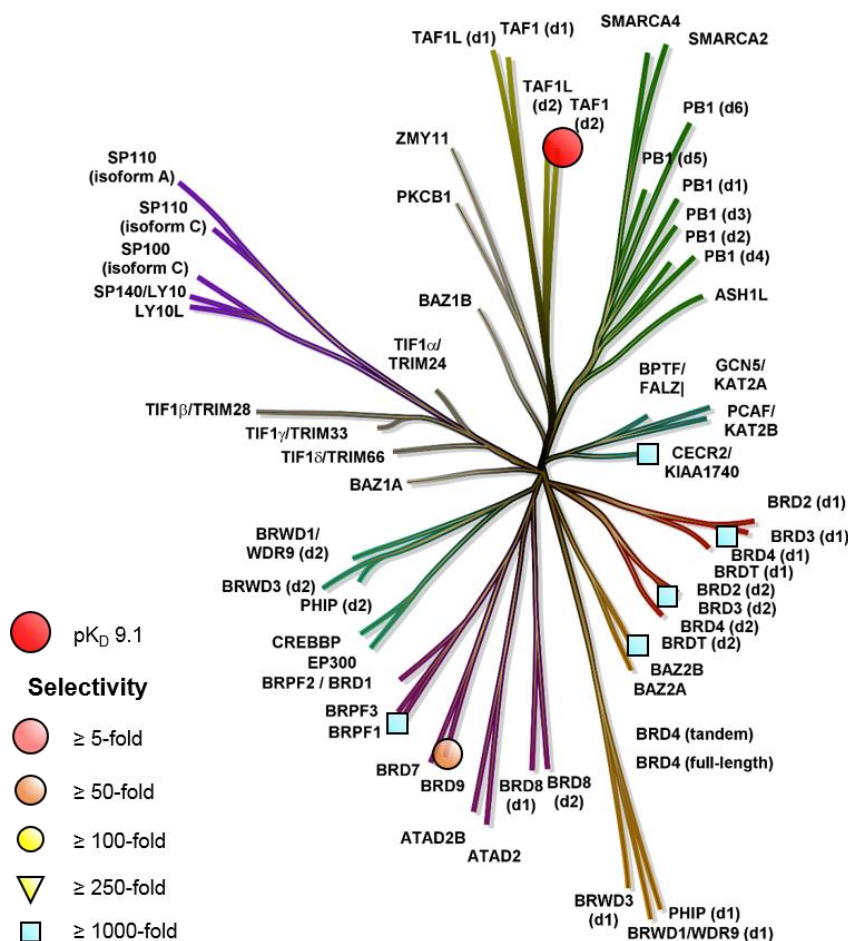

Figure 2.30: Phylogenetic tree inhibition plot generated for 2.061's full curve data generated in the DiscoverX BROMO*scan* assay. Selectivity determined from the difference between TAF1(2) and the relative bromodomain pK$_D$ values.

Compound Number	Bromodomain pK_D						
	TAF1(2)	BRD4(1)	BRD4(2)	BAZ2B	BRD9	CECR2	BRPF1
2.061	9.1	<5.3	6.1	6.0	7.4	6.0	5.3

Table 2.20: pK_D values for compound 2.061 against a selection of bromodomains, calculated from 11-point dose response curves as measured by DiscoverX qPCR assays.

Pleasingly, **2.061** demonstrated sub-nanomolar potency for TAF1(2) (pK_D = 9.1) and ≥1000-fold selectivity against all other bromodomains tested, including both BRD4 bromodomains. An exception to this was BRD9 where 50-fold selectivity was observed.

Having fulfilled the bromodomain selectivity profile desired, the HCl salt of **2.061** (**2.061·HCl**) was then screened against an internal cross-screen panel of kinases, enzymes, GPCRs and ion-channels, to investigate its activity against other pharmacological targets. Compound **2.061·HCl** showed selectivity over the 56 targets tested showing no activity pIC_{50} > 5 excluding CYP3A4 enzyme (pIC_{50} = 5.5) (**Appendix Table 5.02** & **5.03**) which was considered insignificant for the project.

Having fulfilled the selectivity profile desired for a non-BET bromodomain chemical probe the *in vivo* applicability of compound **2.061** was explored.

2.7.2 Metabolic Stability

To investigate the suitability of **2.061** for *in vivo* application, preliminary studies were performed to assess the pharmacokinetic properties of **2.061**. MetaSite, an *in silico* cytochrome P450 (CYP) mediated metabolism predictor,[182,183] was used to first predict the most likely sites of metabolism based on the 3D structure of the molecules and their likelihood to fit into CYP enzyme pockets. Additionally, MetaSite considered the chemical transformations induced by each enzyme and the relative likelihood of these occurring. The carbon atom highlighted in blue was predicted as the most likely site for metabolism, followed by the naphthyridinone methyl substituent (**Figure 2.31**). Three additional sites on the DHP ring, as well as some minor sites on the piperidine ring and terminal amine, were also identified.
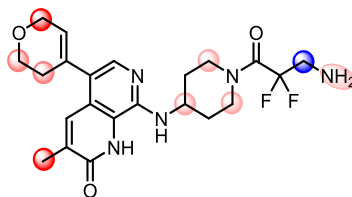
2.061

Figure 2.31: Metasite output for compound 2.061. Most likely site of CYP mediated metabolism highlighted in blue. Additional sites ranked by likelihood from dark red to light red.

After identifying the most likely sites for metabolism, the *in vitro* clearance of compound **2.061** was then measured in human liver microsomes. Pleasingly compound **2.061** showed low clearance (0.83 mL/min/g) and, although further profiling is required, offers promise for potential *in vivo* applications.

2.7.3 Negative Control

One of the key aims at the outset of the project was to synthesize a structurally similar negative control to accompany the resulting chemical probe. Not only would this help mitigate the chance of false phenotype assignment, but also help fulfil one of the main gaps in the TAF1/TAF1L chemical tool box.

Ideally a negative control should be the inactive enantiomer of the tool molecule. However, in the absence of any stereocenters, attempts to reduce activity *via* a one-point change were pursued. It was hypothesized that disruption of the tridentate interaction to the conserved Asn residue *via* removal of a hydrogen bond interaction would reduce TAF1(2) activity (**Figure 2.32a**). To conserve as much of the acetylated Lys mimetic as possible, the anilinic N-H hydrogen bond interaction (shown in blue) was selected for disruption (**Figure 2.32b**). It was hypothesized this could be achieved *via* methylation of the nitrogen (**2.079**) or *via* conversion to an ether linkage (**2.080**) (**Figure 2.32c**).
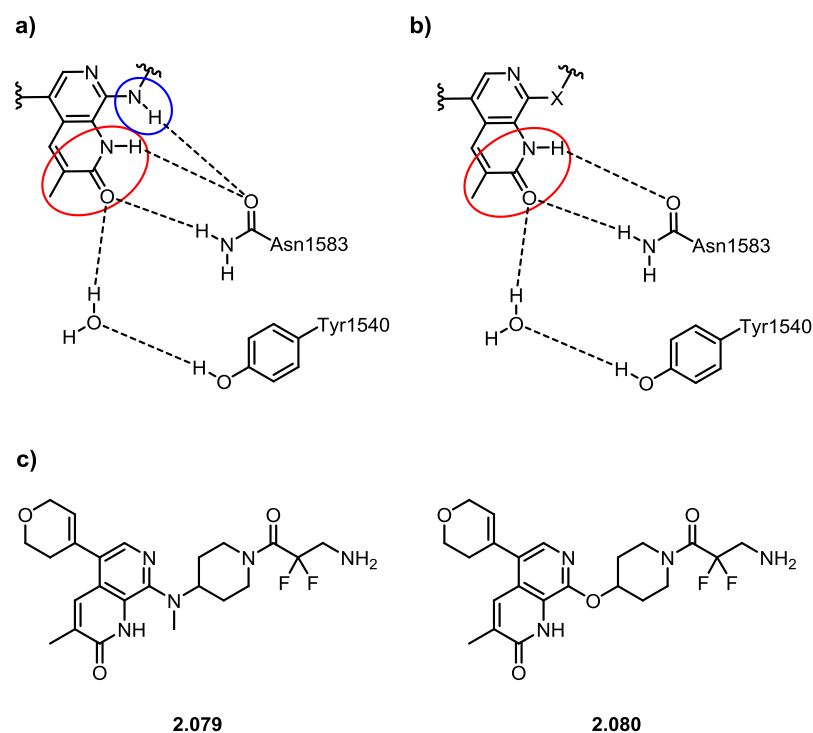
Figure 2.32: a) Schematic of the key interactions between the naphthyridinone scaffold and Asn1583 and Tyr1540 during TAF1(2) binding; b) removal of a hydrogen bond interaction *via* the removal of the N-H hydrogen bond; and c) proposed negative controls 2.079 and 2.080.

2.7.3.1 Synthesis of N-Methyl Negative Control

The synthesis of compound **2.079** began *via* a Buchwald-Hartwig amination between early intermediate **2.029** and *tert*-butyl 4-(methylamino)piperidine-1-carboxylate (**Scheme 2.18**). Despite using a secondary amine, the reaction proceeded well under the BrettPhos conditions previously used, producing **2.081** in 76% yield. Subsequent bromination under standard conditions yielded **2.082** in 69% yield. A Suzuki-coupling using XPhos-Pd-G2 yielded intermediate **2.083** in 62% yield, which was globally deprotected with TFA to give intermediate **2.084**. A HATU promoted coupling with **2.063** then gave intermediate **2.085** which was Boc deprotected to give final compound **2.079** in 66% yield.
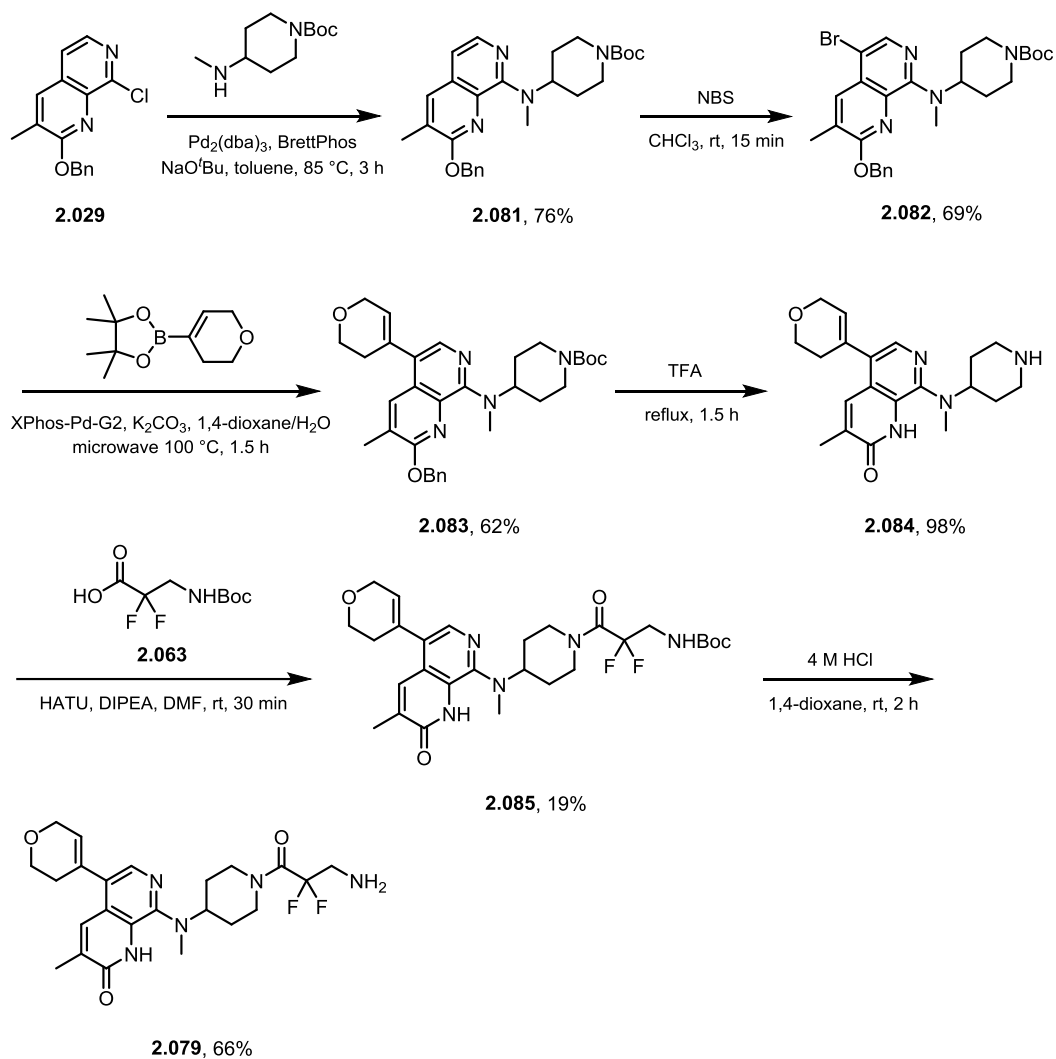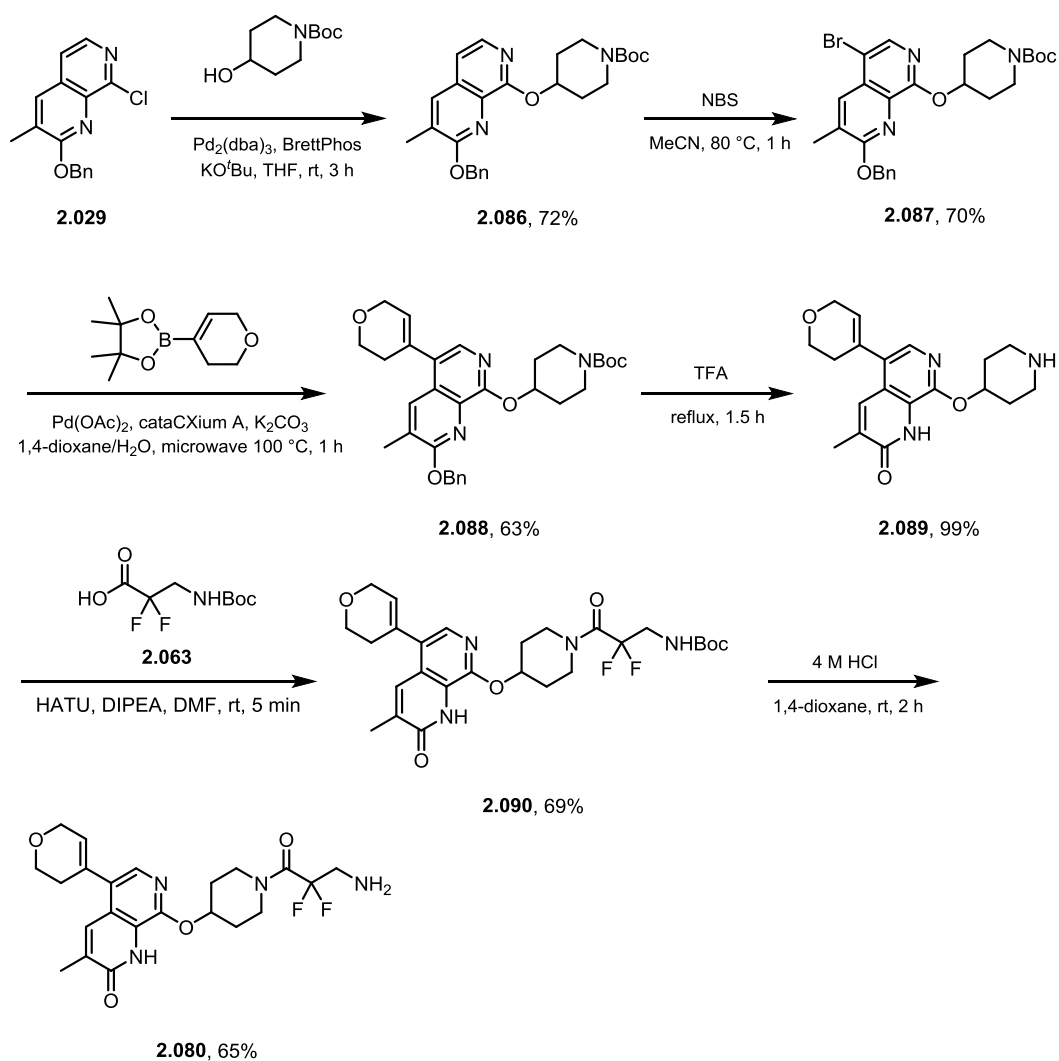
Scheme 2.18: Synthesis of negative control compound 2.079.

2.7.3.2 Synthesis of O-ether linked Negative Control

Synthesis of compound **2.080** began from early intermediate **2.029** (**Scheme 2.19**). An etherification using the preferred Buchwald-Hartwig amination conditions was trialed and showed poor conversion to the desired product. Pleasingly, switching to a weaker coordinating cation *via* KO^{t}Bu, and running the reaction at room temperature, gave an improved conversion, yielding compound **2.086** in 72% yield. Bromination using NBS at room temperature in chloroform was then trialed as before, showing no reactivity. It was hypothesized that in the absence of the strongly activating amine group, the ring was less electron rich and harsher conditions were required to facilitate

electrophilic aromatic substitution. As a result, acetonitrile was used in place of chloroform to facilitate higher reaction temperatures (80 °C) and delivered **2.087** in 70% yield. A Suzuki-coupling under standard conditions followed by removal of the benzyl and Boc groups gave intermediate **2.089**. An amide coupling with **2.063** gave intermediate **2.090** in 69% yield, which was Boc deprotected under standard conditions to yield final compound **2.080** in 65% yield.


Scheme 2.19: Synthesis of negative control compound 2.080.

2.7.3.3 Results and Discussion: Negative Controls

Once synthesized both compounds were screened *via* DiscoverX against TAF1(2) and BRD4(1) and their physicochemical properties measured (**Table 2.21**). As

hypothesized, both compounds showed a dramatic reduction in TAF1(2) potency (>1000-fold), did not show activity against BRD4(1) at 10 µM and possessed reasonable physicochemical properties.
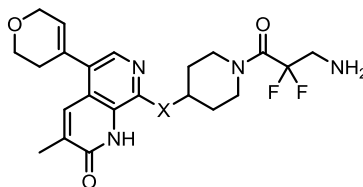
Entry	Compound	X	TAF1(2) pK$_D$	BRD4(1) pK$_D$	AMP (nm/s)	CAD Solubility (µg/mL)	ChromLogD
1	**2.079**	NMe	<5.0	<5.0	150	112	2.90
2	**2.080**	O	5.4	<5.0	76	32	3.13

Table 2.21: Physicochemical properties and potency profile for compounds 2.079 and 2.080. CAD solubility, AMP and ChromLogD measurements were all performed at pH$_{7.4}$.

Despite showing greater activity for TAF1(2) and possessing lower permeability and solubility than **2.079**, compound **2.080** was selected to function as a negative control for **2.061** due to concerns over the extra site of metabolism (N-Me) introduced for compound **2.079**. Metasite predictions were run on compounds **2.079** and **2.080** and confirmed the N-Me group as a potential site of metabolism (**Figure 2.33**). More specifically, metabolic cleavage of the N-Me bond would reveal active compound **2.061** compromising **2.079** as a negative control.
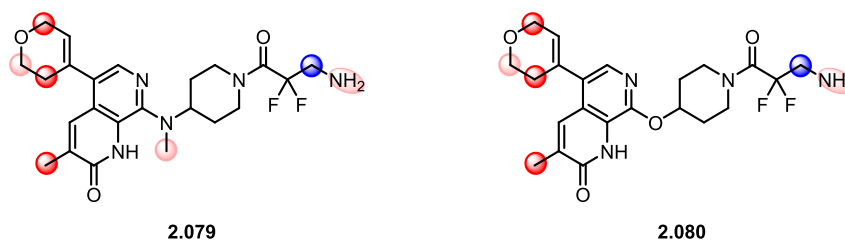

2.079

2.080

Figure 2.33: Metasite output for compounds 2.079 and 2.080. Most likely site of metabolism highlighted in blue. Additional sites ranked by likelihood from dark red to light red.

2.7.4 Summary

Compound **2.061** is a potent and selective inhibitor of the TAF1/TAF1L bromodomains, showing enhanced potency and selectivity compared to other TAF1/TAF1L inhibitors (excluding **2.017**). Additionally, compound **2.061** offers a structurally orthogonal chemotype to reported TAF1/TAF1L probe, **2.017**. Unlike **2.017**, however, compound **2.061** is accompanied by a structurally related negative control to help provide improved confidence in phenotypic assignment. Together with structurally similar negative control **2.080**, compound **2.061** helps expand the diversity of the TAF1/TAF1L chemical tool box and provides an additional pair of high-quality tool molecules for the target validation of the TAF1/TAF1L bromodomains.

2.8 Bromodomain Selectivity Through Conserved Water Interactions

Although **2.061** met the desired bromodomain selectivity profile, activity against BRD9 limited the overall selectivity to 50-fold. In an attempt to further enhance the non-BET selectivity of **2.061**, the concept of conserved water interactions was explored.

As alluded to in **Section 1.3**, the binding pocket of bromodomains contains a conserved network of four water molecules. This water network is seen across all bromodomain binding pockets and is regular in its composition and arrangement. The X-ray crystal structures of apo-TAF1(2), apo-BRD4(1) and apo-BRD9 are shown below (**Figure 2.34**) highlighting the regularity of their respective water networks.
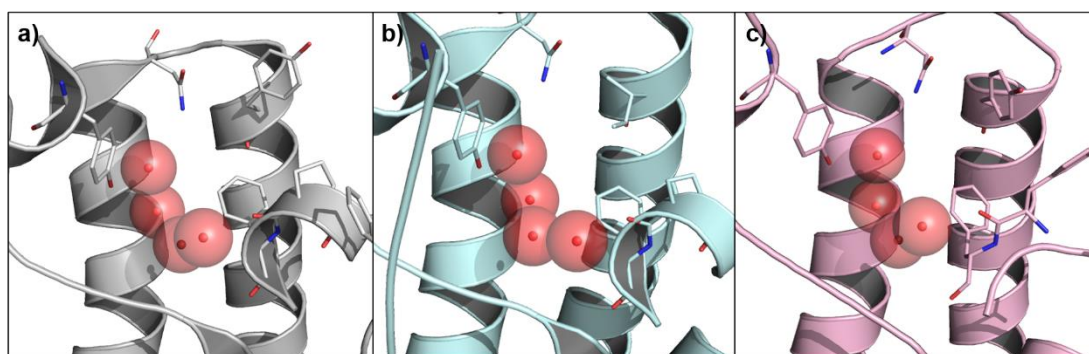

Figure 2.34: a) X-ray crystal structure (PDB: 3UV5) of apo-TAF1(2) (shown in grey); b) X-ray crystal structure (PDB: 2OSS) of apo-BRD4(1) (shown in cyan); and c) GSK internal X-ray crystal structure of apo-BRD9 (shown in pink). Water molecules shown as red spheres.

Despite the structural regularity, the relative stability of each bromodomain water network can vary dramatically, and has been the subject of great interest in recent years.[184,185] Whilst drug discovery has often focused on the displacement of conserved water molecules to produce higher affinity ligands,[186] differential displacement of water molecules can also be exploited to produce selective ligands.[187–189] Displacement of the conserved water molecules within bromodomains has been shown to drastically alter the selectivity profile of compounds. This is in part due to the stability of the water network, which varies between bromodomains, and thus can provide the opportunity for selectivity. The rationale follows that if displacement of the water molecules from bromodomain "X" is easier (a smaller free energy penalty) than displacement from bromodomain "Y", then the difference in displacement free energies will produce a ligand with higher affinity for bromodomain "X".[185]

Multiple groups have attempted to estimate the stability of each bromodomain water network to help explain and predict the selectivity transformations.[185,190] Biggin *et al.* have used all-atom grand canonical Monte Carlo simulations to calculate the binding free energy of 35 bromodomain water networks, thus providing an estimate of their relative stability (**Figure 2.35**).[185]
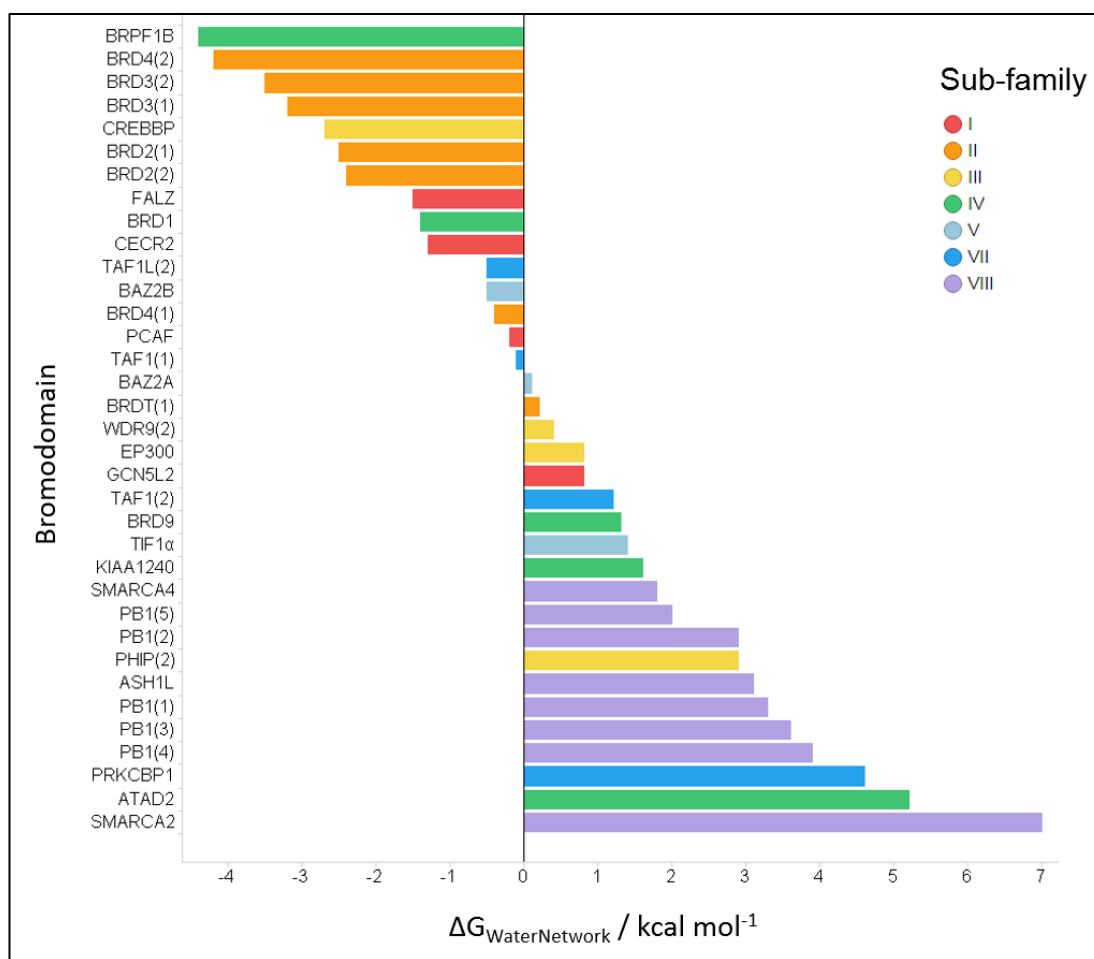
Figure 2.35: Binding energies for the water networks found within bromodomains, coloured by subfamily of bromodomain. Reproduced with permission.[185]

The concept of water displacement has been utilized across academia and industry in the development of selective bromodomain chemical probes, in particular for the subfamily VIII bromodomains, all of which were predicted by Biggin *et al*. to have particularly unstable water networks.[191–193]

As described in **Section 2.2**, elegant work by Genentech and Constellation Pharmaceuticals showed that variation of the acetylated Lys methyl mimetic could produce more subtle effects with the conserved water networks, and in doing so provide selectivity for different bromodomains. This included partial rearrangement of the water network for TAF1(2) and the induction of additional hydrophobic pockets within the binding site of CECR2 and BRD9. Genentech and Constellation Pharmaceuticals also demonstrated that each of these interactions could be favoured

with a specific acetylated Lys methyl mimetic and have developed selective inhibitors for TAF1(2) (**2.017**),[157] CECR2 (**2.091**)[194] and BRD9 (**2.092**)[195] using this methodology (**Figure 2.36**).

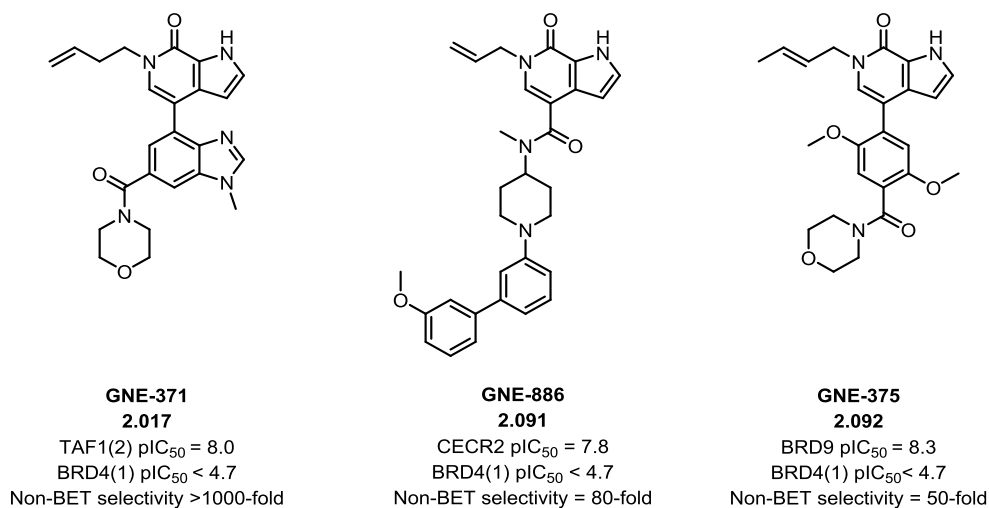| GNE-371	GNE-886	GNE-375
2.017	**2.091**	**2.092**
TAF1(2) pIC_{50} = 8.0	CECR2 pIC_{50} = 7.8	BRD9 pIC_{50} = 8.3
BRD4(1) pIC_{50} < 4.7	BRD4(1) pIC_{50} < 4.7	BRD4(1) pIC_{50}< 4.7
Non-BET selectivity >1000-fold	Non-BET selectivity = 80-fold	Non-BET selectivity = 50-fold

Figure 2.36: Structure of selective TAF1(2) (2.017), CECR2 (2.091) and BRD9 (2.092) inhibitors.

Inspired by the selectivity profile of **2.017** (discussed in **Section 2.2**), in part due to the butenyl acetylated Lys methyl mimetic, it was postulated that similar results could be observed on the naphthyridinone scaffold. Comparison of the X-ray crystal structure of **2.022** (an example naphthyridinone compound) and **2.017** revealed similar vectors for both methyl mimetics (**Figure 2.37**), suggesting this might be possible.
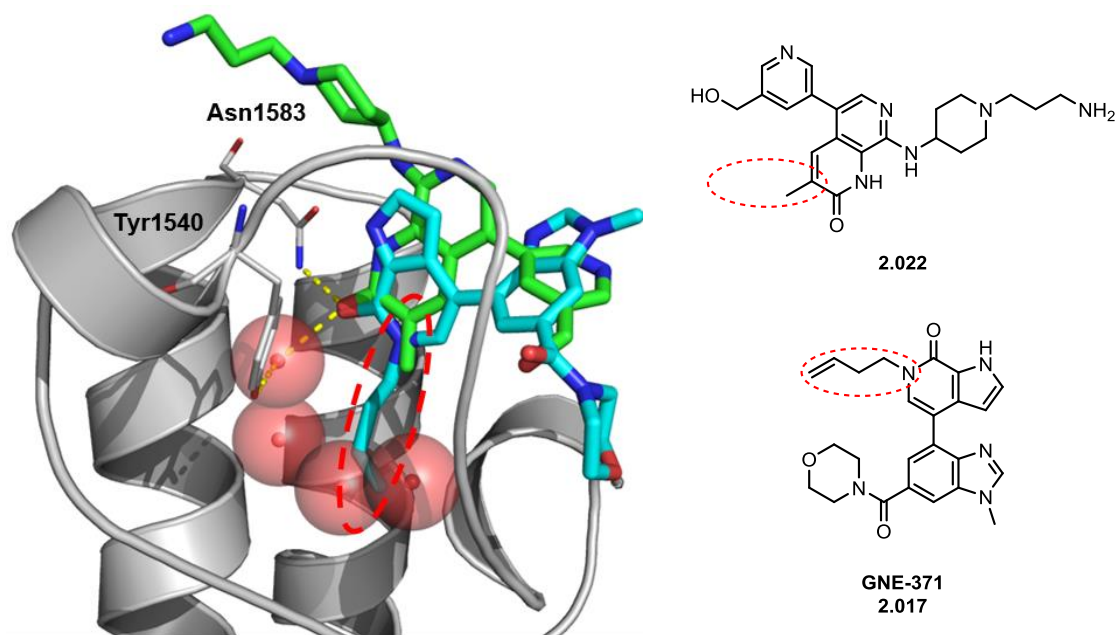
Figure 2.37: Overlay of the crystal structures of 2.022 (shown in green) (GSK internal X-ray crystal structure) and 2.017 (shown in cyan) (PDB:6DF7) bound to TAF1(2) (shown in grey), highlighting the similar methyl mimetic vectors. Acetylated Lys methyl mimetics highlighted with red dashed boxes.

Consequently, compound **2.093** was designed to test this hypothesis (**Figure 2.38**). Additionally, it was hypothesized that incorporation of the butenyl group would likely increase the lipophilicity of the molecule, potentially boosting the permeability of the series further.
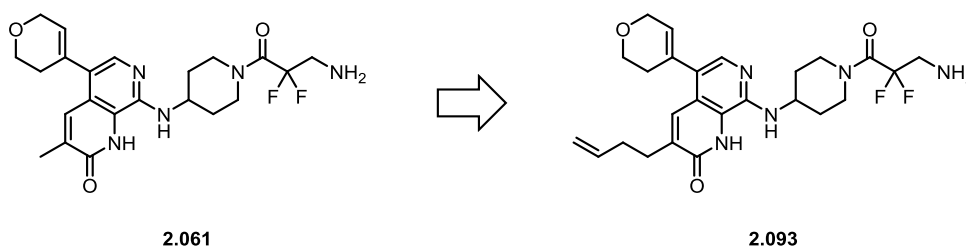

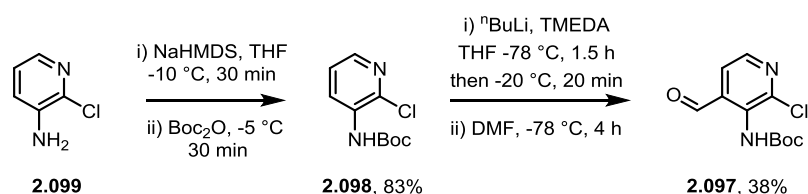**Figure 2.38: Compound 2.061 and proposed butenylated derivative 2.093.**

2.8.1 Synthesis of Butenylated Intermediate 2.094

Retrosynthetic analysis of intermediate **2.094** identified a route to install the butenyl group at an early stage (**Scheme 2.20**). Key intermediate **2.094** could be synthesized from α,β-unsaturated ester **2.095** which in turn could be accessed from the Boc protected derivative **2.096**. Compound **2.096** could be made from aldehyde **2.097** *via* an olefination reaction which in turn could be synthesized *via* Boc protection and carbonylation of **2.099**. A similar set of reactions was previously used to synthesize compound **2.027** (**Section 2.4.3**).[162]

2.094   **2.095**   **2.096**

2.097   **2.098**   **2.099**
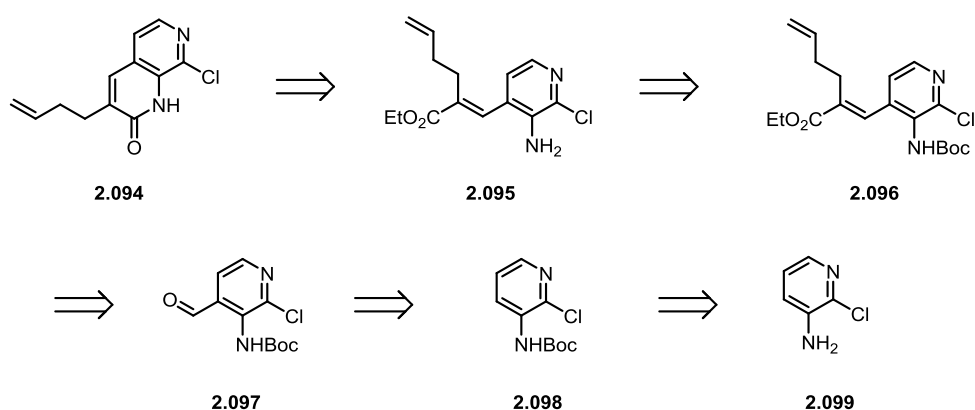
Scheme 2.20: Retrosynthetic route to butenyl intermediate 2.094 from commercially available aminopyridine 2.099.

Commercially available amino pyridine **2.099** was Boc protected under standard conditions to deliver **2.098** in 83% yield (**Scheme 2.21**). Formylation using a directed *ortho* lithiation followed by DMF quenching produced aldehyde **2.097** in 38% yield. Although formylation was expected at the 4-position, the desired regiochemistry was confirmed *via* ^{1}H NMR spectroscopy which agreed with literature spectra.[162] With aldehyde **2.097** in hand, attention was turned to the olefination step.

i) NaHMDS, THF
-10 °C, 30 min

ii) Boc$_2$O, -5 °C
30 min

i) ^{n}BuLi, TMEDA
THF -78 °C, 1.5 h
then -20 °C, 20 min

ii) DMF, -78 °C, 4 h

2.099   **2.098**, 83%   **2.097**, 38%

Scheme 2.21: Synthesis of aldehyde 2.097 from commercially available 2.099.

2.8.1.1 Synthetic Route 1: Horner-Wadsworth-Emmons Olefination

The desired butenyl Horner-Wadsworth-Emmons (HWE) reagent (**2.101**) was synthesized in 70% yield *via* alkylation of **2.100** with butenyl bromide (**Scheme 2.22**). Aldehyde **2.097** was then reacted with **2.101** in an HWE reaction to produce **2.096** in 58% yield. A Boc deprotection under standard conditions delivered free amine **2.095** in 83% yield. A DBU-mediated double bond geometry isomerization enabled a dynamic equilibrium between the *E* and *Z* geometric isomers, the latter of which could spontaneously cyclise to form naphthyridinone **2.094**.[162] Unfortunately, a ~1:1 mixture of regioisomers **2.094** and **2.102** was observed, both in reduced yield due to difficulties separating. It was hypothesized that the more substituted double bond in **2.102** and the extended conjugated system both favoured the formation of **2.102** as the more thermodynamically stable product.
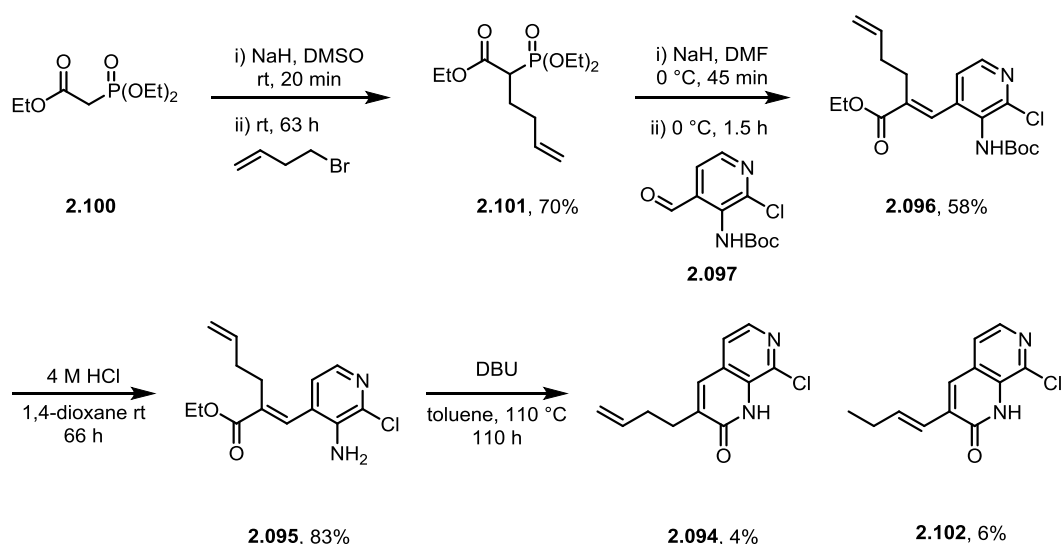
Scheme 2.22: Synthesis of regioisomers 2.094 and 2.102.

To confirm this hypothesis, a conformational search of both regioisomers was conducted using an OPLS3 force field (with the help of Lucia Fusani)[196] and the relative energy of each conformation calculated using density functional theory (B3LYP) quantum mechanics (with the help of Lucia Fusani).[197] As predicted, the conformations calculated for regioisomer **2.102** were all shown to be lower in energy than those of **2.094** by ≥5 kcal/mol (**Table 2.22**), confirming **2.102** as the more thermodynamically stable product.
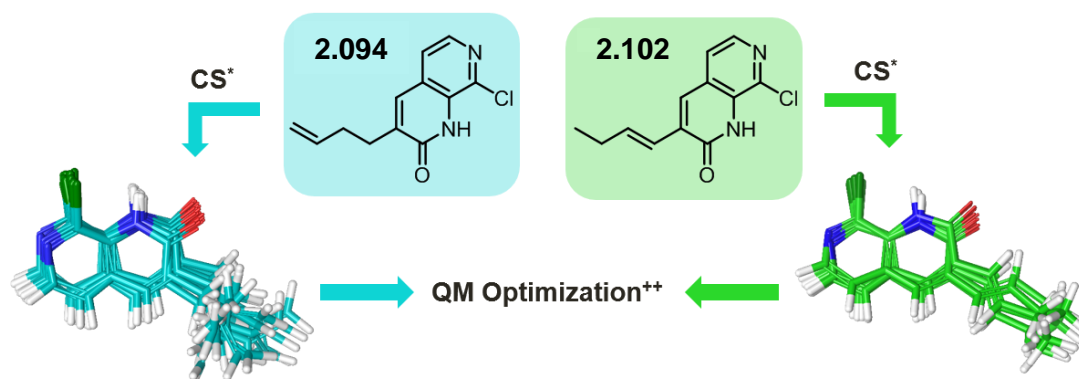
Regioisomer	Solution Phase Relative Energy (kcal/mol)
2.102	0
2.102	0.037
2.102	0.198
2.102	0.211
2.102	0.240
2.102	0.525
2.102	0.603
2.094	6.036
2.094	6.201
2.094	6.235
2.094	6.384
2.094	6.408
2.094	6.737
2.094	6.885
2.094	7.023
2.094	7.424
2.094	7.532
2.094	7.536
2.094	7.871
2.094	8.094

Table 2.22: Solution phase relative energies for each conformation adopted by regioisomers 2.094 and 2.102. *Conformational Search (Macromodel): OPLS3 FF, Energy Window for saving structures = 5.02 kcal/mol. ++Optimization (Jaguar): QM method: DFT(B3LYP) QM basis: 6-3G1. Figure used with permission of Lucia Fusani.

To probe the formation of regioisomer **2.102**, compound **2.094** was stirred at 110 °C in toluene with and without DBU (**Scheme 2.23**). In the absence of DBU, no isomerization occurred and only regioisomer **2.094** was observed, suggesting DBU was actively responsible for the isomerization of the double bond. This was confirmed where, in the presence of DBU, compound **2.094** isomerized to a 1:1 mixture of **2.094** and **2.102**.
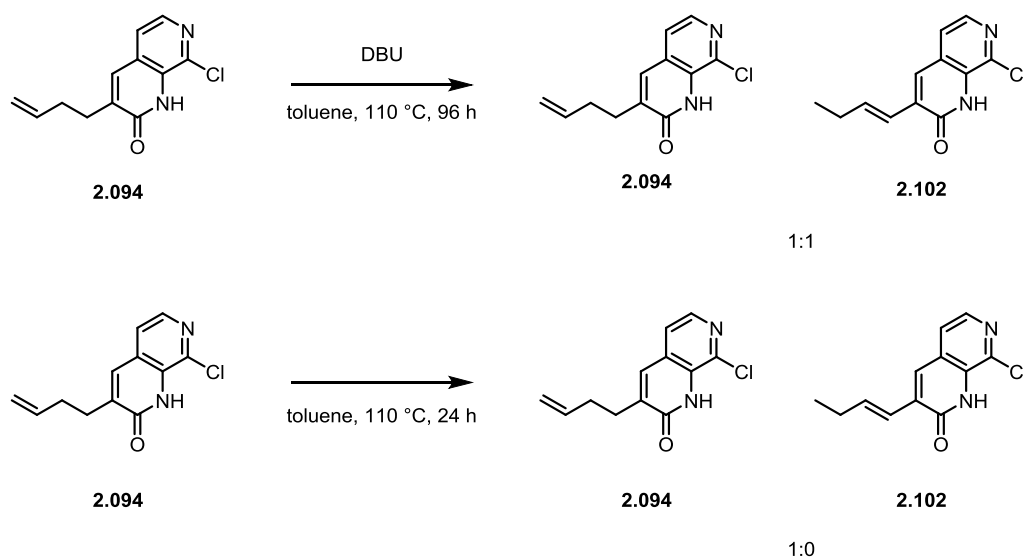

Scheme 2.23: Investigations into the formation of regioisomer 2.102.

In an attempt to avoid the isomerization of the double bond and form regioisomer **2.094** exclusively, a variety of other activating nitrogen/phosphorus nucleophiles were trialed.[198] DABCO, DMAP, NMe$_3$ and PPh$_3$ were all tested and showed no conversion of **2.095** to the desired product **2.094**, suggesting DBU was crucial to cyclisation. It was therefore hypothesized that the double bond could be masked for the cyclisation step and then revealed at a later stage.

2.8.1.2 Synthetic Route 2: Masked Alkene

An acetal group was chosen to test this hypothesis which could be converted to the alkene at a later stage *via* hydrolysis and olefination. Pleasingly, the acetal derivative HWE reagent could be prepared in 76% yield from **2.100** (**Scheme 2.24**). Reaction with aldehyde **2.097** gave a 4:1 (*E:Z*) mixture (estimated *via* LCMS UV area/area ratio) of both diastereomers of **2.104** in 40% yield. The mixture of diastereomers was then

Boc deprotected under standard conditions and cyclized with DBU to yield **2.106** in 92% over the two steps. The next step of the synthesis, a benzyl protection, was then tested and showed a dramatic drop in chemoselectivity towards *O* vs *N*-alkylation, resulting in a poor yield of **2.107**.
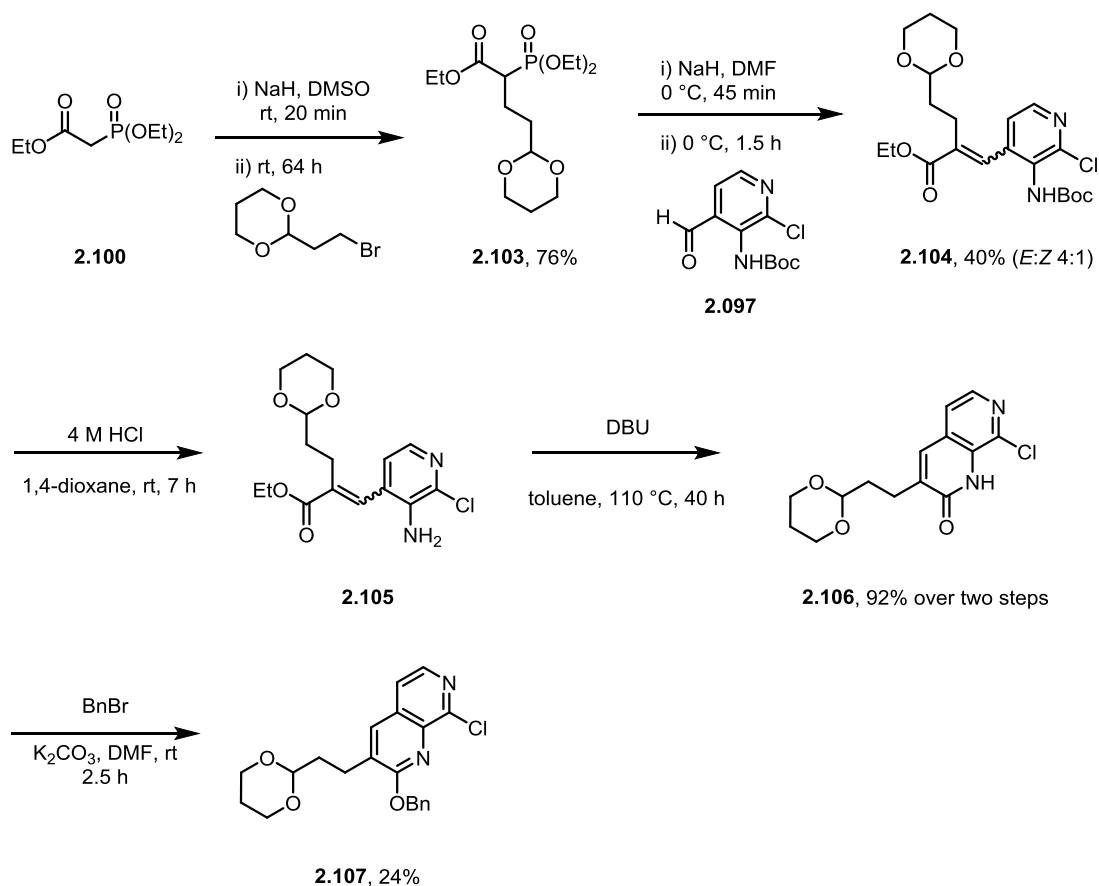
Scheme 2.24: Synthesis of acetal intermediate 2.107.

It was hypothesized that introduction of the 6-membered acetal ring disfavours *O*-alkylation *via* steric hindrance around the oxygen atom. Due to the poor yielding protection step, and the additional two steps that would be required to reveal the alkene, this route was abandoned.

2.8.1.3 Synthetic Route 3: Still-Gennari Olefination

Attention was turned instead to the diastereoselective formation of the *Z*-alkene **2.108** (**Scheme 2.25**). Upon Boc deprotection, **2.108** could spontaneously cyclize, removing the need for DBU and preventing isomerization. It was hypothesized that *Z*-alkene

2.108 could be synthesized *via* a Still-Gennari[199] or Ando[200] variation of the HWE reaction.
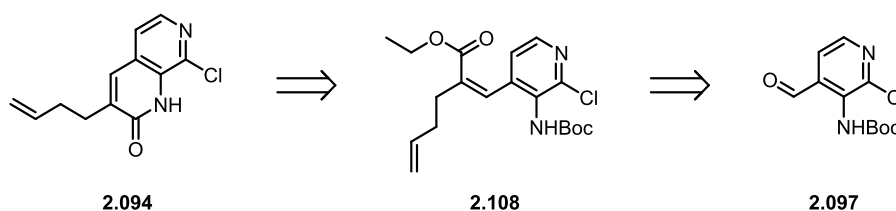
Scheme 2.25: Retrosynthetic route to butenyl intermediate 2.094 *via Z*-alkene 2.108.

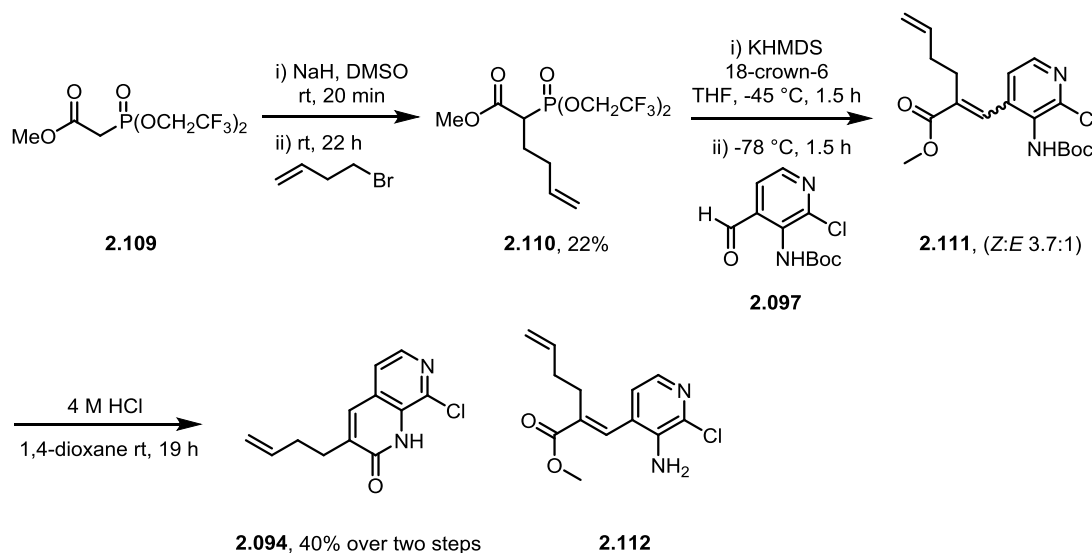Butenyl Still-Gennari reagent **2.110** was synthesized *via* alkylation of **2.109** with butenyl bromide (**Scheme 2.26**). Upon isolation, a poor conversion to **2.110** was observed resulting in 22% yield of **2.110** and **2.109** being recovered in 42% yield. **2.110** was then reacted with aldehyde **2.097** using KHMDS as a base. Additionally, cyclic ether 18-crown-6 was used to sequester the potassium counterion, favouring dissociative conditions and disfavouring reversibility. α,β-Unsaturated ester **2.111** was synthesized as a 3.7:1 *Z:E* mixture (estimated *via* LCMS UV area/area ratio) of inseparable diastereomers. Boc deprotection under standard conditions followed by spontaneous cyclisation produced intermediate **2.094** in 40% yield over two steps, which could be separated *via* silica chromatography from *E*-diastereomer (**2.112**).

Scheme 2.26: *Z*-Diastereoselective synthesis of key intermediate 2.094 using Still-Gennari reagent 2.110.

2.8.1.4 Synthetic Route 4: Ando Olefination

The diphenyl 'Ando reagent' (**2.114**) was prepared from diphenyl phosphonate (**2.113**) and ethyl 2-bromoacetate in 23% yield (**Scheme 2.27**). Butenyl functionalization at the α-position was achieved *via* alkylation using butenyl bromide and NaH. Due to the poor conversion seen during the synthesis of butenyl Still-Gennari reagent **2.110** (**Scheme 2.26**), the alkylation step was heated to 45 °C and yielded **2.115** in 61% yield. **2.115** was then reacted with aldehyde **2.097** under the dissociative Still-Gennari conditions discussed above producing a 1.9:1 *Z:E* mixture of diastereomers (**2.116**) (estimated *via* LCMS UV area/area ratio). Boc deprotection followed by spontaneous cyclisation produced desired intermediate **2.094** in 47% over two steps.
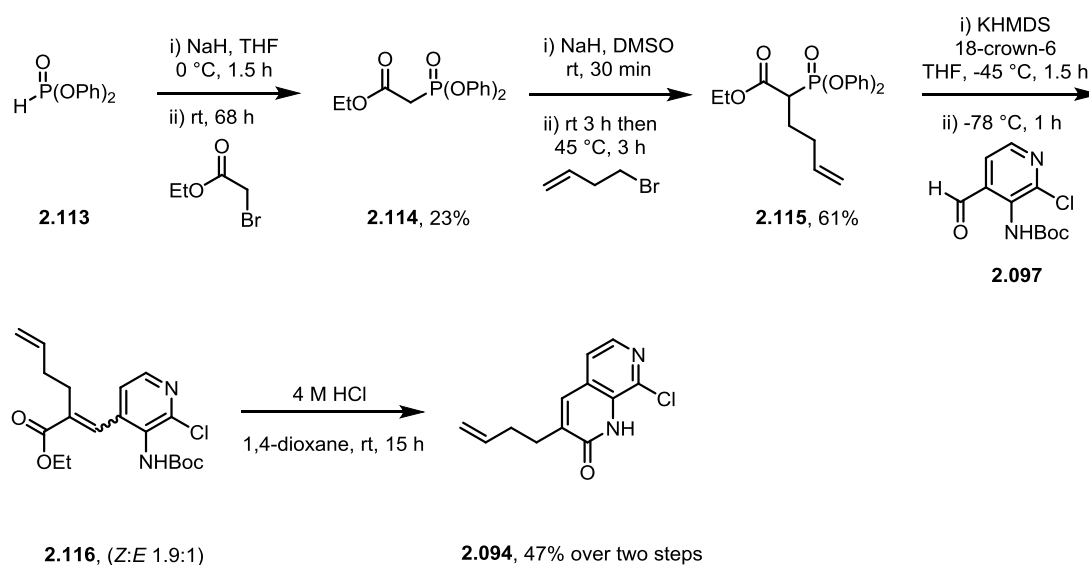
Scheme 2.27: *Z*-Diastereoselective synthesis of 2.094 using Ando reagent 2.115.

2.8.2 Butenylated Compound 2.093: Synthesis

Due to higher *Z*-diastereoselectivity, and requiring one step fewer, the Still-Gennari route was progressed forward. Key intermediate **2.094** was then *O*-benzyl protected yielding **2.117** in 87% (**Scheme 2.28**). A subsequent Buchwald-Hartwig amination yielded intermediate **2.118** in 90%, which was then brominated under standard conditions to give **2.119**. A Suzuki cross-coupling was utilized to attach the DHP group, delivering compound **2.120** in 65% yield. Compound **2.120** was then treated with TFA under refluxing conditions to remove both the benzyl and Boc protecting groups in a 35% yield. An amide coupling with the desired carboxylic acid (**2.063**) followed by Boc deprotection delivered final compound **2.093**. Difficulties isolating the

purified products **2.121**, **2.122** and **2.093** (due to poor solubility) was reflected in the poor yields obtained, despite good conversions being observed *via* LCMS.
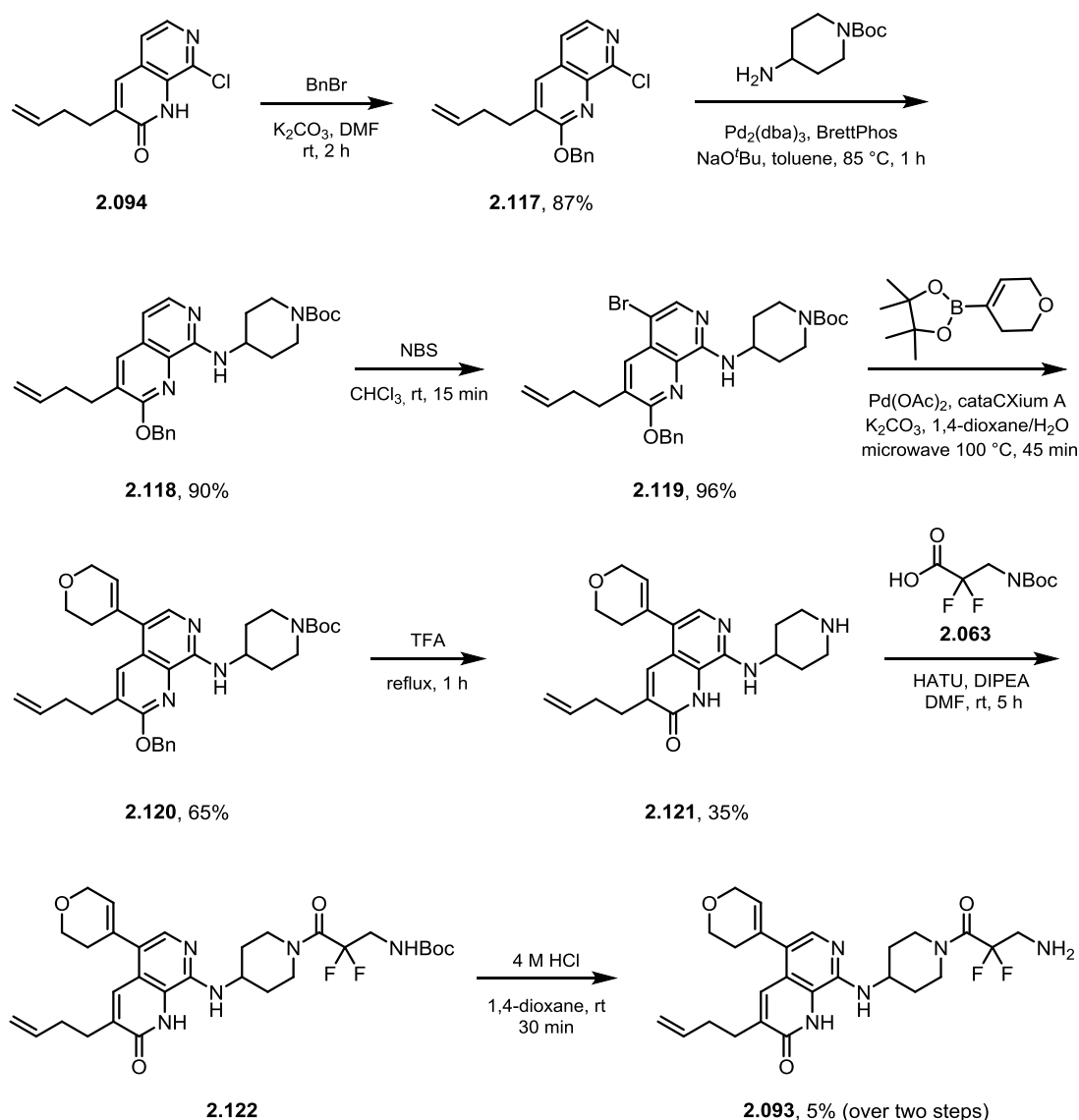
Scheme 2.28: Synthesis of 2.093 from key intermediate 2.094.

2.8.3 Butenylated Compound 2.093: Results and Discussion

Compound **2.093** was first screened against the DiscoverX BROMO*scan* panel at 10 µM to gain an insight into the selectivity profile (**Figure 2.39** and **Table 2.23**). Pleasingly, compound **2.093** appeared selective for TAF1(2) at 10 µM, showing >90% inhibition for TAF1(2) and BRD4(2) only. Additionally, 20/21 of the other non-BET bromodomains (excluding highly homologous TAF1L(2)) showed <50% inhibition at 10 µM, including **2.061**'s closest off-target BRD9.
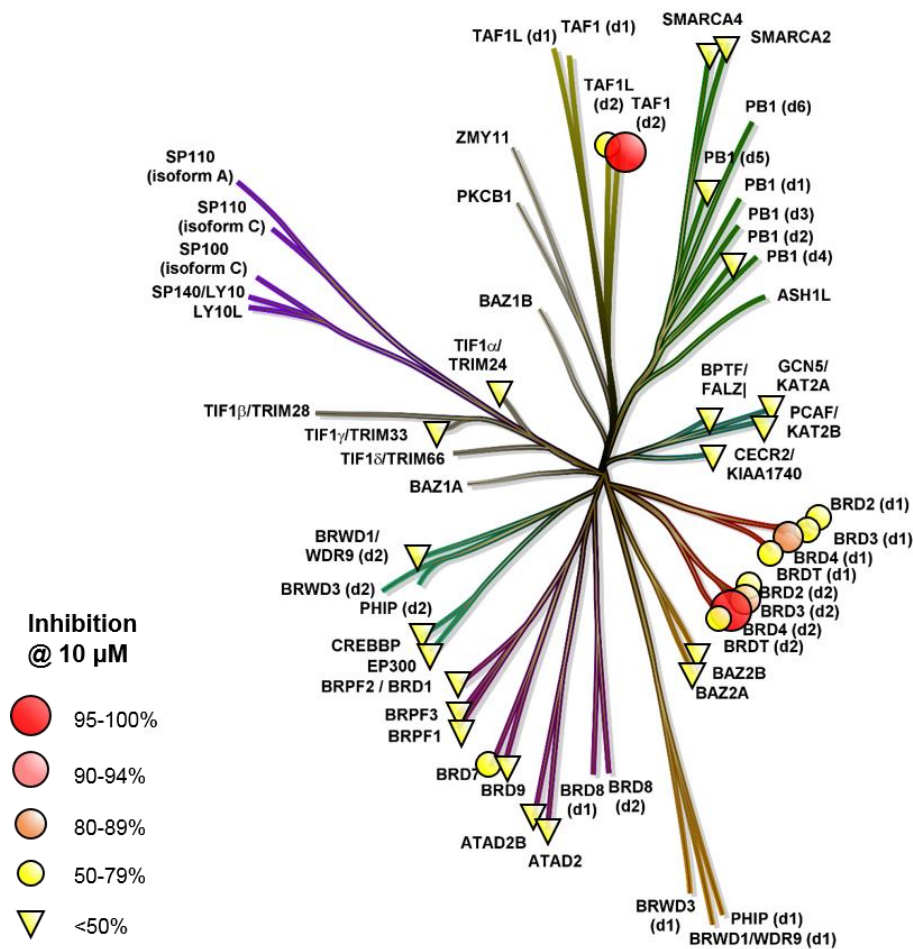
Figure 2.39: Phylogenetic tree inhibition plot of compound 2.093 screened at 10 µM against the DiscoverX BROMO*scan* panel. Data shown in Table 2.23.

Compound Number	ATAD2A	ATAD2B	BAZ2A	BAZ2B	BRD1	BRD2(1)	BRD2(2)	BRD3(1)	BRD3(2)	BRD4(1)	BRD4(2)	BRD7	BRD9	BRDT(1)	BRDT(2)	BRPF1
2.093	0	1	24	0	28	60	73	63	85	88	97	57	9	73	52	27

Compound Number	BRPF3	CECR2	CREBBP	EP300	FALZ	GCN5L2	PB1(2)	PB1(5)	PCAF	SMARCA2	SMARCA4	TAF1(2)	TAF1L(2)	TRIM24	TRIM33	WDR9(2)
2.093	0	21	0	8	13	6	37	0	15	22	36	100	66	6	5	8

Table 2.23: Percentage inhibition of bromodomains tested at 10 µM (DiscoverX BROMO*scan* single-shot assay) for 2.093.

Follow up 11-point dose-response curves were then obtained to quantify potency against TAF1(2), BRD4(1) and BRD4(2) (**Figure 2.40**). Compound **2.093** displayed a reduced potency at TAF1(2) (pK_D = 6.7), falling below the desired threshold for a TAF1/TAF1L chemical probe. Although the butenyl methyl mimetic appeared to show an improved selectivity profile, the substantial reduction in potency against TAF1(2) prevented confirming this quantitatively. The selectivity profile observed at 10 µM and the measured pK_D values suggested that whilst the butenyl methyl mimetic was not well tolerated in other bromodomains, it was also not optimal for TAF1(2) on this series. Additionally, as predicted, introduction of the butenyl chain did provide the expected increase in permeability.
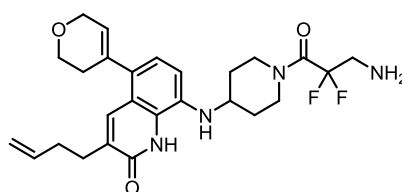
2.093
TAF1(2) pK_D = 6.7
BRD4(1)/(2) pK_D <5.0/<5.0
AMP (nm/s) = 176
CAD Sol. (µg/mL) = 28
ChromLogD = 3.90

Figure 2.40: Compound 2.093 potency and physicochemical profile. CAD solubility, AMP and ChromLogD measurements were all performed at pH$_{7.4}$.

Unfortunately, the necessity to install the alkyl chain at the beginning of the synthesis, prevented further exploration and optimization of this methodology. However, inspired by the perceived dramatic change in selectivity profile of **2.093**, an alternative template was pursued to investigate the methodology further.

Evaluation of the GSK compound database led to BRD7/9 inhibitor **2.123** being identified as a suitable template for further investigation (**Table 2.24**). Compound **2.123** possessed many of the desired criteria for a BRD7/9 chemical probe (discussed in **Section 1.5**), shown in **Table 2.24**, yet was restricted in its potential use as a BRD7/9 chemical probe by poor non-BET bromodomain selectivity, in particular against BRPF1.
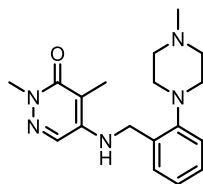
	2.123	Chemical probe requirements
BRD7/9 pK$_D$	7.6/7.4	≥7.0
BRD4(1) pK$_D$ (selectivity)	≥×630	≥×100
BRPF1 pK$_D$ (selectivity)	6.6 (×6)	≥×30
Other non-BET selectivity	×50	≥×30
AMP (nm/s)	330	
CLND Sol. (µg/mL)	178	

Table 2.24: Selectivity and physicochemical profile of 2.123 compared to the requirements of a chemical probe. CAD solubility, AMP and ChromLogD measurements were all performed at pH$_{7.4}$.

The conserved water network found within the binding pocket of major off-target BRPF1 was calculated by Biggin *et al.* to possess the highest free energy score (ΔG_{netw} = -4.4 kcal mol^{-1}) (**Section 2.7**, **Figure 2.35**).[185] It was therefore hypothesized that conserved water interactions could be used to improve selectivity over BRPF1 and non-BET bromodomain selectivity in general, producing a novel chemotype BRD7/9 chemical probe for pre-clinical target validation. This is the subject of the work discussed in **Section 3**.

2.9 Conclusions & Future Work

2.9.1 Conclusions

Lead compound **2.021** was selected as a starting point in the development of a novel chemical probe for TAF1/TAF1L. Statistical analysis and medicinal chemistry knowledge were used to drive the permeability optimization of **2.021** *via* iterative design hypotheses. More specifically, regression modelling was used to highlight a strong dependence between permeability and basicity of the propylamine nitrogen. A series of compounds were prepared to reduce the basicity of **2.021**. Introduction of

geminal fluorine atoms to the propylamine chain resulted in compounds **2.060** and **2.061**, the first permeable compounds produced within the series (AMP = 220 nm/s and 62 nm/s respectively). Disruption of a crucial salt bridge interaction with Asp1539 for compound **2.060**, and an accompanying drop in potency, was recovered *via* rigidification of the propylamine chain (**2.061**). Compound **2.061**'s behaviour within cells was then explored through the use of an intracellular concentration assay, and preliminary work into its PK properties undertaken. Finally, X-ray crystallography guided the design of two negative control compounds which were then triaged based on predicted metabolic stability.

Compounds **2.061** and **2.080** (**Figure 2.41**) offer two complementary novel chemotype tool molecules for the TAF1/TAF1L tool box. Compound **2.061** demonstrates excellent potency for TAF1(2) (pK_D = 9.1) and is the first selective TAF1/TAF1L inhibitor with an accompanying negative control, offering new levels of confidence for phenotypic assignment. Used in conjunction with other high quality TAF1/TAF1L probes, compounds **2.061** and **2.080** will hopefully aid the scientific community in the elucidation of the biological role of the TAF1/TAF1L bromodomains.

2.061
TAF1(2) pK_D = 9.1
BET selectivity = 1000-fold
Non-BET selectivity = 50-fold
CAD Sol. (µg/mL) = 24
AMP (nm/s) = 62

2.080
TAF1(2) pK_D = 5.4
CAD Sol. (µg/mL) = 32
AMP (nm/s) = 76

Figure 2.41: TAF1/TAF1L chemical probe 2.061 and accompanying negative control 2.080. CAD solubility, AMP and ChromLogD measurements were all performed at pH$_{7.4}$.

Inspired by the selectivity profile of **2.017**, the concept of selectivity through conserved water interactions was then explored for the series. A diastereoselective synthesis was utilized to overcome synthetic challenges and ultimately deliver compound **2.093**. Despite appearing highly selective for TAF1(2), reductions in potency suggested that the butenyl acetylated Lys methyl mimetic was suboptimal for this template and would

require further optimization. Due to synthetic complexity, investigation of bromodomain selectivity through conserved water interactions on this template was not explored.

2.9.2 Future Work

As discussed, an effective chemical probe (**2.061**) and an accompanying negative control were developed for the TAF1/TAF1L (**2.061**) bromodomains. Although compound **2.061** appears permeable in both AMP and intracellular concentration assays, future work should focus around demonstrating activity within a cellular assay, such as NanoBRET, or *via* FRAP. Additionally, further profiling into compound **2.061**'s selectivity would provide valuable characterization for the scientific community.

Future work could also provide a more in-depth exploration of conserved water interactions and their application to the template. Compound **2.093** showed potential for the methodology, but challenging synthesis prevented further exploration. To facilitate a more thorough investigation, future work could focus around late stage functionalization of a key intermediate and the introduction of different acetylated Lys methyl mimetics.

Finally, as has been demonstrated with other non-BET bromodomains, inhibition of the bromodomain region is not always sufficient to elicit a therapeutically relevant phenotypic response.[132–134] As a result, investigations into bifunctional TAF1/TAF1L tools, such as bivalent inhibitors and PROTACs, could be particularly valuable. Provided the salt bridge interaction to Asp1539 can be maintained, the primary amine appears by X-ray crystallography to be solvent exposed and a suitable vector for linker attachment. An example TAF1 bivalent inhibitor (**2.124**) and PROTAC (**2.125**) are shown below (**Figure 2.42**) as potential start points, although optimization of linker length (circled in red) and E3 ligase binder (circled in blue) would likely be required.
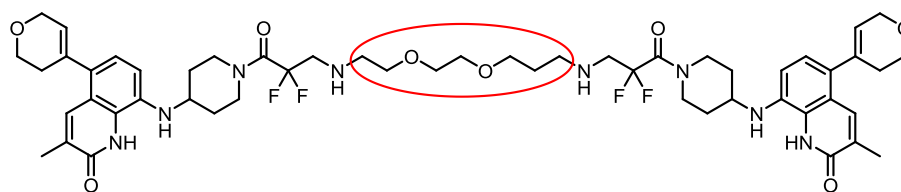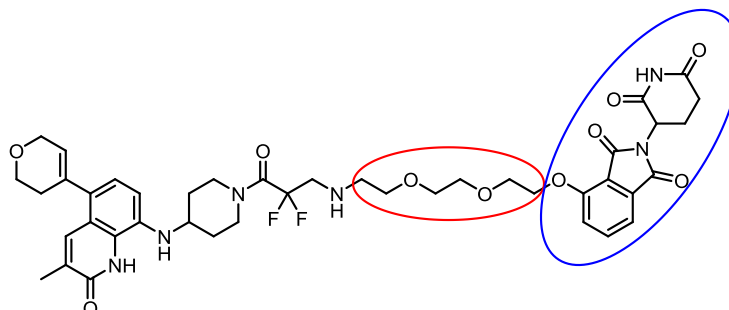
Figure 2.42: Structures of hypothetical bivalent TAF1 inhibitor 2.124 and TAF1/TAF1L PROTAC 2.125.

116

3. Designing a Chemical Probe for BRD7/9

3.1 BRD7/9 as Therapeutic Targets

BRD7/9 are bromodomain containing proteins consisting of 651 and 597 amino acids respectively. Both proteins are comprised of a bromodomain region (BD) and a domain currently of unknown function (DUF) (**Figure 3.01**).
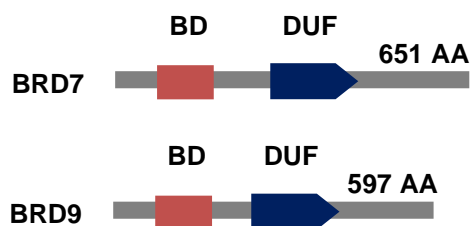

Figure 3.01: Schematic diagram of BRD7 and BRD9, highlighting their bromodomains (BD) and domains of unknown function (DUF).[201,202]

Despite similar structures, BRD7/9 share only 36% residue similarity across the whole protein. A much greater homology (76%) is, however, seen across the bromodomains of BRD7/9 (**Table 3.01**), making the selective targeting of each bromodomain more challenging.

BRD7	BRD9	Comment
Ala154	Gly43	WPF motif
Phe155	Phe44	WPF motif
Phe156	Phe45	WPF motif
Ser157	Ala46	ZA channel
Phe158	Phe47	ZA channel
Pro159	Pro48	ZA channel
Val160	Val49	ZA channel
Thr161	Thr50	ZA loop
Asp162	Asp51	ZA loop
Phe163	Ala52	ZA loop
Ile164	Ile53	ZA loop
Ala165	Ala54	ZA loop
Tyr168	Tyr57	Water-binding Tyr
Ser169	Ser58	
Ile172	Ile61	
Met203	Met92	
Asn206	Asn95	
Ala207	Ala96	Conserved Ala
Tyr210	Tyr99	Conserved Tyr
Asn211	Asn100	Conserved Asn
Thr215	Thr104	
Ile216	Val105	
Tyr217	Tyr106	Gatekeeper
Tyr218	Tyr107	
Lys219	Lys108	
Ala220	Leu109	
Ala221	Ala110	

Table 3.01: The amino acid sequence for BRD7/9 acetyl Lys binding pockets highlighting sequence similarity. Identical residues shown in green, and different residues shown in red.[51]

BRD7 and BRD9 have been implicated in the mammalian chromatin remodeling complexes BAF and PBAF, respectively, two of the most frequently mutated complexes in cancer malignancies.[203,204] As a result, BRD7 and BRD9 are attractive targets in the pursuit of anti-cancer agents.[205]

Hepatocellular carcinoma (HCC) sequencing studies have revealed chromatin-regulatory enzymes, such as BRD9, as particularly prevalent in HCC.[206] Additionally,

a genome-wide CRISPR-Cas9 screen has identified BRD9 as a specific genetic vulnerability associated with rhabdoid tumours, typically found in young children and are most commonly caused by mutation in the SMARCB1 gene. Reduction in SMARCB1 has been shown to cause increased incorporation of BRD9, and has identified a BRD9-containing SWI/SNF subcomplex as crucial for the survival of SMARCB1-mutant rhabdoid tumours.[207]

BRD7 is involved in the pathways of two quintessential tumour suppressors, p53 and BRCA1,[208,209] with expression of BRD7 downregulated in multiple cancers.[210] These include nasopharyngeal carcinoma,[211] colorectal carcinoma,[212] endometrial carcinoma,[213] breast cancer,[214] ovarian cancer,[214] prostate cancer[215] and glioma.[216]

To help divulge the roles that BRD7 and BRD9 (in particular their bromodomain regions) play within these diseases, multiple groups have sought to design chemical probes for their target validation.

3.2 Current BRD7/9 Inhibitors

In 2015 the SGC and the University of Oxford reported the first micromolar BRD7/9 bromodomain inhibitor, LP99 (**3.002**),[217] optimized from initial hit compound **3.001** *via* structure-based design (**Figure 3.02**). BRD9 potency was attributed to functionalization of the pendant aminopiperidinone nitrogen to optimize hydrophobic interactions with Phe47 and hydrogen bonding to Gly43. Compound **3.002** showed potency for BRD9 (pK_D = 7.0) and appeared selective by DSF against 46 other bromodomains (all <1 °C at 10 μM). Activity within FRAP (0.8 μM) and NanoBRET assays (pIC_{50} = 5.3) provided evidence of target engagement. Finally, the enantiomer of **3.002** appeared inactive against BRD9 by ITC, functioning as a suitable negative control.
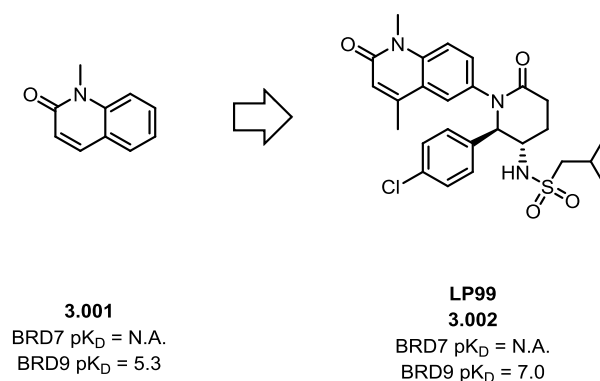
3.001
BRD7 pK$_D$ = N.A.
BRD9 pK$_D$ = 5.3

LP99
3.002
BRD7 pK$_D$ = N.A.
BRD9 pK$_D$ = 7.0

Figure 3.02: BRD7/9 Inhibitor LP99 and initial hit compound 3.001. pK$_D$ values refer to potency measured by ITC.

Since the initial disclosure of **3.002**, numerous BRD7/9 chemical probes have been developed spanning multiple chemotypes, although an unsaturated bicyclic system is common throughout. I-BRD9 (**3.004**) was discovered by GSK and the University of Strathclyde with nanomolar potency for BRD9 (pK$_D$ = 8.7) and was the first inhibitor to display selectivity over BRD7 (200-fold) (**Figure 3.03** & **3.04**).[51] Compound **3.004** was optimized from thienopyridone cross-screen hit **3.003** *via* X-ray crystallography driven structure-based design. Introduction of a basic amidine moiety, to exploit the polarity differences between BRD9 and BRD4, provided the desired selectivity over the BET bromodomains (700-fold). Profiling against other non-BET bromodomains revealed ≥70-fold selectivity and (surprisingly) 200-fold selectivity over BRD7. Although no BRD7 crystal structure is available to rationalize the observed selectivity, it is hypothesized that residue differences within the ZA channel are responsible. Selectivity against a panel of 49 pharmacological targets was also investigated with no activity at less than 5 µM observed. Finally, evidence of target engagement was shown *via* activity within a NanoBRET cellular assay (pIC$_{50}$ = 6.8) supporting the application of **3.004** as a chemical probe for the BRD9 bromodomain.
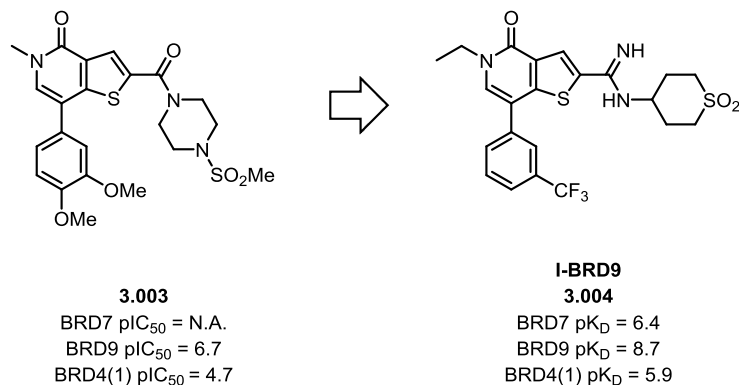
3.003
BRD7 pIC_{50} = N.A.
BRD9 pIC_{50} = 6.7
BRD4(1) pIC_{50} = 4.7

I-BRD9
3.004
BRD7 pK_D = 6.4
BRD9 pK_D = 8.7
BRD4(1) pK_D = 5.9

Figure 3.03: BRD9 chemical probe I-BRD9 and initial hit compound 3.003. pIC_{50} values refer to potency in TR-FRET assays. pK_D values refer to activity in the DiscoverX BROMO*scan* assay.
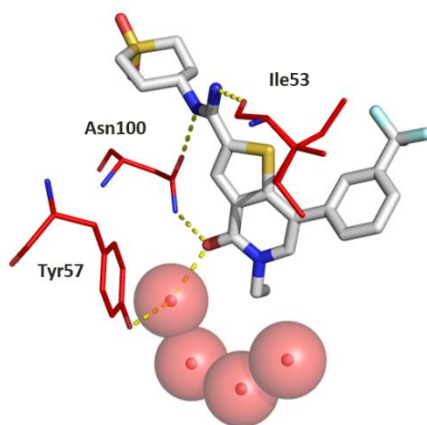

Figure 3.04: Crystal structure (PDB: 4UIW) of 3.004 (grey) bound to human bromodomain BRD9 (red).

Collaborative work between the SGC and Boehringer Ingelheim led to the development of BI-9564 (**3.006**), an *in vivo* capable, potent and selective probe for both BRD7 and BRD9 (**Figures 3.05** & **3.06**).[218] A fragment-based screening approach utilizing a DSF assay to identify initial hits, such as **3.005**, was followed by structure guided design, leading to dual BRD7/9 inhibitors **3.006** and **3.007**. Compound **3.006** displayed potency for BRD9 (pK_D = 8.2) and BRD7 (pK_D = 7.1), and selectivity over the BET subfamily (BRD4(1) pK_D <5.0), as measured by DiscoverX BROMO*scan* assays. Excluding CECR2 (pK_D = 7.1), **3.006** was also shown to be selective against the remaining non-BET bromodomains showing no activity by ITC

121

at the concentrations tested. The cellular activity of **3.006** was demonstrated at 1 μM in a FRAP assay using a green fluorescent protein-BRD9 fusion protein expressed in U2OS cells. Compound **3.006** was also screened against 55 G-protein-coupled receptors (GPCRs) and 324 kinases with only 2 GPCRs and 3 kinases showing >40% inhibition at 10 μM. Additionally, the ability of **3.006** to function as an *in vivo* tool is supported by acceptable aqueous solubility (>90 μg/mL) and permeability (Caco2 P_{app} = 110 nm/s), and suitable PK parameters within a mouse model following intravenous delivery. Likewise, **3.007** displayed subnanomolar potencies for BRD7 (pK_D = 9.5) and BRD9 (pK_D = 9.1) with selectivity over the BET subfamily (BRD4(1) pK_D < 5.0) as demonstrated by the DiscoverX BROMO*scan* assay. Again, **3.007** appeared selective against the remaining non-BET bromodomains (>30-fold) with potency also observed for CECR2 (pK_D = 8.1). Compound **3.007** was also shown to engage both BRD7 and BRD9 with 100% inhibition at 1 μM in FRAP assays, demonstrating target engagement and cellular permeability (Caco2 P_{app} = 14 nm/s), and is accompanied by suitable PK parameters within a mouse model following intravenous delivery. Finally, **3.006** and **3.007** are accompanied by negative control BI-6354 (**3.008**), although it should be acknowledged that the substantial structural differences may give rise to different off-targets.[219]
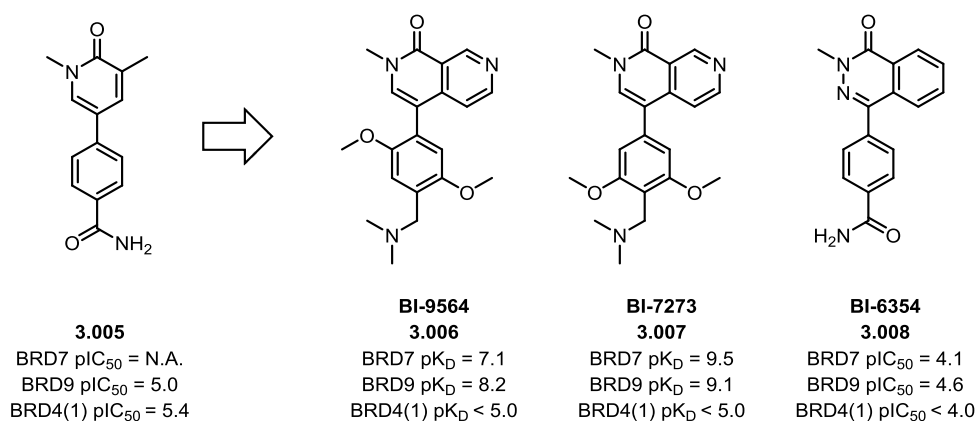

Figure 3.05: Structure of BRD7/9 chemical probe 3.006 and 3.007, accompanying negative control 3.008 and initial hit compound 3.005. pIC_{50} values refer to potency in AlphaScreen assays. pK_D values refer to potency in the DiscoverX BROMO*scan* assay.
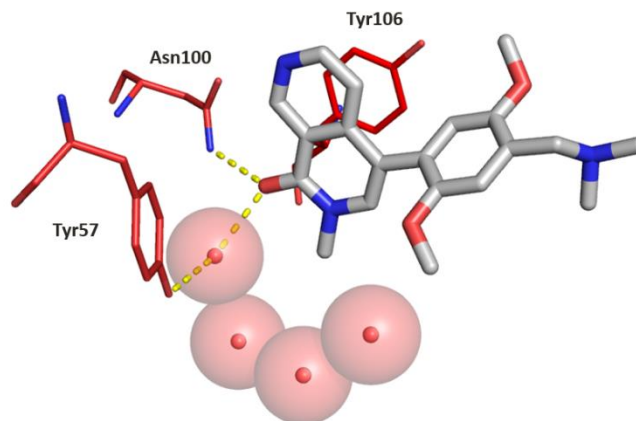
Figure 3.06: Crystal structure (PDB: 5F1H) of 3.006 (grey) bound to human bromodomain BRD9 (red).

TP-472 (**3.009**), another potent and selective BRD7/9 probe, has recently been developed by the SGC and Takeda with a novel BRD7/9 binding chemotype (**Figure 3.07**).[220] Compound **3.009** shows good potency for BRD7 (BRD7 pK_D = 6.5) and BRD9 (BRD9 pK_D = 7.5) and >30-fold selectivity over the remaining bromodomains. Although no solubility or permeability data is supplied for **3.009**, cellular activity was demonstrated (BRD9 pEC_{50} = 6.5) in a BRD9 NanoBRET assay. A negative control, TP-472N (**3.010**), is also reported as being inactive against BRD9 at 20 μM, although the large structural differences should be considered. No data on the selectivity of **3.009** against other pharmacological off-targets is provided.

TP-472
3.009
BRD7 pK_D = 6.5
BRD9 pK_D = 7.5

TP-472N
3.010
BRD7 pK_D = N.A.
BRD9 pK_D < 4.7
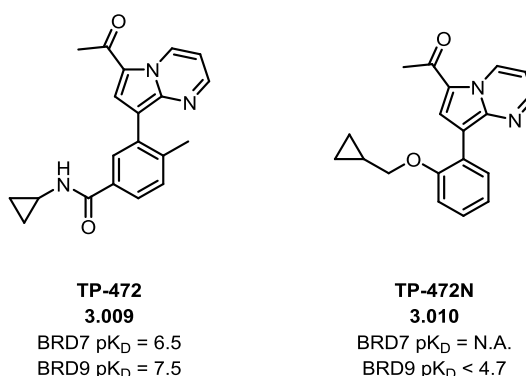
Figure 3.07: Structure of BRD7/9 chemical probe 3.009 and accompanying negative control 3.010. pK_D values refer to potency measured *via* ITC.

As discussed in **Section 2.2**, Crawford and co-workers substituted the *N*-methyl group of **2.013** for a selection of small hydrophobic substituents (**Section 2.2**, **Table 2.03**). The introduction of hydrophobic substituents was shown to induce a narrow hydrophobic channel in the binding pocket of BRD9.[156] Substitution of the *N*-methyl group for a crotyl group (**2.015**) reduced the potency for BRD4, BRPF1, CECR2, CREBBP and TAF1, whilst maintaining submicromolar potency for BRD9 (pIC_{50} = 6.8) (**Figure 3.08**). Although potency at BRD4 (pIC_{50} = 6.3) was reduced, only moderate selectivity was observed. Compound **2.015** was then subject to lead optimization efforts, focusing primarily on occupying accessible space in the ZA channel through *para* substitution of the aromatic ring. Additionally, substitution from the *ortho* and *meta* positions of the ring was hypothesized to occupy a small pocket in BRD9, further enhancing selectivity, leading to GNE-375 (**2.092**).[195] Compound **2.092** exhibited potency at BRD9 (pIC_{50} = 8.3) and >3000-fold selectivity over the BET bromodomains (BRD4(1) pIC_{50} = <4.7) as measured by TR-FRET assays. Potency (BRD9 pK_D = 8.7) and selectivity against other non-BET bromodomains was also confirmed using the DiscoverX BROMO*scan* panel with >1500-fold selectivity observed against the panel, excluding the highly homologous BRD7 (pK_D = 7.0) where 50-fold selectivity was observed. Compound **2.092** was also screened against an Invitrogen 40 kinase panel where no inhibition >20% was observed at 1 µM, and a CEREP panel where activity was observed in a benzodiazepine agonist assay (86% at 10 µM). Compound **2.092** demonstrated target engagement in a cellular thermal shift assay (CETSA), albeit at 2 µM. After demonstrating cellular viability, **2.092** was then used in the target validation of BRD9 bromodomain inhibition. RNA sequencing analysis of gene expression following a 24-hour treatment with **2.092** showed inhibition of seven genes. Of note was the inhibition of aldehyde dehydrogenase 1 family member A1 (ALDH1A1), an enzyme whose levels and activity have been shown to be increased in crizotinib resistant gastric cancer lines.[221] ALDH1A1 and its promoter are regulated by acetylation, suggesting BRD9 could play an active role in either/both of these mechanisms and presents a new area for therapeutic intervention strategies.
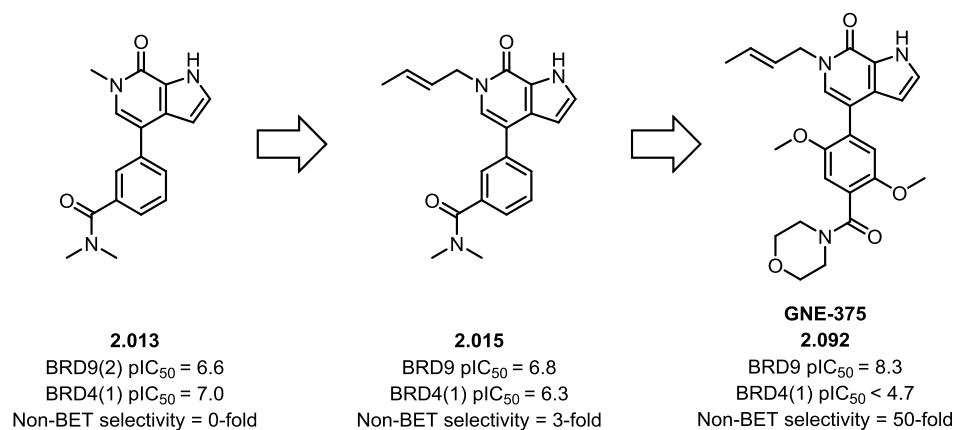
2.013
BRD9(2) pIC$_{50}$ = 6.6
BRD4(1) pIC$_{50}$ = 7.0
Non-BET selectivity = 0-fold

2.015
BRD9 pIC$_{50}$ = 6.8
BRD4(1) pIC$_{50}$ = 6.3
Non-BET selectivity = 3-fold

GNE-375
2.092
BRD9 pIC$_{50}$ = 8.3
BRD4(1) pIC$_{50}$ < 4.7
Non-BET selectivity = 50-fold

Figure 3.08: Structure of BRD7/9 chemical probe 2.092, intermediate 2.015 and starting point 2.013. pIC$_{50}$ values refer to potency in TR-FRET assays.

NMR fragment-based screening has been used to discover five ligand efficient fragments (**3.011**-**3.015**) for future BRD7/9 inhibitor optimization (**Figure 3.09**). Of particular interest is bromo pyrazole fragment **3.013** which appears to show 2.5-fold selectivity for BRD7 over BRD9 and potential for the development of selective BRD7 bromodomain inhibitors.[222]

3.011
BRD7 pK$_D$ = 4.7
BRD9 pK$_D$ = 4.6
LE = 0.50

3.012
BRD7 pK$_D$ = 3.7
BRD9 pK$_D$ = 4.2
LE = 0.49

3.013
BRD7 pK$_D$ = 3.9
BRD9 pK$_D$ = 3.5
LE = 0.45

3.014
BRD7 pK$_D$ = 3.3
BRD9 pK$_D$ = 3.2
LE = 0.36

3.015
BRD7 pK$_D$ = 3.5
BRD9 pK$_D$ = 3.8
LE = 0.38
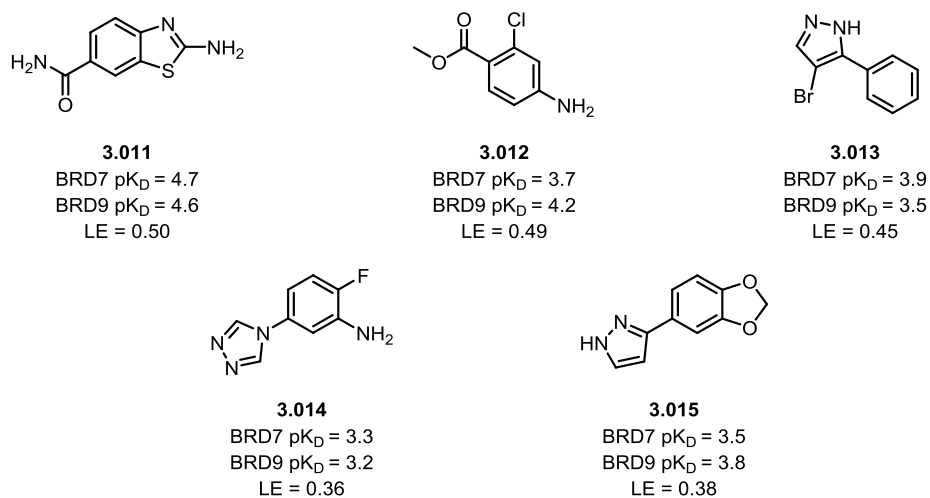
Figure 3.09: Structures of BRD7/9 fragments 3.011-3.015. pK$_D$ values refer to potency calculated from NMR chemical-shift perturbation.

In addition to public literature, several patents disclosing BRD7/9 inhibitors have also been published. Following on from their work developing BRD7/9 chemical probes, Genentech and Constellation Pharmaceuticals have disclosed five additional BRD7/9 inhibitors based around the pyrrolopyridinone scaffold discussed above (**Figure**

3.08).[223] BRD9 potency (pIC_{50} = 7.4) and selectivity data is reported (200-fold selectivity over the BET subfamily of bromodomains and 400-fold selectivity over seven representative non-BET bromodomains) for one compound, although the structure is not specified and no further data is provided.

Similarly, Boehringer Ingelheim have released a patent disclosing numerous BRD9 inhibitors spanning three different, albeit related, chemotypes (**Figure 3.10**).[224] Cellular activity data in either a BRD9 H3 or BRD9 H4 protein-protein interaction assay is provided, and the most potent of each chemotype **3.016** (BRD9 pIC_{50} = 8.5), **3.017** (BRD9 pIC_{50} = 8.3) and **3.018** (BRD9 pIC_{50} = 7.4) are shown below. All three chemotypes show potency for BRD9 and cellular target engagement, however, no further characterization is provided.

3.016
BRD9 pIC_{50} = 8.5

3.017
BRD9 pIC_{50} = 8.3
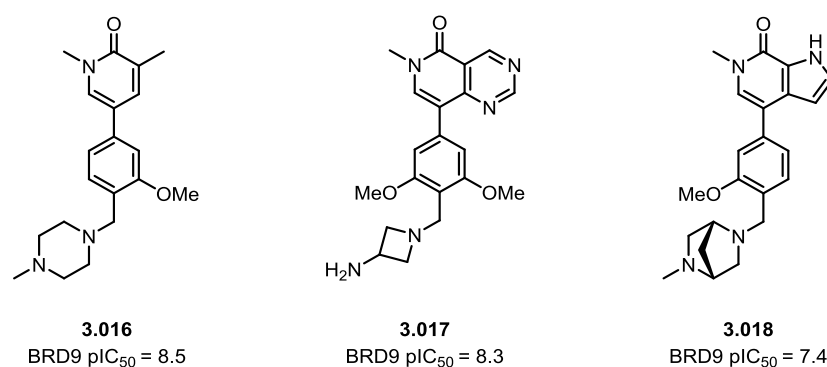
3.018
BRD9 pIC_{50} = 7.4

Figure 3.10: Structure of reference patented BRD7/9 inhibitors 3.016-3.018. pIC_{50} values refer to potency in an AlphaScreen assay.

Finally, Bradner *et al.* have disclosed the most recent addition to the BRD9 chemical tool box dBRD9 (**3.019**), the first BRD9 PROTAC (**Figure 3.11**).[225] A selection of BRD9 PROTACs were synthesized based around three different BRD9 chemical probes, LP99 (**3.002**, **Figure 3.02**), I-BRD9 (**3.004**, **Figure 3.03**) and BI-7273 (**3.007**, **Figure 3.05**). Compound **3.007** was eventually chosen to function as the selective BRD9 inhibitor component of the PROTAC, due to greater BRD9 selectivity (in particular, over the BET subfamily) when compared to **3.002** and **3.004** PROTAC derivatives. To complete the bifunctional PROTAC, an E3 ligase recruiter (a pomalidomide conjugate) was appended *via* a poly-ethylene glycol (PEG) chain to produce **3.019**. Compound **3.019** maintained potency for BRD9 (pIC_{50} = 7.0) and

selectivity over the BET subfamily (BRD4(1) $pIC_{50} < 4.3$). BRD9 was selectively degraded over a range of concentrations using **3.019** (BRD9 $pDC_{50} = 7.0$). The cellular selectivity of **3.019** was then demonstrated using human acute myeloid leukemia (MOLM-13) cells, in which, out of the 7326 proteins quantified, only BRD9 showed a statistically significant difference in abundance (5.5-fold decrease after treatment with 100 nM of **3.019** for 2 hours). A negative control compound for **3.019** was generated through the removal of the acetylated Lys mimetic, thus removing any potency for BRD9 ($pIC_{50} < 5$). Interestingly, both **3.019** and its negative control retained activity against the IKZF family of transcription factors which should be accounted for when using **3.019** for target validation. The development of BRD7/9 PROTACs will help expand the target validation of these proteins into the effects of degradation in comparison to inhibition.

dBRD9
3.019
BRD9 $pIC_{50} = 7.0$
BRD9 $pDC_{50} = 7.0$
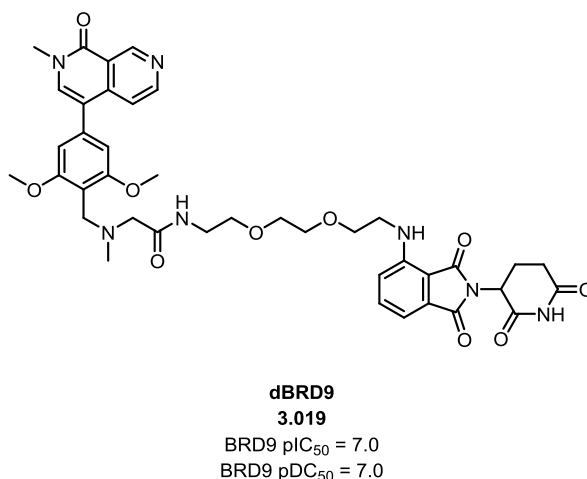
Figure 3.11: Structure of BRD9 degrader 3.019. pIC_{50} values refer to potency in an AlphaScreen assay. pDC_{50} values refer to degradation as measured by western blot analysis.

Despite numerous existing BRD7/9 tool compounds, the target validation of both proteins would benefit from additional probes of different chemotypes to help mitigate any false phenotypic assignment. More specifically, chemotypes avoiding an unsaturated bicyclic scaffold (seen across all existing BRD9 tool molecules, excluding **3.002**) would be particularly valuable.

Methodology to produce selective BRD7/9 inhibitors in a predictable and facile manner would also be extremely valuable for future inhibitor development, as would

the structural information revealed during the SAR exploration, should BRD9 be shown to be a valuable therapeutic target.

3.3 Aims

The aim of the project was to provide a thorough exploration of the conserved water methodology on a synthetically tractable template and, in doing so, provide further evidence to support occupancy of the inducible channel found within the BRD9 bromodomain binding pocket (reported by Genentech and Constellations Pharmaceuticals[156]) as a method for improving BRD9 selectivity. Through application of this methodology the aim is to develop an effective chemical probe for the target validation of the BRD7/9 bromodomains from the pyridazinone scaffold discussed in **Section 2.7.3**. Any probe developed should fulfill the criteria outlined in **Section 1.5** and reproduced below:

1. $pIC_{50} \geq 7$ against BRD9, as determined by a biochemical assay.
2. ≥100-fold selectivity over the BET bromodomain family (using BRD4(1) as a representative example).
3. ≥30-fold selectivity over other non-BET bromodomain families. (Due to the highly homologous nature of the BRD7 and BRD9 bromodomains, selectivity over BRD7 was neither expected nor targeted).
4. ≥30-fold selectivity over other pharmacologically relevant off-targets.
5. Suitable solubility and permeability to ensure exposure at target site.
6. Cellular activity at <1 µM concentrations.
7. Be the product of iterative SAR exploration.
8. Be accompanied by a structurally related negative control.
9. Expand the structural diversity of BRD7/9 chemical probes.

3.4 Identifying Compound 2.123 as a Start Point

The design of a novel chemotype BRD7/9 chemical probe began from compound **3.020** (**Table 3.02**). Compound **3.020** was first designed during GSK's PCAF inhibitor exploration (see **Section 1.4.2.1** for more details), hence the shared pyridazinone scaffold.[108] However, when profiled against other bromodomains, compound **3.020** revealed substantial potency for BRD9. It was therefore hypothesized that a BRD9 chemical probe could be developed from the same series. Work from our laboratories towards the development of **2.123** from initial hit compound **3.020** is summarized below.

SAR was initially focused around the benzyl group of compound **3.020** in an attempt to interact further with the binding pocket of BRD9 and boost BRD9 potency. The *ortho*-position was identified as optimal for BRD9 potency and a selection of ring structures were explored. A range of substituents were shown to be tolerated at this position, including compound **3.021**, which showed a substantial boost in BRD9 potency (pIC_{50} = 7.0). Compound **2.123** was then designed to reduce the lipophilicity of **3.021** and induce a clash with the WPF shelf in the BET bromodomains, improving BET bromodomain selectivity (**Table 3.02**).

Entry	Compound	R =	BRD9 pIC_{50}	BRD4(1) pIC_{50}	ChromLogD
1	**3.020**	Me	6.4	4.6 (×63)	3.57
2	**3.021**		7.0	4.9 (×130)	4.84
3	**2.123**		6.7	<4.3 (>×250)	1.61

Table 3.02: Key SAR breakthroughs in the development of 2.123 from 3.020. Selectivity for BRD9 against the given protein is shown in brackets underneath potency values. ChromLogD measurements were performed at pH7.4.

The broader bromodomain selectivity of compound **2.123** was then investigated *via* screening against the DiscoverX BROMO*scan* panel, as summarized in **Table 3.03**. Unfortunately, substantial activity was observed against non-BET bromodomain BRPF1, resulting in poor selectivity and limiting its application as a chemical probe.
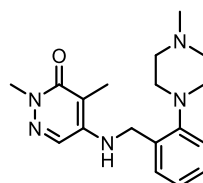
	2.123	**Chemical Probe Requirements**
BRD7/9 pK$_D$	7.6/7.4	≥7.0
BRD4(1) pK$_D$ (selectivity)	4.6 (≥×630)	≥×100
BRPF1 pK$_D$ (selectivity)	6.6 (×6)	≥×30
Other Non-BET selectivity	×50	≥×30

Table 3.03: Bromodomain selectivity profile of compound 2.123.

It was therefore hypothesized that bromodomain conserved water interactions could be used to improve selectivity for BRD9 over BRPF1 and non-BET bromodomain selectivity in general.

3.5 BRD9 Selectivity Through Conserved Water Interactions

Unlike in the TAF1(2) bromodomain, where it was hypothesized that rearrangement/partial displacement of the water molecules could be used improve non-BET selectivity, it was hypothesized that occupation of a narrow hydrophobic channel induced within the binding pocket of BRD9 (reported by Genentech[156]) could provide the desired increase in non-BET bromodomain selectivity.

As discussed in **Section 3.2**, Genentech showed that substituting the acetylated Lys methyl mimetic for different hydrophobic chains induced a narrow hydrophobic channel in BRD9 and CECR2, not possible in other bromodomains.[195] X-ray crystallography has shown that introduction of a crotyl acetylated Lys methyl mimetic leads to a small displacement of the Phe45 side chain in BRD9 and the opening of the hydrophobic pocket (**Figure 3.12**). The crotyl chain can then be accommodated by the induced pocket to avoid clashing with the conserved water network.
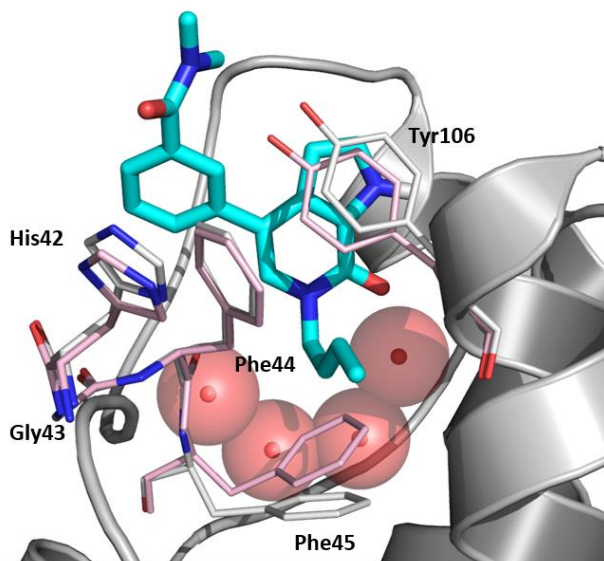
Figure 3.12: Overlay of the crystal structures of compound 2.015 (PDB: 5I7Y) (shown in cyan) bound to BRD9 (shown in grey) and the apo-BRD9 crystal structure (shown in pink) highlighting the small displacement of Phe45 and the conserved water network.

Overlaying the crystal structures of **2.123** and **2.015** bound to BRD9 confirmed the *C*-methyl group as a suitable vector for accessing the induced hydrophobic pocket (**Figure 3.13**).
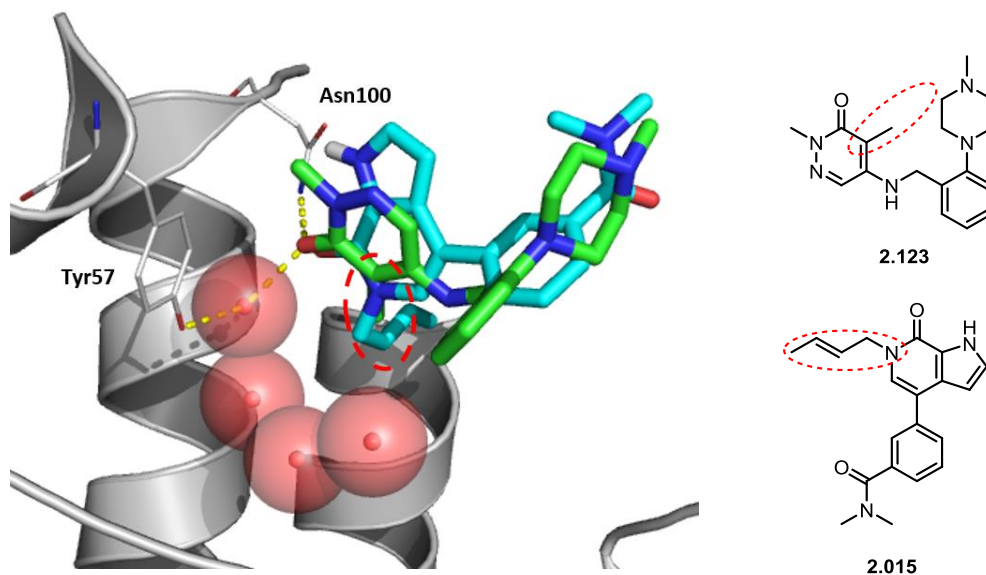

Figure 3.13: Overlay of the crystal structures of compound 2.123 (shown in green) and 2.015 (shown in cyan) (PDB: 5I7Y) bound to BRD9 (shown in grey).

Satisfied that the induced hydrophobic pocket could be accessed from the pyridazinone template, the synthetic practicality of functionalizing this position was assessed. Retrosynthetic analysis was first used to identify two synthetic routes (**Scheme 3.01**) from which a variety of different acetylated Lys methyl mimetics could be accessed. Both synthetic routes would commence from commercially available 4,5-dichloropyridazin-3(2H)-one (**3.022**) and require three steps, allowing for a thorough, yet rapid exploration of this methodology.

Synthetic Route 1 would begin with introduction of the various alkyl chain methyl mimetics *via* a displacement reaction with commercially available organometallic reagents. It was hypothesized that an initial deprotonation of the pyridazinone N-H *via* an equivalent of the chosen organometallic reagent would then disfavour displacement at the 5-position, allowing for a chemoselective displacement of the 4-position chlorine. A subsequent methylation of the pyridazinone nitrogen, and a Buchwald-Hartwig amination to append the amine, would provide access to the final compounds. By contrast, Synthetic Route 2 would commence with methylation of the pyridazinone nitrogen followed by a 1,4-addition of an amine into the α,β-unsaturated lactam. Finally, a Suzuki coupling with commercially available boronic coupling partners would provide access to the desired final compounds.
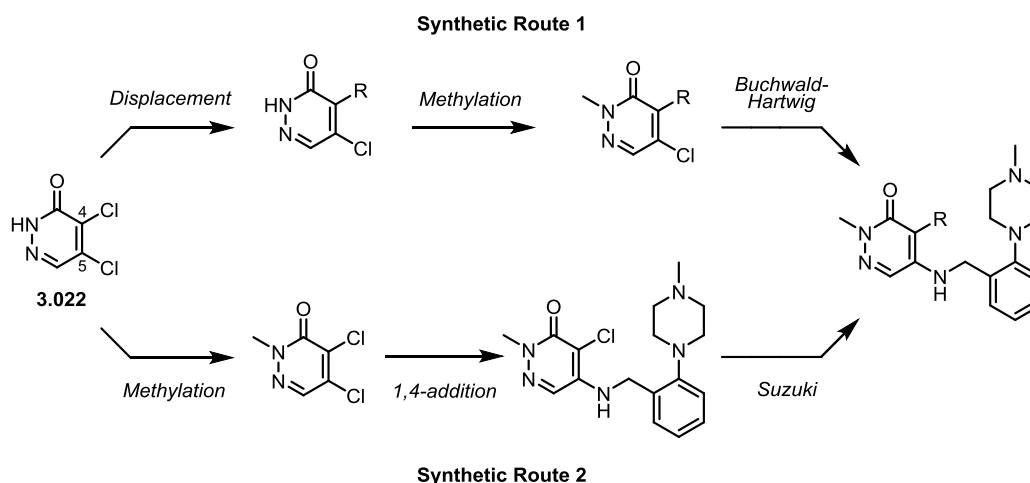
Scheme 3.01: Synthetic routes 1 and 2.

3.5.1 Unsaturated Alkyl Chain Methyl Mimetics
A selection of alkenyl chains, including the reported crotyl group, were first targeted to investigate whether a similar effect could be observed on the pyridazinone template

(**Figure 3.14**). Whilst the *E*-crotyl group was reported as optimal on the pyrrolopyridinone scaffold (**2.015**), it was unknown whether this SAR would transfer to other chemotypes. As a result, the allyl (**3.023**) and butenyl derivatives (**3.026**) were also investigated. Finally, the effect of unsaturation at the adjoining carbon on accessing the induced pocket was unknown. Consequently, 1,2-butenyl compound **3.025** was also investigated.
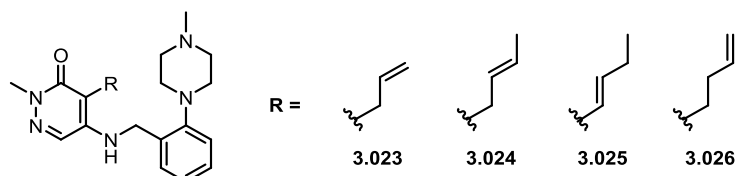

Figure 3.14: Target compounds 3.023-3.026 with unsaturated alkyl chain methyl mimetics.

3.5.1.1 Unsaturated Alkyl Chain Methyl Mimetics: Synthesis

Compounds **3.023**-**3.026** were all synthesized *via* Synthetic Route 2 (**Scheme 3.01**). Commercially available **3.022** was first methylated using methyl iodide and potassium carbonate in refluxing acetonitrile. Additionally, TBAB was used as a promoter to yield **3.027** in 76% (**Scheme 3.02**). Methylation was observed exclusively on the nitrogen, supported by the presence of a carbonyl stretching frequency (1635 cm^{-1}) in the IR spectrum of **3.027**. The right-hand side of the molecule was then appended *via* a 1,4-addition to the α,β-unsaturated lactam in DMSO at 120 °C. Although a mixture of regioisomers was observed, displacement of the 5-chloro group was preferred in a 1.8:1 ratio. The isomers were separated by reverse phase chromatography and the structure of the major isomer confirmed *via* a ROESY signal between the pyridazinone hydrogen and the benzylic hydrogens (see **Appendix**, **Figure 5.01**), as key intermediate **3.028**.
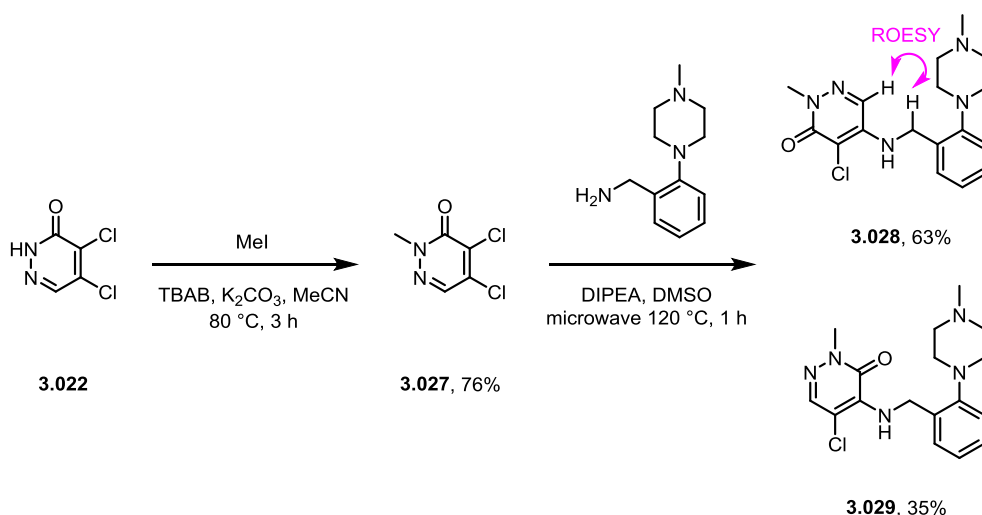
Scheme 3.02: Synthetic route to key intermediate 3.028 and 3.029.

With **3.028** in hand attention was turned to appending the different alkenyl chains. Allyl compound **3.023** was synthesized in 28% yield *via* a Suzuki-coupling with allyl boronic acid pinacol ester and RuPhos-Pd-G2 (**Scheme 3.03**). Similarly, 1,2-butenyl compound **3.025** was synthesized in 47% yield *via* a Suzuki-coupling using a cataCXium A ligand system.
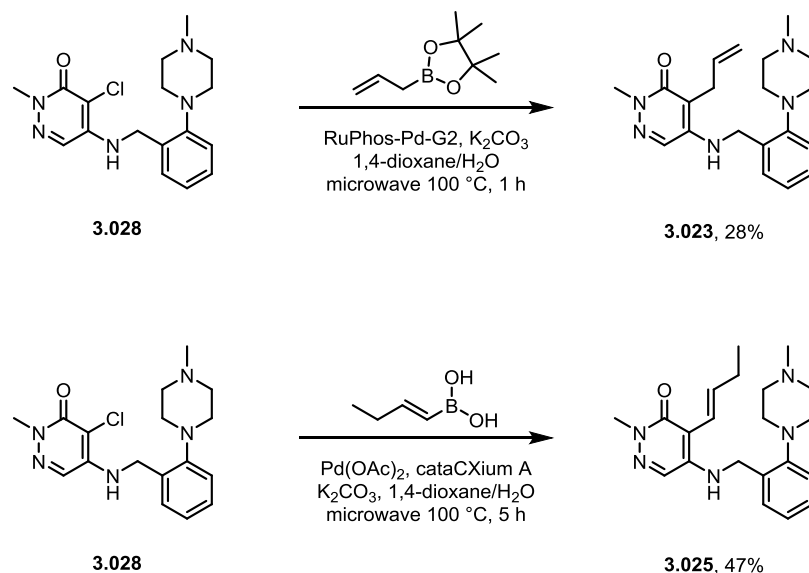
Scheme 3.03: Synthetic routes to compounds 3.023 and 3.025.

A Suzuki coupling with (*E*)-crotyl boronic acid pinacol ester (using the cataCXium A ligand system) resulted in a mixture of four products. Upon separation of the products *via* chiral chromatography it was apparent that under the reaction conditions the double bond geometry had isomerized, giving rise to both crotyl geometric isomers (**3.024** and **3.030**). Additionally, *sec*-butenyl compounds **3.031** and **3.032** were also observed (**Scheme 3.04**). Although not initially targeted, compounds **3.030**-**3.032** had the potential to offer additional information into the steric confinements of the induced pocket, and the effect different geometric isomers might have on accessing the pocket. Consequently, all four compounds were progressed for further profiling.
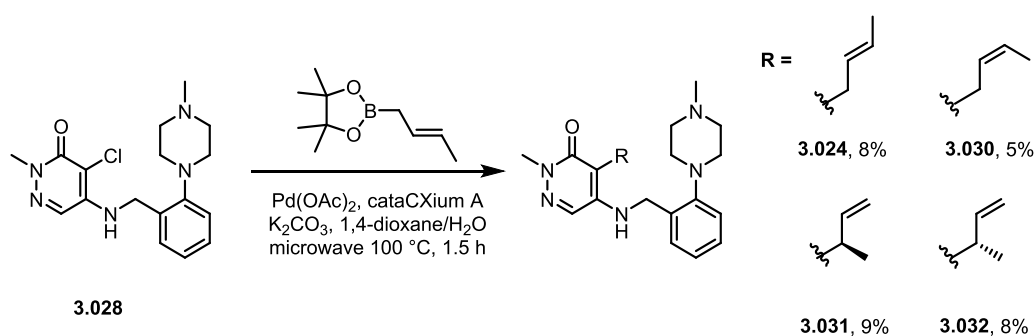
Scheme 3.04: Synthetic route to compounds 3.024, 3.030, 3.031 and 3.032.

Geometric isomers **3.024** and **3.030** where identified *via* characteristic *J*-coupling values (**Figure 3.15**). The alkenyl protons of diastereomer **3.024** showed a splitting of 15.3 Hz, whilst diastereomer **3.030** showed a reduced splitting of 10.5 Hz, characteristic of *E*- and *Z*-alkene geometry, respectively.
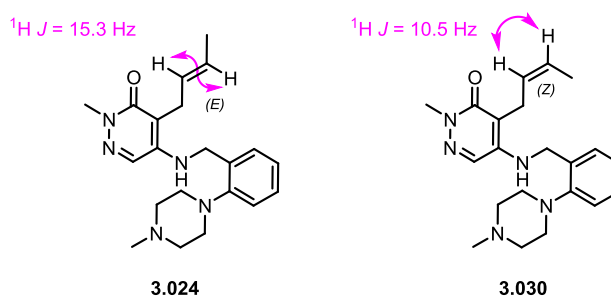
Figure 3.15: Structures of diastereomers 3.024 and 3.030 highlighting the characteristic ^{1}H NMR splitting associated with each double bond geometry.

It was hypothesized that compounds **3.031** and **3.032** were formed *via* donation of hydroxide into the empty p-orbital of boron and subsequent elimination (**Scheme 3.05**). Both **3.031** and **3.032** were isolated as single enantiomers of unknown absolute configuration ([α_D]^{23} (c = 10 mg/mL, MeOH): ±21°). For reader clarity, **3.031** and **3.032** were arbitrarily assigned as the *R*- and *S*-enantiomers, respectively.
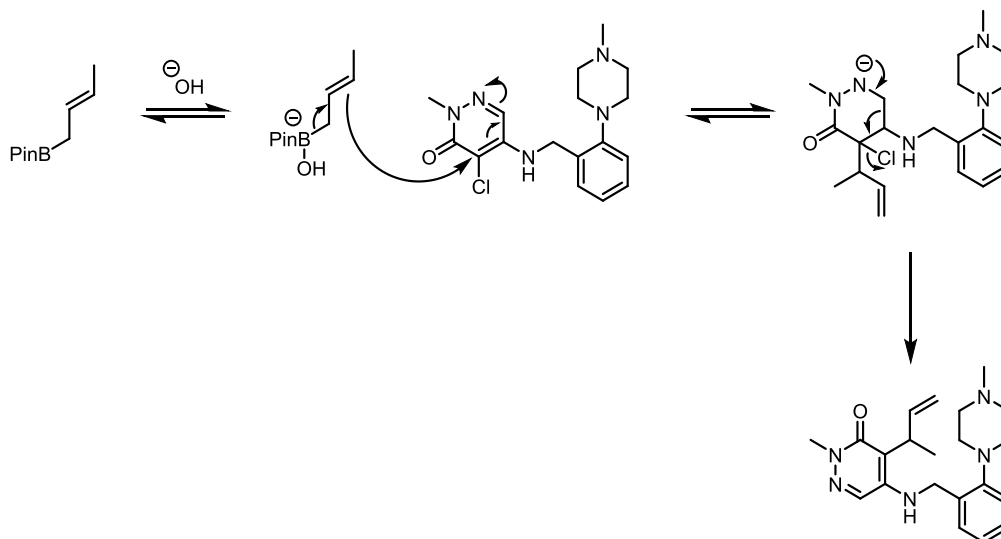
Scheme 3.05: Proposed mechanism for the formation of *sec*-butenyl compounds 3.031 and 3.032.

Finally, the synthesis of butenyl compound **3.026** was attempted *via* both Synthetic Route 1 and Synthetic Route 2. Unfortunately, no desired product was observed for the chlorine displacement or Suzuki reaction stages and so an alternative route was designed from **3.022** (**Scheme 3.06**). Displacement of the 4-chloro group with a methyl Grignard reagent, followed by *N*-methylation under the standard conditions, delivered compounds **3.033** and **3.034** in 81% and 55% yield, respectively. Deprotonation of the enamine γ-position using LiHMDS and alkylation with allyl bromide completed the introduction of the butenyl group in 24% yield. Finally, a Buchwald Hartwig amination was utilized to introduce the amine in 20% yield.
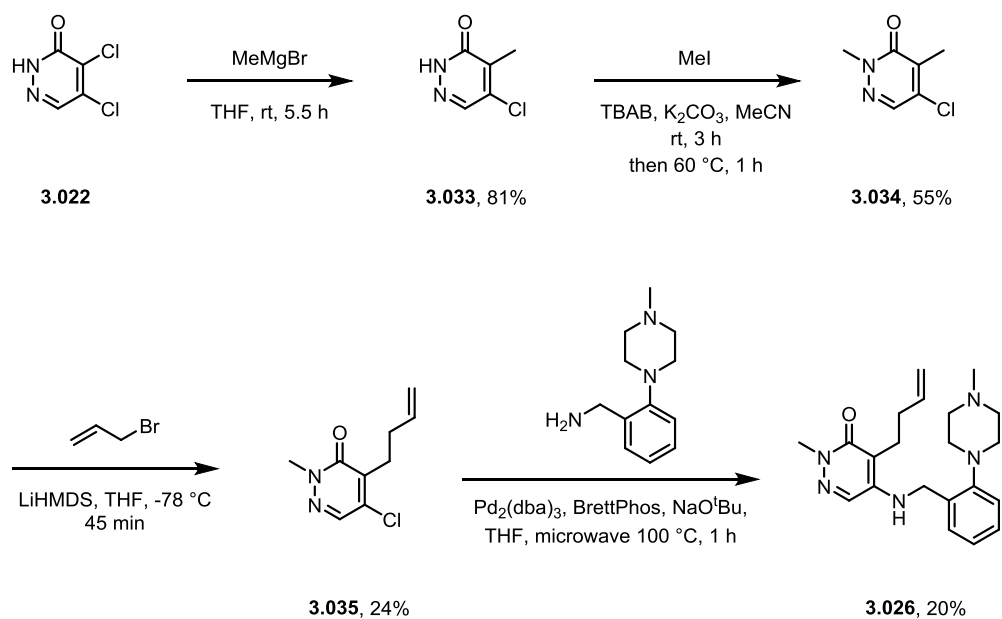
Scheme 3.06: Synthetic route to butenyl compound 3.026.

3.5.1.2 Unsaturated Alkyl Chain Methyl Mimetics: Results and Discussion

Once synthesized compounds **3.023**-**3.026** and **3.030**-**3.032** were screened *via* DiscoverX against BRD9, BRPF1 and BRD4(1), and their physicochemical properties measured (**Table 3.04**). Introduction of an allyl group into the acetylated Lys mimetic (**3.023**) showed a dramatic reduction in BRPF1 potency ($pK_D < 5.0$) as hypothesized, with a minor reduction in BRD9 potency ($pK_D = 7.0$) also observed. Extending the alkyl chain by one carbon to give *E*-crotyl compound **3.024** also reduced BRPF1 potency yet retained all potency for BRD9 ($pK_D = 7.4$). Interestingly, an increase in BRD4(1) potency ($pK_D = 5.4$) was also observed, resulting in similar selectivity over the BET bromodomains (relative to allyl compound **3.023**). Changing the geometric isomer from *E* to *Z* in **3.030** resulted in a reduction in potency against both BRD9 (pK_D = 6.6) and BRD4 ($pK_D < 5.0$) suggesting the *Z* configuration cannot access the induced pocket as effectively as the *E* diastereomer. Moving the double bond to be in conjugation with the rest of the ring in **3.025** dramatically reduced potency against BRD9 ($pK_D < 5.0$), suggesting that the alkyl chain may no longer be able to readily access the required conformation to enter the induced hydrophobic pocket, and was instead clashing with other residues within the binding pocket. Butenyl compound **3.026**, with a terminal alkene, also showed a reduction in BRD9 potency ($pK_D = 6.4$).

Introduction of a branching methyl group at the linker carbon in **3.031** and **3.032** showed further reduction in BRD9 potency (compared to allyl compound **3.023**) for both enantiomers, suggesting increased steric bulk was not well tolerated at this position.
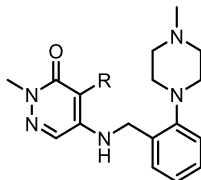
Entry	Compound	R =	CAD Solubility (µg/ mL)	AMP (nm/s)	BRD9 pK$_D$	BRD4(1) pK$_D$	BRPF1 pK$_D$
1	**2.123**	Me	178*	330	7.4	4.6 (×630)	6.6 (×5)
2	**3.023**		>=189	66	7.0	<5.0 (>×100)	<5.0 (>×100)
3	**3.024**	(E)	>=202	375	7.4	5.4 (×100)	<5.0 (>×250)
4	**3.030**	(Z)	>=189	580	6.6	<5.0 (>×40)	<5.0 (>×40)
5	**3.025**	(E)	>=122	190	<5.0	<5.0 (-)	<5.0 (-)
6	**3.026**		>=186	310	6.4	<5.0 (>×25)	<5.0 (>×25)
7	**3.031**		>=94	440	6.6	<5.0 (>×40)	<5.0 (>×40)
8	**3.032**		>=157	550	6.5	<5.0 (>×32)	<5.0 (>×32)

Table 3.04: Physicochemical properties and potency profile for unsaturated compounds 3.023-3.026, 3.030-3.032 and start point 2.123. Selectivity for BRD9 against the given protein is shown in brackets underneath potency values. *CLND solubility. Solubility, AMP and ChromLogD measurements were all performed at pH$_{7.4}$.

To gain further insight into the conformations adopted by each chain, compounds **3.023**-**3.026** and **3.030**-**3.032** were docked (with the help of Dr. Paul Bamborough) within the BRD9 bromodomain (**Figure 3.16**). As expected, the *E*-crotyl chain (**3.024**) showed optimal occupancy of the induced pocket (**Figure 3.16b**). Reducing the length of the chain (**3.023**) showed only partial occupancy of the pocket (**Figure 3.16a**). Alteration of the double bond geometry (**3.030**) and positioning (**3.025** & **3.026**) appeared detrimental to binding, forcing the molecules to twist to accommodate the chain (**Figure 3.16c-e**). Similarly, branching at the adjoining carbon (**3.032**) appeared to cause the molecule to reorder to accommodate the additional steric hindrance (**Figure 3.16f**).
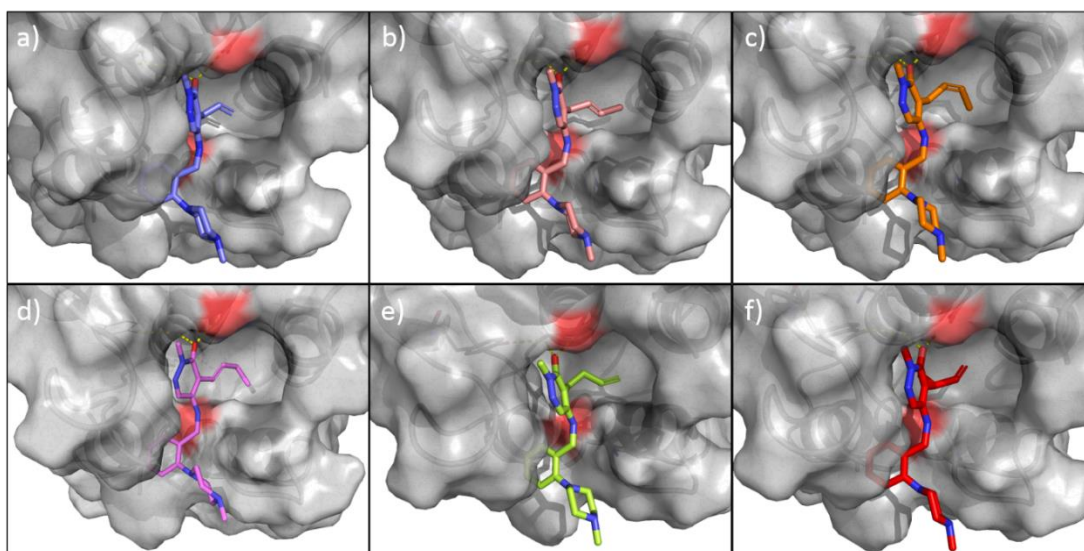
Figure 3.16: Docking of compounds 3.023-3.026 and 3.030-3.032 into the BRD9 bromodomain (shown in grey) from PDB entry 5I7Y and refined using the protein structure preparation module of Maestro. Tyr106 was removed from the protein surface to help show the induced pocket. a) Allyl (3.023); b) *E*-crotyl (3.024); c) *Z*-crotyl (3.030); d) 1,2-butenyl (3.025); e) 3,4-butenyl (3.026); and f) (*R*)-*sec*-butenyl (3.032).

3.5.2 Saturated Alkyl Chain Methyl Mimetics

Attempts to restrict the alkyl chain into preferred conformations using double bonds showed limited success. Consequently, it was hypothesized that greater flexibility within the alkyl chain could alter the chain's ability to access the induced binding pocket and induce further clash in non-tolerated bromodomains. Compounds **3.036**-**3.040**, with saturated alkyl chain methyl mimetics, were designed to test this hypothesis (**Figure 3.17**). As with the unsaturated chains, saturated alkyl chains of

varying length/branching were also prepared to probe the accessible space within the hydrophobic pocket and the effect of saturation/increased flexibility. As a reduction in BRD9 potency was observed when the alkenyl chain was truncated, a broader range of alkyl chain lengths were examined (2-5 carbons) to explore this effect further.
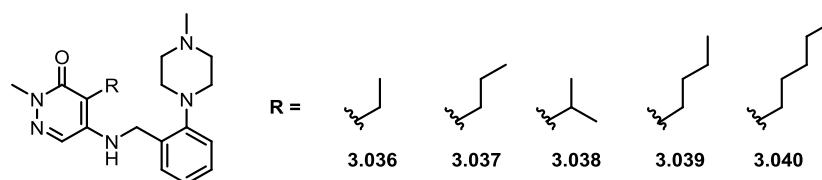

Figure 3.17: Target compounds 3.036-3.040 with saturated alkyl chain methyl mimetics.
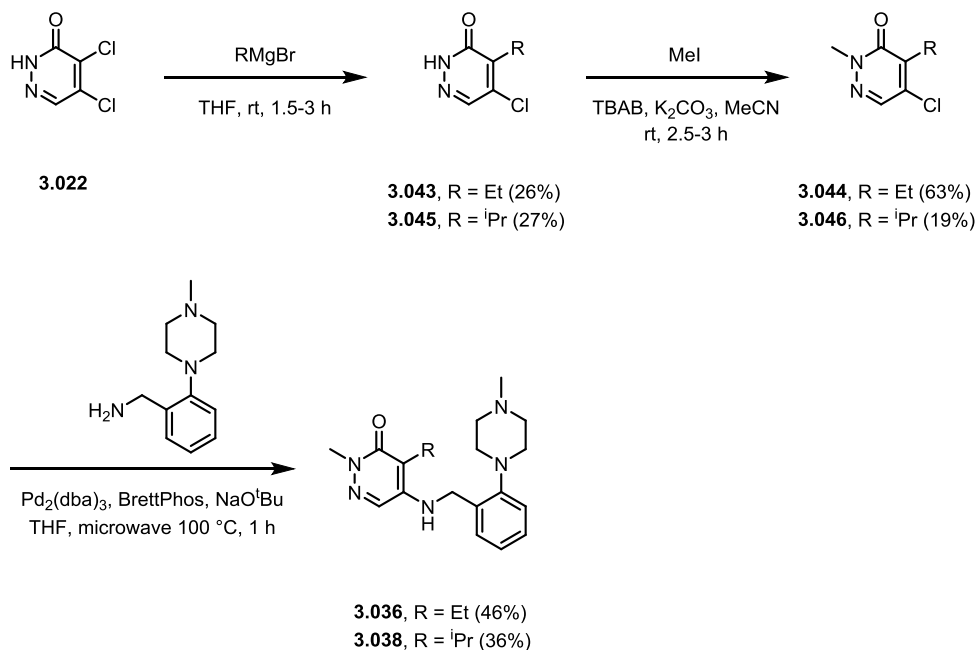
3.5.2.1 Saturated Alkyl Chain Methyl Mimetics: Synthesis

Butyl derivative **3.039** was synthesized first. A chemoselective displacement between **3.022** and ^{n}BuLi at -78 °C delivered compound **3.041** in 63% yield and a subsequent methylation at 60 °C gave intermediate **3.042** in 77% yield (**Scheme 3.07**). Finally, a Buchwald-Hartwig amination with the required amine yielded butyl compound **3.039** in 22%.
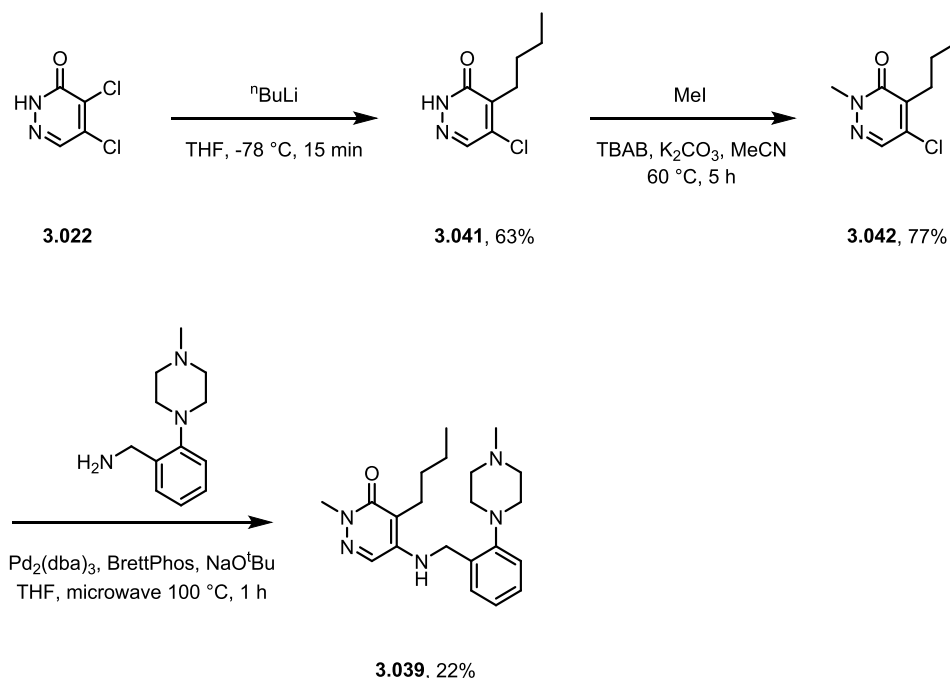
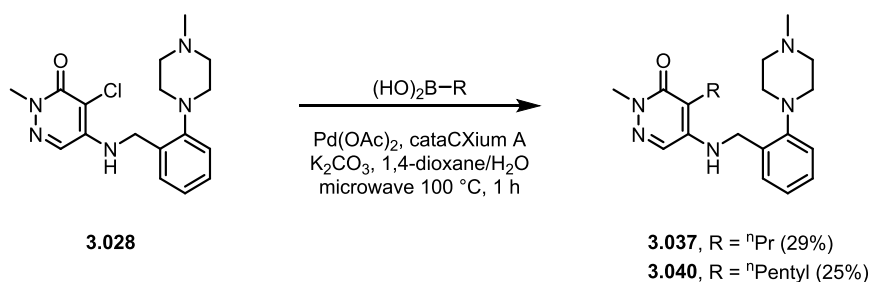**Scheme 3.07: Synthetic route to butyl compound 3.039.**

The ethyl (**3.036**) and isopropyl (**3.038**) derivatives were also synthesized *via* Synthetic Route 1. Introduction of the ethyl and isopopyl chains was achieved (26-27% yield) *via* displacement of the 4-chloro group with the corresponding Grignard reagent at 0 °C (**Scheme 3.08**). A subsequent methylation under standard conditions delivered intermediates **3.044** and **3.046** in 63% and 19% yield respectively. Finally, a Buchwald-Hartwig amination under the preferred conditions yielded final compounds **3.036** (46%) and **3.038** (36%).

3.022

3.043, R = Et (26%)
3.045, R = ^{i}Pr (27%)

3.044, R = Et (63%)
3.046, R = ^{i}Pr (19%)

3.036, R = Et (46%)
3.038, R = ^{i}Pr (36%)

Scheme 3.08: Synthetic routes to compounds 3.036 and 3.038.

Reaction of **3.022** with the corresponding *n*-propyl and *n*-pentyl Grignard reagents failed to give the required product, therefore, attention was shifted to Synthetic Route 2. Suzuki cross-coupling reactions between intermediate **3.028** and the respective boronic acids delivered final compounds **3.037** and **3.040** in 29% and 25% yield respectively (**Scheme 3.09**).

Scheme 3.09: Synthetic routes to *n*-propyl and *n*-pentyl compounds 3.037 and 3.040.

3.5.2.2 Saturated Alkyl Chain Methyl Mimetics: Results and Discussion

Once synthesized compounds **3.036**-**3.040** were screened *via* DiscoverX against BRD9, BRPF1 and BRD4(1), and their physicochemical properties measured (**Table 3.05**). A reduction in BRPF1 potency was observed across all the saturated chains tested, including even the smallest chain, ethyl compound **3.036**, suggesting anything bulkier than a methyl is not well tolerated in BRPF1. Potency for BRD9 remained above the desired threshold for compound **3.036**, although a slight reduction ($pK_D = 7.1$) (relative to methyl derivative **2.123**) was observed. Extending the alkyl chain further to propyl compound **3.037** showed a further reduction in BRD9 potency ($pK_D = 6.9$) and reflects the trends observed for the three-atom unsaturated allyl chain in compound **3.023**. Similarly, introduction of branching at the linker carbon, in isopropyl analogue **3.038**, remained detrimental to the BRD9 potency ($pK_D = 6.5$), confirming the low tolerance for steric bulk at this position. Moving from the *n*-propyl chain to *n*-butyl compound **3.039** showed an increase in BRD9 potency ($pK_D = 7.2$), following the same trends as the unsaturated chain analogues. Interestingly, activity against BRD4(1) remained low ($pK_D < 5.0$) for butyl compound **3.039** demonstrating high BET bromodomain selectivity. *n*-Pentyl derivative **3.040**, designed to gauge the depth of the binding pocket, showed a predicted decrease in BRD9 potency ($pK_D = 6.8$), suggesting four-atom chains are optimal for occupying the induced hydrophobic pocket.
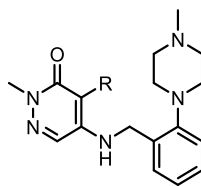
Entry	Compound	R =	CAD Solubility (µg/mL)	AMP (nm/s)	BRD9 pK$_D$	BRD4 pK$_D$	BRPF1 pK$_D$
1	**2.123**	Me	178*	330	7.4	4.6 (×630)	6.6 (×5)
2	**3.036**		>=171	280	7.1	5.1 (×100)	5.2 (×79)
3	**3.037**		>=172	580	6.9	<5.0 (>×79)	<5.0 (>×79)
4	**3.038**		>=201	310	6.5	<5.0 (>×32)	5.1 (×25)
5	**3.039**		>=228	250	7.2	<5.0 (>×160)	<5.0 (>×160)
6	**3.040**		>=190	720	6.8	5.8 (×10)	<5.0 (>×63)

Table 3.05: Physicochemical properties and potency profile for saturated compounds 3.036-3.040 and start point 2.123. Selectivity for BRD9 against the given protein is shown in brackets underneath potency values. *CLND solubility. Solubility, AMP and ChromLogD measurements were all performed at pH$_{7.4}$.

Compounds **3.036-3.040** were docked (with the help of Dr. Paul Bamborough) within the BRD9 bromodomain (**Figure 3.18**), with the four-atom butyl chain (**3.039**) appearing optimal for occupying the induced pocket (**Figure 3.18e** & **3.18f**). Shorter chains (**3.036** & **3.037**) again showed only partial occupancy of the induced pocket (**Figures 3.18a** & **b**) and branching (**3.038**) appeared to cause the molecule to twist within the binding site (**Figure 3.18c**). The larger pentyl chain (**3.040**) was poorly accommodated (**Figure 3.18d**) as expected.
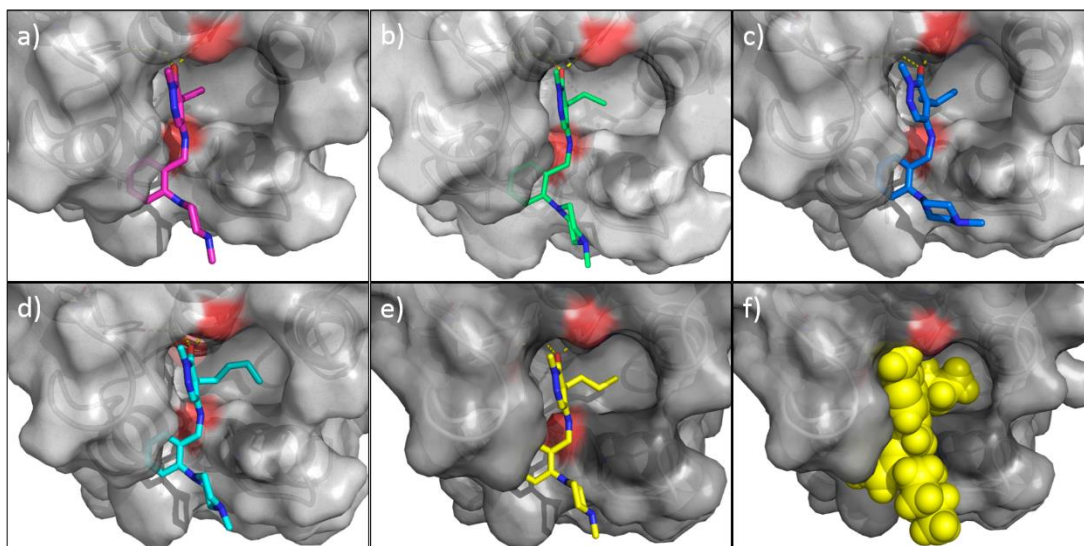
Figure 3.18: Docking of compounds 3.036-3.040 into the BRD9 bromodomain (shown in grey) from PDB entry 5I7Y and refined using the protein structure preparation module of Maestro. Tyr106 was removed from the protein surface to help show the induced pocket. a) Ethyl (3.036); b) propyl (3.037); c) isopropyl (3.038); d) pentyl (3.040); e) butyl (3.039); and f) space fill model of 3.039.

3.5.3 Broader Bromodomain Selectivity Screening

The broader bromodomain selectivity of the most promising compounds (*E*-crotyl compound **3.024** and butyl compound **3.039**) was then investigated. Compounds **3.024** and **3.039** were screened at 10 µM against a DiscoverX BROMO*scan* 32 bromodomain panel (**Figure 3.19** and **Table 3.06**). Pleasingly both compounds appeared selective for BRD7/9 at 10 µM.

Compound **3.024** showed a general improvement in selectivity (**Figure 3.19a**), with many bromodomains showing reduced levels of inhibition compared to start point **2.123** (**Table 3.06**). Exceptions included TAF1(2), where a marginal increase was observed, and the BET family of bromodomains where high levels of inhibition were observed. By contrast **3.039** (**Figure 3.19b**), showed no substantial new off-target activity compared to start point **2.123** (**Table 3.06**).
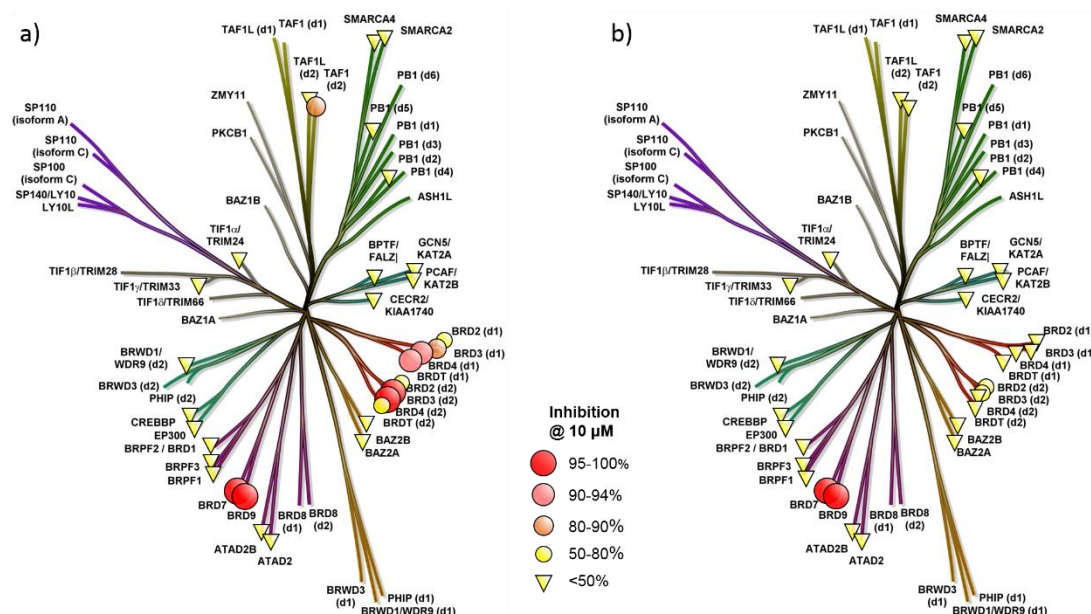
Figure 3.19: a) Compound 3.024 screened at 10 µM against the DiscoverX BROMO*scan* panel; and b) compound 3.039 screened at 10 µM against the DiscoverX BROMO*scan* panel.

Compound Number	ATAD2A	ATAD2B	BAZ2A	BAZ2B	BRD1	BRD2(1)	BRD2(2)	BRD3(1)	BRD3(2)	BRD4(1)	BRD4(2)	BRD7	BRD9	BRDT(1)	BRDT(2)	BRPF1
2.123	0	0	36	18	94	34	49	45	50	50	96	98	99	25	22	97
3.024	0	0	3	49	34	79	66	83	95	91	96	99	100	90	69	11
3.039	0	0	0	15	0	9	60	5	66	4	47	100	100	12	47	2

Compound Number	BRPF3	CECR2	CREBBP	EP300	FALZ	GCN5L2	PB1(2)	PB1(5)	PCAF	SMARCA2	SMARCA4	TAF1(2)	TAF1L(2)	TRIM24	TRIM33	WDR9(2)
2.123	85	63	0	3	28	92	13	0	82	3	0	35	2	31	8	21
3.024	12	0	8	0	0	4	0	0	0	0	0	84	12	0	26	0
3.039	0	0	0	0	23	4	11	29	1	0	0	0	0	1	29	0

Table 3.06: Percentage inhibition of bromodomains tested at 10 µM (DiscoverX BROMO*scan* single-shot assay) for compounds 2.123, 3.024 and 3.039.

145

The (*E*)-crotyl and butyl derivatives were then profiled alongside one another (**Table 3.07**). Despite greater potency for BRD9, compound **3.024** appeared less selective against the BET bromodomains for which a strong biological phenotype is known. Additionally, at 10 µM compound **3.024** reported an increased activity at TAF1(2), and although pK_D values were not measured, provides further support for the preference for a butyl chain. Consequently, butyl compound **3.039** was progressed for further profiling.
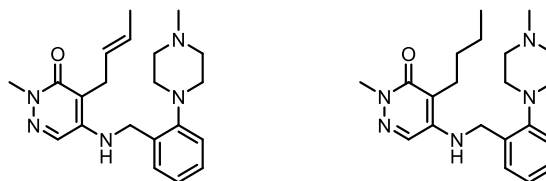
	3.024	3.039
BRD9 BROMO*scan* pK_D	7.4	7.2
BRD4(1) pK_D	5.4	<5.0
BET selectivity	×100	>×160
BRPF1 pK_D	<5.0	<5.0
TAF1(2) inhibition @ 10 µM	84%	0%
ChromLogD	3.11	3.49
CAD solubility (µg/mL)	>=202	>=228
AMP (nm/s)	375	250

Table 3.07: Summary of biochemical and physicochemical properties for 3.024 and 3.039. BET selectivity refers to the difference in pK_D values between BRD9 and BRD4(1). CAD solubility, AMP and ChromLogD measurements were all performed at pH$_{7.4}$.

3.5.4 Metabolic Stability

To investigate the suitability of **3.039** for *in vivo* application, preliminary studies were performed to assess the compound's pharmacokinetic properties. MetaSite was used to first predict the most likely sites of CYP mediated metabolism.[182,183] The pyridazinone *N*-methyl group was predicted to be the major site for metabolism, followed by the piperazine *N*-methyl and two butyl chain carbon atoms (**Figure 3.20**).

Additionally, two other less likely sites of potential metabolism were identified as the benzylamine carbon and a carbon on the substituted aromatic ring.
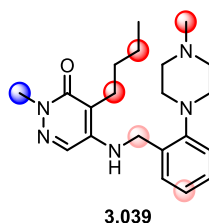

3.039

Figure 3.20: Metasite output for compound 3.039. Most likely site of CYP mediated metabolism highlighted in blue. Additional sites ranked by likelihood from bold red to light red.

The *in vitro* clearance of compound **3.039** was then measured in human liver microsomes and pleasingly showed good microsomal stability (1.99 mL/min/g).

3.6 Compound 3.039, Chemical Probe for the BRD7/9 Bromodomains

3.6.1 Selectivity Profiling
To further investigate the selectivity of compound **3.039**, 11-point dose-response curves (30 μM maximum concentration) were measured to quantify pK_D potency values against the DiscoverX BROMO*scan* panel. Pleasingly, **3.039** showed excellent selectivity against the BET (>500-fold) and non-BET bromodomains (320-fold), excluding the highly homologous BRD7 (pK_D = 6.3) (**Figure 3.21**) (see **Appendix**, **Table 5.04** for pK_D values).

Figure 3.21: DiscoverX BROMO*scan* activity profile for compound 3.039 screened against 40 bromodomains. See Appendix for pK_D values.

Compound **30** was also screened against an internal panel of 40 biological off-targets showing no inhibition $pIC_{50} \geq 5.0$ excluding GPCR MrgX2 (pIC_{50} = 5.3) and serotonin 1B (pIC_{50} = 5.7) (**Appendix**, **Table 5.03**), neither of which were considered as significant for the project.

3.6.2 Negative Control

As discussed in **Section 2.6.2** the importance of structurally similar negative controls in phenotypic assignment is paramount. It was hypothesized that removal of the acetyl Lys methyl mimetic would produce a suitable structurally similar negative control. The des-alkyl derivative (**3.047**) was isolated as the major by-product from the Suzuki reactions performed as part of Synthetic Route 2 (**Section 3.5**). An example is shown

in **Scheme 3.10**. As predicted compound **3.047** was inactive against BRD9 at 50 μM and was therefore selected to function as a negative control for compound **3.039** (**Table 3.08**).

3.028

3.047, 43%
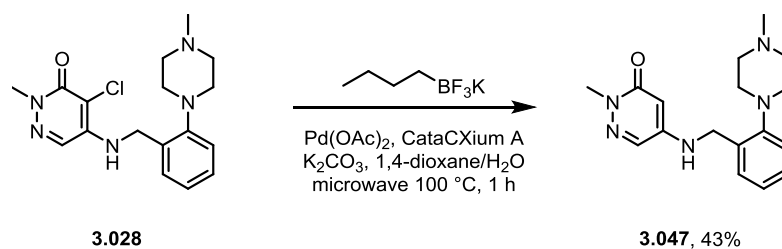
Scheme 3.10: Synthetic route to compound 3.047.

3.6.3 Summary

Compound **3.039** is a potent and highly selective inhibitor of the BRD7/9 bromodomains (**Table 3.08**). Although compound **3.039** appears soluble and permeable, evidence of target engagement *via* a cellular assay should be considered before application as a chemical probe. Together, compound **3.039** and structurally similar negative control **3.047** expand the diversity of the BRD7/9 chemical tool box and provide additional high-quality tool molecules for the target validation of the BRD7/9 bromodomains. Additionally, compound **3.039** provides an alternative ligand efficient BRD7/9 inhibitor for the development of bifunctional tool molecules such as BRD7/9 PROTACs.
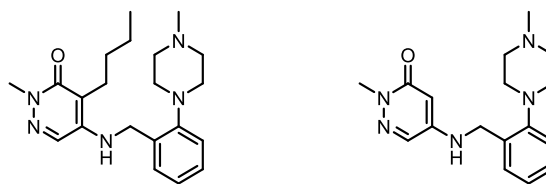
	3.039	3.047
BRD9 pK$_D$	7.2	-
BRD9 pIC$_{50}$	-	<4.3
BET selectivity	>×500	-
Non-BET selectivity	×320	-
ChromLogD	3.49	1.05
CAD solubility (µg/mL)	>=228	>=150
AMP (nm/s)	250	140

Table 3.08: Profile of BRD7/9 chemical probe 3.039 and accompanying negative control 3.047. CAD solubility, AMP and ChromLogD measurements were all performed at pH$_{7.4}$.

3.7 The Broader Applicability of the Butyl Motif

Having demonstrated the utility of bromodomain selectivity through conserved water interactions in the development of **3.039**, focus was moved to testing the transferability of the butyl methyl mimetic to other scaffolds. It was hypothesized that incorporation of this motif into the acetylated Lys mimetics of other bromodomain inhibitors would improve or introduce BRD7/9 selectivity.

Three scaffolds (**Figure 3.22**) were selected to test the utility and applicability of this conserved water interaction concept: 1) compound (**3.048**) an unselective compound from the same template; 2) I-BRD9 (**3.004**) a BRD9 selective compound on a different template; and 3) bromosporine (**3.049**), an unselective compound on a different template.
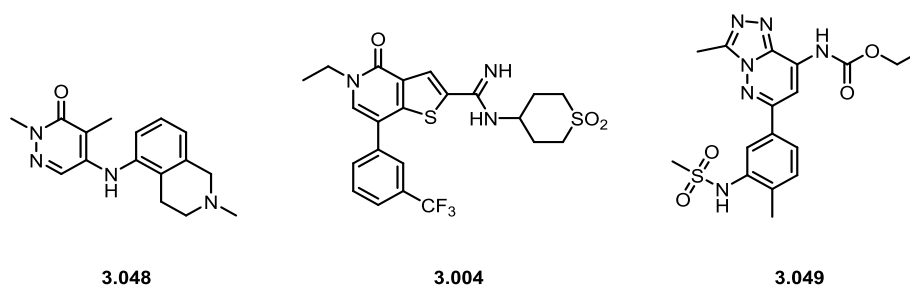
Figure 3.22: Structure of three scaffolds to test the broader applicability of the butyl methyl mimetic.

3.7.1 Pyridazinone BROMObead Scaffold

Compound **3.048** was discovered as part of GSK's PCAF chemical probe work discussed in **Section 1.4.2.1**.[108] Prior to optimization of the RHS, the scaffold appeared unselective for a range of bromodomains (confirmed by screening against the DiscoverX BROMO*scan* panel). Compound **3.048** was used as a promiscuous inhibitor in Cellzome's "BROMObead" assay, highlighting its lack of selectivity. It was hypothesized that incorporation of the butyl group onto compound **3.048** would show an increase in selectivity for BRD9 over a larger selection of non-BET bromodomains, not visible on the BRD9 optimized scaffold.

Sharing the same pyridazinone core as **3.039**, it was assumed that the butyl chain would still be able to access the hydrophobic pocket within BRD9. This was confirmed by overlaying the X-ray crystal structures of chloro derivative **3.050** and **2.015** (**Figure 3.23**). The *C*-chloro group was identified as the acetylated Lys mimetic (*C*-Me in **3.048**) and a suitable vector for accessing the hydrophobic pocket.
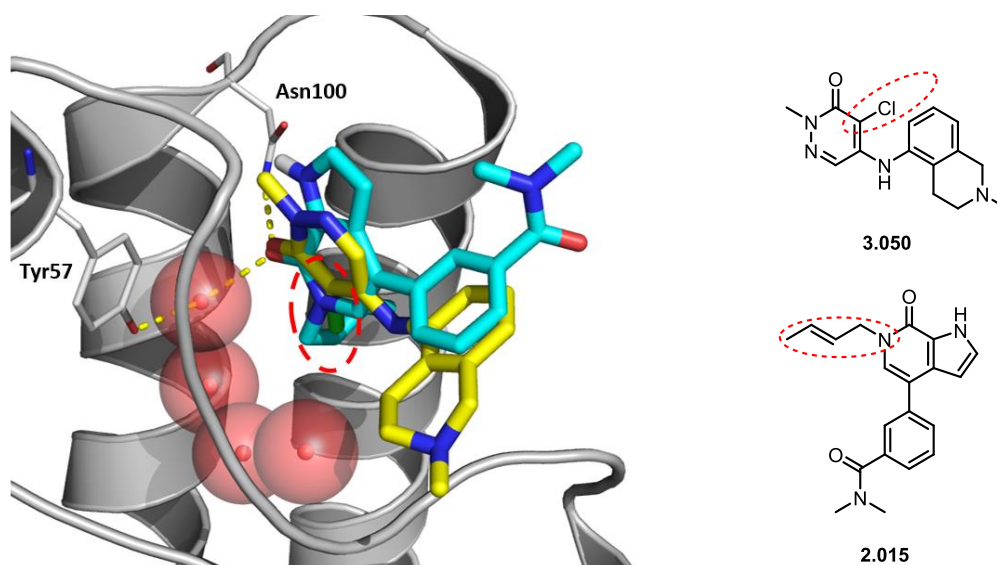
Figure 3.23: Overlay of the crystal structures of compound 3.050 (shown in yellow) (GSK internal X-ray crystal structure) and 2.015 (shown in cyan) (PDB: 5I7Y) bound to BRD9 (shown in grey). Acetylated Lys methyl mimetics highlighted with red dashed boxes.

3.7.1.1 Pyridazinone BROMObead Scaffold: Synthesis

Synthesis of compound **3.053** began from intermediate **3.042** (**Scheme 3.11**). A Buchwald-Hartwig amination using the desired THIQ-aniline delivered intermediate **3.051** in 25% yield. A quantitative Boc deprotection yielded **3.052** which was then methylated under Eschweiler-Clarke conditions, providing access to butylated derivative **3.053** 59% yield.
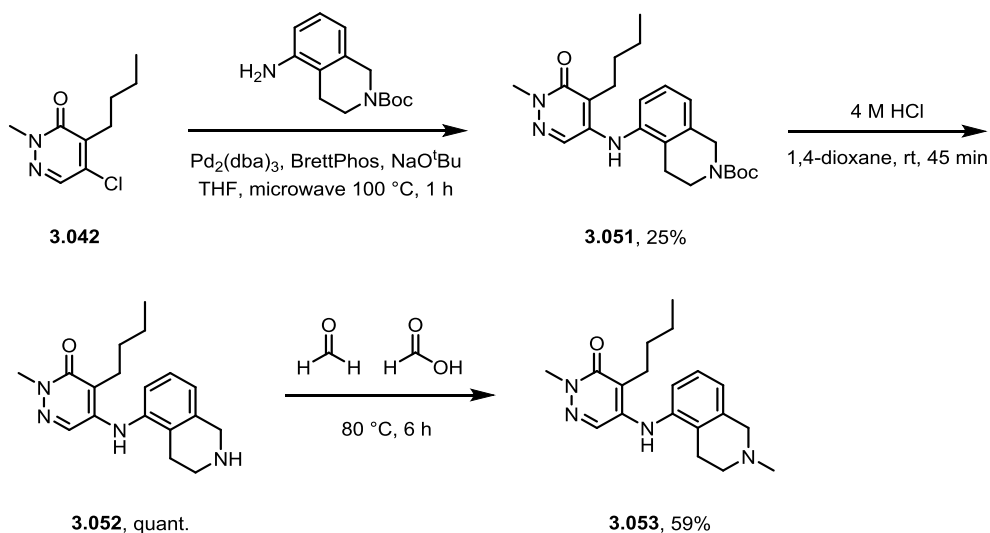
Scheme 3.11: Synthetic route to compound 3.053.

3.7.1.2 Pyridazinone BROMObead Scaffold: Results and Discussion

Compound **3.053** was screened against the DiscoverX BROMO*scan* panel at 10 µM and pleasingly showed exquisite selectivity for BRD7/9 (**Figure 3.24**) and retained activity against BRD9 (100% inhibition). Reduced potency (compared to start point **3.048**) against multiple bromodomains was observed for butylated derivative **3.053** including BAZ2 isoforms, BET bromodomains, BRPF isoforms, CECR2, FALZ and PCAF/GCN5L2 (**Table 3.09**).

153
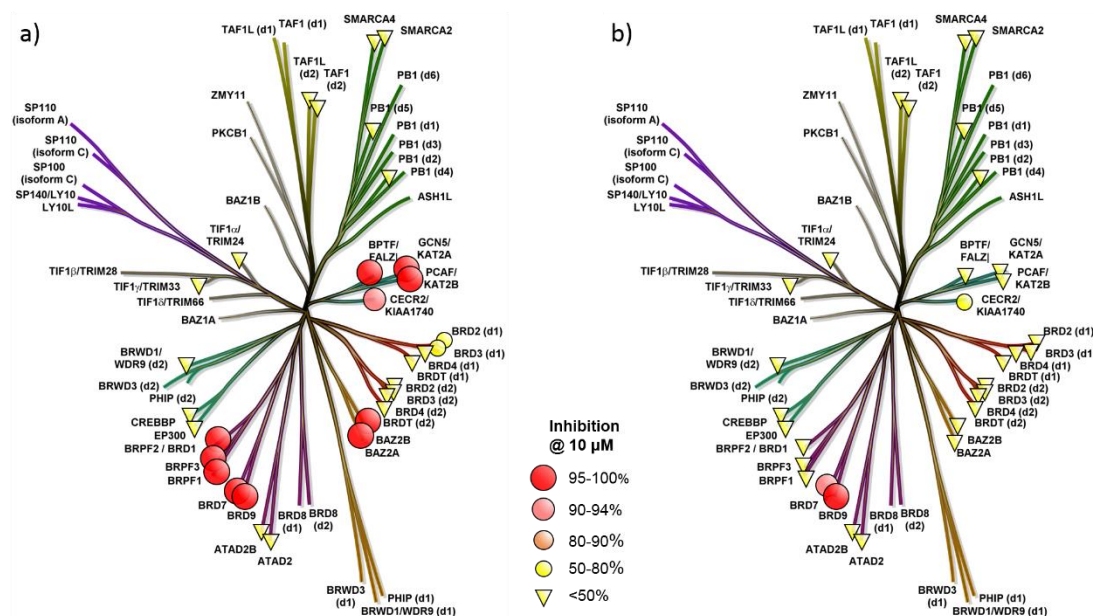
Figure 3.24: a) Compound 3.048 screened at 10 µM against the DiscoverX BROMO*scan* panel; and b) compound 3.053 screened at 10 µM against the DiscoverX BROMO*scan* panel (data shown in Table 3.09).

Compound Number	ATAD2A	ATAD2B	BAZ2A	BAZ2B	BRD1	BRD2(1)	BRD2(2)	BRD3(1)	BRD3(2)	BRD4(1)	BRD4(2)	BRD7	BRD9	BRDT(1)	BRDT(2)	BRPF1
3.048	0	12	100	100	97	53	37	66	48	43	30	100	100	48	15	100
3.053	9	20	8	6	3	12	3	38	27	13	12	93	100	28	11	23

Compound Number	BRPF3	CECR2	CREBBP	EP300	FALZ	GCN5L2	PB1(2)	PB1(5)	PCAF	SMARCA2	SMARCA4	TAF1(2)	TAF1L(2)	TRIM24	TRIM33	WDR9(2)
3.048	100	91	15	1	99	99	9	5	100	2	37	31	9	14	37	2
3.053	21	58	18	6	0	13	15	32	3	6	0	22	0	21	23	0

Table 3.09: Percentage inhibition of bromodomains tested at 10 µM (DiscoverX BROMO*scan* single-shot assay) for 3.048 and butyl derivative 3.053.

154

Compound **3.053**'s potency for BRD9 was measured *via* 11-point dose response curves revealing BRD9 activity had increased upon introduction of the butyl group (**Figure 3.25**).

3.048
BRD9 pK_D = 6.8
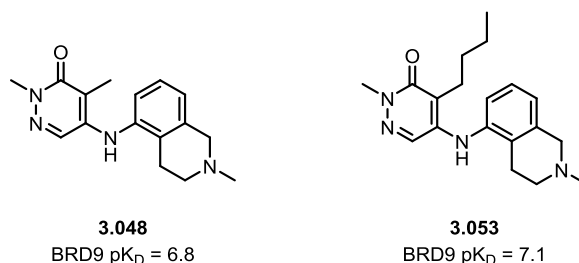
3.053
BRD9 pK_D = 7.1

Figure 3.25: BRD9 potency for compound 3.048 and butylated derivative 3.053.

3.7.2 I-BRD9 Scaffold

Compound **3.053** showed that the butyl motif may be more generally applicable. As such, attention was then shifted to the I-BRD9 (**3.004**) scaffold to investigate whether the methodology could be used to enhance the bromodomain selectivity of existing BRD7/9 inhibitors. **3.004** is a selective BRD9 inhibitor and is discussed further in **Section 3.2**.[51]

Bearing a different core scaffold to **3.039** and **3.053**, the accessibility of the induced hydrophobic pocket from this template was less certain. Overlay of the X-ray crystal structures, however, suggested the ethyl group was functioning as the acetylated Lys methyl mimetic and a suitable vector for the butyl group (**Figure 3.26**).
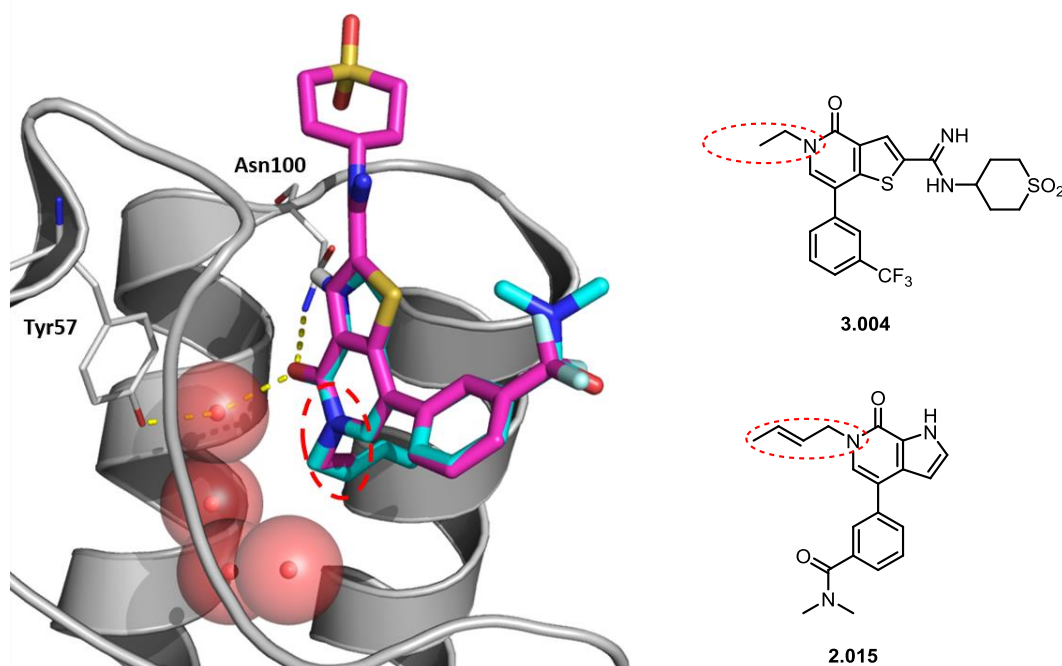
Figure 3.26: Overlay of the crystal structures of compound 3.004 (shown in magenta) (PDB: 4UIW) and 2.015 (shown in cyan) (PDB: 5I7Y) bound to BRD9 (shown in grey). Acetylated Lys methyl mimetics highlighted with red dashed boxes.

3.7.2.1 I-BRD9 Scaffold: Synthesis

The synthesis of compound **3.060** was adapted from the published route to compound **3.004**,[51] starting from commercially available thienopyridinone **3.054** (**Scheme 3.12**). Alkylation with butyl iodide and Cs_2CO_3 at 60 °C introduced the butyl group (**3.055**) in 71% yield. A Negishi cross-coupling with $Zn(CN)_2$ gave nitrile compound **3.056** in 61% yield and a subsequent bromination with NBS delivered intermediate **3.057** in 86% yield. Conversion of the nitrile to the amidine was then attempted *via* a Pinner reaction between **3.057** and the desired amino sulfone, utilizing NaOMe/MeOH as a nucleophilic catalyst. Progression of the reaction stalled at the iminoether intermediate (**3.058**) with further additions of NaOMe and amine having no effect. Consequently, the intermediate was isolated, and the amine reintroduced under alternative conditions. A change in solvent to DMF allowed for higher reaction temperatures (120 °C) and a switch to a non-nucleophilic base (triethylamine) removed the possibility of reversibility. Under these conditions desired amidine **3.059** was obtained (21%) which underwent a Suzuki cross-coupling to deliver final compound **3.060** in 52% yield.

3.054 → **3.055**, 71% → **3.056**, 61%

3.057, 86% → **3.058**, 27%

3.059, 21% → **3.060**, 52%
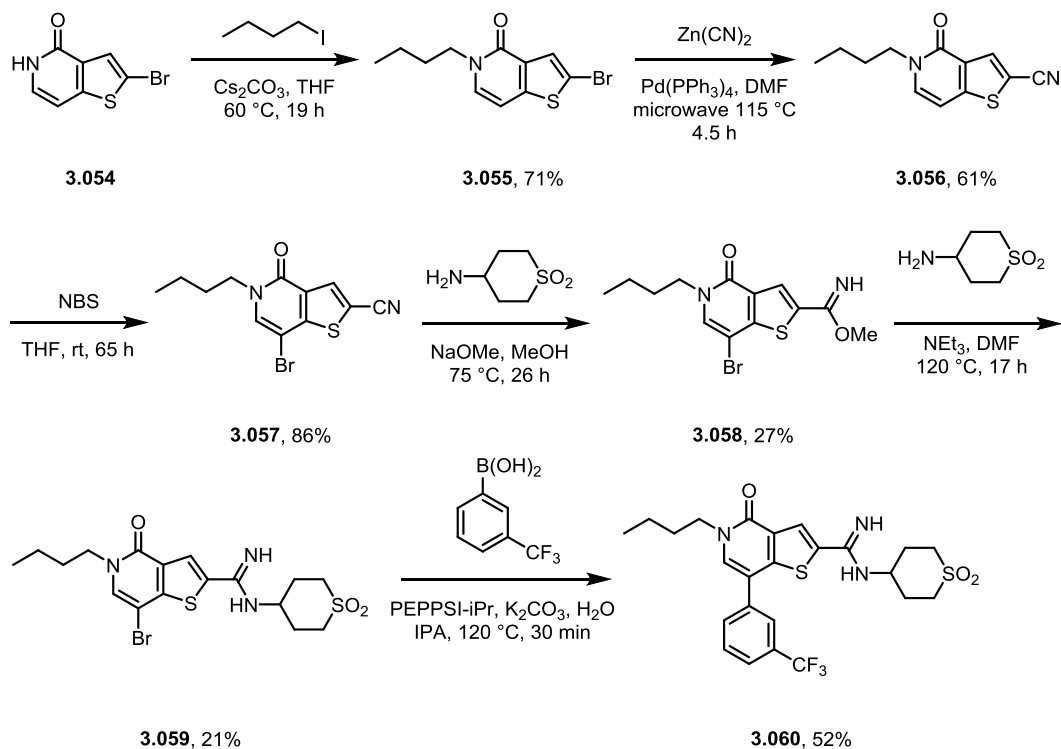
Scheme 3.12: Synthetic route to compound 3.060.

3.7.2.2 I-BRD9 Scaffold: Results and Discussion

Screening of compound **3.060** against the DiscoverX BROMO*scan* panel at 10 µM revealed a reduction in activity against the BET bromodomains, CREBBP/EP300 and a gain in potency against TAF1(2) (**Figure 3.27** & **Table 3.10**), compared to start point **3.004**. Minor reductions were also observed against BRD9 and CECR2 although both appeared potent (94% and 93% inhibition, respectively).

157
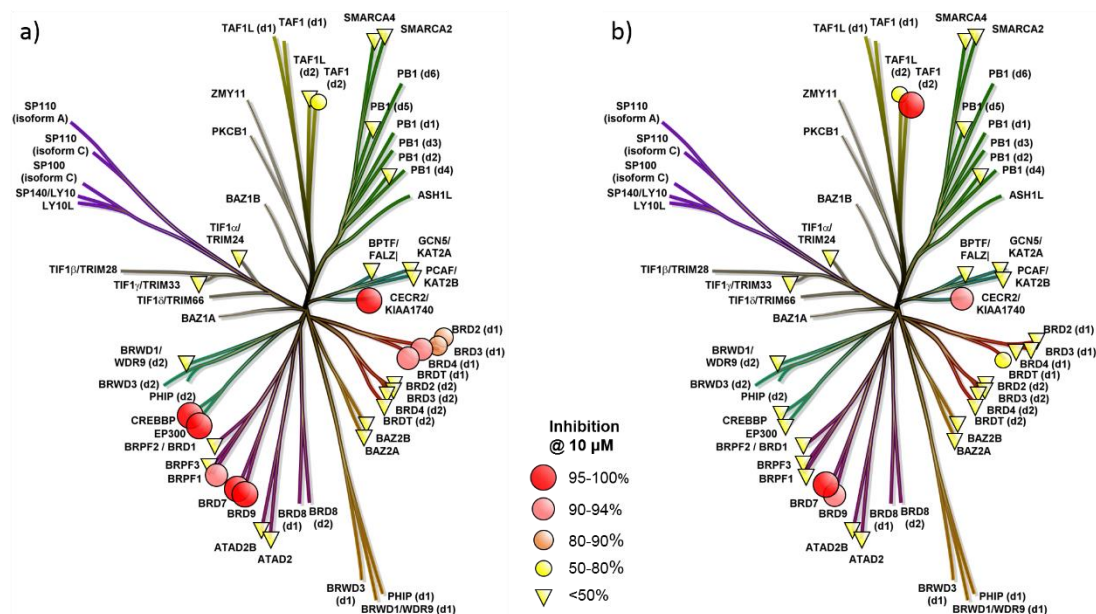
Figure 3.27: a) Compound 3.004 screened at 10 μM against the DiscoverX BROMO*scan* panel; and b) compound 3.060 screened at 10 μM against the DiscoverX BROMO*scan* panel (data shown in Table 3.10).

Compound Number	ATAD2A	ATAD2B	BAZ2A	BAZ2B	BRD1	BRD2(1)	BRD2(2)	BRD3(1)	BRD3(2)	BRD4(1)	BRD4(2)	BRD7	BRD9	BRDT(1)	BRDT(2)	BRPF1
3.004	5	7	10	26	32	80	18	86	36	91	38	98	100	90	19	94
3.060	9	11	1	0	14	38	10	48	18	44	12	97	94	62	9	46

Compound Number	BRPF3	CECR2	CREBBP	EP300	FALZ	GCN5L2	PB1(2)	PB1(5)	PCAF	SMARCA2	SMARCA4	TAF1(2)	TAF1L(2)	TRIM24	TRIM33	WDR9(2)
3.004	5	100	99	99	17	10	3	13	3	24	1	56	9	3	24	0
3.060	25	93	16	15	6	1	0	29	8	8	0	96	57	19	19	2

Table 3.10: Percentage inhibition of bromodomains tested at 10 μM (DiscoverX BROMO*scan* single-shot assay) for 3.004 and butyl derivative 3.060.

158

11-point dose response curves were then obtained to quantify compound **3.060**'s activity against BRD9, TAF1(2) and **3.004**'s closest off-target CECR2 (**Table 3.11**). A reduction in potency against BRD9, CECR2 and the BET bromodomains was confirmed along with increased activity against TAF1(2). Despite losing potency against BRD9, excellent selectivity against the BET bromodomains was maintained and selectivity against CECR2 was improved. Although selectivity over TAF1(2) decreased, compound **3.060** shows an overall improvement in bromodomain selectivity and exemplifies the utility and applicability of the methodology to alternative templates.
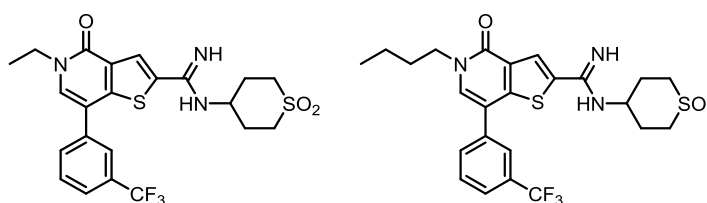
	3.004	**3.060**
BRD9 pK$_D$	8.7	8.0
CECR2 pK$_D$	6.9 (×63)	5.6 (×250)
TAF1(2) pK$_D$	5.1 (×4000)	5.7 (×200)
BRD4(1) pIC$_{50}$	5.3 (×2500)	4.6 (×2500)

Table 3.11: Bromodomain potency profile for compounds 3.004 and 3.060. pK$_D$ values refer to potency in the DiscoverX BROMO*scan* assay. pIC$_{50}$ values refer to potency in a TR-FRET assay.

3.7.3 Bromosporine Scaffold

Bromosporine was discovered by the SGC to function as a pan-bromodomain inhibitor and is notoriously unselective.[226] It was therefore hypothesized that a broader and more complete overview of the effect of the butyl group on bromodomain selectivity could be observed using this template.

X-ray crystallography was used to assess the scaffolds suitability. Overlaying the X-ray crystal structures of **3.049** and **2.015** identified the 3-methyl group of the triazolopyridazine as the acetylated methyl mimetic and a suitable vector for accessing the hydrophobic pocket (**Figure 3.29**).
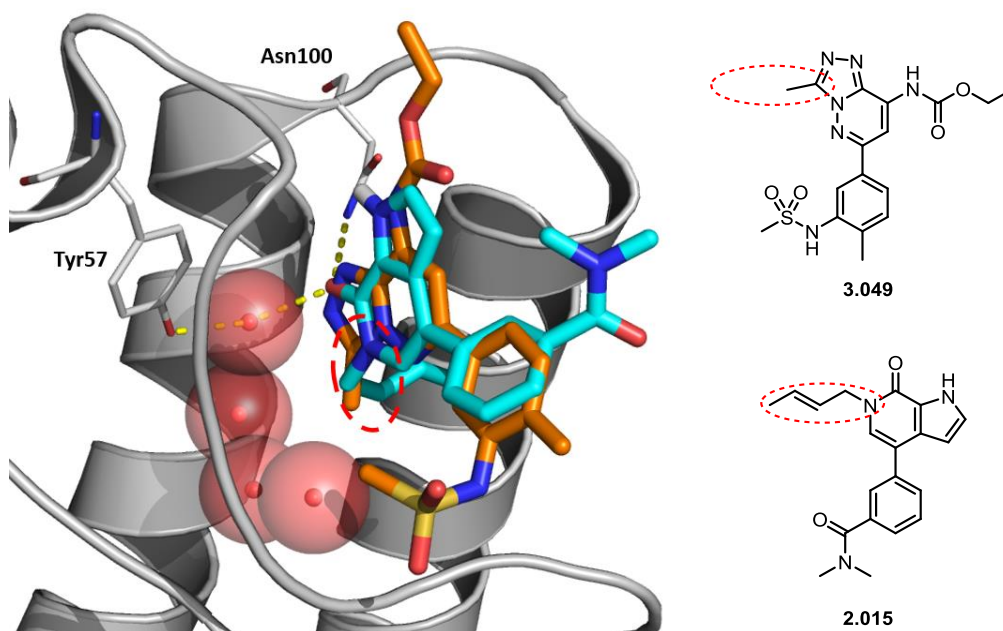
Figure 3.29: Overlay of the crystal structures of compound 3.049 (shown in orange) (PDB: 5IGM) and 2.015 (shown in cyan) (PDB: 5I7Y) bound to BRD9 (shown in grey). Acetylated Lys methyl mimetics highlighted with a red dashed box.

3.7.3.1 Bromosporine Scaffold: Synthesis

The synthesis of compound **3.067** was adapted from a published route to compound **3.049**,[226] starting from commercially available 3,6-dichloropyridazin-4-amine (**3.061**) (**Scheme 3.13**). S_NAr with hydrazine under forcing conditions yielded both regioisomers (**3.062a** and **3.062b**) which, due to similar retention factors on normal and reverse phase columns, could not be separated. Cyclisation with valeric acid produced regioisomers **3.063a** and **3.063b**. The two regioisomers could be separated by silica chromatography and identified *via* ^{1}H-^{15}N HMBC NMR (see **Appendix**, **Figure 5.02**), yielding **3.063a** in 7% and the desired isomer **3.063b** in 43% yield over the two steps. Regioisomer **3.063a** was identified *via* a strong three-bond correlation between proton H_a and N_4 (**Figure 3.30**). By contrast, a strong three-bond signal was observed between H_b and N_5 for regioisomer **3.063b**.
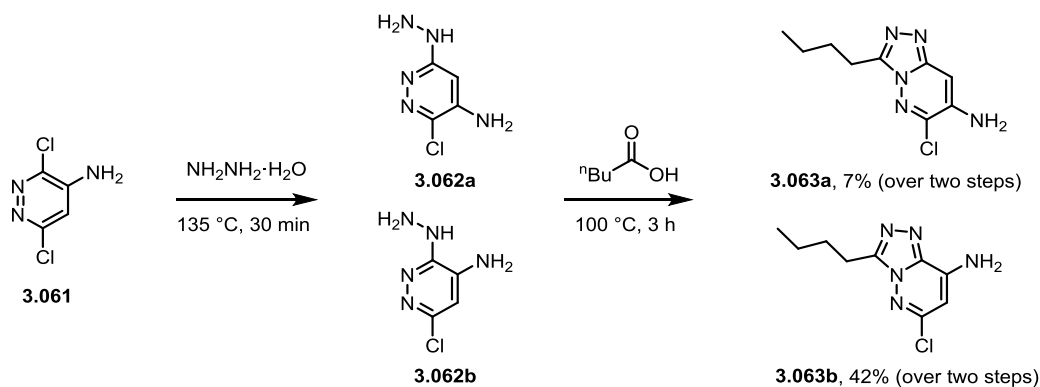
Scheme 3.13: Synthetic route to regioisomers 3.063a and 3.063b.

3.063a
Strong 3-bond ^{1}H-^{15}N
correlation seen between
H_a and N_4

3.063b
Strong 3-bond ^{1}H-^{15}N
correlation seen between
H_b and N_5
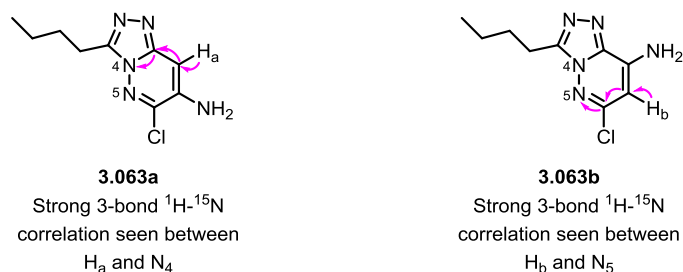
Figure 3.30: Key NMR evidence used to assign regioisomers 3.063a and 3.063b.

Reaction of **3.063b** with ethylchloroformate at room temperature delivered **3.064** in 67% yield and a subsequent Suzuki cross-coupling with the desired aryl boronic acid gave **3.065** in 38% yield (**Scheme 3.14**). Reduction of the nitro group to the aniline (**3.066**) was achieved in 50% yield using powdered iron in acetic acid. Compound **3.066** was then mesylated using MsCl and pyridine as base to give **3.067** in 74% yield.
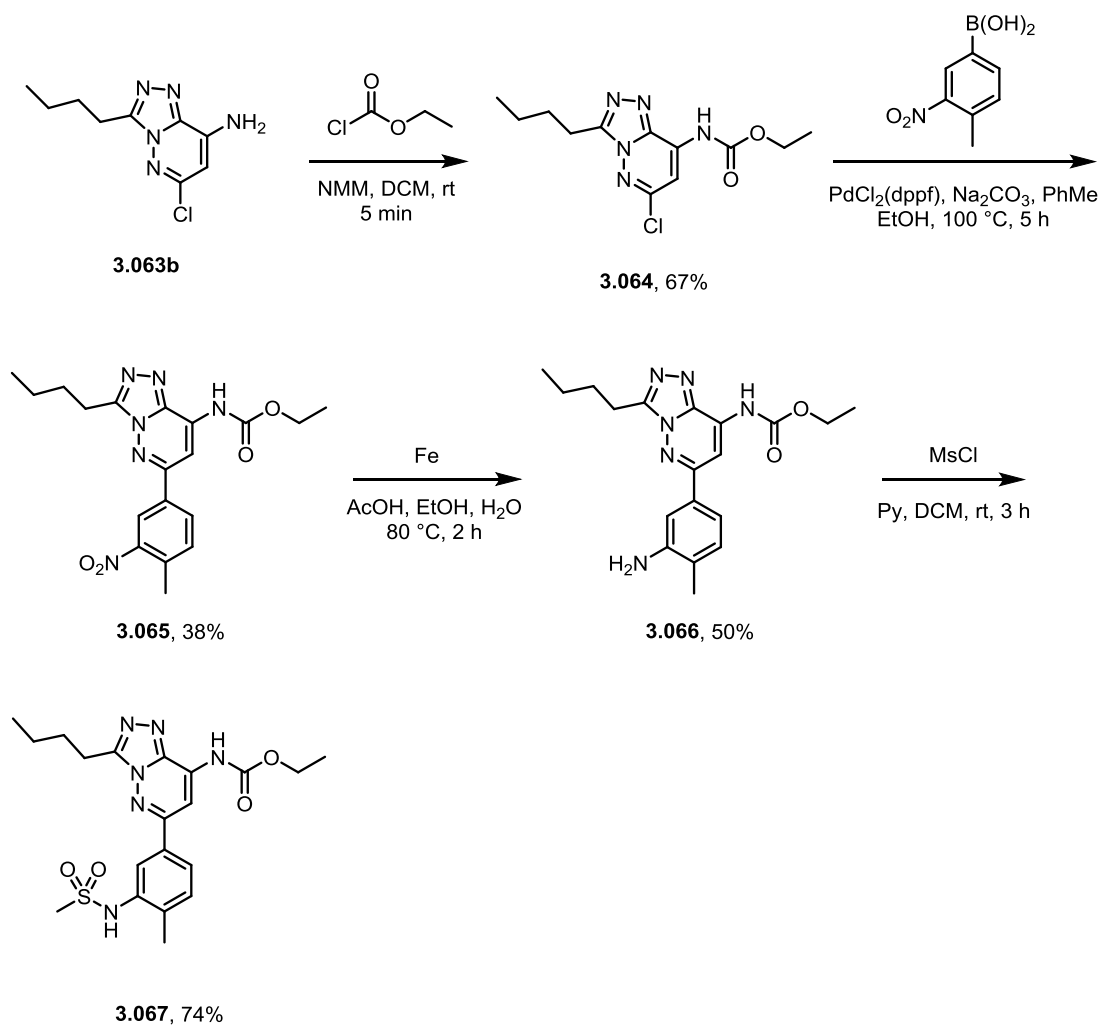
Scheme 3.14: Synthetic route to compound 3.067.

3.7.3.2 Bromosporine Scaffold: Results and Discussion

Screening of **3.067** against the BROMO*scan* panel at 10 µM revealed a reduction in potency, compared to start point **3.049**, against 30/32 bromodomains tested (excluding PB1(2) and WDR9(2) which showed 0% inhibition for **3.049**) (**Figure 3.31** & **Table 3.12**). BRD9 showed the smallest reduction with activity still high (95% inhibition). As before TAF1(2) also retained some activity along with the BET bromodomains. Overall compound **3.067** shows the dramatic shift in selectivity profile and demonstrates the power of the methodology, transforming a promiscuous unselective inhibitor into a potential BRD9 inhibitor.
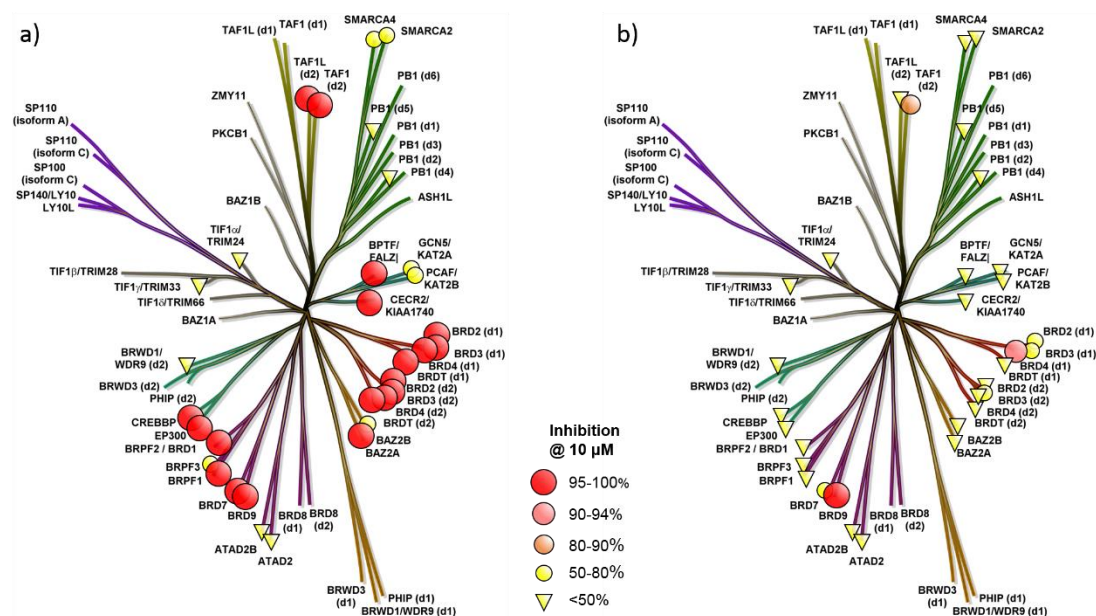
Figure 3.31: a) Compound 3.049 screened at 10 µM against the DiscoverX BROMO*scan* panel; and b) compound 3.067 screened at 10 µM against the DiscoverX BROMO*scan* panel (data shown in Table 3.12).

Compound Number	ATAD2A	ATAD2B	BAZ2A	BAZ2B	BRD1	BRD2(1)	BRD2(2)	BRD3(1)	BRD3(2)	BRD4(1)	BRD4(2)	BRD7	BRD9	BRDT(1)	BRDT(2)	BRPF1
3.049	30	34	100	76	100	100	100	100	100	100	100	100	100	100	100	100
3.067	18	6	0	25	13	68	0	53	63	91	5	63	95	12	16	0

Compound Number	BRPF3	CECR2	CREBBP	EP300	FALZ	GCN5L2	PB1(2)	PB1(5)	PCAF	SMARCA2	SMARCA4	TAF1(2)	TAF1L(2)	TRIM24	TRIM33	WDR9(2)
3.049	78	100	99	99	98	57	0	43	78	76	75	100	100	45	28	0
3.067	3	23	12	22	13	8	4	25	17	27	45	87	30	11	17	0

Table 3.12: Percentage inhibition of bromodomains tested at 10 µM (DiscoverX BROMO*scan* single-shot assay) for 3.049 and butyl derivative 3.067.

163

3.8 Conclusions & Future Work

3.8.1 Conclusions

The concept of bromodomain selectivity through interactions with the conserved water molecules found in the binding pockets of bromodomains was explored. A chemical series was selected, and two synthetic routes designed to allow for a thorough exploration of this methodology. A variety of unsaturated, saturated and branched alkyl chains were investigated probing the effect of conformation, geometric isomerism, alkyl chain length and steric bulk on accessing the induced pocket within BRD9, expanding on previous literature. Four-atom alkyl chains appeared optimal for occupying the induced pocket within BRD9. A flexible butyl chain provided the best selectivity profile and showed a substantial improvement in BET selectivity compared to the literature reported *E*-crotyl chain. The butyl acetylated Lys methyl mimetic was then utilized to develop **3.039** as a high-quality chemical probe for the pre-clinical target validation of the BRD7/9 bromodomains (**Figure 3.32**). **3.039** displays potency for BRD7/9, excellent selectivity against the BET bromodomains and non-BET bromodomains, and good physicochemical properties. Importantly, **3.039** provides a novel chemotype for the BRD7/9 chemical tool box and diverges from the common biaryl scaffold previously seen. An accompanying negative control (**3.047**) was also synthesized to further mitigate false phenotype assignment and improve target validation.

3.039
BRD9 pK_D = 7.2
BET selectivity >500-fold
Non-BET selectivity 320-fold
CAD Sol. (µg/mL) >= 228
AMP (nm/s) = 250

3.047
BRD9 pIC_{50} <4.3
CAD Sol. (µg/mL) >= 150
AMP (nm/s) = 140
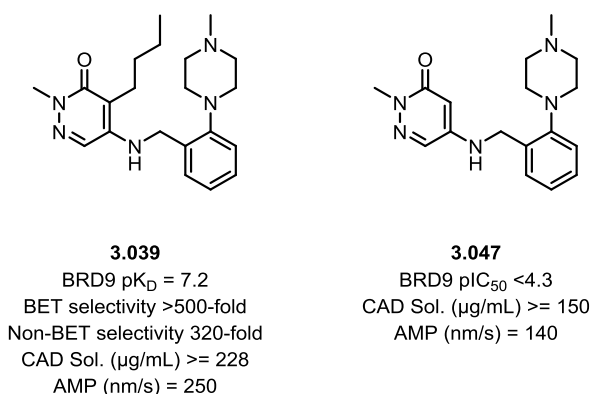
Figure 3.32: BRD7/9 chemical probe 3.039 and accompanying negative control 3.047. CAD solubility, AMP and ChromLogD measurements were all performed at $pH_{7.4}$.

The utility and applicability of this technique was then demonstrated across three templates to prepare BRD9 selective inhibitors in a predictable fashion. First, a selective BRD7/9 inhibitor (**3.053**) was generated on the pyridazinone scaffold from a pan bromodomain inhibitor (**3.048**). The methodology was then applied to existing BRD9 inhibitor **3.004**, to give **3.060**, reducing activity against **3.004**'s closest off-target and improving non-BET bromodomain selectivity overall. Finally, the methodology was applied to pan bromodomain inhibitor bromosporine (**3.049**), to give **3.067**, showcasing the dramatic shift in bromodomain selectivity profile. Including **3.039**, these four examples help support the use of conserved water interactions in the development of selective BRD7/9 bromodomain inhibitors.

3.8.2 Future Work

An effective chemical probe (**3.039**) has been developed for the BRD7/9 bromodomains. Although compound **3.039** appears permeable, activity within cellular assays should be demonstrated before its application in pre-clinical target validation. Future work should focus around demonstrating this *via* a NanoBRET assay or FRAP.

Future work could also explore the possibility of a BRD7/9 PROTAC utilizing **3.039** as the protein binding component (**Figure 3.33**). Additionally, if BRD7/9 selectivity can be biased solely through the use of the butyl motif, the protein binding component can be modified more freely to optimize other properties, such as physicochemical properties, one of the major challenges in PROTAC development. X-ray crystallography suggests that the piperazine nitrogen would be a suitable vector for linker (circled in red) and E3 ligase (circled in blue) placement and offers a suitable starting point (**3.068**) for PROTAC development.
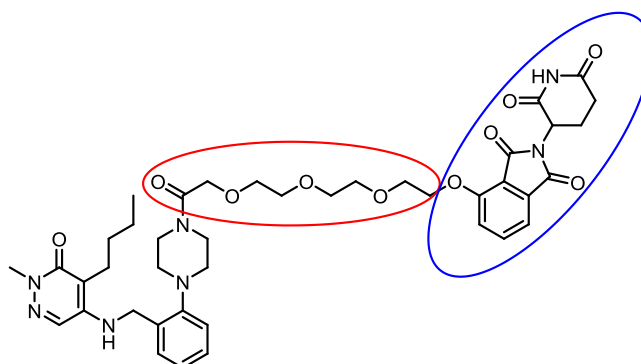
3.068

Figure 3.33: Structure of hypothetical BRD7/9 PROTAC 3.068.

4. Experimental

4.1 General Experimental

The names of the following compounds have been obtained using ChemDraw Ultra 16.0.

NMR Spectroscopy

NMR spectra were recorded on Bruker AV-400 (^{1}H = 400 MHz, ^{13}C = 101 MHz), Bruker AV-500 (^{1}H = 500 MHz, ^{13}C = 125 MHz), Bruker AV-600 (^{1}H = 600 MHz, ^{13}C = 151 MHz) and Bruker AV-700 (^{1}H = 700 MHz, ^{13}C = 176 MHz) instruments.

^{1}H NMR spectra: The chemical shift data for each signal are given as δH in units of parts per million (ppm) relative to tetramethylsilane (TMS) where δ (TMS) = 0.00 ppm. The multiplicity of each signal is indicated by: s (singlet); br. s (broad singlet); d (doublet); t (triplet); q (quartet); quin. (quintet); sext. (sextet); sept. (septet); m (multiplet) or combinations thereof. The number of protons (n) for a given resonance signal is indicated by nH. Coupling constants (J) are quoted in Hz and are recorded to the nearest 0.1 Hz. Identical proton coupling constants (J) are averaged in each spectrum and reported to the nearest 0.1 Hz. All NMR spectra were recorded at room temperature unless otherwise stated.

^{13}C NMR spectra: Recorded with broadband proton decoupling. The chemical shift data for each signal are given as δC in units of parts per million (ppm) relative to tetramethylsilane (TMS) where δC (TMS) = 0.00 ppm. All NMR spectra were recorded at room temperature unless stated.

^{19}F NMR spectra: Recorded with broadband proton and carbon decoupling. The chemical shift data for each signal are given as δF in units of parts per million (ppm). All NMR spectra were recorded at room temperature unless stated.

High Resolution Mass Spectrometry (HRMS)

Chromatography and analysis conditions:

An Agilent 1100 Liquid Chromatograph equipped with a model G1367A autosampler, a model G1312A binary pump and a HP1100 model G1315B diode array detector was used. The method used was generic for all experiments. All separations were achieved using a C18 reversed phase column (100 × 2.1 mm, 3 μm particle size) or equivalent. Gradient elution was carried out with the mobile phases as (A) water containing 0.1% (v/v) TFA and (B) acetonitrile containing 0.1% (v/v) TFA. The conditions for the gradient elution were initially 0% B, increasing linearly to 95% B over 8 min, remaining at 95% B for 0.5 min then decreasing linearly to 0% B over 0.1 min followed by an equilibration period of 1.49 min prior to the next injection. The flow rate was 1 mL/min, split to source and the temperature controlled at 40 °C with an injection volume of between 2 to 5 μL.

Mass Spectrometry conditions:

Positive ion mass spectra were acquired using a Thermo LTQ–Orbitrap FT mass spectrometer, equipped with an ESI interface, over a mass range of 100 – 1100 Da, with a *scan* time of 1 second. The elemental composition was calculated using Xcalibur software and processed using RemoteAnalyzer (Spectral Works Ltd) for the [M+H]+ and the mass error quoted as ppm.

LCMS Methodology

Method using formic acid modifier – LCMS (formic)

LC conditions:

The UPLC analysis was conducted on a Waters Acquity UPLC BEH C18 column (50 mm × 2.1 mm, i.d. 1.7 μm packing diameter) at 40 ˚C. The solvents employed were: A = 0.1% v/v solution of formic acid in water; B = 0.1% v/v solution of formic acid in acetonitrile. The gradient (A:B) employed was from 97:3 to 3:97 over 2 min. The UV detection was a summed signal from wavelength of 210 nm to 350 nm.

MS conditions:

The mass spectrometry was conducted on a Waters ZQ mass spectrometer, with an ionisation mode of alternate–scan positive and negative electrospray. The scan range

was 100 to 1000 AMU, the scan time was 0.27 seconds and the inter–scan delay was 0.10 seconds.

Method using ammonium bicarbonate modifier – LCMS (high pH)

LC conditions:

The UPLC analysis was conducted on a Waters Acquity UPLC BEH C18 column (50 mm × 2.1 mm, i.d. 1.7 µm packing diameter) at 40 °C. The solvents employed were: A = ammonium hydrogen carbonate in water adjusted to pH 10 with ammonia solution; B = acetonitrile. The gradient (A:B) employed was from 99:1 to 0:100 over 2 min. The UV detection was a summed signal from wavelength of 210 nm to 350 nm.

MS conditions:

The mass spectrometry was conducted on a Waters ZQ mass spectrometer, with an ionisation mode of alternate–scan positive and negative electrospray. The scan range was 100 to 1000 AMU, the scan time was 0.27 seconds and the inter–scan delay was 0.10 seconds.

Infrared Spectroscopy Analysis

IR spectra were obtained on a Perkin Elmer Spectrum 1 FTIR apparatus, with major peaks reported.

Melting Point Analysis

Melting point analysis was carried out using Buchi M-565 melting point apparatus.

Flash column chromatography

Purification was performed using Biotage SP4, Isolera One or Teledyne ISCO apparatus with SNAP KP, SNAP ULTRA or RediSepRf pre-packed silica cartridges, eluting with solvents as supplied, under a positive pressure of compressed air.

MDAP Methodology

Method using formic acid modifier – MDAP (formic)

LC conditions:

The HPLC analysis was conducted on either a Sunfire C18 column (100 mm × 19 mm, i.d 5 µm packing diameter) or a Sunfire C18 column (150 mm × 30 mm, i.d. 5 µm packing diameter) at ambient temperature. The solvents employed were: A = 0.1% v/v solution of formic acid in water; B = 0.1% v/v solution of formic acid in acetonitrile. The purification was run as a gradient (A:B) over either 15 or 25 minutes, with a flow rate of 20 mL/min (100 mm × 19 mm, i.d 5 µm packing diameter) or 40 mL/min (150 mm × 30 mm, i.d. 5 µm packing diameter). The UV detection was a summed signal from wavelength of 210 nm to 350 nm.

MS conditions:

The mass spectrometry was conducted on a Waters ZQ mass spectrometer, with an ionisation mode of alternate–scan positive and negative electrospray. The scan range was 100 to 1000 AMU, the scan time was 0.50 secs and the inter–scan delay was 0.20 sec.

Method using ammonium bicarbonate modifier – MDAP (high pH)

LC conditions:

The HPLC analysis was conducted on either an Xbridge C18 column (100 mm × 19 mm, i.d 5 µm packing diameter) or an Xbridge C18 column (100 mm × 30 mm, i.d. 5 µm packing diameter) at ambient temperature. The solvents employed were: A = 10 mM ammonium bicarbonate in water, adjusted to pH 10 with ammonia solution; B = acetonitrile. The purification was run as a gradient (A:B) over either 15 min or 25 min, with a flow rate of 20 mL/min (100 mm × 19 mm, i.d 5 µm packing diameter) or 40 mL/min (150 mm × 30 mm, i.d. 5 µm packing diameter). The UV detection was a summed signal from wavelength of 210 nm to 350 nm.

MS conditions:

The mass spectrometry was conducted on a Waters ZQ mass spectrometer, with an ionisation mode of alternate–scan positive and negative electrospray. The scan range

was 100 to 1000 AMU, the scan time was 0.50 seconds and the inter–scan delay was 0.20 seconds.

Microwave Reactor

Reactions heated under microwave conditions were heated in a Biotage Initiator microwave. All reactions were set with 30 seconds pre-stirring.

Reagents and solvents

All commercial chemicals and solvents were used without further purification unless otherwise specified. All reactions except those in aqueous media were carried out with the use of standard techniques for the exclusion of moisture. *In vacuo* refers to the use of a rotary evaporator attached to a diaphragm pump. Brine refers to a saturated aqueous solution of sodium chloride.

Compound Purity

The purity of compound tested in *in vitro* assays was greater than 95% as determined by LCMS and ^{1}H NMR. All compounds were isolated at >90 wt% unless stated.

TR-FRET Assays

The TR-FRET assays were experimentally performed by members of the GSK SPMB department as described previously.[51,108]

DiscoverX BROMO*scan* Assay

The DiscoverX BROMO*scan* assay was experimentally performed *via* DiscoverX as described.[227]

DiscoverX qPCR Assays

The DiscoverX BROMO*scan* qPCR assays were experimentally performed *via* DiscoverX as described.[227]

Intracellular Concentration Assay

The intracellular concentration assay was experimentally performed by members of the GSK SPMB department using the method outlined below. Hela cells were continuously cultured in MR1-4 custom media (Gibco Life Technologies) + 10% FBS (Gibco Life Technologies) (assay media) at 37 °C, 5% CO_2, with shaking @ 120 RPM. Prior to assay start, the compounds were thawed and the media placed in a 37 °C water bath. 1 mL of HeLa suspension was counted using a Vi-Cell XR counter (Beckman Coulter). An appropriate quantity of cell suspension (4 mL/compound required + 20 mL excess) at 2×10^6 cells/mL in pre-warmed assay media. 4 µl test compound at 10mM in DMSO was added to the columns of two 96 V bottom deep well plates (Greiner-780271) in the following configuration: compound 1 was added to wells A1, C1, and D1 in one 96 deep well plate (Greiner) and E1 and F1 in a second plate. Whilst compound 2 was added to wells A2, C2, and D2 in plate one and E2 and F2 in the second plate and so on.

In plate 1, 2 mL of pre-warmed media (MR1-4 without FBS) was added to row A containing compound. And 2 mL of pre-warmed media (MR1-4 with 10% FBS) was added to rows C and D containing compound. All other wells were left empty. In plate 2 (M-PER), 2 mL cell suspension at 2×10^6 was added to rows E and F containing compound. All other wells were left empty. The plates were covered with a plate lid (Greiner) and incubated for 2.5 hours at 37 °C, 5% CO_2 and with shaking @ 120 RPM. After 2.5 hours the plates were removed from the incubator. Plate 1 remained on the bench until needed and plate 2 (M-PER) containing cell suspension was centrifuged at 500 g for 5 minutes in a centrifuge pre-cooled to 4 °C. The supernatant was discarded and 1 mL/well PBS (Sigma) was added to rows E and F using a multidrop combi. An Agilent Bravo was then used to resuspend the pellet in the PBS by repeat aspiration and ejection. After the wash with PBS, the plate was centrifuged at 500 g for 5 minutes at 4 °C, and the supernatant was discarded, but retaining the cell pellets.

180 µl of M-PER (Thermo-Fisher Scientific) was then added to rows E and F of plate 2 using a multidrop combi to disrupt the cells and generate the total cell condition. Plate 2 was returned to the BRAVO, and the M-PER/cell pellet was mixed and transferred into rows E and F of a standard 96 well V-bottom plate (Greiner), this will now be known as plate 3. Plate 3 was covered and left to incubate for 15 minutes at 37 °C, 5% CO_2 with shaking @ 120 RPM. Plate 3 containing the cell suspension and M-PER in rows E and F were centrifuged at 3300 g for 30 minutes at 4 °C. The supernatants were then removed from Plate 3 using the BRAVO and transferred to another standard 96 well V-bottom plate in the same well positions. This will now be known as Plate 4 or the cell concentration assay master plate. The cell pellets were left in Plate 3 and discarded. Manually, 260 µL of row A of Plate 1 was transferred to row A of Plate 4 (Cell Concentration Assay Master Plate), and 180 µl of rows C and D from Plate 1 (NCC) was transferred to each rows C and D of Plate 4 (cell concentration assay master plate). The final assay plate for Rapidfire – MS analysis was generated using the BRAVO by transferring 5 µl of each sample in plate 4 columns C-F (cell concentration assay master plate) into a new standard 96 V-bottom well plate. This will be known as the cell concentration assay plate (Plate 5). A prepared mixture of 45 parts RPMI media/5 parts internal standard solution (containing 100 ng/mL Sulfamethazine in 5% MeCN)/95 parts of 50% MeCN (aq.) was then added to all wells using a multidrop combi. The samples were then analysed using the Rapidfire-MSMS Mass Spectrometer (API5500 or equivalent).

4.2 Experimental Procedures

2-(Benzyloxy)-8-chloro-3-methyl-1,7-naphthyridine (2.029)
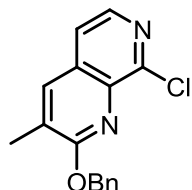
To a solution of 8-chloro-3-methyl-1,7-naphthyridin-2(1H)-one (3.083 g, 15.84 mmol) in DMF (23 mL) was added potassium carbonate (2.850 g, 20.62 mmol). The resulting suspension was stirred at rt for 15 min before being treated with benzyl bromide (2.07 mL, 17.4 mmol). The suspension was then stirred at rt for 2.5 hours. The suspension was diluted with water (20 mL) and EtOAc (20 mL), filtered, and the resulting white solid washed with water (15 mL) and Et_2O (15 mL) before being dried under vacuum for 72 hours at 45 °C yielding **2.029** (3.796 g, 13.33 mmol, 84%) as a white solid. ^{1}H NMR (400 MHz, CHLOROFORM-*d*) δ ppm 8.23 (d, *J*=5.4 Hz, 1 H), 7.81-7.78 (m, 1 H), 7.66-7.61 (m, 2 H), 7.47-7.39 (m, 3 H), 7.38-7.32 (m, 1 H), 5.68 (s, 2 H), 2.44 (d, *J*=1.0 Hz, 3 H); LCMS (formic): R_t = 1.38 min (100%) $[M+H]^+$ = 285.

***tert*-Butyl 4-((2-(benzyloxy)-3-methyl-1,7-naphthyridin-8-yl)amino)piperidine-1-carboxylate (2.030)**
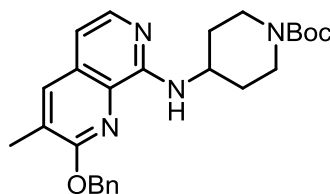
tert-Butyl 4-aminopiperidine-1-carboxylate (1.265 g, 6.320 mmol) was added to a solution of **2.029** (1.200 g, 4.214 mmol), sodium *tert*-butoxide (1.622 g, 16.87 mmol), $Pd_2(dba)_3$ (0.216 g, 0.236 mmol) and 2-(dicyclohexylphosphino)3,6-dimethoxy-2′,4′,6′-triisopropyl-1,1′-biphenyl (0.225 g, 0.419 mmol) in THF (19 mL). The reaction mixture was then stirred at 60 °C for 4 hours before being allowed to cool to rt and then concentrated *in vacuo*. The resultant residue was then diluted with DCM (40 mL) and washed with water (40 mL). The separated organic layer was then passed through a hydrophobic frit and concentrated *in vacuo.* The residue was purified by silica chromatography (0-60% EtOAc in cyclohexane) and the appropriate fractions combined and concentrated *in vacuo* yielding **2.030** (1.360 g, 3.032 mmol, 72%) as an orange solid. m.p. 133–134 °C; v_{max} (solid)/cm^{-1}: 3367 (N-H), 2939, 1682 (C=O), 1516, 1421, 1162, 734; ^{1}H NMR (400 MHz, METHANOL-d_4) δ ppm 7.78-7.76 (m, 1 H), 7.71 (d, *J*=6.0 Hz, 1 H), 7.53-7.47 (m, 2 H), 7.41-7.34 (m, 2 H), 7.33-7.27 (m, 1 H), 6.79 (d, *J*=6.0 Hz, 1 H), 5.55 (s, 2 H), 4.17-4.08 (m, 1 H), 4.08-4.00 (m, 2 H), 3.12-2.98 (m, 2 H), 2.38 (d, *J*=1.0 Hz, 3

H), 2.10-2.01 (m, 2 H), 1.58-1.46 (m, 11 H) (N.B. exchangeable proton not visible); LCMS (formic): R_t = 0.93 min (100%) [M+H]$^+$ = 449.

tert-Butyl 4-((2-(benzyloxy)-5-bromo-3-methyl-1,7-naphthyridin-8-yl)amino)piperidine-1-carboxylate (2.031)

N-Bromosuccinimide (0.824 g, 4.63 mmol) was added to a solution of **2.030** (2.066 g, 4.606 mmol) in chloroform (52 mL) and stirred at rt for 1.5 hours before being diluted with water (30 mL). The organic phase was then passed through a hydrophobic frit and concentrated *in vacuo* to yield **2.031** (2.414 g, 4.577 mmol, 99%) as an orange solid. m.p. 149–152 °C; v_{max} (solid)/cm^{-1}: 3405 (N-H), 2930, 2812, 1660 (C=O), 1594, 1519, 1253, 1165, 1127; ^{1}H NMR (400 MHz, CHLOROFORM-*d*) δ ppm 8.01 (s, 1 H), 7.98-7.95 (m, 1 H), 7.51-7.46 (m, 2 H), 7.44-7.38 (m, 2 H), 7.37-7.32 (m, 1 H), 6.19 (d, *J*=8.1 Hz, 1 H), 5.51 (s, 2 H), 4.28-4.16 (m, 1 H), 4.14-3.99 (m, 2 H), 3.12-3.00 (m, 2 H), 2.45 (d, *J*=1.0 Hz, 3 H), 2.17-2.07 (m, 2 H), 1.57-1.47 (m, 11 H); ^{13}C NMR (101 MHz, CHLOROFORM-*d*) δ ppm 160.3, 154.8, 153.2, 141.2, 137.1, 135.8, 130.1, 128.6, 127.9, 127.8, 127.4, 127.2, 103.2, 79.5, 68.4, 47.5, 42.7, 32.3, 28.5, 16.6; HRMS (M+H)$^+$ calculated for $C_{26}H_{32}BrN_4O_3$ 527.1658; found 527.1655; LCMS (formic): R_t = 1.66 min (97%) [M+H]$^+$ = 527.

tert-Butyl 4-((2-(benzyloxy)-5-(3,6-dihydro-2H-pyran-4-yl)-3-methyl-1,7-naphthyridin-8-yl)amino)piperidine-1-carboxylate (2.032)
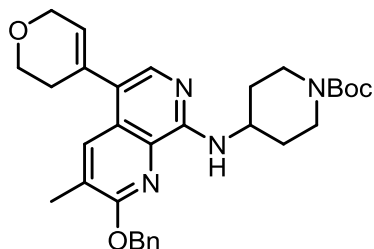
2-(3,6-Dihydro-2H-pyran-4-yl)-4,4,5,5-tetramethyl-1,3,2-dioxaborolane (0.593 g, 2.82 mmol) was added at rt to a stirred mixture of **2.031** (1.163 g, 2.205 mmol), potassium carbonate (0.609 g, 4.41 mmol), Pd(OAc)$_2$ (0.044 g, 0.20 mmol), and butyldi-1-adamantylphosphine (0.070 g, 0.20 mmol) in 1,4-dioxane (9.80 mL) and water (4.90 mL). The resultant reaction mixture was then heated at 100 °C for 1 hour in a microwave reactor. This was repeated a further three

times across three different vessels. The third repeat required a further addition of 2-(3,6-dihydro-2H-pyran-4-yl)-4,4,5,5-tetramethyl-1,3,2-dioxaborolane (0.710 g, 3.38 mmol) and was heated to 100 °C for a further 30 min in a microwave reactor. The four reaction mixtures were allowed to cool to rt before being combined and diluted with EtOAc (80 mL). The combined mixture was filtered through Celite and concentrated *in vacuo* before being purified by silica chromatography (0-50% EtOAc in cyclohexane). The relevant fractions were combined and concentrated *in vacuo* to yield **2.032** (4.42 g, 8.33 mmol, 86%) as an orange solid. m.p. 163-169 °C; v_{max} (solid)/cm^{-1}: 3385 (N-H), 2926, 2849, 1683 (C=O), 1517, 1422, 1151, 701; ^{1}H NMR (400 MHz, CHLOROFORM-*d*) δ ppm 7.89-7.87 (m, 1 H), 7.78 (s, 1 H), 7.56-7.50 (m, 2 H), 7.47-7.40 (m, 2 H), 7.38 (m, 1 H), 6.24 (d, *J*=8.3 Hz, 1 H), 5.84-5.80 (m, 1 H), 5.55 (s, 2 H), 4.41 (app. q, *J*=2.8 Hz, 2 H), 4.35-4.23 (m, 1 H), 4.16-4.06 (m, 2 H), 4.02 (t, *J*=5.4 Hz, 2 H), 3.16-3.04 (m, 2 H), 2.52-2.46 (m, 2 H), 2.44 (d, *J*=1.0 Hz, 3 H), 2.21-2.13 (m, 2 H), 1.60-1.52 (m, 11 H); HRMS (M+H)$^+$ calculated for $C_{31}H_{39}N_4O_4$ 531.2971; found 531.2978; LCMS (formic): Rt = 1.00 min (98%) [M+H]+ = 531.

5-(3,6-Dihydro-2H-pyran-4-yl)-3-methyl-8-(piperidin-4-ylamino)-1,7-naphthyridin-2(1H)-one (2.033)
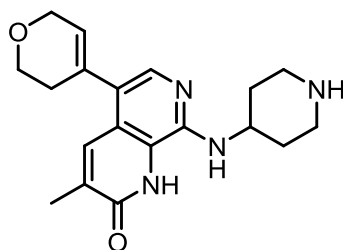
2.032 (0.878 g, 1.66 mmol) was dissolved in TFA (7 mL) and stirred at reflux for 3 hours. The volatile components were removed *in vacuo*. To the resultant residue was added toluene (15 mL) and concentrated *in vacuo* (× 3). The resulting residue was diluted with MeOH (20 mL) and passed through a preconditioned (100 mL MeOH) aminopropyl column (70 g). The column was washed with MeOH (150 mL) and the desired fractions combined and concentrated *in vacuo* yielding **2.033** (0.536 g, 1.57 mmol, 95%) as a yellow solid. m.p. 252–256 °C; v_{max} (solid)/cm^{-1}: 3395 (N-H), 2925, 1658 (C=O), 1593, 1524, 1450, 1127, 845; ^{1}H NMR (400 MHz, CHLOROFORM-*d*) δ ppm 7.86-7.83 (m, 1 H), 7.79 (s, 1 H), 6.59 (d, *J*=6.8 Hz, 1 H), 5.80-5.65 (m, 1 H), 4.43-4.36 (m, 2 H), 4.33-4.21 (m, 1 H), 4.01 (t, *J*=5.3 Hz, 2 H), 3.27-3.16 (m, 2 H), 2.92-2.81 (m, 2 H), 2.49-2.42 (m, 2 H), 2.37 (d, *J*=1.0 Hz, 3 H), 2.27-2.18 (m, 2 H), 1.62 (qd, *J*=11.8, 3.9 Hz, 2 H) (N.B. exchangeable lactam and piperidine amine protons not visible); ^{13}C NMR (101 MHz, CHLOROFORM-*d*) δ ppm 164.4, 146.0,

138.5, 135.7, 132.9, 131.6, 127.0, 122.5, 122.4, 120.3, 65.7, 64.5, 48.8, 45.9, 34.1, 31.1, 17.6; HRMS $(M + H)^+$ calculated for $C_{19}H_{25}N_4O_2$, 341.1978; found 341.1976; LCMS (formic): R_t = 0.39 min (96%) $[M+H]^+$ = 341.

tert-Butyl (3-oxopropyl)carbamate (2.035)
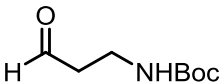
Dess-Martin periodinane (787 mg, 1.86 mmol) was added to a stirred solution of *tert*-butyl (3-hydroxypropyl)carbamate (0.244 mL, 1.43 mmol) in DCM (5 mL) at 0 °C. The resultant reaction mixture was stirred at 0 °C for 15 hours whilst warming to rt. The mixture was diluted with Et_2O (20 mL) and treated with 20% aq. $Na_2S_2O_3$ solution (5 mL) and saturated aq. $NaHCO_3$ solution (5 mL) and stirred vigorously for 1 hour. The organic layer was separated and the aqueous layer extracted with EtOAc (3 × 10 mL). The organic fractions were combined and washed sequentially with 10 wt% aq. $Na_2S_2O_3$ solution (10 mL), saturated aq. $NaHCO_3$ solution (10 mL) and brine (10 mL). The resultant solution was passed through a hydrophobic frit and concentrated *in vacuo* yielding **2.035** (237 mg, 1.368 mmol, 96%). ^{1}H NMR (400 MHz, CHLOROFORM-*d*) δ ppm 9.83 (s, 1 H), 4.99-4.81 (m, 1 H), 3.48-3.42 (m, 2 H), 2.73 (t, *J*=5.8 Hz, 2 H), 1.46 (s, 9 H).

tert-Butyl (3-(4-((5-(3,6-dihydro-2H-pyran-4-yl)-3-methyl-2-oxo-1,2-dihydro-1,7-naphthyridin-8-yl)amino)piperidin-1-yl)propyl)carbamate (2.036)
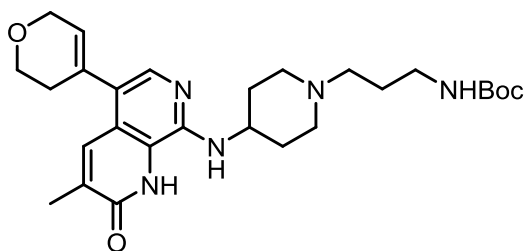
A mixture of **2.033** (0.800 g, 2.35 mmol) and **2.035** (0.244 g, 1.41 mmol) in MeOH (30 mL) and AcOH (3 mL) was stirred at 50 °C for 3 hours. Picoline borane complex (0.251 g, 2.35 mmol) was added and the mixture stirred at 50 °C for a further 24 hours. The reaction mixture was concentrated *in vacuo* and the resultant residue diluted with saturated aq. $NaHCO_3$ solution (5 mL) and DCM (5 mL). The layers were separated and the aqueous layer extracted further with DCM (3 × 5 mL). The organic fractions were combined and passed through a hydrophobic frit before being concentrated *in vacuo*. The resultant solid was dissolved in minimal DCM and purified

by silica chromatography (0-100% EtOH in EtOAc). The desired fractions were combined and concentrated *in vacuo* to yield **2.036** (441 mg, 0.886 mmol, 63%) as a yellow solid. v_{max} (solid)/cm^{-1}: 3395 (N-H), 2930, 1659 (C=O), 1595, 1451, 1126; ^{1}H NMR (400 MHz, DMSO-d_6) δ ppm 11.37 (br. s, 1 H), 7.71-7.69 (m, 1 H), 7.61 (s, 1 H), 6.81-6.75 (m, 1 H), 6.67 (d, *J*=6.8 Hz, 1 H), 5.74-5.71 (m, 1 H), 4.26-4.21 (m, 2 H), 3.98-3.88 (m, 1 H), 3.86 (t, *J*=5.3 Hz, 2 H), 2.95 (app. q, *J*=6.8 Hz, 2 H), 2.87-2.80 (m, 2 H), 2.36-2.24 (m, 4 H), 2.14 (d, *J*=1.0 Hz, 3 H), 2.05-1.92 (m, 4 H), 1.59-1.44 (m, 4 H), 1.39 (s, 9 H); HRMS (M+H)$^+$ calculated for $C_{27}H_{40}N_5O_4$ 498.3080; found 498.3077; LC/MS (high pH): R_t = 1.02 min (94%) [M+H]$^+$ = 498.

8-((1-(3-Aminopropyl)piperidin-4-yl)amino)-5-(3,6-dihydro-2H-pyran-4-yl)-3-methyl-1,7-naphthyridin-2(1H)-one (2.021)

2.036 (55 mg, 0.11 mmol) was dissolved in 4 M HCl in 1,4-dioxane (3 mL) and stirred for 18 hours at rt before being concentrated *in vacuo.* The resultant solid was dissolved in 1:1 MeOH:DMSO and purified by MDAP (high pH: extended). The desired fractions were concentrated *in vacuo* yielding **2.021** (25 mg, 0.063 mmol, 57%) as a yellow solid. m.p. 219–220 °C; v_{max} (solid)/cm^{-1}: 3390 (N-H), 2935, 1659 (C=O), 1594, 1525, 1452, 1126, 843; ^{1}H NMR (400 MHz, DMSO-d_6) δ ppm 7.70-7.67 (m, 1 H), 7.60 (s, 1 H), 6.67 (d, *J*=6.8 Hz, 1 H), 5.74-5.70 (m, 1 H), 4.26-4.21 (m, 2 H), 3.97-3.89 (m, 1 H), 3.86 (t, *J*=5.4 Hz, 2 H), 2.89-2.81 (m, 2 H), 2.63-2.54 (m, 2 H), 2.36-2.28 (m, 4 H), 2.13 (d, *J*=1.0 Hz, 3 H), 2.04-1.91 (m, 4 H), 1.55-1.41 (m, 4 H) (N.B. exchangeable lactam and propylamine protons not visible); ^{13}C NMR (151 MHz, DMSO-d_6) δ ppm 162.6, 145.8, 137.6, 134.0, 133.8, 131.6, 127.1, 122.6, 121.3, 121.1, 65.3, 64.1, 56.3, 52.8, 48.4, 40.6, 32.3, 30.9, 17.3 (one carbon not visible); HRMS (M + H)$^+$ calculated for $C_{22}H_{32}N_5O_2$, 397.2556; found 397.2558; LCMS(high pH): R_t = 0.77 min (97%) [M+H]$^+$ = 398

5-Bromo-3-methyl-8-(piperidin-4-ylamino)-1,7-naphthyridin-2(1H)-one (2.041)
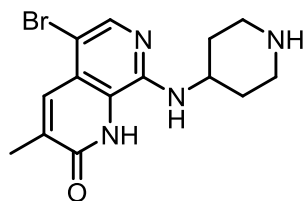
2.031 (9.18 g, 17.4 mmol) was dissolved in TFA (60 mL) at rt. The solution was then heated to reflux and stirred for 18 hours. The volatile components were removed *in vacuo*. To the residue was added toluene (15 mL) and the mixture concentrated *in vacuo* (× 3). The resultant solid was dissolved in MeOH (50 mL) and passed through a preconditioned (100 mL MeOH) aminopropyl column (70 g) and eluted with MeOH (500 mL). The desired fractions were combined and concentrated *in vacuo* yielding **2.041** (5.56 g, 16.5 mmol, 95%) as an orange solid. m.p. 241–244 °C; v_{max} (solid)/cm^{-1}: 3473 (N-H), 3377 (N-H), 2845, 1672 (C=O), 1596, 1434, 1131, 800; ^{1}H NMR (400 MHz, DMSO-d_6) δ ppm 7.92 (s, 1 H), 7.82-7.77 (m, 1 H), 6.95 (d, *J*=6.4 Hz, 1 H), 4.24-4.12 (m, 1 H), 3.43-3.27 (m, 2 H), 3.17 (s, 1 H), 3.12-3.00 (m, 2 H), 2.24-2.08 (m, 5 H), 1.75-1.61 (m, 2 H) (N.B. exchangeable lactam proton not visible); LCMS (formic): Rt = 0.53 min (96%) [M+H]+ = 337.

***tert*-Butyl (3-(4-((5-bromo-3-methyl-2-oxo-1,2-dihydro-1,7-naphthyridin-8-yl)amino)piperidin-1-yl)-3-oxopropyl)(methyl)carbamate (2.039)**
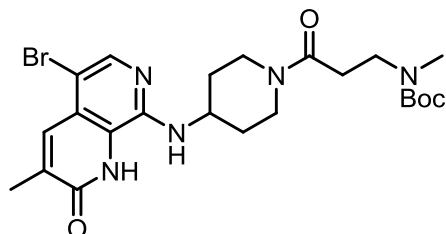
2.041 (200 mg, 0.593 mmol) was added at rt to a stirred solution of 3-((*tert*-butoxycarbonyl)(methyl)amino)propanoic acid (133 mg, 0.652 mmol), HATU (451 mg, 1.19 mmol) and DIPEA (0.310 mL, 1.78 mmol) in DMF (3 mL). The resultant solution was stirred at rt for 3 hours before being diluted with EtOAc (40 mL) and washed with water (40 mL). A precipitate formed and was collected containing the desired product. The organic layer of the resultant filtrate was separated and the aqueous layer extracted with EtOAc (3 × 20 mL). The organic fractions were combined and concentrated *in vacuo*. The resultant solid was dissolved in DCM and purified by silica chromatography (0-50% 3:1 EtOAc:EtOH in cyclohexane). The desired fractions were combined and concentrated *in vacuo* yielding a yellow solid which was combined with the precipitate yielding **2.039** (220 mg, 0.42 mmol, 71%) as a yellow solid. m.p. 191-198 °C; ^{1}H NMR (400 MHz, DMSO-

d_6, 393 K) δ ppm 11.18 (br. s, 1 H), 7.91 (s, 1 H), 7.82-7.79 (m, 1 H), 6.64 (d, J=6.5 Hz, 1 H), 4.30-4.16 (m, 1 H), 4.13-3.98 (m, 2 H), 3.49-3.40 (m, 2 H), 3.21-3.04 (m, 2 H), 2.61-2.55 (m, 2 H), 2.23 (d, J=1.3 Hz, 3 H), 2.10-2.01 (m, 2 H), 1.55-1.47 (m, 2 H), 1.44 (s, 9 H) (N.B. *N*-methyl group peak hidden under water peak visible on rt ^{1}H NMR spectrum at 2.80 ppm); HRMS (M+H)$^+$ calculated for $C_{23}H_{33}BrN_5O_4$ 522.1716; found 522.1713; LCMS (high pH): R_t = 1.07 min (99%) [M+H]+ = 522.

tert-Butyl   (3-(4-((5-bromo-3-methyl-2-oxo-1,2-dihydro-1,7-naphthyridin-8-yl)amino)piperidin-1-yl)propyl)(methyl)carbamate (2.042)
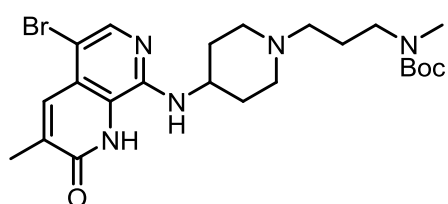
2.039 (169 mg, 0.323 mmol) was dissolved in THF (3.5 mL) at rt under a nitrogen atmosphere. 1 M BH$_3$·THF complex in THF solution (12.94 mL, 12.94 mmol) was then added under nitrogen and the resulting solution stirred at rt for 1 hour.

To the resultant solution was added MeOH (13 mL) at 0 °C under nitrogen (effervescence and an exotherm were observed) and the solution stirred at rt for 96 hours before being concentrated *in vacuo* producing a yellow solid. The resultant solid was dissolved in DCM (40 mL) and diluted with water (40 mL) and the layers separated. The aqueous layer was extracted further with DCM (3 × 20 mL). The organic fractions were combined and washed with brine (20 mL) and passed through a hydrophobic frit before being concentrated *in vacuo* to produce a yellow solid. The resultant solid was dissolved in minimal DCM and purified by silica chromatography (0-100% 3:1 EtOAc:EtOH in cyclohexane. The desired fractions were combined and concentrated *in vacuo* yielding **2.042** (108 mg, 0.212 mmol, 66%). m.p. 190-192 °C; v_{max} (solid)/cm^{-1}: 3392 (N-H), 2929, 1698 (C=O), 1657, 1598, 1449, 1152; ^{1}H NMR (400 MHz, DMSO-d_6, 393 K) δ ppm 11.57 (br. s, 1 H), 7.92 (s, 1 H), 7.81-7.79 (m, 1 H), 6.84 (d, J=6.5 Hz, 1 H), 3.95-3.84 (m, 1 H), 3.20 (t, J=7.2 Hz, 2 H), 2.91-2.83 (m, 2 H), 2.79 (s, 3 H), 2.33-2.26 (m, 2 H), 2.19 (d, J=1.0 Hz, 3 H), 2.10-1.95 (m, 4 H), 1.68-1.60 (m, 2 H), 1.56-1.45 (m, 2 H), 1.41 (s, 9 H); HRMS (M + H)$^+$ calculated for $C_{23}H_{35}BrN_5O_3$, 508.1910; found 508.1917; LCMS (high pH): R_t = 1.22 min (100%) [M+H]$^+$ = 508.

***tert*-Butyl (3-(4-((5-(3,6-dihydro-2H-pyran-4-yl)-3-methyl-2-oxo-1,2-dihydro-1,7-naphthyridin-8-yl)amino)piperidin-1-yl)propyl)(methyl)carbamate (2.043)**
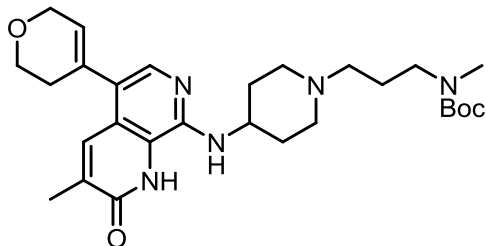
2-(3,6-Dihydro-2H-pyran-4-yl)-4,4,5,5-tetramethyl-1,3,2-dioxaborolane (67 mg, 0.32 mmol) was added at rt to a stirred mixture of **2.042** (81 mg, 0.16 mmol), potassium carbonate (40 mg, 0.29 mmol), Pd(OAc)$_2$ (4 mg, 0.02 mmol) and butyldi-1-adamantylphosphine (6 mg, 0.02 mmol) in 1,4-dioxane (10 mL) and water (5 mL). The resultant solution was then heated at 100 °C for 2 hours in a microwave reactor. Further 2-(3,6-dihydro-2H-pyran-4-yl)-4,4,5,5-tetramethyl-1,3,2-dioxaborolane (67 mg, 0.32 mmol), potassium carbonate (40 mg, 0.29 mmol), Pd(OAc)$_2$ (4 mg, 0.02 mmol) and butyldi-1-adamantylphosphine (6 mg, 0.02 mmol) were added and the reaction mixture stirred at 100 °C for 1 hour in a microwave reactor. The resultant solution was allowed to cool to rt before being diluted with EtOAc (15 mL) and filtered through Celite. The resultant solution was concentrated *in vacuo* yielding an orange solid which was then dissolved in minimal DCM and purified by silica chromatography (0-75% 10% MeOH in DCM in DCM). The desired fractions were combined and concentrated *in vacuo* yielding **2.043** (50 mg, 0.10 mmol, 61%) as a yellow solid. m.p. 200-202 °C; ν$_{max}$ (solid)/cm^{-1}: 3390 (N-H), 2925, 1659 (C=O), 1448, 1125, 843; ^{1}H NMR (400 MHz, DMSO-d_6, 393 K) δ ppm 7.70-7.69 (m, 1 H), 7.63 (s, 1 H), 6.46-6.42 (m, 1 H), 5.77-5.73 (m, 1 H), 4.27 (app. q, *J*=2.7 Hz, 2 H), 4.07-4.03 (m, 1 H), 3.90 (t, *J*=5.4 Hz, 2 H), 3.27-3.24 (m, 2 H), 2.83 (s, 3 H), 2.49-2.39 (m, 2 H), 2.38-2.33 (m, 2 H), 2.30-2.21 (m, 2 H), 2.18 (d, *J*=1.3 Hz, 3 H), 2.08-1.99 (m, 2 H), 1.75-1.68 (m, 2 H), 1.66-1.57 (m, 2 H), 1.45 (s, 9 H) (N.B. exchangeable lactam proton not visible and a further signal hidden under water peak but visible on rt NMR at 2.93-2.83 (m, 2 H)); HRMS (M+H)$^+$ calculated for C$_{28}$H$_{42}$N$_5$O$_4$ 512.3237; found 512.3232; LCMS (high pH): R$_t$ = 1.09 min (92%) [M+H]+ = 512.

5-(3,6-Dihydro-2H-pyran-4-yl)-3-methyl-8-((1-(3-(methylamino)propyl)piperidin-4-yl)amino)-1,7-naphthyridin-2(1H)-one (2.037)
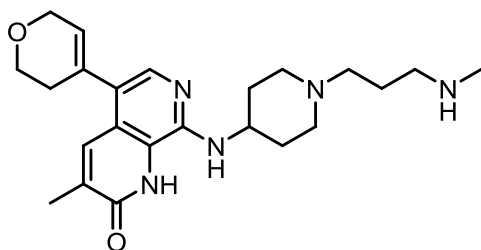
2.043 (47 mg, 0.092 mmol) was dissolved in 4 M HCl in 1,4-dioxane (7 mL) at rt. The resultant solution was stirred at rt for 2 hours before being concentrated *in vacuo*. The resultant solid was dissolved in 1:1 MeOH:DMSO and purified by MDAP (high pH). The desired fractions were combined and concentrated *in vacuo* to yield **2.037** (24 mg, 0.058 mmol, 64%) as a yellow solid. m.p. 212–214 °C; v_{max} (solid)/cm^{-1}: 3386 (N-H), 2930, 1658 (C=O), 1597, 1447, 1122, 667; ^{1}H NMR (400 MHz, DMSO-d_6, 393 K) δ ppm 7.70-7.67 (m, 1 H), 7.62 (s, 1 H), 6.50-6.38 (m, 1 H), 5.79-5.70 (m, 1 H), 4.27 (app. q, J=2.8 Hz, 2 H), 4.10-3.95 (m, 1 H), 3.89 (t, J=5.4 Hz, 2 H), 2.87 (dt, J=11.8, 3.3 Hz, 2 H), 2.59-2.54 (m, 2 H), 2.44-2.30 (m, 7 H), 2.23-2.10 (m, 5 H), 2.05-1.96 (m, 2 H), 1.65-1.52 (m, 4 H) (N.B. exchangeable lactam and methylamine proton not visible); HRMS (M+H)$^+$ calculated for $C_{23}H_{34}N_5O_2$ 412.2713; found 412.2712; LCMS (high pH): R_t = 0.85 min (100%) [M+H]$^+$ = 412.

## 5-Bromo-8-((1-(3-(dimethylamino)propanoyl)piperidin-4-yl)amino)-3-methyl-1,7-naphthyridin-2(1H)-one (2.040)
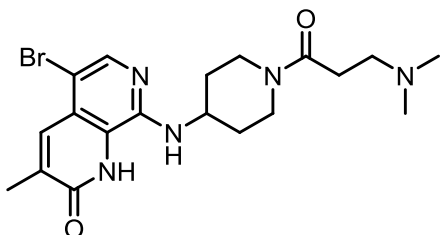
DIPEA (0.232 mL, 1.33 mmol) was added to a stirred solution of 3-(dimethylamino)propanoic acid (57 mg, 0.49 mmol), **2.041** (150 mg, 0.445 mmol) and HATU (338 mg, 0.890 mmol) in DMF (2 mL) at rt. The reaction mixture was stirred for 30 min before being purified *via* MDAP (high pH: extended). The desired fractions were combined yielding **2.040** (55 mg, 0.13 mmol, 28%) as a yellow solid. m.p. 115-118 °C; v_{max} (solid)/cm^{-1}: 3383 (N-H), 2948, 1596 (C=O), 1441, 1033; ^{1}H NMR (400 MHz, DMSO-d_6, 393 K) δ ppm 7.89 (s, 1 H), 7.78 (s, 1 H), 6.69 (br. s, 1 H), 4.29-4.16 (m, 1 H), 4.11-3.98 (m, 2 H), 3.18-3.03 (m, 2 H), 2.57 (t, J=7.1 Hz, 2 H), 2.47 (t, J=7.1 Hz, 2 H), 2.22 (s, 3 H), 2.20 (s, 6 H), 1.98 - 2.09 (m, 2 H), 1.41 - 1.54 (m, 2 H) (N.B. exchangeable lactam proton not visible);^{13}C NMR (101 MHz, DMSO-d_6) δ ppm 169.9,

162.7, 146.2, 139.9, 135.8, 134.2, 123.0, 121.9, 103.7, 48.2, 45.6, 44.3, 32.4, 31.6, 31.3, 17.2; HRMS (M+H)$^+$ calculated for $C_{19}H_{27}BrN_5O_2$ 436.1348; found 436.1348; LC/MS (high pH): Rt = 0.79 min(100%) [M+H]+ = 436

3-(4-((5-Bromo-3-methyl-2-oxo-1,2-dihydro-1,7-naphthyridin-8-yl)amino)piperidin-1-yl)-*N,N*-dimethylpropanamide (2.045)
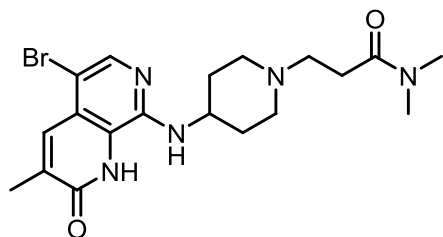
N,N-Dimethylacrylamide (0.459 mL, 4.45 mmol) was added at rt to a stirred solution of **2.041** (300 mg, 0.890 mmol) and dolomite (164 mg, 0.890 mmol) in water (10 mL). The reaction mixture was heated to 100 °C and stirred for 6 hours. The reaction mixture was decanted off from the dolomite and allowed to cool to rt. The aqueous layer was diluted with water (20 mL) and washed with EtOAc (2 × 30 mL). The aqueous layer was concentrated *in vacuo* yielding **2.045** (355 mg, 0.814 mmol, 91%) as an orange solid. m.p. 219–221 °C; v_{max} (solid)/cm^{-1}: 3382 (N-H), 2927, 1650 (C=O), 1597 (C=O), 1436, 1129, 718; ^{1}H NMR (400 MHz, DMSO-d_6, 393 K) δ ppm 7.92 (s, 1 H), 7.81 (s, 1 H), 6.71 (br. s, 1 H), 4.26-4.12 (m, 1 H), 3.50-3.35 (m, 2 H), 3.33-3.21 (m, 2 H), 3.16-3.03 (m, 2 H), 2.96 (s, 6 H), 2.81 (t, *J*=6.8 Hz, 2 H), 2.28-2.12 (m, 5 H), 1.95-1.77 (m, 2 H) (N.B. exchangeable lactam proton not visible); HRMS (M+H)$^+$ calculated for $C_{19}H_{27}BrN_5O_2$ 436.1348; found 436.1346; LC/MS (high pH): Rt = 0.83 min (97%) [M+H]+ = 436.

5-Bromo-8-((1-(3-(dimethylamino)propyl)piperidin-4-yl)amino)-3-methyl-1,7-naphthyridin-2(1H)-one (2.046)
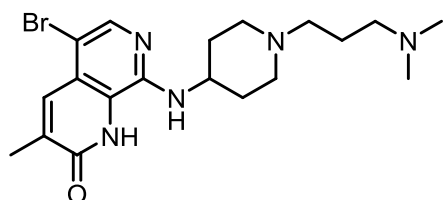
2.045 (333 mg, 0.763 mmol) was dissolved in THF (8 mL) at rt under nitrogen. 1 M BH$_3$·THF complex in THF solution (30.5 mL, 30.5 mmol) was added to the reaction mixture at rt under nitrogen and the resulting solution stirred at rt for 4 hours. To the reaction mixture was added MeOH (10 mL) at 0 ºC. The solution was then concentrated *in vacuo* yielding a yellow solid. The solid was dissolved in MeOH

(6 mL) and 2 M aq. HCl solution (2 mL) and heated at 80 °C for 3 hours. The solution was allowed to cool to rt before being concentrated under a positive flow of nitrogen. The resultant residue was dissolved in water and purified *via* MDAP (high pH). The desired fractions were combined and concentrated *in vacuo* yielding **2.046** (70 mg, 0.17 mmol, 22%) as a yellow solid. m.p. 197–200 °C; v_{max} (solid)/cm^{-1}: 3390 (N-H), 2939, 2759, 1661 (C=O), 1596 (C=O), 1442; ^{1}H NMR (400 MHz, DMSO-d_6, 393 K) δ ppm 7.83 (s, 1 H), 7.76-7.71 (m, 1 H), 6.71-6.56 (m, 1 H), 4.00-3.90 (m, 1 H), 2.86-2.78 (m, 2 H), 2.35 (t, *J*=7.2 Hz, 2 H), 2.28 (t, *J*=7.2 Hz, 2 H), 2.21 (s, 3 H), 2.18-2.09 (m, 8 H), 2.02-1.93 (m, 2 H), 1.62-1.50 (m, 4 H) (N.B. exchangeable lactam proton not visible); HRMS (M+H)$^+$ calculated for $C_{19}H_{29}BrN_5O$ 422.1555; found 422.1550; LC/MS (formic): Rt = 0.43 min (100%) [M+H]+ = 422.

5-(3,6-Dihydro-2H-pyran-4-yl)-8-((1-(3-(dimethylamino)propyl)piperidin-4-yl)amino)-3-methyl-1,7-naphthyridin-2(1H)-one (2.038)
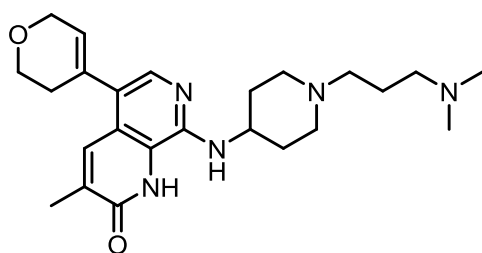
2-(3,6-Dihydro-2H-pyran-4-yl)-4,4,5,5-tetramethyl-1,3,2-dioxaborolane (30 mg, 0.14 mmol) was added at rt to a stirred mixture of **2.046** (30 mg, 0.071 mmol), potassium carbonate (29 mg, 0.21 mmol), Pd(OAc)$_2$ (2 mg, 0.007 mmol) and butyldi-1-adamantylphosphine (3 mg, 0.007 mmol) in 1,4-dioxane (7 mL) and water (3.5 mL). The resultant solution was then heated at 100 °C for 1 hour 45 min in a microwave reactor. 2-(3,6-Dihydro-2H-pyran-4-yl)-4,4,5,5-tetramethyl-1,3,2-dioxaborolane (30 mg, 0.14 mmol), potassium carbonate (30 mg, 0.21 mmol), Pd(OAc)$_2$ (2 mg, 0.007 mmol) and butyldi-1-adamantylphosphine (3 mg, 0.007 mmol) were added and the reaction mixture heated for 1 hour at 100 ºC in a microwave reactor. 2-(3,6-dihydro-2H-pyran-4-yl)-4,4,5,5-tetramethyl-1,3,2-dioxaborolane (30 mg, 0.14 mmol), potassium carbonate (30 mg, 0.21 mmol), Pd(OAc)$_2$ (2 mg, 0.007 mmol) and butyldi-1-adamantylphosphine (3 mg, 0.007 mmol) were added and the reaction mixture heated for 45 min at 100 ºC in a microwave reactor. The resultant mixture was diluted with EtOAc (5 mL) and passed through Celite. The Celite was washed with EtOAc and the resultant solution concentrated *in vacuo* yielding an orange solid. The solid was dissolved in 1:1:2 MeOH:DMSO:water (0.8 mL) and purified by MDAP (high pH:

extended). The desired fractions were combined yielding **2.038** (9 mg, 0.02 mmol, 30%) as an orange solid. m.p. 208–212 °C; v_{max} (solid)/cm^{-1}: 3396, (N-H), 2923, 1657 (C=O), 1594, 1449, 1126, 841, 663; ^{1}H NMR (400 MHz, DMSO-d_6, 393 K) δ ppm 7.70-7.68 (m, 1 H), 7.63 (s, 1 H), 6.44 (d, J=6.3 Hz, 1 H), 5.77-5.73 (m, 1 H), 4.27 (app. q, J=2.6 Hz, 2 H), 4.08-3.96 (m, 1 H), 3.90 (t, J=5.4 Hz, 2 H), 2.40-2.34 (m, 4 H), 2.30 (t, J=7.2 Hz, 2 H), 2.17-2.11 (m, 9 H), 2.17-2.11 (m, 2 H), 2.04-1.98 (m, 2 H), 1.64-1.53 (m, 4 H) (N.B. exchangeable lactam proton not visible and a further 2 H signal obscured by water peak); HRMS (M+H)$^+$ calculated for $C_{24}H_{36}N_5O_2$ 426.2869; found 426.2863; LCMS (high pH): R_t = 0.97 min (96%) [M+H]$^+$ = 426.

8-((1-(3-Aminopropanoyl)piperidin-4-yl)amino)-5-(3,6-dihydro-2H-pyran-4-yl)-3-methyl-1,7-naphthyridin-2(1H)-one (2.049)
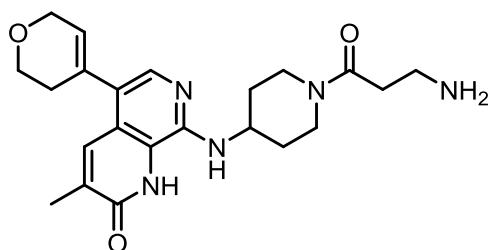
HATU (241 mg, 0.634 mmol) and DIPEA (0.166 mL, 0.951 mmol) were added at rt to a stirred solution of 3-((*tert*-butoxycarbonyl)amino)propanoic acid (60 mg, 0.32 mmol) in DMF (3 mL). After 5 minutes **2.033** (108 mg, 0.317 mmol) was added at rt to the stirred solution and the reaction mixture stirred for 6.5 hours. The reaction mixture was then diluted with water (10 mL) and extracted with EtOAc (4 × 10 mL). The combined organic fractions were washed with brine (10 mL), passed through a hydrophobic frit and concentrated *in vacuo*. The resultant solid was dissolved in 4 M HCl in 1,4-dioxane (14 mL) at rt. The resultant solution was stirred at rt for 2 hours before being concentrated *in vacuo*. The resultant solid was dissolved in 1:1 MeOH:DMSO and purified by MDAP (high pH). The desired fractions were combined and concentrated *in vacuo* to yield **2.049** (24 mg, 0.058 mmol, 18%) as a yellow solid. v_{max} (solid)/cm^{-1}: 3390 (N-H), 2935, 1680 (C=O), 1621, 1513, 1417, 1364, 1126, 761; ^{1}H NMR (400 MHz, DMSO-d_6, 393 K) δ ppm 7.71-7.67 (m, 1 H), 7.64 (s, 1 H), 6.51-6.44 (m, 1 H), 5.77-5.73 (m, 1 H), 4.33-4.23 (m, 3 H), 4.12-4.01 (m, 2 H), 3.89 (t, J=5.4 Hz, 2 H), 3.19-3.08 (m, 2 H), 2.45 (t, J=6.5 Hz, 2 H), 2.38-2.32 (m, 2 H), 2.17 (d, J=1.0 Hz, 3 H), 2.09-2.00 (m, 2 H), 1.54-1.42 (m, 2 H) (N.B. exchangeable lactam and primary amine protons not visible and signal obscured by water peak but visible on rt ^{1}H NMR spectrum at 2.78-2.73 ppm (m, 2 H)); HRMS (M+H)$^+$ calculated

for $C_{22}H_{30}N_5O_3$ 412.2349; found 412.2341; LCMS (high pH): R_t = 0.68 min (95%) $[M+H]^+$ = 412.

3-(4-((5-(3,6-Dihydro-2H-pyran-4-yl)-3-methyl-2-oxo-1,2-dihydro-1,7-naphthyridin-8-yl)amino)piperidin-1-yl)propanamide (2.050)
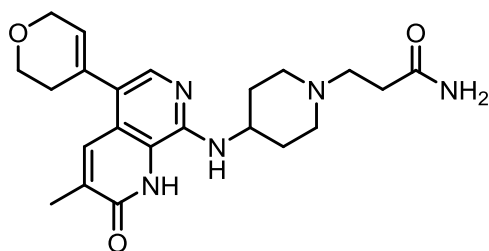

Acrylamide (0.017 g, 0.24 mmol) was added at rt to a stirred solution of **2.033** (0.081 g, 0.24 mmol) and dolomite (0.022 g, 0.12 mmol) in water (2 mL). The reaction was stirred vigorously at rt for 96 hours. Further acrylamide (0.068 g, 0.95 mmol) was added and the reaction stirred vigorously for 5 hours. The reaction mixture was allowed to settle, and the solution decanted away from the dolomite and concentrated *in vacuo*. The resultant solid was dissolved in 1:1 MeOH:DMSO and purified by MDAP (high pH). The relevant fractions were combined and concentrated *in vacuo* yielding **2.050** (22 mg, 0.053 mmol, 23%) as a yellow solid. m.p. 241–246 °C; v_{max} (solid)/cm^{-1}: 3398 (N-H), 2940, 1660 (C=O), 1594, 1455, 1123, 843; ^{1}H NMR (400 MHz, DMSO-d_6, 393 K) δ ppm 7.68-7.66 (m, 1 H), 7.60 (s, 1 H), 6.76-6.49 (m, 2 H), 6.47-6.39 (m, 1 H), 5.77-5.72 (m, 1 H), 4.26 (app. q, *J*=2.8 Hz, 2 H), 4.08-3.95 (m, 1 H), 3.89 (t, *J*=5.4 Hz, 2 H), 2.62 (t, *J*=7.1 Hz, 2 H), 2.40-2.32 (m, 2 H), 2.27 (t, *J*=7.1 Hz, 2 H), 2.25-2.14 (m, 5 H), 2.05-1.95 (m, 2 H), 1.63-1.51 (m, 2 H) (N.B. exchangeable lactam proton not visible and signal obscured by water peak but visible on rt ^{1}H NMR spectrum at 2.89-2.80 ppm (m, 2 H)); ^{13}C NMR (151 MHz, DMSO-d_6) δ ppm 173.9, 162.6, 145.7, 137.6, 134.1, 133.8, 131.7, 127.2, 122.7, 121.3, 65.3, 64.1, 54.5, 52.4, 48.2, 33.7, 32.2, 30.9, 17.3 (N.B. one carbon not visible); HRMS (M+H)$^+$ calculated for $C_{22}H_{30}N_5O_3$ 412.2349; found 412.2352; LCMS (high pH): R_t = 0.71 min (100%) $[M+H]^+$ = 412.

***tert*-Butyl (3-(4-((5-(3,6-dihydro-2H-pyran-4-yl)-3-methyl-2-oxo-1,2-dihydro-1,7-naphthyridin-8-yl)amino)piperidin-1-yl)-3-oxopropyl)carbamate (2.051)**
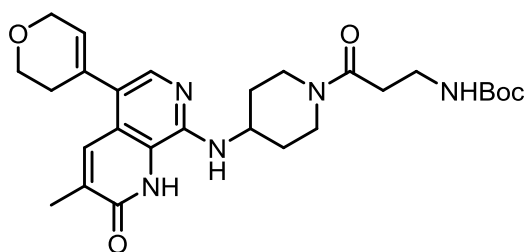
HATU (378 mg, 0.993 mmol) and DIPEA (0.259 mL, 1.49 mmol) were added at rt to a stirred solution of 3-((*tert*-butoxycarbonyl)amino)propanoic acid (113 mg, 0.596 mmol) and **2.033** (169 mg, 0.496 mmol) in DMF (3 mL). The reaction mixture was stirred at rt for 5 hours before being diluted with water (10 mL) and extracted with EtOAc (4 × 10 mL). The combined organic fractions were washed with brine (10 mL), passed through a hydrophobic frit and concentrated *in vacuo*. The resultant solid was dissolved in 1:1 MeOH:DMSO and purified by MDAP (formic). The desired fractions were combined and concentrated *in vacuo* yielding **2.051** (104 mg, 0.203 mmol, 41%) as a cream solid. ^{1}H NMR (400 MHz, DMSO-d_6, 393 K) δ ppm 11.06 (br. s, 1 H), 7.71-7.67 (m, 1 H), 7.64 (s, 1 H), 6.53-6.40 (m, 1 H), 6.19-5.95 (m, 1 H), 5.78-5.70 (m, 1 H), 4.27 (app. q, J=2.8 Hz, 2 H), 4.10-3.95 (m, 1 H), 3.89 (t, J=5.4 Hz, 2 H), 3.30-3.06 (m, 4 H), 2.56-2.51 (m, 2 H), 2.43-2.30 (m, 2 H), 2.17 (d, J=1.0 Hz, 3 H), 2.11-1.99 (m, 2 H), 1.56-1.34 (m, 11 H) (N.B. signal obscured by water peak); LCMS (formic): R_t = 0.69 min (100%) [M+H]$^+$ = 512.

8-((1-(3-Aminopropanoyl)piperidin-4-yl)amino)-5-(3,6-dihydro-2H-pyran-4-yl)-3-methyl-1,7-naphthyridin-2(1H)-one, hydrochloride (2.049·HCl)
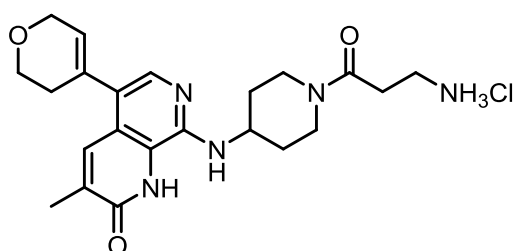
2.051 (93 mg, 0.18 mmol) was dissolved in 4 M HCl in 1,4-dioxane (2 mL) at rt. The resultant solution was stirred at rt for 2 hours before being concentrated *in vacuo* producing a yellow solid. The resultant solid was washed with Et$_2$O and dried under reduced pressure yielding **2.049·HCl** (20 mg, 0.05 mmol, 25%) as a cream solid. ^{1}H NMR uninterpretable due to salt nature. LCMS (formic): R_t = 0.37 min (100%) [M+H]$^+$ = 412.

3-((*tert*-Butoxycarbonyl)amino)-2-fluoropropanoic acid (2.055)
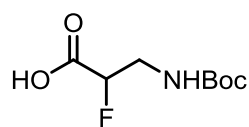
2-Carboxy-2-fluoroethan-1-aminium chloride (0.499 g, 3.48 mmol) was dissolved in 1 M sodium hydroxide (10 mL) and *tert*-butanol (20 mL). Di-*tert*-butyl dicarbonate (0.987 g, 4.52 mmol) was then added slowly at 0 °C to the stirred reaction mixture. The reaction mixture was stirred for 18 hours whilst warming to rt. The resultant solution was concentrated *in vacuo* before being diluted with EtOAc and acidified to pH 2 using HCl solution (1 M). The solution was then diluted with water (10 mL) and the layers separated. The aqueous layer was then extracted further with EtOAc (2 × 5 mL). The combined organic fractions were washed with brine (5 mL) and passed through a hydrophobic frit. The resultant solution was then concentrated *in vacuo* to yield **2.055** (0.679 g, 3.28 mmol, 94%) as a colourless oil. ^{1}H NMR (400 MHz, DMSO-d_6, 393 K) δ ppm 12.79 (br. s, 1 H), 6.46 (br. s, 1 H), 4.98-4.82 (m, 1 H), 3.56-3.31 (m, 2 H), 1.37 (s, 9 H).

tert-Butyl (3-(4-((5-bromo-3-methyl-2-oxo-1,2-dihydro-1,7-naphthyridin-8-yl)amino)piperidin-1-yl)-2-fluoro-3-oxopropyl)carbamate (2.056)
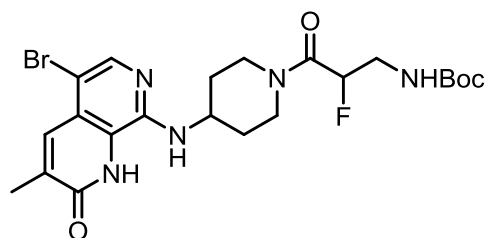
DIPEA (0.155 mL, 0.890 mmol) was added to a stirred mixture of **2.041** (100 mg, 0.297 mmol), HATU (135 mg, 0.356 mmol) and **2.055** (153 mg, 0.741 mmol) in DMF (2.5 mL). The resultant solution was stirred at rt for 15 min before being purified by MDAP (high pH). The desired fractions were combined and concentrated *in vacuo* yielding **2.056** (67 mg, 0.13 mmol, 43%) as an orange solid. m.p. 258-262 °C; ν$_{max}$ (solid)/cm^{-1}: 3379 (N-H), 2923, 1661 (C=O), 1601 (C=O), 1162; ^{1}H NMR (400 MHz, DMSO-d_6, 393 K) δ ppm 11.19 (br. s, 1 H), 7.91 (s, 1 H), 7.82-7.77 (m, 1 H), 6.68 (d, *J*=6.1 Hz, 1 H), 6.46-6.37 (m, 1 H), 5.35 (ddd, *J*=48.7, 7.2, 4.0 Hz, 1 H), 4.31-4.20 (m, 1 H), 4.12-4.00 (m, 2 H), 3.53-3.32 (m, 2 H), 3.27-3.15 (m, 2 H), 2.22 (d, *J*=1.2 Hz, 3 H), 2.13-2.05 (m, 2 H), 1.61-1.49 (m, 2 H), 1.43 (s, 9 H); HRMS (M+H)$^+$ calculated for $C_{22}H_{30}BrFN_5O_4$ 526.1449; found 526.1449; LC/MS (high pH): R_t = 1.04 min (89%) [M+H]$^+$ = 526.

***tert*-Butyl (3-(4-((5-bromo-3-methyl-2-oxo-1,2-dihydro-1,7-naphthyridin-8-yl)amino)piperidin-1-yl)-2-fluoropropyl)carbamate (2.057)**
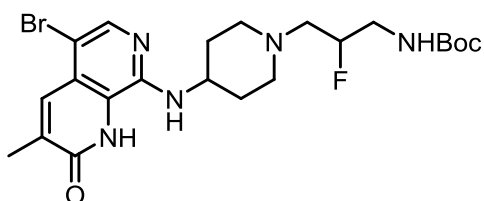
Under an inert atmosphere of nitrogen, **2.056** (564 mg, 1.07 mmol) was dissolved in anhydrous THF (40 mL) at rt. The stirred solution was then cooled to 0 °C before 2 M $LiAlH_4$ in THF solution (2.68 mL, 5.36 mmol) was added dropwise. The reaction mixture was stirred for a further 30 min at 0 °C. EtOAc (40 mL) was added slowly under nitrogen at 0 °C with vigorous stirring. Saturated aq. Rochelle's salt solution (40 mL) was then added slowly under nitrogen at 0 °C with vigorous stirring. The resultant solution was stirred for 63 hours until two distinct layers were visible. The organic layer was separated and the aqueous layer extracted with EtOAc (2 × 40 mL). The combined organic layers were concentrated *in vacuo* producing a yellow solid which was purified by silica chromatography (0-30% EtOH in EtOAc). The desired fractions were combined and concentrated *in vacuo* yielding **2.057** (151 mg, 0.295 mmol, 28%) as a yellow solid. ^{1}H NMR (400 MHz, DMSO-d_6, 393 K) δ ppm 11.20 (br. s, 1 H), 7.89 (s, 1 H), 7.80-7.78 (m, 1 H), 6.64-6.56 (m, 1 H), 6.39-6.32 (m, 1 H), 4.78-4.56 (m, 1 H), 4.04-3.92 (m, 1 H), 3.36-3.15 (m, 2 H), 2.92-2.87 (m, 2 H), 2.65-2.56 (m, 2 H), 2.35-2.26 (m, 2 H), 2.22 (d, *J*=1.3 Hz, 3 H), 2.04-1.96 (m, 2 H), 1.65-1.54 (m, 2 H), 1.43 (s, 9 H); LCMS (high pH): R_t = 1.14 min (100%) [M+H]+ = 512.

***tert*-Butyl (3-(4-((5-(3,6-dihydro-2H-pyran-4-yl)-3-methyl-2-oxo-1,2-dihydro-1,7-naphthyridin-8-yl)amino)piperidin-1-yl)-2-fluoropropyl)carbamate (2.058)**
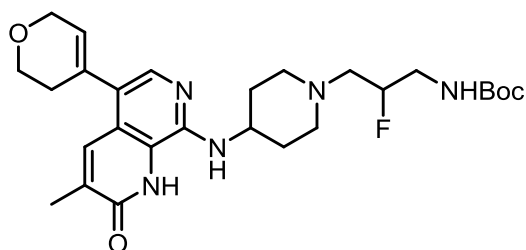
2-(3,6-Dihydro-2H-pyran-4-yl)-4,4,5,5-tetramethyl-1,3,2-dioxaborolane (79 mg, 0.38 mmol) was added at rt to a stirred mixture of **2.057** (150 mg, 0.29 mmol), potassium carbonate (81 mg, 0.59 mmol), Pd(OAc)₂ (8 mg, 0.03 mmol) and butyldi-1-adamantylphosphine (12 mg, 0.034 mmol) in 1,4-dioxane (2 mL) and water (1 mL). The resultant reaction mixture was then heated at 100 °C for 1 hour in a microwave

reactor then allowed to cool down to rt over 13 hours. The reaction mixture was diluted with EtOAc (20 mL) and filtered through Celite. The solution was concentrated *in vacuo* before being purified by silica chromatography (0-30% EtOH in EtOAc). The relevant fractions were combined and concentrated *in vacuo* to yield **2.058** (75 mg, 0.15 mmol, 50%) as a yellow solid. ^{1}H NMR (400 MHz, DMSO-d_6, 393 K) δ ppm 10.95 (br. s, 1 H), 7.68 (s, 1 H), 7.62 (s, 1 H), 6.42 (d, *J*=6.8 Hz, 1 H), 6.39-6.32 (m, 1 H), 5.76-5.72 (m, 1 H), 4.77-4.58 (m, 1 H), 4.26 (app. q, *J*=2.8 Hz, 2 H), 4.06-3.97 (m, 1 H), 3.89 (t, *J*=5.4 Hz, 2 H), 3.32-3.19 (m, 2 H), 2.94-2.86 (m, 2 H), 2.65-2.56 (m, 2 H), 2.40-2.25 (m, 4 H), 2.17 (d, *J*=1.0 Hz, 3 H), 2.04-1.96 (m, 2 H), 1.65-1.53 (m, 2 H), 1.43 (s, 9 H); HRMS (M+H)$^+$ calculated for $C_{27}H_{39}FN_5O_4$ 516.2986; found 516.2987; LCMS (high pH): R_t = 1.02 min (84%) [M+H]+ = 516.

8-((1-(3-Amino-2-fluoropropyl)piperidin-4-yl)amino)-5-(3,6-dihydro-2H-pyran-4-yl)-3-methyl-1,7-naphthyridin-2(1H)-one (2.052)
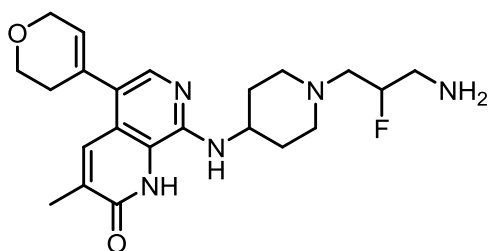
2.058 (69 mg, 0.13 mmol) was dissolved in 4 M HCl in 1,4-dioxane (7 mL) at rt. The resultant solution was stirred at rt for 2 hours before being concentrated *in vacuo*. The resultant solid was dissolved in 1:1 MeOH:DMSO and purified by MDAP (high pH). The desired fractions were combined and concentrated *in vacuo* to yield **2.052** (29 mg, 0.070 mmol, 52%) as a yellow solid. m.p. 225–227 °C; v_{max} (solid)/cm^{-1}: 3390 (N-H), 2940, 1683 (C=O), 1519, 1418, 1363, 1155, 736, 698; ^{1}H NMR (400 MHz, DMSO-d_6, 393 K) δ ppm 7.70-7.67 (m, 1 H), 7.62 (s, 1 H), 6.42 (d, *J*=6.5 Hz, 1 H), 5.77-5.72 (m, 1 H), 4.57 (dquin., *J*=49.4, 5.4 Hz, 1 H), 4.26 (app. q, *J*=2.7 Hz, 2 H), 4.08-3.95 (m, 1 H), 3.89 (t, *J*=5.4 Hz, 2 H), 2.95-2.87 (m, 2 H), 2.86-2.76 (m, 2 H), 2.66-2.56 (m, 2 H), 2.39-2.25 (m, 4 H), 2.17 (d, *J*=1.3 Hz, 3 H), 2.05-1.94 (m, 2 H), 1.65-1.52 (m, 2 H) (N.B. exchangeable lactam and primary amine protons not visible); ^{13}C NMR (151 MHz, DMSO-d_6) δ ppm 162.4, 145.5, 137.7, 134.1, 133.9, 131.6, 127.2, 122.7, 121.3, 120.8, 94.1 (d, *J*=169.2 Hz,1 C), 65.3, 64.1, 59.9 (d, *J*=22.1 Hz, 1 C), 53.3, 48.1, 44.5 (d, *J*=22.1 Hz, 1 C), 32.2, 30.9, 17.3; ^{19}F NMR (376 MHz, DMSO-d_6) δ ppm -184.64 (s, 1 F); HRMS (M+H)$^+$ calculated for $C_{22}H_{31}FN_5O_2$ 416.2462; found 416.2458; LCMS (high pH): R_t = 0.75 min (100%) [M+H]$^+$ = 416.

***tert*-Butyl   (3-(4-((5-(3,6-dihydro-2H-pyran-4-yl)-3-methyl-2-oxo-1,2-dihydro-1,7-naphthyridin-8-yl)amino)piperidin-1-yl)-2-fluoro-3-oxopropyl)carbamate (2.059)**
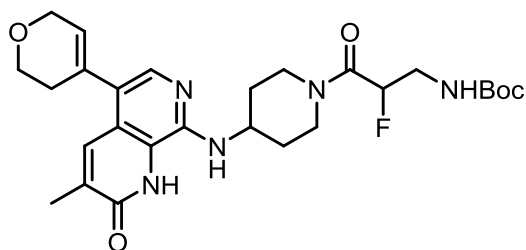
DIPEA (0.154 mL, 0.881 mmol) was added to a stirred mixture of **2.033** (0.100 g, 0.294 mmol), HATU (134 mg, 0.352 mmol) and **2.055** (151 mg, 0.734 mmol) in DMF (2.5 mL) at rt. The resultant solution was stirred at rt for 15 minutes before being purified by MDAP (high pH). The desired fractions were combined yielding **2.059** (115 mg, 0.217 mmol, 74%) as an orange solid. m.p. 183-185 °C; v_{max} (solid)/cm^{-1}: 3385 (N-H), 2927, 1651 (C=O), 1448, 1128, 722; ^{1}H NMR (400 MHz, DMSO-d_6, 393 K) δ ppm 7.71-7.67 (m, 1 H), 7.64 (s, 1 H), 6.38 (br. s, 1 H), 5.79-5.73 (m, 1 H), 5.35 (ddd, *J*=48.9, 7.1, 4.2 Hz, 1 H), 4.34-4.24 (m, 3 H), 4.12-4.00 (m, 2 H), 3.89 (t, *J*=5.4 Hz, 2 H), 3.55-3.33 (m, 2 H), 3.28-3.16 (m, 2 H), 2.40-2.32 (m, 2 H), 2.17 (d, *J*=1.0 Hz, 3 H), 2.14-2.05 (m, 2 H), 1.62-1.50 (m, 2 H), 1.43 (s, 9 H) (N.B. exchangeable lactam and amine proton not visible); HRMS (M+H)$^+$ calculated for $C_{27}H_{37}FN_5O_5$ 530.2779; found 530.2780; LC/MS (high pH): R_t = 0.97 min (96%) [M+H]$^+$ = 530.

8-((1-(3-Amino-2-fluoropropanoyl)piperidin-4-yl)amino)-5-(3,6-dihydro-2H-pyran-4-yl)-3-methyl-1,7-naphthyridin-2(1H)-one (2.053)
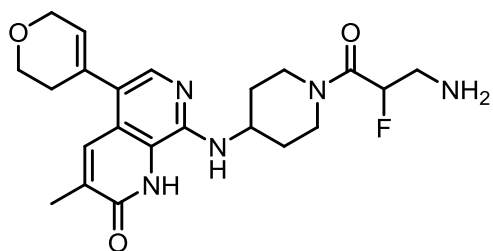
2.059 (85 mg, 0.16 mmol) was dissolved in 4 M HCl in 1,4-dioxane (2 mL) and stirred at rt for 2 hours. The reaction mixture was concentrated *in vacuo* before being dissolved in 1:1 MeOH:DMSO and purified by MDAP (high pH). The desired fractions were combined and reduced under a positive pressure of nitrogen yielding **2.053** (30 mg, 0.070 mmol, 44%) as a yellow solid. v_{max} (solid)/cm^{-1}: 3381 (N-H), 2924, 1655 (C=O), 1591, 1448, 1128, 843; ^{1}H NMR (400 MHz, DMSO-d_6, 393 K) δ ppm 7.69 (s, 1 H), 7.64 (s, 1 H), 6.50 (d, *J*=5.4 Hz, 1 H), 5.77-5.71 (m, 1 H), 5.30-5.12 (m, 1 H), 4.37-4.23 (m, 3 H), 4.15-4.01 (m, 2 H), 3.89 (t, *J*=5.4 Hz, 2 H), 3.26-3.15 (m, 2 H),

3.05-2.95 (m, 2 H), 2.39-2.32 (m, 2 H), 2.17 (s, 3 H), 2.12-2.04 (m, 2 H), 1.59-1.47 (m, 2 H) (N.B. exchangeable lactam and primary amine protons not visible); HRMS (M+H)$^+$ calculated for $C_{22}H_{29}FN_5O_3$ 430.2254; found 430.2253; LC/MS (high pH): R_t = 0.70 min (97%) [M+H]$^+$ = 430.

3-((*tert*-Butoxycarbonyl)amino)-2,2-difluoropropanoic acid (2.063)
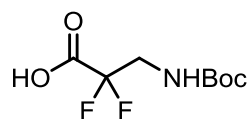
2-Carboxy-2,2-difluoroethan-1-aminium chloride (351 mg, 2.17 mmol) was dissolved in *tert*-butanol (15 mL) and 1 M aq. NaOH (5.43 mL, 5.43 mmol) at rt. The resultant solution was cooled to 0 °C and di-*tert*-butyl dicarbonate (619 mg, 2.84 mmol) added slowly. The solution was allowed to warm to rt and stirred for 20 hours. The resultant solution was acidified to pH 2 using aq. 2 M HCl. The solution was then washed with EtOAc (15 mL) and the aqueous layer separated. The aqueous layer was concentrated *in vacuo* yielding **2.063** (452 mg, 2.01 mmol, 92 %) as a white solid. ^{1}H NMR (400 MHz, DMSO-d_6, 393 K) δ ppm 6.09 (br. s, 1 H), 3.44 (td, *J*=14.3, 5.6 Hz, 2 H), 1.42 (s, 9 H) (N.B. carboxylic acid proton not visible).

tert-Butyl (3-(4-((5-bromo-3-methyl-2-oxo-1,2-dihydro-1,7-naphthyridin-8-yl)amino)piperidin-1-yl)-2,2-difluoro-3-oxopropyl)carbamate (2.064)
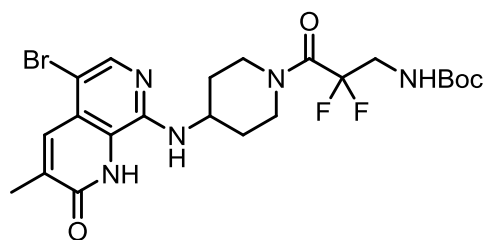
2.041 (1141 mg, 3.383 mmol) was added at rt to a stirred solution of **2.063** (750 mg, 3.33 mmol), HATU (3.799 g, 9.991 mmol) and DIPEA (2.61 mL, 15.0 mmol) in DMF (17 mL). The resultant solution was stirred at rt for 3 hours before being diluted with EtOAc (40 mL) and washed with water (40 mL). A precipitate formed and was collected under reduced pressure yielding **2.064** (648 mg, 1.19 mmol, 36%) as a yellow solid. v_{max} (solid)/cm^{-1}: 3390 (N-H), 2930, 1681 (C=O), 1519, 1418, 1364, 1161, 699; ^{1}H NMR (400 MHz, DMSO-d_6, 393 K) δ ppm 11.18 (br. s, 1 H), 7.92 (s, 1 H), 7.82-7.79 (m, 1 H), 6.73-6.64 (m, 1 H), 6.56-6.44 (m, 1 H), 4.35-4.24 (m, 1 H), 4.20-4.09 (m, 2 H), 3.72 (td, *J*=15.4, 6.4 Hz, 2 H), 3.39-3.26 (m, 2 H),

2.23 (d, *J*=1.3 Hz, 3 H), 2.18-2.07 (m, 2 H), 1.64–1.52 (m, 2 H), 1.44 (s, 9 H); LCMS (high pH): R_t = 1.15 min (100%) [M+H]+ = 544.

8-((1-(3-Amino-2,2-difluoropropyl)piperidin-4-yl)amino)-5-bromo-3-methyl-1,7-naphthyridin-2(1H)-one (2.065)
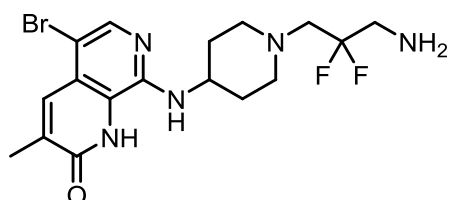
2.064 (530 mg, 0.97 mmol) was dissolved in THF (10 mL) at rt under a nitrogen atmosphere. 1 M BH_3·THF complex in THF solution (49 mL, 49 mmol) was then added under nitrogen and stirred at rt for 2 hours. To the solution was added MeOH (1 mL) dropwise at rt under nitrogen (solution effervesced and generated an exotherm). The solution was stirred for 1.5 hours before being concentrated *in vacuo* producing a yellow solid. The resultant solid was dissolved in MeOH (20 mL) and diluted with aq. 1 M HCl solution (20 mL) before being heated to 80 °C for 45 min. The solution was neutralised with saturated aq. $NaHCO_3$ solution and extracted with DCM (40 mL). The organic layer was separated and the aqueous layer extracted further with DCM (3 × 20 mL). The organic fractions were combined, washed with brine (40 mL) and concentrated *in vacuo* generating **2.065** (370 mg, 0.86 mmol, 88%) as a yellow solid. m.p. 204–209 °C; v_{max} (solid)/cm^{-1}: 3395 (N-H), 2935, 1658 (C=O), 1524, 1444, 1044, 857; ^{1}H NMR (400 MHz, DMSO-d_6, 393 K) δ ppm 7.91 (s, 1 H), 7.83-7.79 (m, 1 H), 6.83 (d, *J*=6.6 Hz, 1 H), 3.94-3.83 (m, 1 H), 3.00-2.89 (m, 4 H), 2.80 (t, *J*=14.4 Hz, 2 H), 2.38-2.30 (m, 2 H), 2.19 (d, *J*=1.2 Hz, 3 H), 2.00-1.90 (m, 2 H), 1.56-1.45 (m, 2 H) (N.B. exchangeable lactam and primary amine protons not visible); HRMS (M+H)$^+$ calculated for $C_{17}H_{23}F_2N_5O$ 430.1054; found 430.1053; LCMS (high pH): R_t = 0.92 min (91%) [M+H]+ = 430.

8-((1-(3-Amino-2,2-difluoropropyl)piperidin-4-yl)amino)-5-(3,6-dihydro-2H-pyran-4-yl)-3-methyl-1,7-naphthyridin-2(1H)-one (2.060)
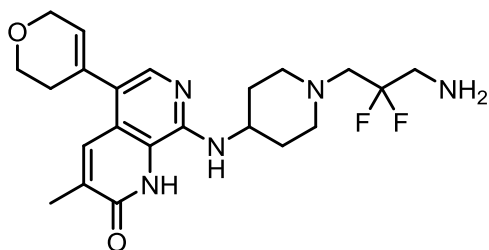
2-(3,6-Dihydro-2H-pyran-4-yl)-4,4,5,5-tetramethyl-1,3,2-dioxaborolane (209 mg, 0.997 mmol) was added at rt to a stirred mixture of **2.065** (335 mg, 0.779 mmol), potassium carbonate (215 mg, 1.56 mmol), Pd(OAc)$_2$ (18 mg, 0.078 mmol) and butyldi-1-adamantylphosphine (33 mg, 0.091 mmol) in 1,4-dioxane (7 mL) and water (3.5 mL). The resultant reaction mixture was then heated at 100 °C for 1 hour in a microwave reactor. The reaction mixture was allowed to cool to rt before being diluted with EtOAc (20 mL) and filtered through Celite. The resultant solution was concentrated *in vacuo* and dissolved in 1:1 MeOH:EtOAc (0.8 mL) and DCM (0.2 mL) before being purified by MDAP (high pH). The desired fractions were combined and concentrated *in vacuo* yielding **2.060** (61 mg, 0.14 mmol, 18%) as a yellow solid. m.p. 220–223 °C; v$_{max}$ (solid)/cm^{-1}: 3395 (N-H), 2925, 1657 (C=O), 1593, 1452, 1121, 842; ^{1}H NMR (400 MHz, DMSO-d_6) δ ppm 7.71-7.69 (m, 1 H), 7.61 (s, 1 H), 6.66 (d, *J*=6.5 Hz, 1 H), 5.75-5.70 (m, 1 H), 4.26-4.22 (m, 2 H), 3.99-3.89 (m, 1 H), 3.86 (t, *J*=5.3 Hz, 2 H), 2.98-2.88 (m, 4 H), 2.79 (t, *J*=14.4 Hz 2 H), 2.35-2.27 (m, 4 H), 2.14 (d, *J*=1.0 Hz, 3 H), 1.99-1.91 (m, 2 H), 1.55-1.44 (m, 2 H) (N.B. exchangeable lactam and primary amine protons not visible); ^{13}C NMR (101 MHz, DMSO-d_6) δ ppm 162.4, 145.5, 137.7, 134.2, 133.9, 131.6, 127.2, 122.7, 121.3, 120.8, 65.3, 64.1, 58.9 (t, *J*=26.4 Hz, 1 C), 53.8, 49.1, 47.7, 32.3, 30.9, 17.3 (N.B. one carbon signal missing); ^{19}F NMR (376 MHz, DMSO-d_6) δ ppm −105.01 (s, 2 F); HRMS (M+H)$^+$ calculated for C$_{22}$H$_{30}$F$_2$N$_5$O$_2$ 433.2289; found 434.2363; LCMS (high pH): R$_t$ = 0.84 min (98%) [M+H]+ = 434.

***tert*-Butyl (3-(4-((5-(3,6-dihydro-2H-pyran-4-yl)-3-methyl-2-oxo-1,2-dihydro-1,7-naphthyridin-8-yl)amino)piperidin-1-yl)-2,2-difluoro-3-oxopropyl)carbamate (2.066)**
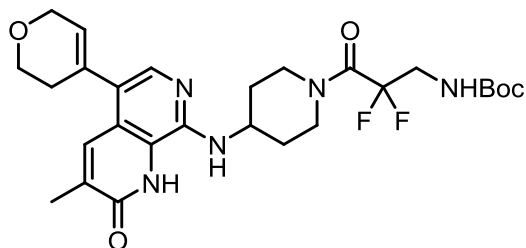
HATU (894 mg, 2.35 mmol) and DIPEA (0.819 mL, 4.70 mmol) were added at rt to a stirred solution of **2.063** (318 mg, 1.41 mmol) in DMF (7 mL). After 30 minutes **2.033** (0.400 g, 1.18 mmol) was added at rt to the resultant stirred solution and the reaction mixture stirred for 5 hours. The reaction mixture was then diluted with water (10 mL) and extracted with EtOAc (4 × 10 mL). The combined organic fractions were washed with brine (10 mL), passed through a hydrophobic frit and concentrated *in vacuo*. The resultant solid was dissolved in 1:1 MeOH:DMSO and purified by MDAP (formic). The desired fractions were combined and concentrated *in vacuo* yielding **2.066** (168 mg, 0.307 mmol, 26%) as a cream solid. ^{1}H NMR (400 MHz, DMSO-d_6, 393 K) δ ppm 7.71-7.68 (m, 1 H), 7.65-7.61 (m, 1 H), 6.53-6.44 (m, 2 H), 5.76 (br. s, 1 H), 4.40-4.30 (m, 1 H), 4.27 (app. q, J=2.4 Hz, 2 H), 4.17-4.11 (m, 2 H), 3.89 (t, J=5.4 Hz, 2 H), 3.72 (td, J=15.4, 6.4 Hz, 2 H), 3.40-3.26 (m, 2 H), 2.38-2.32 (m, 2 H), 2.17 (d, J=1.0 Hz, 3 H), 2.16-2.08 (m, 2 H), 1.66-1.52 (m, 2 H), 1.45-1.42 (m, 9 H) (N.B. exchangeable lactam proton not visible); LCMS (formic): R_t = 0.81 min (100%) [M+H]+ = 548.

8-((1-(3-Amino-2,2-difluoropropanoyl)piperidin-4-yl)amino)-5-(3,6-dihydro-2H-pyran-4-yl)-3-methyl-1,7-naphthyridin-2(1H)-one (2.061)
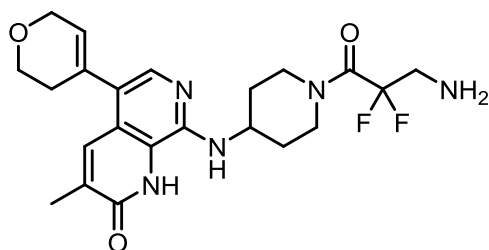
A mixture of **2.066** (129 mg, 0.236 mmol) in 4 M HCl in 1,4-dioxane (7 mL) was stirred for 2 hours at rt before being concentrated *in vacuo*. The resultant solid was dissolved in 1:1 MeOH:DMSO and purified by MDAP (high pH) to yield **2.061** (42 mg, 0.094 mmol, 40%) as a yellow solid. m.p. 263–266 °C; v_{max} (solid)/cm^{-1}: 3390 (N-H), 2935, 1658 (C=O), 1622, 1449, 1121, 844; ^{1}H NMR (400 MHz, CHLOROFORM-*d*) δ ppm 13.19

(br. s, 1 H), 7.86-7.83 (m, 1 H), 7.79 (s, 1 H), 6.67 (d, J=7.1 Hz, 1 H), 5.83-5.75 (m, 1 H), 4.61-4.46 (m, 2 H), 4.44-4.35 (m, 3 H), 4.01 (t, J=5.4 Hz, 2 H), 3.44-2.94 (m, 4 H), 2.50-2.40 (m, 2 H), 2.37-2.24 (m, 5 H), 1.91-1.61 (m, 2 H) (N.B. exchangeable primary amine protons not visible); ^{13}C NMR (101 MHz, CHLOROFORM-d) δ ppm 164.4, 145.7, 138.6, 135.9, 133.0, 131.4, 127.4, 123.0, 122.6, 120.3, 119.6, 65.7, 64.4, 47.8, 46.0, 42.5, 33.0, 32.2, 31.0, 17.6; ^{19}F NMR (376 MHz, DMSO-d_6) δ ppm −105.49 (br. s, 2 F); HRMS (M+H)$^+$ calculated for $C_{22}H_{28}F_2N_5O_3$ 448.2160; found 448.2162; LCMS (high pH): R_t = 0.79 min (100%) [M+H]$^+$ = 448.

8-((1-(3-Amino-2,2-difluoropropanoyl)piperidin-4-yl)amino)-5-(3,6-dihydro-2H-pyran-4-yl)-3-methyl-1,7-naphthyridin-2(1H)-one, hydrochloride (2.061·HCl)
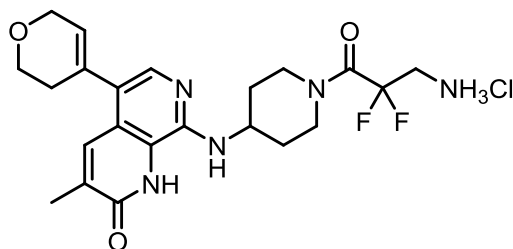
2.066 (163 mg, 0.298 mmol) was dissolved in 4 M HCl in 1,4-dioxane (4 mL) at rt. The resultant solution was stirred at rt for 2 hours before being concentrated *in vacuo* yielding **2.061·HCl** (143 mg, 0.295 mmol, 99%) as a pale orange solid. ^{1}H NMR (400 MHz, DMSO-d_6, 393 K) δ ppm 7.74-7.70 (m, 1 H), 7.59 (s, 1 H), 5.79 (br. s, 1 H), 4.49-4.39 (m, 1 H), 4.29-4.24 (m, 2 H), 4.17 (d, J=13.6 Hz, 2 H), 3.90 (t, J=5.4 Hz, 2 H), 3.70-3.57 (m, 4 H), 3.38 (br. s, 2 H), 2.41-2.31 (m, 2 H), 2.25-2.08 (m, 5 H), 1.74-1.57 (m, 2 H) (N.B. exchangeable lactam and amine proton not visible, NH_3^+ signal visible on rt ^{1}H NMR at 8.69 ppm (br. s, 3 H)); HRMS (M+H)$^+$ calculated for $C_{22}H_{28}F_2N_5O_3$ 448.2160; found 448.2156; LC/MS (High pH): R_t = 0.81 min (99%) [M+H]$^+$ = 448.

tert-Butyl (3*S*,4*R*)-4-((2-(benzyloxy)-3-methyl-1,7-naphthyridin-8-yl)amino)-3-fluoropiperidine-1-carboxylate (2.069)
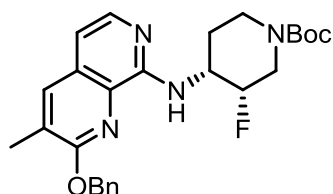
tert-Butyl (3*S*,4*R*)-4-amino-3-fluoropiperidine-1-carboxylate (501 mg, 2.30 mmol) was added at rt to a solution of **2.029** (545 mg, 1.91 mmol), Pd$_2$(dba)$_3$ (88 mg, 0.096 mmol), sodium *tert*-butoxide (736 mg, 7.66 mmol) and 2-(dicyclohexylphosphino)3,6-dimethoxy-2′,4′,6′-triisopropyl-1,1′-biphenyl (103

mg, 0.191 mmol) in toluene (16 mL). The resultant solution was stirred at 60 °C for 6 hours. *tert*-Butyl (3*S*,4*R*)-4-amino-3-fluoropiperidine-1-carboxylate (251 mg, 1.15 mmol), Pd$_2$(dba)$_3$ (88 mg, 0.096 mmol), sodium *tert*-butoxide (368 mg, 3.83 mmol) and 2-(dicyclohexylphosphino)3,6-dimethoxy-2′,4′,6′-triisopropyl-1,1′-biphenyl (103 mg, 0.191 mmol) were added and the reaction stirred at 85 °C for 1.5 hours before being allowed to cool to rt. The solution was diluted with EtOAc (15 mL) and MeOH (10 mL) and filtered through Celite. The Celite was washed with EtOAc (10 mL) and MeOH (5 mL) and the combined washings concentrated *in vacuo* producing an orange oil. The resultant oil was dissolved in minimal DCM and purified by silica chromatography (0-60% EtOAc in cyclohexane). The desired fractions were combined yielding **2.069** (657 mg, 1.41 mmol, 74%). ^{1}H NMR (400 MHz, DMSO-d_6, 393 K) δ ppm 7.91-7.88 (m, 1 H), 7.84 (d, *J*=5.8 Hz, 1 H), 7.57-7.50 (m, 2 H), 7.43-7.36 (m, 2 H), 7.32 (s, 1 H), 6.86 (d, *J*=5.8 Hz, 1 H), 6.51 (d, *J*=8.0 Hz, 1 H), 5.58 (s, 2 H), 5.03-4.86 (m, 1 H), 4.55-4.40 (m, 1 H), 4.39-4.29 (m, 1 H), 4.15-4.07 (m, 1 H), 3.23 (ddd, *J*=39.2, 14.8, 1.3 Hz, 1 H), 3.06-2.97 (m, 1 H), 2.38 (d, *J*=1.0 Hz, 3 H), 1.95-1.73 (m, 2 H), 1.48 (s, 9 H); HRMS (M+H)$^+$ calculated for C$_{26}$H$_{32}$FN$_4$O$_3$ 467.2458; found 467.2455; LCMS (formic): R$_t$ = 1.01 min (100%) [M+H]$^+$ = 467.

tert-Butyl (3*S*,4*R*)-4-((2-(benzyloxy)-5-bromo-3-methyl-1,7-naphthyridin-8-yl)amino)-3-fluoropiperidine-1-carboxylate (2.070)
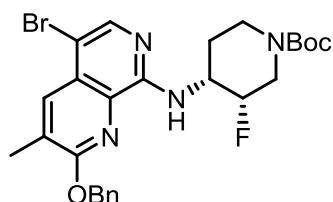

N-Bromosuccinimide (272 mg, 1.53 mmol) was added at rt to a stirred solution of **2.069** (647 mg, 1.39 mmol) in chloroform (13 mL). The resultant solution was then stirred for 1 hour at rt, before being diluted with water (20 mL). The organic phase was separated, passed through a hydrophobic frit and concentrated *in vacuo* to yield **2.070** (728 mg, 1.34 mmol, 96%) as an orange solid. m.p. 77-83 °C; ν$_{max}$ (solid)/cm^{-1}: 3412 (N-H), 2980, 1694 (C=O), 1518, 1419, 1158; ^{1}H NMR (400 MHz, DMSO-d_6, 393 K) δ ppm 8.03-8.02 (m, 1 H), 8.01 (s, 1 H), 7.56-7.51 (m, 2 H), 7.42-7.37 (m, 2 H), 7.36-7.30 (m, 1 H), 6.65-6.59 (m, 1 H), 5.61 (s, 2 H), 5.02-4.87 (m, 1 H), 4.51-4.40 (m, 1 H), 4.39-4.29 (m, 1 H), 4.15-4.06 (m, 1 H), 3.22 (ddd, *J*=39.2, 14.8, 1.3 Hz, 1 H), 3.06-2.97 (m, 1 H), 2.45 (d, *J*=1.3 Hz, 3 H), 1.95-1.81 (m, 2 H), 1.51-1.46 (m, 9 H); HRMS (M+H)$^+$ calculated for

$C_{26}H_{31}BrFN_4O_3$ 545.1564; found 545.1564; LCMS (formic): R_t = 1.66 min (100%) [M+H]$^+$ = 545.

tert-Butyl (3_S_,4_R_)-4-((2-(benzyloxy)-5-(3,6-dihydro-2H-pyran-4-yl)-3-methyl-1,7-naphthyridin-8-yl)amino)-3-fluoropiperidine-1-carboxylate (2.071)
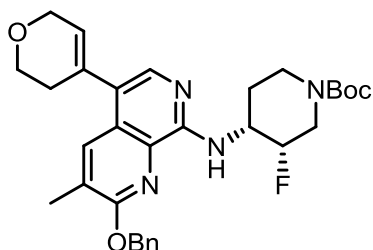
The solvent system was sparged with nitrogen for 20 min prior to use. 2-(3,6-Dihydro-2H-pyran-4-yl)-4,4,5,5-tetramethyl-1,3,2-dioxaborolane (362 mg, 1.72 mmol), **2.070** (723 mg, 1.33 mmol), potassium carbonate (366 mg, 2.65 mmol), Pd(OAc)$_2$ (30 mg, 0.13 mmol) and butyldi-1-adamantylphosphine (48 mg, 0.13 mmol) were dissolved in 1,4-dioxane (10 mL) and water (5 mL). The resultant reaction mixture was then heated at 100 °C for 1 hour in a microwave reactor. The reaction mixture was diluted with EtOAc (15 mL), filtered through Celite and concentrated *in vacuo*. The resultant residue was dissolved in minimal DCM and purified by silica chromatography (0-50% EtOAc in cyclohexane). The desired fractions were combined yielding **2.071** (633 mg, 1.15 mmol, 87%) as a yellow solid. m.p. 70-78 °C; v_{max} (solid)/cm^{-1}: 3408 (N-H), 2984, 1694 (C=O), 1519, 1421, 1150; ^{1}H NMR (400 MHz, DMSO-d_6, 393 K) δ ppm 7.98 (s, 1 H), 7.72 (s, 1 H), 7.55-7.50 (m, 2 H), 7.42-7.35 (m, 2 H), 7.34-7.28 (m, 1 H), 6.52 (d, *J*=8.0 Hz, 1 H), 5.83-5.79 (m, 1 H), 5.59 (s, 2 H), 5.03-4.83 (m, 1 H), 4.55-4.40 (m, 1 H), 4.39-4.25 (m, 3 H), 4.16-4.05 (m, 1 H), 3.92 (t, *J*=5.4 Hz, 2 H), 3.32-3.13 (m, 1 H), 3.07-2.95 (m, 1 H), 2.48-2.37 (m, 5 H), 1.93-1.76 (m, 2 H), 1.51-1.43 (m, 9 H); HRMS (M+H)$^+$ calculated for $C_{31}H_{38}FN_4O_4$ 549.2877; found 549.2876; LCMS (formic): R_t = 1.13 min (99%) [M+H]$^+$ = 549.

5-(3,6-Dihydro-2H-pyran-4-yl)-8-(((3*S*,4*R*)-3-fluoropiperidin-4-yl)amino)-3-methyl-1,7-naphthyridin-2(1H)-one (2.072)
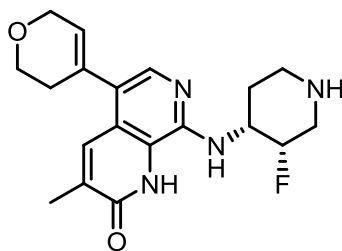
2.071 (617 mg, 1.13 mmol) was dissolved in TFA (5 mL) at rt. The resultant solution was then heated to reflux and stirred for 2 hours before being allowed to cool to rt. The volatile components were then removed *in vacuo*. Toluene (10 mL) was then added to the resulting residue and removed under reduced pressure (× 3). The resulting residue was diluted with MeOH (5 mL) and passed through a preconditioned (15 mL MeOH) aminopropyl column (10 g). The column was washed with MeOH (50 mL) and the desired fractions combined and concentrated *in vacuo* yielding **2.072** (245 mg, 0.684 mmol, 61%) as a yellow solid. m.p. 249–254 °C; v_{max} (solid)/cm^{-1}: 3393 (N-H), 2921, 1656 (C=O), 1593, 1450, 1128, 842; ^{1}H NMR (400 MHz, DMSO-d_6, 393 K) δ ppm 7.74-7.70 (m, 1 H), 7.63 (s, 1 H), 6.68 (d, *J*=6.8 Hz, 1 H), 5.76 (tt, *J*=2.8, 1.5 Hz, 1 H), 4.94-4.69 (m, 1 H), 4.48-4.31 (m, 1 H), 4.28 (app. q, *J*=2.8 Hz, 2 H), 3.90 (t, *J*=5.5 Hz, 2 H), 3.28-3.20 (m, 1 H), 3.10-3.04 (m, 1 H), 2.86 (ddd, *J*=37.4, 14.3, 1.0 Hz, 1 H), 2.74-2.66 (m, 1 H), 2.39-2.34 (m, 2 H), 2.19 (d, *J*=1.3 Hz, 3 H), 1.84-1.72 (m, 2 H) (N.B. exchangeable lactam and amino piperidine proton not visible); ^{19}F NMR (376 MHz, DMSO-d_6) δ ppm −73.41 (s, 1 F); HRMS (M+H)$^{+}$ calculated for $C_{19}H_{24}FN_4O_2$ 359.1883; found 359.1878; LCMS (formic): R_t = 0.43 min (100%) [M+H]$^{+}$ = 359.

tert-Butyl (3-((3*S*,4*R*)-4-((5-(3,6-dihydro-2H-pyran-4-yl)-3-methyl-2-oxo-1,2-dihydro-1,7-naphthyridin-8-yl)amino)-3-fluoropiperidin-1-yl)propyl)carbamate (2.073)
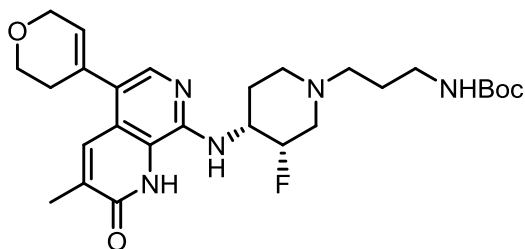
A mixture of **2.072** (125 mg, 0.349 mmol) and **2.035** (120 mg, 0.69 mmol) in MeOH (6 mL) and AcOH (0.60 mL) was stirred at 50 °C for 3 hours before picoline borane complex (37 mg, 0.35 mmol) was added and the mixture stirred at 50 °C for 15 hours. The solution was then allowed to cool to rt before being concentrated *in vacuo*.

The resultant residue was dissolved in DCM (10 mL) and washed with saturated aq. NaHCO$_3$ solution (10 mL). The aqueous layer was separated and extracted further with DCM (3 × 5 mL). The organic fractions were combined and passed through a hydrophobic frit before being concentrated *in vacuo*. The resultant solid was purified by silica chromatography (0-100% EtOH in EtOAc). The desired fractions were combined and concentrated *in vacuo* to yield **2.073** (102 mg, 0.198 mmol, 57%) as a cream solid. v_{max} (solid)/cm^{-1}: 3393 (N-H), 2965, 1656 (C=O), 1594, 1449, 1168; ^{1}H NMR (400 MHz, DMSO-d_6, 393 K) δ ppm 11.34-11.15 (br. s, 1 H), 7.72-7.69 (m, 1 H), 7.63 (s, 1 H), 6.66 (d, *J*=7.3 Hz, 1 H), 6.22-6.11 (m, 1 H), 5.81-5.73 (m, 1 H), 4.97-4.80 (m, 1 H), 4.37-4.22 (m, 3 H), 3.90 (t, *J*=5.4 Hz, 2 H), 3.23-3.12 (m, 1 H), 3.05 (app. q, *J*=6.8 Hz, 2 H), 2.98-2.89 (m, 1 H), 2.48-2.21 (m, 6 H), 2.19 (d, *J*=0.8 Hz, 3 H), 2.05-1.90 (m, 1 H), 1.85-1.75 (m, 1 H), 1.63 (quin., *J*=6.8 Hz, 2 H), 1.44 (s, 9 H); HRMS (M+H)$^+$ calculated for C$_{27}$H$_{39}$FN$_5$O$_4$ 516.2986; found 516.2982; LCMS (high pH): R$_t$ = 1.05 min (97%) [M+H]$^+$ = 516.

8-(((3*S*,4*R*)-1-(3-Aminopropyl)-3-fluoropiperidin-4-yl)amino)-5-(3,6-dihydro-2H-pyran-4-yl)-3-methyl-1,7-naphthyridin-2(1H)-one (2.067)
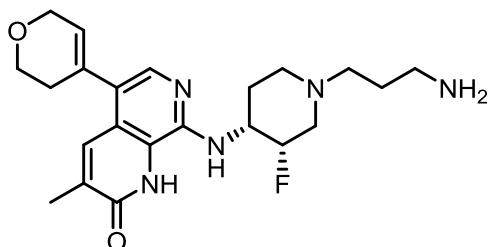

2.073 (93 mg, 0.18 mmol) was dissolved in 4 M HCl in 1,4-dioxane (5 mL) at rt and stirred for 1 hour. The solution was concentrated *in vacuo*, dissolved in 1:1 MeOH:DMSO and purified by MDAP (high pH). The desired fractions were combined and concentrated *in vacuo* yielding **2.067** (42 mg, 0.10 mmol, 56%) as a cream solid. m.p. 204–209 °C; v_{max} (solid)/cm^{-1}: 3393 (N-H), 2938, 1656 (C=O), 1594, 1444, 1123, 843; [α$_D$]^{23} (c = 10 mg/mL, MeOH): +8°; ^{1}H NMR (400 MHz, DMSO-d_6, 393 K) δ ppm 7.72-7.69 (m, 1 H), 7.63 (s, 1 H), 6.67 (d, *J*=5.3 Hz, 1 H), 5.82-5.72 (m, 1 H), 5.00-4.79 (m, 1 H), 4.41-4.19 (m, 3 H), 3.90 (t, *J*=5.4 Hz, 2 H), 3.22-3.13 (m, 1 H), 2.98-2.88 (m, 1 H), 2.67 (t, *J*=6.7 Hz, 2 H), 2.49-2.41 (m, 2 H), 2.37 (td, *J*=4.9, 2.8 Hz, 2 H), 2.33-2.21 (m, 1 H), 2.19 (d, *J*=1.3 Hz, 3 H), 2.04-1.90 (m, 1 H), 1.85-1.74 (m, 1 H), 1.58 (quin., *J*=6.8 Hz, 2 H), 1.45 (s, 1 H) (N.B. exchangeable lactam and primary amine protons not visible); ^{13}C NMR (101 MHz, DMSO-d_6) δ ppm 162.7, 145.6, 137.2, 134.1, 133.7, 131.6, 127.2, 123.3, 121.7, 121.6, 87.8 (d, *J*=175.3 Hz, 1 C), 65.3, 64.1, 56.0 (d, *J*=19.0 Hz, 1 C),

55.7, 52.2, 50.3 (d, J=19.0 Hz, 1 C), 30.9, 30.3, 26.8, 17.4 (N.B. one carbon signal missing); ^{19}F NMR (376 MHz, DMSO-d_6) δ ppm −198.74 (s, 1 F); HRMS (M+H)$^+$ calculated for $C_{22}H_{31}FN_5O_2$ 416.2448; found 416.2457; LCMS (high pH): R_t = 0.76 min (99%) [M+H]$^+$ = 416.

tert-Butyl 4-((2-(benzyloxy)-3-methyl-1,7-naphthyridin-8-yl)amino)-3,3-difluoropiperidine-1-carboxylate (2.074)
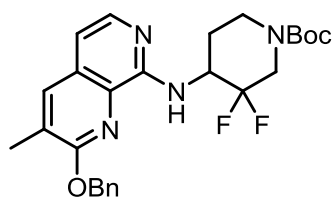
tert-Butyl 4-amino-3,3-difluoropiperidine-1-carboxylate (448 mg, 1.90 mmol) was added to a solution of **2.029** (450 mg, 1.58 mmol), sodium *tert*-butoxide (607 mg, 6.32 mmol), Pd$_2$(dba)$_3$ (72 mg, 0.079 mmol) and 2-(dicyclohexylphosphino)3,6-dimethoxy-2′,4′,6′-triisopropyl-1,1′-biphenyl (85 mg, 0.16 mmol) in toluene (16 mL) and stirred at 85 °C for 5 hours. The resultant reaction mixture was diluted with EtOAc (20 mL) and filtered through Celite. The Celite was washed with EtOAc (10 mL) and the combined washings concentrated *in vacuo* producing an orange oil. The resultant oil was partitioned between DCM (30 mL) and water (30 mL). The organic layer was separated and the aqueous layer extracted further with DCM (3 × 15 mL). The organic fractions were combined and concentrated *in vacuo* producing an orange oil. The resultant oil was dissolved in minimal DCM and purified by silica chromatography (0-40% EtOAc in cyclohexane). The desired fractions were combined yielding **2.074** (649 mg, 1.34 mmol, 85%) as a cream solid. m.p. 119-120 °C; ν$_{max}$ (solid)/cm^{-1}: 3430, (N-H), 2935, 1698 (C=O), 1423, 1157, 901; ^{1}H NMR (400 MHz, DMSO-d_6, 300 K) δ ppm 7.93-7.90 (m, 1 H), 7.85 (d, J=5.5 Hz, 1 H), 7.57-7.50 (m, 2 H), 7.42-7.36 (m, 2 H), 7.32 (s, 1 H), 6.90 (d, J=5.5 Hz, 1 H), 6.51 (d, J=9.3 Hz, 1 H), 5.64-5.55 (m, 2 H), 5.00-4.86 (m, 1 H), 4.31-4.20 (m, 1 H), 4.06-3.97 (m, 1 H), 3.45 (ddd, J=29.1, 14.6, 1.5 Hz, 1 H), 3.24-3.14 (m, 1 H), 2.39 (d, J=1.0 Hz, 3 H), 2.13-2.04 (m, 1 H), 1.82-1.70 (m, 1 H), 1.50 (s, 9 H); ^{19}F NMR (376 MHz, DMSO-d_6) δ ppm −111.07-−109.20 (m, 1 F), −120.46-−118.80 (m, 1 F); HRMS (M+H)$^+$ calculated for $C_{26}H_{31}F_2N_4O_3$ 485.2364; found 485.2372; LCMS (formic): R_t = 1.14 min (100%) [M+H]$^+$ = 485.

tert-Butyl 4-((2-(benzyloxy)-5-bromo-3-methyl-1,7-naphthyridin-8-yl)amino)-3,3-difluoropiperidine-1-carboxylate (2.075)
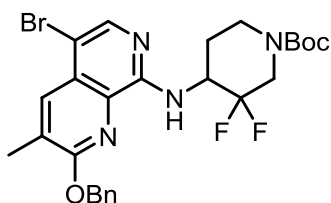
N-Bromosuccinimide (0.250 g, 1.41 mmol) was added at rt to a stirred solution of **2.074** (619 mg, 1.28 mmol) in chloroform (10 mL). The solution was then stirred at rt for 1 hour before being diluted with water (20 mL). The organic phase was separated, passed through a hydrophobic frit and concentrated *in vacuo* to yield **2.075** (663 mg, 1.18 mmol, 92%) as an orange solid. m.p. 129-131 °C; v_{max} (solid)/cm^{-1}: 3426 (N-H), 2978, 1699 (C=O), 1520, 1421, 1155; ^{1}H NMR (400 MHz, DMSO-d_6) δ ppm 8.03-8.02 (m, 1 H), 8.00 (s, 1 H), 7.57-7.52 (m, 2 H), 7.42-7.35 (m, 2 H), 7.35-7.29 (m, 1 H), 6.80 (d, J=9.8 Hz, 1 H), 5.67-5.55 (m, 2 H), 5.04-4.88 (m, 1 H), 4.36-4.14 (m, 1 H), 4.09-3.94 (m, 1 H), 3.62-3.36 (m, 1 H), 3.22-2.99 (m, 1 H), 2.40 (d, J=1.2 Hz, 3 H), 2.00-1.92 (m, 1 H), 1.91-1.77 (m, 1 H), 1.44 (s, 9 H); HRMS (M+H)$^+$ calculated for $C_{26}H_{30}BrF_2N_4O_3$ 563.1469; found 563.1467; LCMS (high pH): R_t = 1.67 min (100%) [M+H]$^+$ = 563.

tert-Butyl 4-((2-(benzyloxy)-5-(3,6-dihydro-2H-pyran-4-yl)-3-methyl-1,7-naphthyridin-8-yl)amino)-3,3-difluoropiperidine-1-carboxylate (2.076)
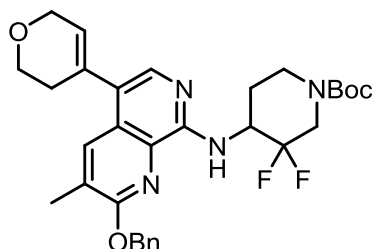
The solvent system was sparged with nitrogen for 30 min prior to use. 2-(3,6-Dihydro-2H-pyran-4-yl)-4,4,5,5-tetramethyl-1,3,2-dioxaborolane (281 mg, 1.34 mmol) was added at rt to a stirred mixture of **2.075** (588 mg, 1.04 mmol), potassium carbonate (288 mg, 2.09 mmol), Pd(OAc)$_2$ (23 mg, 0.10 mmol) and butyldi-1-adamantylphosphine (37 mg, 0.10 mmol) in 1,4-dioxane (10 mL) and water (5 mL). The resultant reaction mixture was then heated at 100 °C for 1 hour in a microwave reactor. The reaction mixture was allowed to cool to rt before being diluted with EtOAc (30 mL) and filtered through Celite. The resultant solution was concentrated *in vacuo,* dissolved in minimal DCM and purified by silica chromatography (0-50% EtOAc in cyclohexane). The desired fractions were combined and concentrated *in vacuo* yielding **2.076** (482 mg, 0.851 mmol, 82%) as a yellow solid. m.p. 91–99 °C; ^{1}H NMR (400 MHz, DMSO-d_6, 393 K) δ ppm 8.00-7.98

(m, 1 H), 7.73 (s, 1 H), 7.56-7.51 (m, 2 H), 7.42-7.35 (m, 2 H), 7.35-7.29 (m, 1 H), 6.55-6.49 (d, J=9.3 Hz, 1 H), 5.84-5.80 (m, 1 H), 5.65-5.55 (m, 2 H), 4.99-4.85 (m, 1 H), 4.29 (app. q, J=2.7 Hz, 2 H), 4.27-4.20 (m, 1 H), 4.05-3.97 (m, 1 H), 3.92 (t, J=5.4 Hz, 2 H), 3.23-3.14 (m, 1 H), 2.45-2.38 (m, 5 H), 2.12-2.04 (m, 1 H), 1.82-1.70 (m, 1 H), 1.50 (s, 9 H); ^{13}C NMR (101 MHz, DMSO-d_6) δ ppm 159.9, 154.3, 153.0, 138.0, 137.9, 135.0, 131.8, 128.8, 128.7, 128.3, 128.2, 127.1, 127.0, 126.4, 123.1, 80.1, 74.0, 68.2, 65.3, 64.2, 50.5, 30.7, 28.4, 26.8, 25.4, 16.7 (N.B. one carbon signal missing); HRMS (M+H)$^+$ calculated for $C_{31}H_{37}F_2N_4O_4$ 567.2783; found 567.2783; LCMS (formic): R_t = 1.33 min (98%) [M+H]$^+$ = 567.

8-((3,3-Difluoropiperidin-4-yl)amino)-5-(3,6-dihydro-2H-pyran-4-yl)-3-methyl-1,7-naphthyridin-2(1H)-one (2.077)
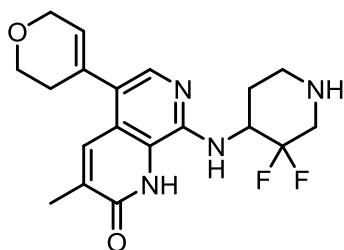
2.076 (467 mg, 0.824 mmol) was dissolved in TFA (5 mL) at rt. The resultant solution was then heated to reflux and stirred for 2 hours before being allowed to cool to rt. Volatile components were then removed *in vacuo*. Toluene (10 mL) was then added to the resulting residue and concentrated *in vacuo* (× 3). The residue was dissolved in MeOH (5 mL) and passed through a preconditioned (15 mL MeOH) aminopropyl column (10 g). The column was washed with MeOH (50 mL) and the desired fractions combined and concentrated *in vacuo* yielding **2.077** (244 mg, 0.648 mmol, 79%) as a yellow solid. m.p. 267–272 °C; v_{max} (solid)/cm^{-1}: 3381 (N-H), 2885, 1662 (C=O), 1599, 1446, 1127, 844; ^{1}H NMR (400 MHz, CHLOROFORM-d) δ ppm 13.60 (br. s, 1 H), 7.86-7.82 (m, 1 H), 7.78 (s, 1 H), 6.86 (d, J=8.6 Hz, 1 H), 5.82-5.78 (m, 1 H), 5.18-5.02 (m, 1 H), 4.39 (app. q, J=2.5 Hz, 2 H), 4.01 (t, J=5.4 Hz, 2 H), 3.41-3.33 (m, 1 H), 3.26-3.17 (m, 1 H), 3.02 (app. dd, J=30.1, 13.9 Hz, 1 H), 2.92-2.81 (m, 1 H), 2.49-2.42 (m, 2 H), 2.37 (d, J=1.2 Hz, 3 H), 2.26-2.12 (m, 1 H), 1.95 (qd, J=12.6, 4.2 Hz, 1 H) (N.B. exchangeable piperidine amine proton not visible); ^{13}C NMR (101 MHz, CHLOROFORM-d) δ ppm 164.5, 145.8, 138.2, 135.5, 133.7, 131.6, 128.6, 127.3 (t, J=33.7 Hz, 1 C), 123.7, 122.9, 120.4, 65.7, 64.5, 51.8 (t, J=24.9 Hz, 1 C), 51.2 (t, J=24.9 Hz, 1 C), 44.8, 32.9, 32.8, 17.2; ^{19}F NMR (376 MHz, CHLOROFORM-d) δ ppm −111.6 (d, J=241 Hz, 1 F), −120.0 (d, J=241 Hz, 1 F);

HRMS (M+H)$^+$ calculated for $C_{19}H_{23}F_2N_4O_2$ 377.1789; found 377.1792; LCMS (formic): R_t = 0.47 min (100%) [M+H]$^+$ = 377.

tert-Butyl (3-(4-((5-(3,6-dihydro-2H-pyran-4-yl)-3-methyl-2-oxo-1,2-dihydro-1,7-naphthyridin-8-yl)amino)-3,3-difluoropiperidin-1-yl)propyl)carbamate (2.078)
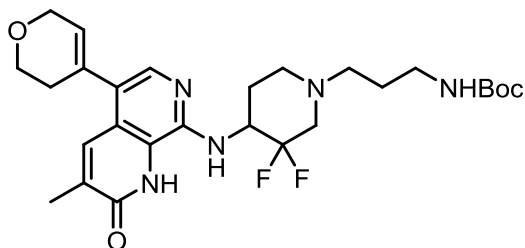
A mixture of **2.077** (125 mg, 0.332 mmol) and **2.035** (120 mg, 0.69 mmol) in MeOH (5 mL) and AcOH (0.5 mL) was stirred at 50 °C for 3 hours before picoline borane complex (36 mg, 0.33 mmol) was added and the mixture stirred at 50 °C for 18 hours. The solution was then allowed to cool to rt before concentrated *in vacuo* and the resultant residue dissolved in DCM (5 mL) and washed with saturated aq. NaHCO$_3$ solution (5 mL). The aqueous layer was separated and extracted with DCM (3 × 5 mL). The organic fractions were combined, passed through a hydrophobic frit and concentrated *in vacuo*. The resultant solid was purified by silica chromatography (0-100% EtOH in EtOAc). The desired fractions were combined and concentrated *in vacuo*. The remaining fractions were combined and re-purified by silica chromatography (0-30% 3:1 EtOAc:EtOH in cyclohexane). The desired fractions were combined and concentrated *in vacuo* yielding **2.078** (0.100 g, 0.187 mmol, 56%) as a cream solid. m.p. 217-223 °C; ν_{max} (solid)/cm^{-1}: 3385 (N-H), 2966, 1696 (C=O), 1654 (C=O), 1594, 1437, 1130; ^{1}H NMR (400 MHz, DMSO-d_6) δ ppm 11.27 (br. s, 1 H), 7.74-7.70 (m, 1 H), 7.64 (s, 1 H), 6.68 (d, *J*=8.3 Hz, 1 H), 6.23-6.11 (m, 1 H), 5.81-5.74 (m, 1 H), 4.87-4.71 (m, 1 H), 4.28 (app. q, *J*=2.8 Hz, 2 H), 3.90 (t, *J*=5.4 Hz, 2 H), 3.19-3.08 (m, 1 H), 3.05 (q, *J*=6.8 Hz, 2 H), 2.95-2.87 (m, 1 H), 2.41-2.30 (m, 3 H), 2.20 (d, *J*=1.0 Hz, 3 H), 2.06-1.93 (m, 1 H), 1.85-1.73 (m, 1 H), 1.64 (quin., *J*=6.8 Hz, 2 H), 1.44 (s, 9 H) (N.B. three protons missing, signal obscured by solvent peak); ^{19}F NMR (376 MHz, DMSO-d_6) δ ppm −75.12 (s, 1 F), −167.32 (s, 1 F); HRMS (M+H)$^+$ calculated for $C_{27}H_{38}F_2N_5O_4$ 534.2892; found 534.2883; LCMS (high pH): R_t = 1.04 min (95%) [M+H]$^+$ = 534.

8-((1-(3-Aminopropyl)-3,3-difluoropiperidin-4-yl)amino)-5-(3,6-dihydro-2H-pyran-4-yl)-3-methyl-1,7-naphthyridin-2(1H)-one (2.068)
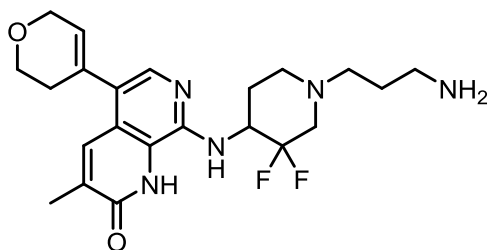
2.078 (89 mg, 0.17 mmol) was dissolved in 4 M HCl in 1,4-dioxane (5 mL) and stirred at rt for 1 hour. The solution was concentrated *in vacuo*, dissolved in 1:1 MeOH:DMSO and purified by MDAP (high pH). The desired fractions were combined yielding **2.068** (29 mg, 0.067 mmol, 40%) as a white solid. m.p. 157–160 °C; v_{max} (solid)/cm^{-1}: 3388 (N-H), 2944, 1659 (C=O), 1598, 1436, 908; ^{1}H NMR (400 MHz, DMSO-d_6, 393 K) δ ppm 7.73-7.70 (m, 1 H), 7.63 (s, 1 H), 6.69 (br. s, 1 H), 5.81-5.74 (m, 1 H), 4.87-4.70 (m, 1 H), 4.28 (app. q, *J*=2.8 Hz, 2 H), 3.90 (t, *J*=5.4 Hz, 2 H), 3.20-3.09 (m, 1 H), 2.96-2.86 (m, 1 H), 2.67 (t, *J*=6.8 Hz, 2 H), 2.60-2.53 (m, 2 H), 2.41-2.27 (m, 3 H), 2.20 (d, *J*=1.3 Hz, 3 H), 2.04-1.92 (m, 1 H), 1.85-1.71 (m, 1 H), 1.59 (quin., *J*=6.8 Hz, 2 H) (N.B. exchangeable lactam and amine protons not visible. one proton missing, signal obscured by DMSO solvent peak); ^{13}C NMR (101 MHz, CHLOROFORM-*d*) δ ppm 164.4, 145.9, 138.1, 135.3, 133.8, 131.6, 127.2, 123.6, 122.9, 120.5, 65.6, 64.5, 58.5 (t, *J*=20.5 Hz, 1 C), 55.5, 51.9, 51.2 (t, *J*=20.5 Hz, 1 C), 40.7, 31.0, 29.9, 29.7, 26.9, 17.2; ^{19}F NMR (376 MHz, CHLOROFORM-*d*) δ ppm −108.06 (d, *J*=240.6 Hz, 1 F), −115.3 (d, *J*=240.6 Hz, 1 F); HRMS (M+H)$^+$ calculated for $C_{22}H_{30}F_2N_5O_2$ 434.2343; found 434.2364; LCMS (high pH): R_t = 0.78 min (100%) [M+H]$^+$ = 434.

***tert*-Butyl 4-((2-(benzyloxy)-3-methyl-1,7-naphthyridin-8-yl)(methyl)amino)piperidine-1-carboxylate (2.081)**
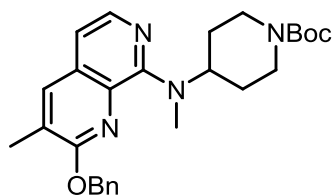
tert-butyl 4-(methylamino)piperidine-1-carboxylate (0.374 mL, 1.76 mmol) was added to a solution of **2.029** (0.500 g, 1.76 mmol), sodium *tert*-butoxide (675 mg, 7.02 mmol), Pd$_2$(dba)$_3$ (0.080 g, 0.088 mmol), 2-(dicyclohexylphosphino)3,6-dimethoxy-2′,4′,6′-triisopropyl-1,1′-biphenyl (94 mg, 0.18 mmol) in toluene (15 mL). The resulting reaction mixture was then stirred at 85 °C for 3 hours. The resultant solution was allowed to cool to rt before being diluted with EtOAc (15 mL) and water (15 mL). The organic layer was separated, washed with

brine (20 mL), passed through a hydrophobic frit, and concentrated *in vacuo*. The resultant residue was purified by silica chromatography (0-50% EtOAc in cyclohexane). The desired fractions were combined and concentrated *in vacuo* yielding **2.081** (616 mg, 1.33 mmol, 76%) as an orange solid. v_{max} (solid)/cm^{-1}: 2923, 1689 (C=O), 1419, 732; ^{1}H NMR (400 MHz, DMSO-d_6) δ ppm 7.99-7.96 (m, 1 H), 7.95 (d, J=5.4 Hz, 1 H), 7.52-7.48 (m, 2 H), 7.46-7.39 (m, 2 H), 7.38-7.32 (m, 1 H), 7.03 (d, J=5.4 Hz, 1 H), 5.50 (s, 2 H), 5.04-4.95 (m, 1 H), 4.11-3.98 (m, 2 H), 3.03 (s, 3 H), 2.84-2.67 (m, 2 H), 2.34 (d, J=1.0 Hz, 3 H), 1.83-1.67 (m, 4 H), 1.41 (s, 9 H); ^{13}C NMR (101 MHz, DMSO-d_6) δ ppm 158.5, 157.2, 154.3, 140.0, 137.5, 137.4, 132.0, 130.9, 129.0, 128.2, 127.9, 126.0, 111.4, 79.1, 67.7, 57.1, 32.9, 29.4, 28.6, 26.8, 16.5; HRMS (M+H)$^+$ calculated for $C_{27}H_{35}N_4O_3$ 463.2709; found 463.2712; LC/MS (formic): R_t = 0.96 min (99%) [M+H]$^+$ = 463.

tert-Butyl 4-((2-(benzyloxy)-5-bromo-3-methyl-1,7-naphthyridin-8-yl)(methyl)amino)piperidine-1-carboxylate (2.082)
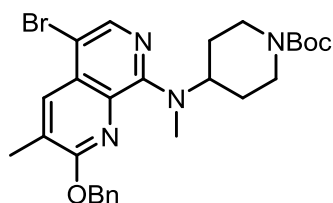

N-Bromosuccinimide (254 mg, 1.427 mmol) was added at rt to a stirred solution of **2.081** (0.600 g, 1.30 mmol) in chloroform (11 mL). The resultant solution was then stirred at rt for 15 min before being diluted with water (30 mL). The organic phase was passed through a hydrophobic frit and concentrated *in vacuo*. The resultant residue was dissolved in minimal DCM and purified by silica chromatography (0-15% EtOAc in cyclohexane). The desired fractions were combined and concentrated *in vacuo* yielding **2.082** (484 mg, 0.894 mmol, 69%) as a yellow oil. ^{1}H NMR (400 MHz, DMSO-d_6) δ ppm 8.12 (s, 1 H), 8.08 (br. s, 1 H), 7.54-7.47 (m, 2 H), 7.46-7.39 (m, 2 H), 7.39-7.32 (m, 1 H), 5.51 (s, 2 H), 5.00-4.88 (m, 1 H), 4.11-3.94 (m, 2 H), 3.04 (s, 3 H), 2.82-2.65 (m, 2 H), 2.40 (s, 3 H), 1.76-1.67 (m, 2 H), 1.43-1.32 (m, 11 H); ^{13}C NMR (101 MHz, DMSO-d_6) δ ppm 159.2, 156.8, 154.3, 141.0, 137.2, 136.0, 132.7, 129.2, 129.0, 128.4, 127.9, 127.8, 105.6, 79.1, 68.2, 57.3, 33.2, 29.3, 28.6, 26.8, 16.6; LC/MS (TFA): R_t = 1.19 min (100%) [M+H]$^+$ = 541.

***tert*-Butyl 4-((2-(benzyloxy)-5-(3,6-dihydro-2H-pyran-4-yl)-3-methyl-1,7-naphthyridin-8-yl)(methyl)amino)piperidine-1-carboxylate (2.083)**
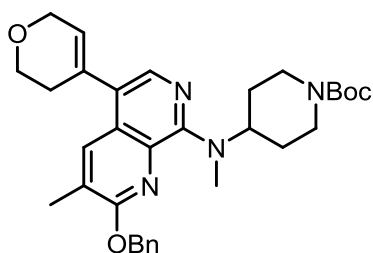
2-(3,6-Dihydro-2H-pyran-4-yl)-4,4,5,5-tetramethyl-1,3,2-dioxaborolane (252 mg, 1.20 mmol) was added at rt to a stirred mixture of **2.082** (464 mg, 0.857 mmol), potassium carbonate (355 mg, 2.57 mmol) and XPhos-Pd-G2 (67 mg, 0.086 mmol) in 1,4-dioxane (1.33 mL) and water (0.66 mL). The resultant reaction mixture was then heated to 100 °C for 1 hour in a microwave reactor. A further portion of XPhos-Pd-G2 (67 mg, 0.086 mmol) was added and the reaction heated at 100 °C for 30 min. The reaction mixture was allowed to cool down to rt before being diluted with EtOAc (20 mL) and filtered through Celite. The resultant solution was concentrated *in vacuo*. The resultant residue was dissolved in EtOAc (15 mL) and washed sequentially with water (15 mL) and brine (15 mL). The organic layer was passed through a hydrophobic frit and concentrated *in vacuo*. The resultant residue was dissolved in minimal DCM and purified by silica chromatography (0-50% EtOAc in cyclohexane). The desired fractions were combined and concentrated *in vacuo* yielding **2.083** (288 mg, 0.529 mmol, 62%) as a yellow solid. m.p. 137–139 °C; v_{max} (solid)/cm^{-1}: 2928, 1689 (C=O), 1422, 1151; ^{1}H NMR (400 MHz, DMSO-d_6) δ ppm 8.03-8.00 (m, 1 H), 7.82 (s, 1 H), 7.53-7.47 (m, 2 H), 7.46-7.39 (m, 2 H), 7.38-7.32 (m, 1 H), 5.83-5.79 (m, 1 H), 5.51 (s, 2 H), 4.97-4.88 (m, 1 H), 4.30-4.25 (m, 2 H), 4.11-3.97 (m, 2 H), 3.90 (t, *J*=5.4 Hz, 2 H), 3.02 (s, 3 H), 2.81-2.65 (m, 2 H), 2.43-2.33 (m, 5 H), 1.83-1.67 (m, 4 H), 1.41 (s, 9 H); ^{13}C NMR (101 MHz, DMSO-d_6) δ ppm 158.4, 156.7, 154.3, 138.0, 137.5, 135.2, 131.8, 131.7, 129.0, 128.6, 128.2, 127.9, 127.2, 125.9, 124.9, 79.1, 67.7, 65.3, 64.2, 57.3, 32.9, 30.6, 29.4, 28.6, 26.8, 16.7; HRMS (M+H)$^+$ calculated for $C_{32}H_{41}N_4O_4$ 545.3128; found 545.3130; LC/MS (formic): R_t = 1.05 min (100%) [M+H]$^+$ = 545.

5-(3,6-Dihydro-2H-pyran-4-yl)-3-methyl-8-(methyl(piperidin-4-yl)amino)-1,7-naphthyridin-2(1H)-one (2.084)
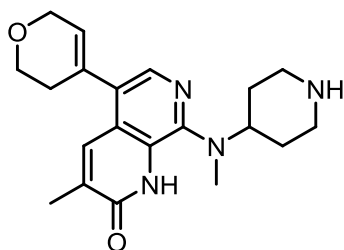
2.083 (278 mg, 0.510 mmol) was dissolved in TFA (8 mL) at rt. The resultant solution was then heated to reflux and stirred for 1.5 hours before being allowed to cool down to rt. Volatile components were then removed *in vacuo*. Toluene (10 mL) was then added to the resulting residue and evaporated off *in vacuo* (× 3). The resultant residue was dissolved in minimal MeOH and passed through a preconditioned aminopropyl column (20 g) and washed with MeOH (50 mL). The desired fractions were combined and concentrated *in vacuo* yielding **2.084** (178 mg, 0.502 mmol, 98%) as a cream solid. m.p. 164-168 °C; ν_{max} (solid)/cm^{-1}: 2928, 1689 (C=O), 1423, 1150, 734; ^{1}H NMR (400 MHz, DMSO-d_6) δ ppm 7.92 (s, 1 H), 7.82-7.75 (m, 1 H), 5.88-5.80 (m, 1 H), 4.26 (app. q, J=2.4 Hz, 2 H), 3.88 (t, J=5.3 Hz, 2 H), 3.24-3.18 (m, 1 H), 3.00-2.88 (m, 2 H), 2.67 (s, 3 H), 2.46-2.32 (m, 4 H), 2.17 (d, J=1.0 Hz, 3 H), 1.76-1.65 (m, 2 H), 1.47 (qd, J=11.7, 3.9 Hz, 2 H) (N.B. exchangeable lactam and piperidine amine proton not visible); HRMS (M+H)$^+$ calculated for $C_{20}H_{27}N_4O_2$ 355.2134; found 355.2135; LC/MS (high pH): R_t = 0.84 min (96%) [M+H]$^+$ = 355.

tert-Butyl (3-(4-((5-(3,6-dihydro-2H-pyran-4-yl)-3-methyl-2-oxo-1,2-dihydro-1,7-naphthyridin-8-yl)(methyl)amino)piperidin-1-yl)-2,2-difluoro-3-oxopropyl)carbamate (2.085)
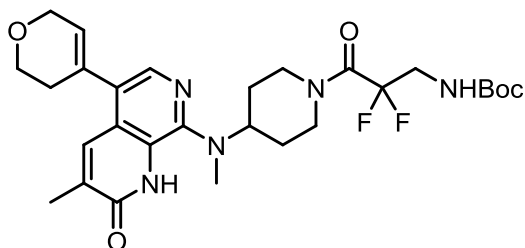
HATU (386 mg, 1.02 mmol) and DIPEA (0.354 mL, 2.03 mmol) were added at rt to a stirred solution of **2.063** (229 mg, 1.02 mmol) and **2.084** (180 mg, 0.508 mmol) in DMF (10 mL). The resultant solution was stirred at rt for 30 min before being diluted with water (15 mL) and extracted with EtOAc (15 mL). The organic layer was separated, and the aqueous layer extracted further (15 mL). The organic fractions were combined and washed sequentially with 10 wt% aq. LiCl solution (30 mL) and brine (20 mL). The organic layer was passed through a hydrophobic frit and

concentrated *in vacuo*. The resultant residue was dissolved in 1:1 DMSO:DCM and purified by MDAP (high pH). The desired fractions were combined and concentrated *in vacuo* yielding **2.085** (54 mg, 0.096 mmol, 19%) as a cream solid. m.p. 221-222 °C; v_{max} (solid)/cm^{-1}: 3450, 2970, 1721, 1645 (C=O), 1495, 1130; ^{1}H NMR (400 MHz, DMSO-d_6, 393 K) δ ppm 9.89 (br. s, 1 H), 7.94 (s, 1 H), 7.80-7.74 (m, 1 H), 6.54-6.43 (m, 1 H), 5.89-5.83 (m, 1 H), 4.30 (app. q, J=2.7, 2 H), 4.25-4.12 (m, 2 H), 3.92 (t, J=5.4 Hz, 2 H), 3.68 (td, J=15.3, 6.5 Hz, 2 H), 3.63-3.51 (m, 1 H), 3.16-3.00 (m, 2 H), 2.72 (s, 3 H), 2.45-2.39 (m, 2 H), 2.20 (d, J=1.0 Hz, 3 H), 1.98-1.89 (m, 2 H), 1.74-1.60 (m, 2 H), 1.42 (s, 9 H); HRMS (M+H)$^+$ calculated for $C_{28}H_{38}F_2N_5O_5$ 562.2841; found 562.2845; LC/MS (high pH): R_t = 1.11 min (100%) [M+H]$^+$ = 562.

8-((1-(3-amino-2,2-difluoropropanoyl)piperidin-4-yl)(methyl)amino)-5-(3,6-dihydro-2H-pyran-4-yl)-3-methyl-1,7-naphthyridin-2(1H)-one (2.079)
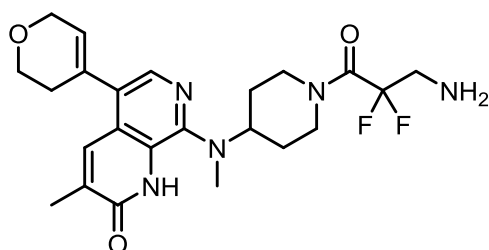

2.085 (44 mg, 0.078 mmol) was dissolved in 4 M HCl in 1,4-dioxane (3 mL) and stirred at rt for 2 hours before being concentrated *in vacuo*. The resultant residue was dissolved in minimal 1:1 MeOH:DMSO and purified by MDAP (high pH). The desired fractions were combined and concentrated *in vacuo* yielding **2.079** (24 mg, 0.052 mmol, 66%) as a cream solid. m.p. 231–237 °C; v_{max} (solid)/cm^{-1}: 2928, 1644 (C=O), 1610, 1450, 1048; ^{1}H NMR (400 MHz, DMSO-d_6, 393 K) δ ppm 7.94 (s, 1 H), 7.80-7.74 (m, 1 H), 5.90-5.83 (m, 1 H), 4.30 (app. q, J=2.6 Hz, 2 H), 4.26-4.17 (m, 2 H), 3.92 (t, J=5.3 Hz, 2 H), 3.63-3.54 (m, 1 H), 3.15 (t, J=15.3 Hz, 2H), 3.10-3.02 (m, 2 H), 2.72 (s, 3 H), 2.46-2.39 (m, 2 H), 2.20 (d, J=1.3 Hz, 3 H), 1.98-1.89 (m, 2 H), 1.71-1.57 (m, 2 H) (N.B. exchangeable lactam and amine protons not visible); ^{13}C NMR (101 MHz, DMSO-d_6) δ ppm 161.9, 161.3 (t, J=28.6 Hz, 1 C), 150.6, 138.1, 136.0, 133.1, 131.0, 130.3, 128.7, 128.1, 123.2, 66.8, 65.2, 64.0, 56.8, 45.8 (t, J=26.1 Hz, 1 C), 37.3, 30.4, 30.2, 29.2, 17.5; ^{19}F NMR (376 MHz, DMSO-d_6) δ ppm −105.44 (s, 2 F); HRMS (M+H)$^+$ calculated for $C_{23}H_{30}F_2N_5O_3$ 462.2317; found 462.2321; LC/MS (high pH): R_t = 0.84 min (100%) [M+H]$^+$ = 462.

tert-Butyl 4-((2-(benzyloxy)-3-methyl-1,7-naphthyridin-8-yl)oxy)piperidine-1-carboxylate (2.086)
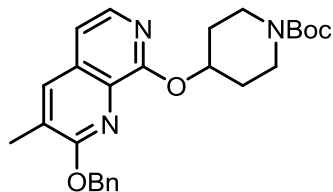
tert-Butyl 4-hydroxypiperidine-1-carboxylate (459 mg, 2.28 mmol), **2.029** (0.500 mg, 1.76 mmol), potassium *tert*-butoxide (591 mg, 5.27 mmol), Pd₂(dba)₃ (16 mg, 0.018 mmol) and 2-(dicyclohexylphosphino)3,6-dimethoxy-2′,4′,6′-triisopropyl-1,1′-biphenyl (19 mg, 0.035 mmol) were dissolved in THF (13 mL) under nitrogen. The reaction was then stirred at rt for 3 hours. The solution was diluted with EtOAc (20 mL) and water (15 mL) and the layers separated. The aqueous layer was extracted further with EtOAc (3 × 10 mL). The organic fractions were combined, washed with brine (10 mL), passed through a hydrophobic frit, and concentrated *in vacuo*. The resultant residue was dissolved in minimal DCM and purified by silica chromatography (0-45% EtOAc in cyclohexane). The desired fractions were combined and concentrated *in vacuo* yielding **2.086** (568 mg, 1.26 mmol, 72%) as a white solid. m.p. 100-104 °C; v_{max} (solid)/cm^{-1}: 2976, 1686 (C=O), 1425, 1234, 763; ^{1}H NMR (400 MHz, DMSO-d_6) δ ppm 8.04-8.01 (m, 1 H), 7.92 (d, *J*=5.6 Hz, 1 H), 7.65-7.60 (m, 2 H), 7.39-7.33 (m, 2 H), 7.33-7.27 (m, 1 H), 7.22 (d, *J*=5.6 Hz, 1 H), 5.62 (s, 2 H), 5.53-5.47 (m, 1 H), 3.75-3.67 (m, 2 H), 3.48-3.40 (m, 2 H), 2.34 (d, *J*=0.7 Hz, 3 H), 2.06-2.01 (m, 2 H), 1.87-1.82 (m, 2 H), 1.47 (s, 9 H); ^{13}C NMR (101 MHz, DMSO-d_6) δ ppm 160.7, 158.1, 154.5, 138.6, 137.6, 136.6, 131.0, 130.9, 129.2, 128.6, 128.3, 127.6, 114.0, 79.2, 70.2, 67.8, 30.8, 28.6, 28.5, 16.7; HRMS (M+H)$^+$ calculated for $C_{26}H_{32}N_3O_4$ 450.2393; found 450.2397; LCMS (formic): R$_t$ = 1.58 min (96%) [M+H]$^+$ = 450.

tert-Butyl 4-((2-(benzyloxy)-5-bromo-3-methyl-1,7-naphthyridin-8-yl)oxy)piperidine-1-carboxylate (2.087)
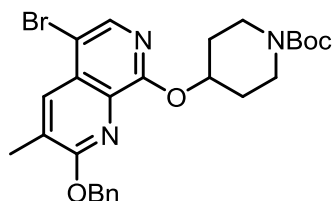
N-Bromosuccinimide (243 mg, 1.37 mmol) was added at rt to a stirred solution of **2.086** (558 mg, 1.24 mmol) in acetonitrile (10 mL). The resultant solution was then heated to 80 °C and stirred for 1 hour. The reaction mixture was allowed to cool to rt. The resultant precipitate was filtered under reduced pressure and washed with water (2 × 5 mL) yielding **2.087**

(456 mg, 0.863 mmol, 70%) as a white solid. m.p. 136-139 °C; v_{max} (solid)/cm^{-1}: 2957, 1693 (C=O), 1417, 1274, 763; ^{1}H NMR (400 MHz, DMSO-d_6) δ ppm 8.14 (s, 1 H), 8.09-8.06 (m, 1 H), 7.65-7.58 (m, 2 H), 7.39-7.27 (m, 3 H), 5.57 (s, 2 H), 5.47-5.39 (m, 1 H), 3.71-3.60 (m, 2 H), 3.44-3.34 (m, 2 H), 2.40 (d, J=1.0 Hz, 3 H), 2.05-1.95 (m, 2 H), 1.81-1.70 (m, 2 H), 1.43 (s, 9 H); HRMS (M+H)$^+$ calculated for $C_{26}H_{31}BrN_3O_4$ 528.1498; found 528.1505; LCMS (high pH): R_t = 1.77 min (98%) [M+H]$^+$ = 528.

tert-Butyl 4-((2-(benzyloxy)-5-(3,6-dihydro-2H-pyran-4-yl)-3-methyl-1,7-naphthyridin-8-yl)oxy)piperidine-1-carboxylate (2.088)
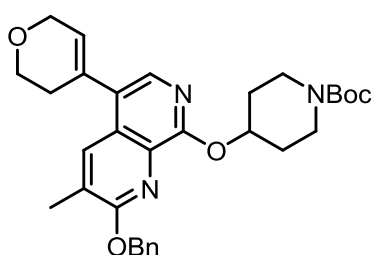

2-(3,6-Dihydro-2H-pyran-4-yl)-4,4,5,5-tetramethyl-1,3,2-dioxaborolane (245 mg, 1.17 mmol) was added at rt to a stirred mixture of **2.087** (440 mg, 0.83 mmol), potassium carbonate (345 mg, 2.50 mmol), Pd(OAc)$_2$ (15 mg, 0.067 mmol) and butyldi-1-adamantylphosphine (48 mg, 0.13 mmol) in 1,4-dioxane (1.33 mL) and water (0.66 mL). The resultant reaction mixture was then heated to 100 °C for 1 hour in a microwave reactor. The reaction mixture was allowed to cool to rt before being diluted with EtOAc (10 mL), passed through Celite and concentrated *in vacuo*. The resultant residue was dissolved in minimal DCM and purified by silica chromatography (0-100% EtOAc in cyclohexane). The desired fractions were combined and concentrated *in vacuo* yielding **2.088** (280 mg, 0.53 mmol, 63%) as a colourless oil. ^{1}H NMR (400 MHz, DMSO-d_6) δ ppm 8.04-8.00 (m, 1 H), 7.78 (s, 1 H), 7.67-7.60 (m, 2 H), 7.40-7.27 (m, 3 H), 5.86-5.81 (m, 1 H), 5.57 (s, 2 H), 5.50-5.41 (m, 1 H), 4.31-4.24 (m, 2 H), 3.89 (t, J=5.4 Hz, 2 H), 3.71-3.61 (m, 2 H), 3.45-3.34 (m, 2 H), 2.44-2.34 (m, 5 H), 2.05-1.94 (m, 2 H), 1.82-1.70 (m, 2 H), 1.43 (s, 9 H); ^{13}C NMR (101 MHz, DMSO-d_6) δ ppm 157.3, 154.5, 137.6, 136.5, 134.6, 131.4, 130.7, 129.3, 128.7, 128.6, 128.3, 127.9, 127.6, 127.5, 79.2, 70.1, 67.8, 65.3, 64.1, 30.8, 30.6, 28.6, 26.8, 16.8 (N.B. one carbon signal missing); HRMS (M+H)$^+$ calculated for $C_{31}H_{38}N_3O_5$ 532.2811; found 532.2819; LCMS (formic): R_t = 1.61 min (98%) [M+H]$^+$ = 532.

5-(3,6-Dihydro-2H-pyran-4-yl)-3-methyl-8-(piperidin-4-yloxy)-1,7-naphthyridin-2(1H)-one (2.089)
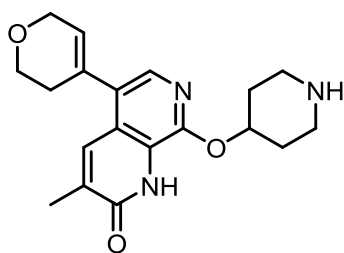
2.088 (227 mg, 0.427 mmol) was dissolved in TFA (4 mL) at rt. The resultant solution was then heated to reflux and stirred for 1.5 hours before being allowed to cool to rt. Volatile components were then removed *in vacuo*. Toluene (3 mL) was then added to the resulting residue and concentrated *in vacuo* (× 3). The resultant residue was dissolved in MeOH (20 mL) and passed through a preconditioned (25 mL MeOH) aminopropyl column (10 g) and washed with MeOH (100 mL). The desired fractions were combined and concentrated *in vacuo* yielding **2.089** (144 mg, 0.422 mmol, 99%) as a cream solid. m.p. 204-207 °C; v_{max} (solid)/cm^{-1}: 3168, 2957, 1653 (C=O), 1422, 1119; ^{1}H NMR (400 MHz, DMSO-d_6) δ ppm 7.80-7.72 (m, 1 H), 7.66 (s, 1 H), 5.86-5.77 (m, 1 H), 5.21-5.11 (m, 1 H), 4.30-4.22 (m, 2 H), 3.88 (t, *J*=5.4 Hz, 2 H), 3.08-2.99 (m, 2 H), 2.63-2.54 (m, 2 H), 2.41-2.31 (m, 2 H), 2.21-2.13 (m, 3 H), 2.00-1.88 (m, 2 H), 1.72-1.59 (m, 2 H) (N.B. exchangeable lactam and amine protons not visible); ^{13}C NMR (101 MHz, DMSO-d_6) δ ppm 162.0, 149.9, 136.3, 135.8, 132.8, 131.0, 128.2, 127.7, 122.8, 122.7, 73.2, 65.2, 64.0, 44.3, 32.6, 30.6, 17.6; HRMS (M+H)$^+$ calculated for $C_{19}H_{24}N_3O_3$ 342.1818; found 342.1825; LCMS (formic): R_t = 0.49 min (100%) [M+H]$^+$ = 342.

***tert*-Butyl (3-(4-((5-(3,6-dihydro-2H-pyran-4-yl)-3-methyl-2-oxo-1,2-dihydro-1,7-naphthyridin-8-yl)oxy)piperidin-1-yl)-2,2-difluoro-3-oxopropyl)carbamate (2.090)**
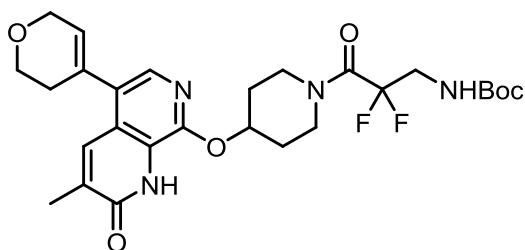
HATU (297 mg, 0.782 mmol) and DIPEA (0.182 mL, 1.04 mmol) were added at rt to a stirred solution of **2.063** (117 mg, 0.521 mmol) and **2.089** (89 mg, 0.26 mmol) in DMF (8 mL). The solution was stirred at rt for 5 min before being diluted with water (15 mL) and EtOAc (15 mL). The layers were separated and the aqueous extracted further with EtOAc (15 mL). The organic layers were combined and washed

sequentially with 10 wt% aq. LiCl solution (15 mL) and brine (15 mL). The organic layer was passed through a hydrophobic frit and concentrated *in vacuo*. The resultant residue was dissolved in 1:1 MeOH:DCM and purified by MDAP (high pH). The desired fractions were combined yielding **2.090** (98 mg, 0.18 mmol, 69%) as a cream solid. m.p. 173-177 °C; v_{max} (solid)/cm^{-1}: 2978, 1652 (C=O), 1250, 1165; ^{1}H NMR (400 MHz, DMSO-d_6, 393 K) δ ppm 10.61 (br. s, 1 H), 7.75-7.70 (m, 1 H), 7.67 (s, 1 H), 6.54-6.44 (m, 1 H), 5.85-5.80 (m, 1 H), 5.54-5.45 (m, 1 H), 4.28 (app. q, *J*=2.7 Hz, 2 H), 4.05-3.94 (m, 2 H), 3.91 (t, *J*=5.4 Hz, 2 H), 3.78-3.62 (m, 4 H), 2.42-2.37 (m, 2 H), 2.20 (d, *J*=1.0 Hz, 3 H), 2.11-2.00 (m, 2 H), 2.00-1.89 (m, 2 H), 1.42 (s, 9 H); ^{13}C NMR (101 MHz, DMSO-d_6) δ ppm 162.2, 156.2, 149.5, 136.5, 135.8, 132.8, 131.0, 128.3, 128.1, 123.1, 122.7, 78.9, 69.8, 65.2, 64.0, 55.4, 31.1, 30.6, 30.0, 28.6, 26.8, 17.6 (N.B. one carbon signal missing); HRMS (M+H)$^+$ calculated for $C_{27}H_{35}F_2N_4O_6$ 549.2525; found 549.2529; LCMS (high pH): R_t = 1.15 min (97%) [M+H]$^+$ = 549.

8-((1-(3-Amino-2,2-difluoropropanoyl)piperidin-4-yl)oxy)-5-(3,6-dihydro-2H-pyran-4-yl)-3-methyl-1,7-naphthyridin-2(1H)-one (2.080)
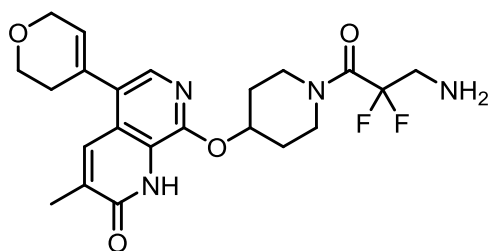
2.090 (85 mg, 0.16 mmol) was dissolved in 4 M HCl in 1,4-dioxane (3 mL) and stirred at rt for 2 hours before being concentrated *in vacuo*. The resultant residue was dissolved in minimal 1:1 MeOH:DMSO and purified by MDAP (high pH). The desired fractions were combined and concentrated *in vacuo* yielding **2.080** (45 mg, 0.10 mmol, 65%) as a cream solid. m.p. 204–208 °C; v_{max} (solid)/cm^{-1}: 2945, 1651 (C=O), 1615, 1421, 1359; ^{1}H NMR (400 MHz, DMSO-d_6, 393 K) δ ppm 7.74-7.70 (m, 1 H), 7.67 (s, 1 H), 5.87-5.80 (m, 1 H), 5.55-5.47 (m, 1 H), 4.28 (app. q, *J*=2.5 Hz, 2 H), 4.07-3.95 (m, 2 H), 3.91 (t, *J*=5.4 Hz, 2 H), 3.75-3.61 (m, 2 H), 3.19 (t, *J*=15.2 Hz, 2 H), 2.44-2.36 (m, 2 H), 2.20 (d, *J*=1.3 Hz, 3 H), 2.11-2.00 (m, 2 H), 1.99-1.88 (m, 2 H) (N.B. exchangeable lactam and amine protons not visible. Lactam proton visible on rt NMR 11.40 ppm (br. s, 1 H)); ^{13}C NMR (151 MHz, DMSO-d_6) δ ppm 162.2, 161.5 (t, *J*=27.9 Hz, 1 C), 149.5, 136.5, 135.7, 132.8, 131.0, 128.3, 128.1, 123.1, 122.7, 118.4 (t, *J*=254.3 Hz, 1 C) 69.8, 65.2, 64.0, 45.9 (t, *J*=26.5, 1 C), 42.2, 30.6, 30.2, 17.6; ^{19}F NMR (376 MHz,

DMSO-d_6) δ ppm −105.7- -105.5 (m, 2 F); HRMS (M+H)$^+$ calculated for $C_{22}H_{27}F_2N_4O_4$ 449.2000; found 449.2010; LCMS (high pH): R_t = 0.87 min (100%) [M+H]$^+$ = 449.

tert-Butyl (2-chloropyridin-3-yl)carbamate (2.098)
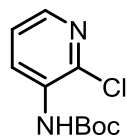
2-Chloropyridin-3-amine (10 g, 80 mmol) in THF (20 mL) was added in portions to a 1 M NaHMDS in THF solution (171 mL, 171 mmol) at -10 °C under nitrogen. The resultant solution was stirred at -10 °C for 30 min before Boc-anhydride (19.87 mL, 85.54 mmol) in THF (40 mL) was added at -5 °C under nitrogen. The resultant solution was stirred at -5 °C for 30 min before 2M HCl (90 mL) was added followed by EtOAc (100 mL). The phases were separated and the organic layer washed with water (80 mL), brine (80 mL), passed through a hydrophobic frit and concentrated *in vacuo*. The resultant residue was dissolved in minimal DCM and purified by silica chromatography (0-40% EtOAc in cyclohexane). The desired fractions were combined and concentrated *in vacuo* to yield **2.098** (14.68 g, 64.19 mmol, 83%) as a white solid. ^{1}H NMR (400 MHz, CHLOROFORM-*d*) δ ppm 8.49 (d, *J*=8.1 Hz, 1 H), 8.02 (d, *J*=4.6 Hz, 1 H), 7.21 (dd, *J*=8.1, 4.6 Hz, 1 H), 7.01 (br. s, 1 H), 1.53 (s, 9 H); ^{13}C NMR (101 MHz, CHLOROFORM-*d*) δ ppm 152.1, 142.5, 139.1, 132.6, 127.1, 123.2, 81.8, 28.2; LC/MS (formic): R_t = 1.04 min (96%) [M+H]$^+$ = 229.

tert-Butyl (2-chloro-4-formylpyridin-3-yl)carbamate (2.097)
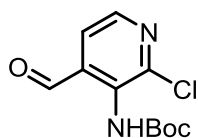
To a solution of **2.098** (3.000 g, 13.12 mmol) in THF (60 mL) under nitrogen was added TMEDA (4.36 mL, 28.9 mmol). The solution was cooled to -78 °C and 1.6 M ^{n}BuLi in hexanes (18.0 mL, 28.9 mmol) added dropwise over 15 min. The resultant solution was stirred at -78 °C for 1.5 hours before being warmed to -20 °C and stirred for 20 min. The resultant solution was cooled to -78 °C and DMF (2.03 mL, 26.2 mmol) added dropwise over 5 min. The resultant solution was stirred at -78 °C for 2.5 hours. Another portion of DMF (2.03 mL, 26.2 mmol) was added and the solution stirred for a further 1.5 hours. The solution was diluted with saturated aq. NH$_4$Cl solution (45 mL) and EtOAc (45 mL). The organic layer was separated and washed with brine (45 mL) before being passed through a

hydrophobic frit and concentrated *in vacuo*. The resultant residue was dissolved in minimal DCM and purified by silica chromatography (0-30% EtOAc in cyclohexane). The desired fractions were combined yielding **2.097** (1.28 g, 4.97 mmol, 38%) as a yellow solid. ^{1}H NMR (400 MHz, CHLOROFORM-*d*) δ ppm 10.00 (s, 1 H), 8.38 (d, *J*=4.9 Hz, 1 H), 7.68 (d, *J*=4.9 Hz, 1 H), 6.91 (br. s, 1 H), 1.55 (s, 9 H); LC/MS (formic): R_t = 0.92 min (99%) $[M+H+H_2O]^+$ = 275.

Ethyl 2-(diethoxyphosphoryl)hex-5-enoate (2.101)
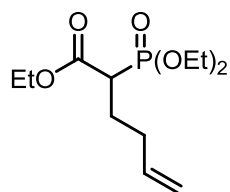
To a stirred solution of ethyl 2-(diethoxyphosphoryl)acetate (3.54 mL, 17.8 mmol) in DMSO (20 mL) was added sodium hydride in oil 60 wt % (0.785 g, 19.6 mmol). The resultant reaction mixture was stirred at rt for 20 min before 4-bromobut-1-ene (2.35 mL, 23.2 mmol) was added dropwise at rt. The resultant solution was stirred at rt for 63 hours. The solution was then diluted with saturated aq. NH₄Cl solution (50 mL). The aqueous layer was separated and extracted with EtOAc (3 × 50 mL). The combined organic fractions were passed through a hydrophobic frit and concentrated *in vacuo*. The resultant orange oil was purified by silica chromatography (0-90% EtOAc in cyclohexane). The desired fractions were combined and concentrated *in vacuo* yielding **2.101** (3.472 g, 12.48 mmol, 70%) as a pale-yellow oil. ^{1}H NMR (400 MHz, CHLOROFORM-*d*) δ ppm 5.77 (ddt, *J*=17.0, 10.4, 6.4, 6.4 Hz, 1 H), 5.09-5.01 (m, 2 H), 4.27-4.11 (m, 6 H), 3.07-2.91 (m, 1 H), 2.27-1.88 (m, 4 H), 1.35 (td, *J*=7.2, 2.6 Hz, 6 H), 1.31 (t, *J*=7.2 Hz, 3 H).
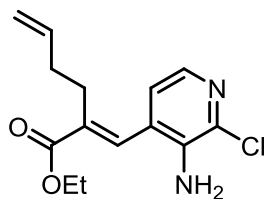
Ethyl (*E*)-2-((3-((*tert*-butoxycarbonyl)amino)-2-chloropyridin-4-yl)methylene)hex-5-enoate (2.096)
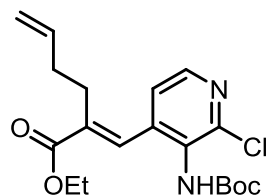
Sodium hydride in oil 60 wt % (0.339 g, 8.473 mmol) was added to a solution of **2.101** (2.358 g, 8.473 mmol) in DMF (20 mL) at 0 °C and left to stir for 45 min. A solution of **2.097** (1.500 g, 5.843 mmol) in DMF (20 mL) was added drop wise over 10 min at 0 °C. The reaction mixture was left to stir at 0 °C for 1.5 hours. The resultant solution was diluted with saturated aq. NH₄Cl solution (30 mL) and EtOAc (30 mL).

The organic layer was separated and the aqueous layer extracted with EtOAc (2 × 30 mL). The combined organic layers were washed with brine (20 mL), passed through a hydrophobic frit and concentrated *in vacuo*. The resultant oil was dissolved in DCM and passed through a hydrophobic frit. The resultant solution was concentrated *in vacuo* and dissolved in minimal DCM before being purified by silica chromatography (0-50% Et$_2$O in cyclohexane). The desired fractions were concentrated *in vacuo* yielding **2.096** (1.282 g, 3.366 mmol, 58%) as a colourless oil. ^{1}H NMR (400 MHz, CHLOROFORM-*d*) δ ppm 8.27 (d, *J*=5.0 Hz, 1 H), 7.56 (s, 1 H), 7.17 (d, *J*=5.0 Hz, 1 H), 6.27 (br. s, 1 H), 5.75 (ddt, *J*=17.0, 10.2, 6.7, 6.7 Hz, 1 H), 5.05-4.95 (m, 2 H), 4.29 (q, *J*=7.1 Hz, 2 H), 2.47-2.39 (m, 2 H), 2.30-2.20 (m, 2 H), 1.48 (s, 9 H), 1.35 (t, *J*=7.1 Hz, 3 H); ^{13}C NMR (101 MHz, CHLOROFORM-*d*) δ ppm 167.0, 152.3, 146.2, 143.8, 137.4, 133.7, 122.9, 115.4, 81.7, 61.1, 32.9, 28.1, 27.5, 26.9, 14.3; LC/MS (formic): R$_t$ = 1.26 min (100%) [M+H]$^+$ = 381.

Ethyl (*E*)-2-((3-amino-2-chloropyridin-4-yl)methylene)hex-5-enoate (2.095)

To a solution of ethyl 2-((3-((*tert*-butoxycarbonyl)amino)-2-chloropyridin-4-yl)methylene)hex-5-enoate (0.100 g, 0.263 mmol) in 1,4-dioxane (2 mL) was added 4 M HCl in 1,4-dioxane (4 mL) drop-wise at 0 °C. The resultant solution was stirred at rt for 15 hours. A further portion of 4 M HCl in 1,4-dioxane (2 mL) was added at rt and the reaction mixture stirred at rt for 7 hours. A further portion of 4 M HCl in 1,4-dioxane (6 mL) was added at rt and the reaction mixture stirred at rt for 44 hours before being concentrated *in vacuo*. The resultant oil was dissolved in DCM (5 mL) and washed sequentially with saturated aq. NaHCO$_3$ solution (5 mL) and brine (5 mL). The resultant solution was concentrated *in vacuo* yielding **2.095** (61 mg, 0.22 mmol, 83%) as a yellow oil. ^{1}H NMR (400 MHz, CHLOROFORM-*d*) δ ppm 7.82 (d, *J*=4.9 Hz, 1 H), 7.43 (s, 1 H), 6.93 (d, *J*=4.9 Hz, 1 H), 5.69 (ddt, *J*=17.0, 10.1, 6.7, 6.7 Hz, 1 H), 5.02-4.94 (m, 2 H), 4.32 (q, *J*=7.2 Hz, 2 H), 4.16 (br. s, 2 H), 2.53-2.44 (m, 2 H), 2.27-2.19 (m, 2 H), 1.38 (t, *J*=7.2 Hz, 3 H); LC/MS (formic): R$_t$ = 1.12 min (88%) [M+H]$^+$ = 281.

### (*E*)-3-(But-1-en-1-yl)-8-chloro-1,7-naphthyridin-2(1H)-one (2.102)
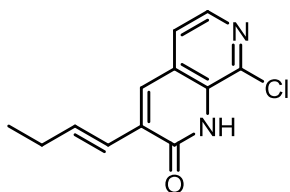
A solution of ethyl 2-((3-amino-2-chloropyridin-4-yl)methylene)hex-5-enoate (546 mg, 1.95 mmol) and DBU (3.52 mL, 23.3 mmol) in toluene (10 mL) were stirred at 110 °C for 110 hours. The solution was allowed to cool to rt before being diluted with saturated aq. NH$_4$Cl solution (30 mL) and Et$_2$O (30 mL). The organic layer was separated and the aqueous extracted further with Et$_2$O (3 × 15 mL). The organic layers were combined, washed with brine (15 mL) and passed through a hydrophobic frit, before being concentrated *in vacuo*. The resulting residue was dissolved in minimal DCM and purified by silica chromatography (0-50% EtOAc in cyclohexane). The desired fractions were combined yielding **2.102** (29 mg, 0.12 mmol, 6%) as a white solid. m.p. 129–132 °C; ν$_{max}$ (solid)/cm^{-1}: 2970, 1652 (C=O), 1472; ^{1}H NMR (400 MHz, CHLOROFORM-*d*) δ ppm 9.23 (br. s, 1 H), 8.17 (d, *J*=5.1 Hz, 1 H), 7.68 (s, 1 H), 7.37 (d, *J*=5.1 Hz, 1 H), 6.90 (dt, *J*=15.9, 6.6 Hz, 1 H), 6.63 (d, *J*=15.9 Hz, 1 H), 2.40-2.27 (m, 2 H), 1.15 (t, *J*=7.5 Hz, 3 H); ^{13}C NMR (101 MHz, CHLOROFORM-*d*) δ ppm 160.8, 141.3, 140.9, 137.0, 136.1, 130.5, 129.3, 126.7, 122.4, 119.9, 26.8, 13.1; HRMS (M+H)$^+$ calculated for C$_{12}$H$_{12}$ClN$_2$O 235.0638; found 235.0638; LC/MS (formic): R$_t$ = 0.94 min (100%) [M+H]$^+$ = 235.

Ethyl 2-(diethoxyphosphoryl)-4-(1,3-dioxan-2-yl)butanoate (2.103)
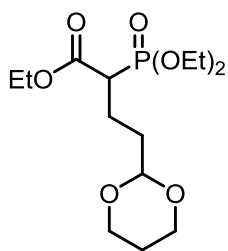
To a stirred solution of ethyl 2-(diethoxyphosphoryl)acetate (3.54 mL, 17.84 mmol) in DMSO (20 mL) was added sodium hydride in oil 60 wt % (0.928 g, 23.2 mmol). The resultant reaction mixture was stirred at rt for 20 min before 2-(2-bromoethyl)-1,3-dioxane (3.16 mL, 23.2 mmol) was added dropwise at rt. The resultant solution was stirred at rt for 1 hour before being left unstirred for 63 hours. The resultant solution was diluted with saturated aq. NH$_4$Cl solution (50 mL) and EtOAc (50 mL). The aqueous layer was separated and extracted with EtOAc (2 × 50 mL). The combined organic fractions were combined and passed through a hydrophobic frit before being concentrated *in vacuo*. The resultant oil was dissolved in minimal DCM and purified by silica chromatography (0-100% EtOAc in cyclohexane). The desired fractions were combined and concentrated *in vacuo* yielding **2.103** (4.583 g, 13.55 mmol, 76%) as a pale-yellow oil. ^{1}H NMR (400 MHz,

CHLOROFORM-*d*) δ ppm 4.53 (t, *J*=5.1 Hz, 1 H), 4.27-4.03 (m, 8 H), 3.79-3.69 (m, 2 H), 3.06-2.92 (m, 1 H), 2.14-1.94 (m, 3 H), 1.71-1.57 (m, 2 H), 1.39-1.25 (m, 10 H).

Ethyl 2-((3-((*tert*-butoxycarbonyl)amino)-2-chloropyridin-4-yl)methylene)-4-(1,3-dioxan-2-yl)butanoate (2.104)
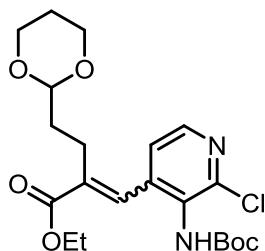

Sodium hydride in oil 60 wt % (0.267 g, 6.67 mmol) was added to a solution **2.103** (2.255 g, 6.665 mmol) in DMF (20 mL) at 0 °C and left to stir for 45 min. A solution of **2.097** (1.180 g, 4.597 mmol) in DMF (20 mL) was added drop wise over 10 min at 0 °C. The reaction mixture was left to stir at 0 °C for 1.5 hours. The resultant solution was diluted with saturated aq. NH_4Cl solution (30 mL) and EtOAc (30 mL). The organic layer was separated and the aqueous layer extracted with EtOAc (2 × 30 mL). The combined organic layers were washed with brine (20 mL), passed through a hydrophobic frit and concentrated *in vacuo*. The resultant oil was dissolved in DCM and passed through a hydrophobic frit. The resultant solution was concentrated *in vacuo* and dissolved in minimal DCM before being purified by silica chromatography (0-50% EtOAc in cyclohexane). The desired fractions were concentrated *in vacuo* yielding ethyl (*E*)-2-((3-((*tert*-butoxycarbonyl)amino)-2-chloropyridin-4-yl)methylene)-4-(1,3-dioxan-2-yl)butanoate (817 mg, 1.85 mmol, 40%) as a yellow oil. Product contains a 4:1 *E:Z* mixture of diastereomers; NMR for *E*-diastereomer given. ^{1}H NMR (400 MHz, CHLOROFORM-*d*) δ ppm 8.26 (d, *J*=5.1 Hz, 1 H), 7.53 (s, 1 H), 7.22 (d, *J*=5.1 Hz, 1 H), 6.58 (br. s, 1 H), 4.52 (t, *J*=4.8 Hz, 1 H), 4.27 (q, *J*=7.1 Hz, 2 H), 4.09-4.04 (m, 2 H), 3.75-3.67 (m, 2 H), 2.43-2.34 (m, 2 H), 1.87-1.80 (m, 3 H), 1.47 (s, 10 H), 1.34 (t, *J*=7.1 Hz, 3 H); HRMS (M+H)[+] calculated for $C_{21}H_{30}ClN_2O_6$ 441.1792; found 441.1788; LC/MS (formic): R_t = 1.14 min (99%) [M+H][+] = 441.

**3-(2-(1,3-Dioxan-2-yl)ethyl)-8-chloro-1,7-naphthyridin-2(1H)-one (2.106)**
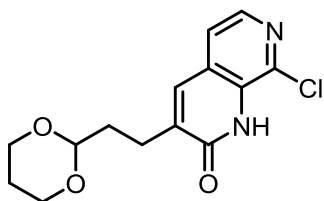
To a solution of **2.104** (705 mg, 1.60 mmol) in 1,4-dioxane (10 mL) was added 4 M HCl in 1,4-dioxane (20 mL) at rt. The resultant solution was stirred at rt for 7 hours. The resultant solution was concentrated *in vacuo.* The resultant residue was dissolved in DCM (10 mL) and washed sequentially with saturated aq. NaHCO$_3$ solution (10 mL) and brine (10 mL). The resultant solution was concentrated *in vacuo* yielding a yellow oil. The oil was dissolved in toluene (10 mL). To the solution was added DBU (4.93 mL, 32.7 mmol) and the solution stirred at 110 °C for 16 hours. A further portion of DBU (4.93 mL, 32.7 mmol) was added at rt and the resultant solution stirred at 110 °C for 6 hours before a further portion of DBU (2.50 mL, 16.6 mmol) was added and the reaction stirred at 110 °C for 18 hours. The resultant solution was diluted with washed with saturated aq. NH$_4$Cl solution (15 mL) and the organic layer separated. The aqueous layer was extracted further with EtOAc (2 × 10 mL) and concentrated *in vacuo*. The resultant residue was dissolved in minimal DCM and purified by silica chromatography (0-50% EtOAc in cyclohexane). The desired fractions were combined and concentrated *in vacuo* yielding **2.106** (434 mg, 1.473 mmol, 92%) as a white solid. m.p. 154–158 °C; v_{max} (solid)/cm^{-1}: 2930, 1648 (C=O), 1141, 826, 439; ^{1}H NMR (400 MHz, CHLOROFORM-*d*) δ ppm 8.18 (d, *J*=5.1 Hz, 1 H), 7.56 (s, 1 H), 7.36 (d, *J*=5.1 Hz, 1 H), 4.64 (t, *J*=5.0 Hz, 1 H), 4.17-4.08 (m, 2 H), 3.83-3.73 (m, 2 H), 2.86-2.77 (m, 2 H), 2.17-2.02 (m, 2 H), 2.03-1.94 (m, 2 H) (N.B. exchangeable lactam proton not visible); HRMS (M+H)$^+$ calculated for C$_{14}$H$_{16}$ClN$_2$O$_3$ 295.0849; found 295.0851; LC/MS (formic): R$_t$ = 0.71 min (97%) [M+H]$^+$ = 295.

3-(2-(1,3-Dioxan-2-yl)ethyl)-2-(benzyloxy)-8-chloro-1,7-naphthyridine (2.107)
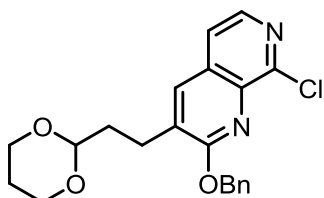
To a solution of **2.106** (0.100 mg, 0.339 mmol) in DMF (2.5 mL) was added potassium carbonate (56 mg, 0.41 mmol). The resulting suspension was stirred at rt for 15 min before being treated with benzyl bromide (0.04 mL, 0.37 mmol). The solution was then stirred at rt for 2.5 hours. The solution was diluted with water (6 mL) and EtOAc (6 mL). The organic layer was

separated, washed with saturated aq. LiCl solution (5 mL), brine (5 mL), and passed through a hydrophobic frit before being concentrated *in vacuo*. The resultant residue was purified by silica chromatography (0-50% EtOAc in cyclohexane). The desired fractions were combined and concentrated *in vacuo* yielding **2.107** (31 mg, 0.081 mmol, 24%) as a white solid. m.p. 102–104 °C; v_{max} (solid)/cm^{-1}: 2957, 2862, 1448, 1266, 1141, 695; ^{1}H NMR (400 MHz, CHLOROFORM-*d*) δ ppm 8.23 (d, *J*=5.4 Hz, 1 H), 7.80 (s, 1 H), 7.68- 7.61 (m, 2 H), 7.47 (d, *J*=5.4 Hz, 1 H), 7.44-7.38 (m, 2 H), 7.37-7.32 (m, 1 H), 5.69 (s, 2 H), 4.57 (t, *J*=5.1 Hz, 1 H), 4.18-4.09 (m, 2 H), 3.80-3.70 (m, 2 H), 2.92 (t, *J*=7.3 Hz, 2 H), 2.18-2.06 (m, 1 H), 2.05-1.99 (m, 2 H), 1.40-1.32 (m, 1 H); HRMS (M+H)$^+$ calculated for $C_{21}H_{22}ClN_2O_3$ 385.1319; found 385.1319; LC/MS (formic acid): R_t = 1.36 min (94%) [M+H]$^+$ = 385.

Methyl 2-(bis(2,2,2-trifluoroethoxy)phosphoryl)hex-5-enoate (2.110)
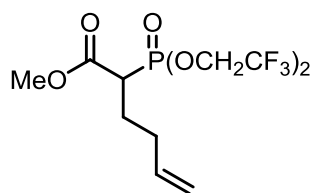
To a stirred solution of methyl 2-(bis(2,2,2-trifluoroethoxy)phosphoryl)acetate (1.33 mL, 6.29 mmol) in DMSO (10 mL) was added sodium hydride in oil 60 wt % (0.166 g, 6.92 mmol). The resultant reaction mixture was stirred at rt for 20 min before 4-bromobut-1-ene (0.83 mL, 8.2 mmol) was added dropwise at rt. The resultant solution was stirred at rt for 21 hours. A further portion of 4-bromobut-1-ene (0.32 mL, 3.1 mmol) was added and the solution stirred for 1 hour at rt. The solution was then diluted with saturated aq. NH$_4$Cl solution (50 mL) and EtOAc (50 mL). The aqueous layer was separated and extracted with EtOAc (2 × 50 mL). The combined organic fractions were passed through a hydrophobic frit and concentrated *in vacuo*. The resultant orange oil was purified by silica chromatography (0-100% EtOAc in cyclohexane). The desired fractions were combined and concentrated *in vacuo* yielding **2.110** (509 mg, 1.37 mmol, 22%) as a colourless oil. ^{1}H NMR (400 MHz, CHLOROFORM-*d*) δ ppm 5.75 (ddt, *J*=17.6, 9.8, 6.6, 6.6 Hz, 1 H), 5.11-5.08 (m, 1 H), 5.08-5.05 (m, 1 H), 4.51-4.36 (m, 4 H), 3.80 (s, 3 H), 3.23-3.13 (m, 1 H), 2.28-1.93 (m, 4 H).

**3-(But-3-en-1-yl)-8-chloro-1,7-naphthyridin-2(1H)-one (2.094)**
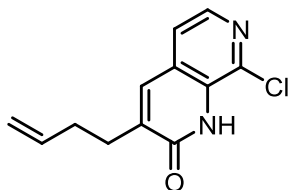
To a solution of **2.110** (509 mg, 1.37 mmol) in THF (15 mL) was added 18-crown-6 (772 mg, 2.92 mmol). The resulting solution was cooled to -78 °C and potassium bis(trimethylsilyl)amide (291 mg, 1.461 mmol) added in portions. The resultant mixture was allowed to warm to -45 °C and stirred for 1.5 hours. **2.097** (0.250 g, 0.974 mmol) in THF (2.26 mL) was then added to the solution at -78 °C and the resultant solution stirred at -78 °C for 1.5 hours. To the stirred solution at -78 °C was added saturated aq. NH₄Cl solution (15 mL) and Et₂O (15 mL) and the solution allowed to warm to rt. The layers were separated and the aqueous extracted further with Et₂O (10 mL). The organic layers were combined, washed with brine (10 mL) and passed through a hydrophobic frit before being concentrated *in vacuo*. The resultant residue was dissolved in 1,4-dioxane (10 mL). To the solution was added 4 M HCl in 1,4-dioxane (20 mL) drop-wise at rt. The resultant solution was stirred at rt for 19 hours before being concentrated *in vacuo*. The resultant residue was dissolved in minimal DCM and purified by silica chromatography (0-40% EtOAc in cyclohexane). The desired fractions were combined and concentrated *in vacuo* yielding **2.094** (91 mg, 0.39 mmol, 40%). m.p. 114–116 °C; v_{max} (solid)/cm⁻¹: 3169 (N-H), 3079, 2916, 1653 (C=O), 1470, 929; ^{1}H NMR (400 MHz, CHLOROFORM-*d*) δ ppm 9.19 (br. s, 1 H), 8.19 (d, *J*=5.1 Hz, 1 H), 7.57-7.52 (m, 1 H), 7.36 (d, *J*=5.1 Hz, 1 H), 5.87 (ddt, *J*=16.9, 10.3, 6.6, 6.6 Hz, 1 H), 5.14-5.07 (m, 1 H), 5.07-5.02 (m, 1 H), 2.86-2.75 (m, 2 H), 2.52-2.43 (m, 2 H); ^{13}C NMR (101 MHz, CHLOROFORM-*d*) δ ppm 161.5, 141.3, 141.1, 137.1, 137.0, 134.0, 129.9, 126.5, 119.9, 115.9, 31.8, 30.0; HRMS (M+H)⁺ calculated for $C_{12}H_{11}ClN_2O$ 235.0638; found 235.0633; LC/MS (formic): R_t = 0.86 min (100%) [M+H]⁺ = 235.

**Ethyl 2-(diphenoxyphosphoryl)acetate (2.114)**
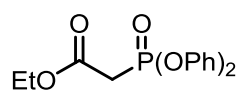
To a stirred suspension of sodium hydride in oil 60 wt % (1.025 g, 25.62 mmol) in THF (21.35 mL) was added diphenyl phosphonate (4.09 mL, 21.4 mmol) dropwise over 15 min at 0 °C. The suspension was then stirred at 0 °C for 1.5 hours. Ethyl 2-bromoacetate (2.84 mL, 25.6 mmol) was then added dropwise over 5 min at 0 °C before allowing the solution to warm to

rt and left to stir at rt for 68 hours. To the stirred suspension was added saturated aq. NH_4Cl solution (5 mL) and water (10 mL). The organic layer was separated and the aqueous extracted further with Et_2O (3 × 10 mL). The organic fractions were combined, washed with brine (10 mL), passed through a hydrophobic frit, and concentrated *in vacuo*. The resultant residue was dissolved in minimal DCM and purified by silica chromatography (0-20% EtOAc in cyclohexane). The desired fractions were combined and concentrated *in vacuo* yielding **2.114** (1.581 g, 4.936 mmol, 23%) as a colourless oil. ^{1}H NMR (400 MHz, METHANOL-d_4) δ ppm 7.44-7.36 (m, 4 H), 7.32-7.17 (m, 6 H), 4.81 (s, 2 H), 4.23 (q, *J*=7.1 Hz, 2 H), 1.27 (t, *J*=7.1 Hz, 3 H); HRMS (M+H)$^+$ calculated for $C_{16}H_{17}O_5P$ 321.0892; found 321.0887; LC/MS (formic): R_t = 1.07 min (100%) [M+H]$^+$ = 321.

Ethyl 2-(diphenoxyphosphoryl)hex-5-enoate (2.115)
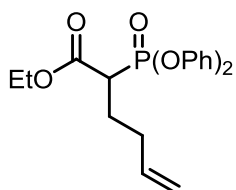
To a stirred solution of **2.114** (1.227 g, 3.831 mmol) in DMSO (5.5 mL) was added sodium hydride in oil 60 wt % (0.199 g, 4.98 mmol). The resultant reaction mixture was stirred at rt for 30 min before 4-bromobut-1-ene (0.500 mL, 4.98 mmol) was added dropwise at rt. The resultant solution was stirred at rt for 3 hours before being heated to 45 °C and stirred for 3 hours. The solution was allowed to cool to rt before being diluted with saturated aq. NH_4Cl solution (10 mL). The aqueous layer was separated and extracted with EtOAc (3 × 10 mL). The combined organic fractions were passed through a hydrophobic frit and concentrated *in vacuo*. The resultant orange oil was purified by silica chromatography (0-30% EtOAc in cyclohexane). The desired fractions were combined and concentrated *in vacuo* yielding **2.115** (869 mg, 2.32 mmol, 61%) as a colourless oil. ^{1}H NMR (400 MHz, DMSO-d_6) δ ppm 7.46-7.37 (m, 4 H), 7.27-7.22 (m, 2 H), 7.20-7.13 (m, 4 H), 5.80 (ddt, *J*=17.0, 10.4, 6.4, 6.4 Hz, 1 H), 5.08-4.99 (m, 2 H), 4.18 (q, *J*=7.3 Hz, 2 H), 3.55-3.44 (m, 1 H), 2.21-1.96 (m, 4 H), 1.18 (t, *J*=7.3 Hz, 3 H); LC/MS (formic acid): R_t = 1.30 min (100%) [M+H]$^+$ = 375.

2-(Benzyloxy)-3-(but-3-en-1-yl)-8-chloro-1,7-naphthyridine (2.117)
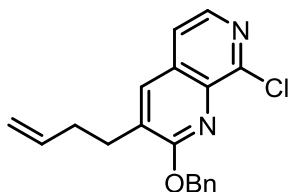
To a solution of **2.094** (1024 mg, 4.363 mmol) in DMF (10 mL) was added potassium carbonate (0.724 g, 5.24 mmol). The resulting suspension was stirred at rt for 20 min before being treated with benzyl bromide (0.57 mL, 4.8 mmol). The suspension was then stirred at rt for 2 hours. The solution was diluted with water (15 mL) and EtOAc (15 mL). The organic layer was separated, washed with saturated aq. LiCl solution (5 mL), brine (5 mL), and passed through a hydrophobic frit before being concentrated *in vacuo*. The resultant residue was purified by silica chromatography (0-30% EtOAc in cyclohexane). The desired fractions were combined and concentrated *in vacuo* yielding **2.117** (1.226 g, 3.775 mmol, 87%) as a white solid. m.p. 86–87°C; v_{max} (solid)/cm^{-1}: 2951, 1412, 1264, 698; ^{1}H NMR (400 MHz, CHLOROFORM-*d*) δ ppm 8.24 (d, *J*=5.4 Hz, 1 H), 7.78 (s, 1 H), 7.66-7.60 (m, 2 H), 7.47 (d, *J*=5.4 Hz, 1 H), 7.45-7.39 (m, 2 H), 7.38-7.32 (m, 1 H), 5.92-5.80 (m, 1 H), 5.69 (s, 2 H), 5.10-4.98 (m, 2 H), 2.91 (t, *J*=7.5 Hz, 2 H), 2.54-2.43 (m, 2 H). ^{13}C NMR (101 MHz, CHLOROFORM-*d*) δ ppm 161.6, 150.4, 140.6, 137.6, 137.1, 136.8, 135.3, 132.3, 130.7, 128.7, 128.4, 128.1, 119.4, 115.8, 68.5, 32.5, 29.8; HRMS (M+H)$^+$ calculated for $C_{19}H_{18}ClN_2O$ 325.1108; found 325.1105; LC/MS (formic acid): R_t = 1.50 min (100%) [M+H]$^+$ = 325.

tert-Butyl 4-((2-(benzyloxy)-3-(but-3-en-1-yl)-1,7-naphthyridin-8-yl)amino)piperidine-1-carboxylate (2.118)
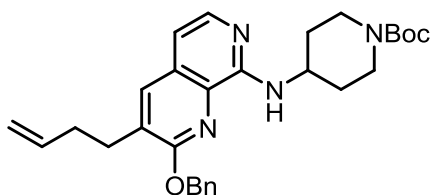
tert-Butyl 4-aminopiperidine-1-carboxylate (906 mg, 4.52 mmol) was added to a solution of **2.117** (1224 mg, 3.768 mmol), sodium *tert*-butoxide (1449 mg, 15.07 mmol), Pd$_2$(dba)$_3$ (173 mg, 0.188 mmol), 2-(dicyclohexylphosphino)3,6-dimethoxy-2′,4′,6′-triisopropyl-1,1′-biphenyl (202 mg, 0.377 mmol) in toluene (15 mL). The resulting reaction mixture was then stirred at 85 °C for 1 hour. The resultant reaction mixture was allowed to cool to rt before being diluted with EtOAc (30 mL) and filtered through Celite. The Celite was washed with EtOAc (10 mL) and the combined washings concentrated *in vacuo* producing an orange oil. The resultant oil was partitioned between DCM (30 mL) and

water (30 mL). The organic layer was separated and the aqueous layer extracted further with DCM (3 × 15 mL). The organic fractions were combined and concentrated *in vacuo* producing an orange oil. The resultant oil was dissolved in minimal DCM and purified by silica chromatography (0-60% EtOAc in cyclohexane). The desired fractions were combined and concentrated *in vacuo* yielding **2.118** (1.663 g, 3.403 mmol, 90%) as an orange oil. ^{1}H NMR (400 MHz, CHLOROFORM-*d*) δ ppm 7.90 (d, *J*=5.9 Hz, 1 H), 7.65 (s, 1 H), 7.50 (d, *J*=7.1 Hz, 2 H), 7.44-7.38 (m, 2 H), 7.37-7.31 (m, 1 H), 6.75 (d, *J*=5.9 Hz, 1 H), 6.20 (d, *J*=8.1 Hz, 1 H), 5.88 (ddt, *J*=17.1, 10.3, 6.6, 6.6 Hz, 1 H), 5.52 (s, 2 H), 5.09-4.98 (m, 2 H), 4.33-4.22 (m, 1 H), 4.16-4.00 (m, 2 H), 3.08 (br. s, 2 H), 2.88 (t, *J*=7.5 Hz, 2 H), 2.52-2.43 (m, 2 H), 2.19-2.10 (m, 2 H), 1.55-1.49 (m, 11 H); ^{13}C NMR (101 MHz, CHLOROFORM-*d*) δ ppm 159.5, 154.9, 153.9, 140.4, 137.5, 137.4, 135.8, 130.0, 129.5, 128.6, 128.0, 127.8, 127.4, 115.5, 108.1, 79.5, 68.0, 47.3, 32.8, 32.5, 29.9, 28.5, 26.9; HRMS (M+H)$^+$ calculated for $C_{29}H_{36}N_4O_3$ 489.2866; found 489.2865; LC/MS (formic acid): R_t = 1.05 min (100%) [M+H]$^+$ = 489.

tert-Butyl 4-((2-(benzyloxy)-5-bromo-3-(but-3-en-1-yl)-1,7-naphthyridin-8-yl)amino)piperidine-1-carboxylate (2.119)
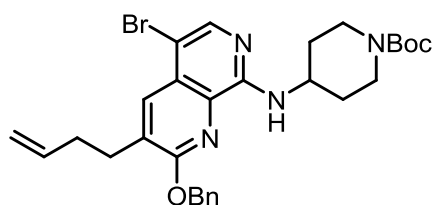
N-Bromosuccinimide (661 mg, 3.71 mmol) was added at rt to a stirred solution of **2.118** (1650 mg, 3.38 mmol) in chloroform (27 mL). The resultant solution was then stirred at rt for 15 min before being diluted with water (0.5 mL). The organic phase was then passed through a hydrophobic frit and concentrated *in vacuo* to yield **2.119** (1.833 g, 3.230 mmol, 96%) as a yellow solid. m.p. 130–135 °C; v_{max} (solid)/cm^{-1}: 3412 (N-H), 2944, 1688 (C=O), 1523, 1419, 1155, 701; ^{1}H NMR (400 MHz, CHLOROFORM-*d*) δ ppm 8.02 (s, 1 H), 7.96 (s, 1 H), 7.51-7.46 (m, 2 H), 7.44-7.38 (m, 2 H), 7.38-7.32 (m, 1 H), 6.18 (d, *J*=8.1 Hz, 1 H), 5.95-5.83 (m, 1 H), 5.53 (s, 2 H), 5.11-5.01 (m, 2 H), 4.27-4.17 (m, 1 H), 4.15-4.01 (m, 2 H), 3.12-3.01 (m, 2 H), 2.92 (t, *J*=7.6 Hz, 2 H), 2.54-2.46 (m, 2 H), 2.17-2.08 (m, 2 H), 1.56-1.48 (m, 11 H); ^{13}C NMR (101 MHz, CHLOROFORM-*d*) δ ppm 160.0, 154.8, 153.2, 141.3, 137.3, 137.1, 135.4, 131.1, 130.1, 128.6, 127.9, 127.4, 127.2, 115.7, 103.3, 79.5, 68.4, 47.5, 32.8, 32.3, 29.9, 28.5 (N.B. one carbon signal missing); HRMS (M+H)$^+$ calculated for

$C_{29}H_{35}BrN_4O_3$ 567.1971; found 567.1973; LC/MS (formic): R_t = 1.59 min (96%) $[M+H]^+$ = 567.

tert-Butyl 4-((2-(benzyloxy)-3-(but-3-en-1-yl)-5-(3,6-dihydro-2H-pyran-4-yl)-1,7-naphthyridin-8-yl)amino)piperidine-1-carboxylate (2.120)
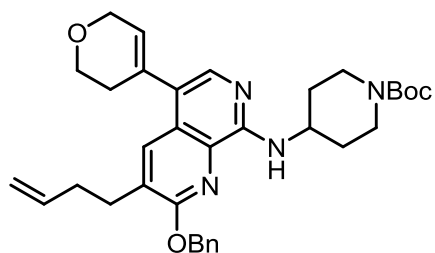

2-(3,6-Dihydro-2H-pyran-4-yl)-4,4,5,5-tetramethyl-1,3,2-dioxaborolane (256 mg, 1.22 mmol) was added at rt to a stirred mixture of **2.119** (541 mg, 0.953 mmol), potassium carbonate (263 mg, 1.91 mmol), Pd(OAc)$_2$ (11 mg, 0.048 mmol) and butyldi-1-adamantylphosphine (17 mg, 0.048 mmol) in 1,4-dioxane (5.5 mL) and water (2.75 mL). The resultant reaction mixture was then heated at 100 °C for 45 min in a microwave reactor. The reaction mixture was allowed to cool to rt before being diluted with EtOAc (10 mL) and passed through Celite. The resultant solution was concentrated *in vacuo*. The resultant residue was dissolved in EtOAc (20 mL) and washed with water (20 mL). The layers were separated and the aqueous layer extracted further with EtOAc (20 mL). The organic layers were combined, washed with brine (15 mL), passed through a hydrophobic frit and concentrated *in vacuo*. The resultant residue was dissolved in minimal DCM and purified by MDAP (high pH). The desired fractions were combined and concentrated *in vacuo* yielding **2.120** (354 mg, 0.620 mmol, 65%) as a pale-yellow solid. m.p. 84–87 °C; v_{max} (solid)/cm^{-1}: 3412 (N-H), 2926, 1687 (C=O), 1519, 1418, 1153; ^{1}H NMR (400 MHz, DMSO-d_6) δ ppm 7.92 (s, 1 H), 7.68 (s, 1 H), 7.54 (d, *J*=7.1 Hz, 2 H), 7.42-7.36 (m, 2 H), 7.35-7.28 (m, 1 H), 6.64 (d, *J*=8.3 Hz, 1 H), 5.85 (ddt, *J*=17.0, 10.3, 6.5, 6.5 Hz, 1 H), 5.78-5.74 (m, 1 H), 5.61 (s, 2 H), 5.03-4.93 (m, 2 H), 4.29-4.15 (m, 3 H), 4.02-3.91 (m, 2 H), 3.87 (t, *J*=5.4 Hz, 2 H), 3.04-2.88 (m, 2 H), 2.84 (t, *J*=7.5 Hz, 2 H), 2.44-2.32 (m, 4 H), 1.97-1.87 (m, 2 H), 1.60-1.47 (m, 2 H), 1.43 (s, 9 H); ^{13}C NMR (101 MHz, DMSO-d_6) δ ppm 159.2, 154.3, 153.2, 138.6, 138.2, 138.1, 134.6, 131.9, 129.6, 128.8, 128.2, 128.1, 126.5, 126.1, 121.7, 116.0, 79.0, 68.1, 65.4, 64.2, 55.4, 47.4, 32.9, 32.1, 30.6, 29.5, 28.6 (N.B. one sp^2 carbon signal missing); HRMS (M+H)$^+$ calculated for $C_{34}H_{43}N_4O_4$ 571.3284; found 571.3287; LC/MS (formic): R_t = 1.11 min (100%) $[M+H]^+$ = 571.

3-(But-3-en-1-yl)-5-(3,6-dihydro-2H-pyran-4-yl)-8-(piperidin-4-ylamino)-1,7-naphthyridin-2(1H)-one (2.121)
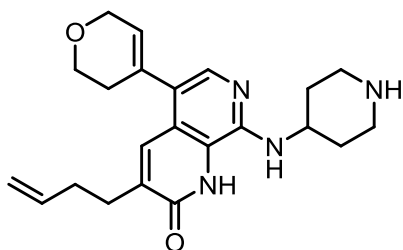
2.120 (931 mg, 1.63 mmol) was dissolved in TFA (10 mL) at rt. The resultant solution was then heated to reflux and stirred for 1 hour before being allowed to cool down to rt. Volatile components were then removed *in vacuo*. Toluene was added to the resulting residue and evaporated off *in vacuo* (3 × 10 mL). The resultant residue was dissolved in minimal MeOH and passed through a preconditioned aminopropyl column (25 mL) and washed with MeOH (50 mL). The desired fractions were combined and concentrated *in vacuo.* The resultant residue was dissolved in 1:1 MeOH:DCM and purified by MDAP (high pH). The desired fractions were combined and concentrated *in vacuo* yielding **2.121** (219 mg, 0.576 mmol, 35%) as a yellow solid. m.p. 207–210 °C; v_{max} (solid)/cm^{-1}: 3390 (N-H), 2921, 1653 (C=O), 1592, 1440, 1127, 903; ^{1}H NMR (400 MHz, DMSO-d_6) δ ppm 7.63 (s, 1 H), 7.60 (s, 1 H), 6.69 (d, *J*=6.8 Hz, 1 H), 5.84 (ddt, *J*=17.0, 10.4, 6.5, 6.5 Hz, 1 H), 5.74-5.68 (m, 1 H), 5.08-4.94 (m, 2 H), 4.23 (d, *J*=2.5 Hz, 2 H), 4.08-3.94 (m, 1 H), 3.85 (t, *J*=5.3 Hz, 2 H), 3.06-2.87 (m, 2 H), 2.63 (t, *J*=7.4 Hz, 2 H), 2.38-2.25 (m, 4 H), 2.00-1.81 (m, 2 H), 1.41-1.23(m, 2 H) (N.B. one signal obscured by solvent peak, exchangeable lactam and amine protons not visible); ^{13}C NMR (101 MHz, DMSO-d_6) δ ppm 162.1, 145.5, 138.4, 137.6, 136.9, 133.6, 131.6, 127.1, 122.6, 121.2, 120.9, 115.8, 65.3, 64.1, 48.7, 45.5, 33.6, 32.2, 30.8, 29.7; HRMS (M+H)$^+$ calculated for $C_{22}H_{29}N_4O_2$ 381.2291; found 381.2296; LC/MS (high pH): R_t = 0.96 min (100%) [M+H]$^+$ = 381.

8-((1-(3-Amino-2,2-difluoropropanoyl)piperidin-4-yl)amino)-3-(but-3-en-1-yl)-5-(3,6-dihydro-2H-pyran-4-yl)-1,7-naphthyridin-2(1H)-one (2.093)
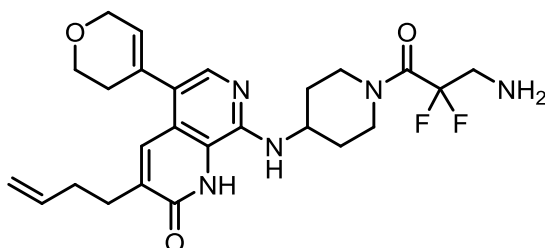
HATU (300 mg, 0.788 mmol) and DIPEA (0.229 mL, 1.31 mmol) were added at rt to a stirred solution of **2.063** (118 mg, 0.526 mmol) in DMF (2 mL). After 15 minutes **2.121** (0.100 g, 0.263 mmol)

was added at rt to the stirred solution and the reaction mixture stirred for 5 hours. The reaction mixture was then diluted with water (10 mL) and extracted with EtOAc (4 × 10 mL). The combined organic fractions were washed with brine (10 mL) and passed through a hydrophobic frit. The resultant solution was then concentrated *in vacuo*. The resultant solid was dissolved in 1:1 MeOH:DMSO and purified by MDAP (formic). The desired fractions were combined and concentrated *in vacuo* yielding a cream solid. The solid was dissolved in 4 M HCl in 1,4-dioxane (4 mL) at rt. The resultant solution was stirred at rt for 30 min before being filtered under reduced pressure. The filtrate was concentrated *in vacuo* and the resulting residue dissolved in 1:1 MeOH:DMSO and purified by MDAP (high pH). The desired fractions were combined and concentrated *in vacuo* yielding **2.093** (7 mg, 0.02 mmol, 5%) as a yellow solid. ^{1}H NMR (400 MHz, DMSO-d_6, 393 K) δ ppm 7.71-7.60 (m, 2 H), 6.58-6.47 (m, 1 H), 5.88 (ddt, *J*=16.9, 10.3, 6.6, 6.6 Hz, 1 H), 5.80-5.71 (m, 1 H), 5.14-4.95 (m, 2 H), 4.42-4.31 (m, 1 H), 4.31-4.25 (m, 2 H), 4.23-4.12 (m, 2 H), 3.95-3.86 (m, 2 H), 3.40-3.13 (m, 4 H), 2.75-2.65 (m, 2 H), 2.46-2.31 (m, 4 H), 2.19-2.07(m, 2 H), 1.66-1.51 (m, 2 H) (N.B. exchangeable lactam and primary amine protons not visible); ^{13}C NMR (151 MHz, DMSO-d_6) δ ppm 162.0, 161.4, 145.2, 138.4, 137.6, 137.3, 133.6, 131.5, 127.4, 123.2, 121.3, 120.8, 118.4, 115.9, 65.3, 64.1, 47.4, 45.7, 44.4, 42.0, 40.6, 32.2, 30.8, 29.6; ^{19}F NMR (376 MHz, DMSO-d_6) δ ppm -105.58 - -105.41 (m, 2 F); HRMS (M+H)$^+$ calculated for $C_{25}H_{32}F_2N_5O_3$ 488.2473; found 488.2473; LC/MS (high pH): R_t = 0.96 min (97%) [M+H]$^+$ = 488.

4,5-Dichloro-2-methylpyridazin-3(2H)-one (3.027)
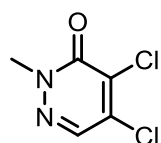
Methyl iodide (0.627 mL, 10.0 mmol) was added to a stirred mixture of tetrabutylammonium bromide (4.410 g, 13.67 mmol), 4,5-dichloropyridazin-3(2H)-one (1.504 g, 9.117 mmol) and potassium carbonate (2.520 g, 18.23 mmol) in MeCN (30 mL) at rt. The resultant mixture was heated to 80 °C for 3 hours before being allowed to cool to rt. The resultant mixture was filtered under reduced pressure and the filtrate concentrated *in vacuo*. The resultant solid was dissolved in EtOAc (50 mL) and washed with 2 M aq. HCl solution (30 mL). MeOH was added dropwise to dissolve the white precipitate. The organic layer was then washed with brine (30 mL), passed through a hydrophobic frit and concentrated *in vacuo*. The resultant solid was dissolved in minimal DCM and a white

precipitate filtered under reduced pressure. The resulting filtrate was concentrated *in vacuo* before being dissolved in minimal DCM and purified by silica chromatography (0-50% EtOAc in cyclohexane). The desired fractions were concentrated *in vacuo* yielding **3.027** (1.234 g, 6.894 mmol, 76%) as a white solid. m.p. 89–90 °C; v_{max} (solid)/cm^{-1}: 3047, 1635 (C=O), 1580, 1231, 714, 628; ^{1}H NMR (400 MHz, CHLOROFORM-*d*) δ ppm 7.78 (s, 1 H), 3.84 (s, 3 H); ^{13}C NMR (101 MHz, CHLOROFORM-*d*) δ ppm 156.8, 136.5, 135.3, 134.0, 41.0; HRMS (M+H)$^+$ calculated for $C_5H_5Cl_2N_2O$ 178.9779; found 178.9774; LC/MS (formic): R_t = 0.65 min (100%) [M+H]$^+$ = 179.

4-Chloro-2-methyl-5-((2-(4-methylpiperazin-1-yl)benzyl)amino)pyridazin-3(2H)-one (3.028) and 5-chloro-2-methyl-4-((2-(4-methylpiperazin-1-yl)benzyl)amino)pyridazin-3(2H)-one (3.029)
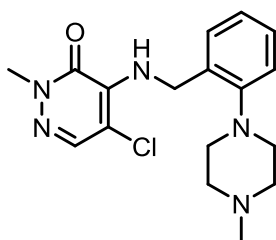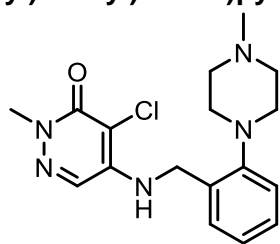
DIPEA (0.742 mL, 4.25 mmol) was added to a stirred solution of **3.027** (507 mg, 2.83 mmol) and (2-(4-methylpiperazin-1-yl)phenyl)methanamine (0.655 mL, 3.40 mmol) in DMSO (12 mL) at rt. The resultant solution was heated to 120 °C and stirred for 1 hour in a microwave reactor. The resultant solution was diluted with saturated aq. NH$_4$Cl solution (15 mL) and EtOAc (15 mL) and the layers separated. The aqueous layer was then extracted further with EtOAc (15 mL). The organic fractions were combined, washed with brine, passed through a hydrophobic frit and concentrated *in vacuo*. The resultant solid was dissolved in 1:1 MeOH:DMSO and purified by MDAP (high pH). The desired fractions were combined yielding **3.028** (616 mg, 1.77 mmol, 63%) as a cream solid. m.p. 109–111 °C; v_{max} (solid)/cm^{-1}: 3342 (N-H), 2939, 2801, 1606 (C=O), 1451; ^{1}H NMR (400 MHz, METHANOL-*d$_4$*) δ ppm 7.65 (s, 1 H), 7.39-7.35 (m, 1 H), 7.34-7.30 (m, 1 H), 7.29-7.23 (m, 1 H), 7.17 (td, *J*=7.6, 1.1 Hz, 1 H), 4.67 (s, 2 H), 3.67 (s, 3 H), 3.24-3.10 (m, 8 H), 2.77 (s, 3 H) (N.B. exchangeable amine proton not visible); ^{13}C NMR (101 MHz, METHANOL-*d$_4$*) δ ppm 160.0, 151.2, 146.8, 134.6, 130.0, 129.8, 128.6, 126.7, 121.7, 107.5, 56.0, 52.3, 44.9, 42.9, 40.7; HRMS (M+H)$^+$ calculated for $C_{17}H_{23}ClN_5O$ 348.1591; found 348.1590;

LC/MS (high pH): R_t = 0.87 min (100%) $[M+H]^+$ = 348; and **3.029** (348 mg, 1.000 mmol, 35%) as an orange solid; m.p. 97–99 °C; v_{max} (solid)/cm^{-1}: 3335 (N-H), 1615 (C=O), 1200, 720; ^{1}H NMR (600 MHz, METHANOL-d_4) δ ppm 8.40 (s, 1 H), 8.13 (t, J=6.8 Hz, 1 H), 8.10-8.06 (m, 1 H), 8.02-7.97 (m, 2 H), 7.95-7.90 (m, 1 H), 5.74 (d, J=6.8 Hz, 2 H), 4.43 (s, 3 H), 3.99 (br. s, 4 H), 3.87-3.78 (m, 4 H), 3.54 (s, 3 H); HRMS $(M+H)^+$ calculated for $C_{17}H_{23}ClN_5O$ 348.1591; found 348.1603; LC/MS (high pH): R_t = 1.08 min (100%) $[M+H]^+$ = 348.

4-Allyl-2-methyl-5-((2-(4-methylpiperazin-1-yl)benzyl)amino)pyridazin-3(2H)-one (3.023)
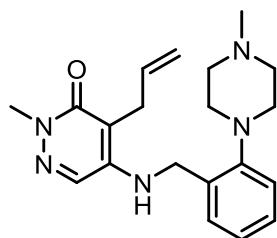
The solvent system was sparged with nitrogen for 30 min prior to use. 2-Allyl-4,4,5,5-tetramethyl-1,3,2-dioxaborolane (0.05 mL, 0.3 mmol) was added to a stirred solution of **3.028** (0.050 g, 0.14 mmol), potassium carbonate (0.050 g, 0.36 mmol) and RuPhos-Pd-G2 (17 mg, 0.022 mmol) in 1,4-dioxane (2 mL) and water (1 mL) under nitrogen at rt. The resultant mixture was heated to 100 °C and stirred for 1 hour. The resultant solution was diluted with EtOAc and filtered through Celite before being concentrated *in vacuo*. The resultant residue was dissolved in EtOAc (10 mL) and washed with water (10 mL). The organic layer was passed through a hydrophobic frit and concentrated *in vacuo*. The resultant residue was dissolved in 1:1 MeOH:DMSO and purified by MDAP (high pH: extended). The desired fractions were combined and concentrated *in vacuo* yielding **3.023** (14 mg, 0.040 mmol, 28%) as a colourless oil. ^{1}H NMR (400 MHz, METHANOL-d_4) δ ppm 7.59 (s, 1 H), 7.34-7.30 (m, 1 H), 7.26 (td, J=7.6, 1.2 Hz, 1 H), 7.20 (dd, J=7.6, 1.2 Hz, 1 H), 7.08 (td, J=7.6, 1.2 Hz, 1 H), 5.87 (ddt, J=17.1, 10.3, 5.7 Hz, 1 H), 5.11-5.01 (m, 2 H), 4.56 (s, 2 H), 3.63 (s, 3 H), 3.00 (t, J=4.8 Hz, 4 H), 2.70 (app. br. s, 4 H), 2.40 (s, 3 H) (N.B. exchangeable amine proton not visible and CH$_2$ allyl proton signal obscured by MeOH solvent peak); ^{13}C NMR (101 MHz, METHANOL-d_4) δ ppm 161.7, 150.5, 146.1, 133.3, 132.9, 128.3, 128.1, 128.0, 124.1, 119.5, 114.4, 109.1, 55.1, 52.1, 44.8, 40.9, 38.9, 26.6; HRMS $(M+H)^+$ calculated for $C_{20}H_{28}N_5O$ 354.2294; found 354.2299; LC/MS (high pH): R_t = 0.90 min (100%) $[M+H]^+$ = 354.

(*E*)-4-(But-1-en-1-yl)-2-methyl-5-((2-(4-methylpiperazin-1-yl)benzyl)amino) pyridazin-3(2H)-one (3.025)
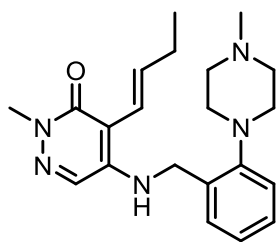
The solvent system was sparged with nitrogen for 20 min prior to use. (*E*)-But-1-en-1-ylboronic acid (15 mg, 0.15 mmol), **3.028** (24 mg, 0.069 mmol), potassium carbonate (24 mg, 0.17 mmol), Pd(OAc)$_2$ (2 mg, 0.01 mmol) and butyldi-1-adamantylphosphine (4 mg, 0.01 mmol) were dissolved in 1,4-dioxane (2 mL) and water (1 mL) under nitrogen at rt. The resultant mixture was heated to 100 °C and stirred for 1 hour in a microwave reactor. A further portion of (*E*)-but-1-en-1-ylboronic acid (15 mg, 0.15 mmol), potassium carbonate (24 mg, 0.17 mmol), Pd(OAc)$_2$ (2 mg, 0.01 mmol) and butyldi-1-adamantylphosphine (4 mg, 0.01 mmol) were added under nitrogen and the reaction stirred at 100 °C for 2 hours in a microwave reactor. A further portion of (*E*)-but-1-en-1-ylboronic acid (15 mg, 0.15 mmol), potassium carbonate (24 mg, 0.17 mmol), Pd(OAc)$_2$ (2 mg, 0.01 mmol) and butyldi-1-adamantylphosphine (4 mg, 0.01 mmol) were added under nitrogen and the reaction stirred at 100 °C for 2 hours. The solution was allowed to cool to rt before being diluted with EtOAc (10 mL), filtered through Celite, and concentrated *in vacuo*. The resultant residue was dissolved in EtOAc (5 mL) and washed sequentially with water (5 mL) and brine (5 mL) before being passed through a hydrophobic frit and concentrated *in vacuo*. The resultant residue was dissolved in 1:1 MeOH:DMSO and purified by MDAP (high pH). the desired fractions were combined yielding **3.025** (12 mg, 0.033 mmol, 47%) as a colourless oil. ^{1}H NMR (400 MHz, METHANOL-d_4) δ ppm 7.60 (s, 1 H), 7.34 (dd, *J*=7.6, 1.2 Hz, 1 H), 7.31-7.25 (m, 1 H), 7.24-7.19 (m, 1 H), 7.10 (td, *J*=7.6, 1.2 Hz, 1 H), 6.77 (dt, *J*=16.0, 6.6 Hz, 1 H), 6.30 (dt, *J*=16.0, 1.7 Hz, 1 H), 4.57 (s, 2 H), 3.63 (s, 3 H), 3.00 (t, *J*=4.8 Hz, 4 H), 2.70 (app. br. s, 4 H), 2.39 (s, 3 H), 2.36-2.27 (m, 2 H), 1.14 (t, *J*=7.5 Hz, 3 H) (N.B. exchangeable amine proton not visible); ^{13}C NMR (101 MHz, METHANOL-d_4) δ ppm 160.8, 150.6, 144.6, 139.3, 133.2, 128.4, 128.2, 128.1, 124.3, 119.7, 118.1, 108.5, 55.2, 52.1, 44.8, 41.6, 38.8, 27.0, 12.6; HRMS (M+H)$^+$ calculated for $C_{21}H_{30}N_5O$ 368.2450; found 368.2461; LC/MS (high pH): R_t = 1.01 min (98%) [M+H]$^+$ = 368.

(*E*)-4-(But-2-en-1-yl)-2-methyl-5-((2-(4-methylpiperazin-1-yl)benzyl)amino)pyridazin-3(2H)-one (3.024), (*Z*)-4-(But-2-en-1-yl)-2-methyl-5-((2-(4-methylpiperazin-1-yl)benzyl)amino)pyridazin-3(2H)-one (3.030), (*R*)-4-(But-3-en-2-yl)-2-methyl-5-((2-(4-methylpiperazin-1-yl)benzyl)amino)pyridazin-3(2H)-one (3.031) and (*S*)-4-(But-3-en-2-yl)-2-methyl-5-((2-(4-methylpiperazin-1-yl)benzyl)amino)pyridazin-3(2H)-one (3.032)
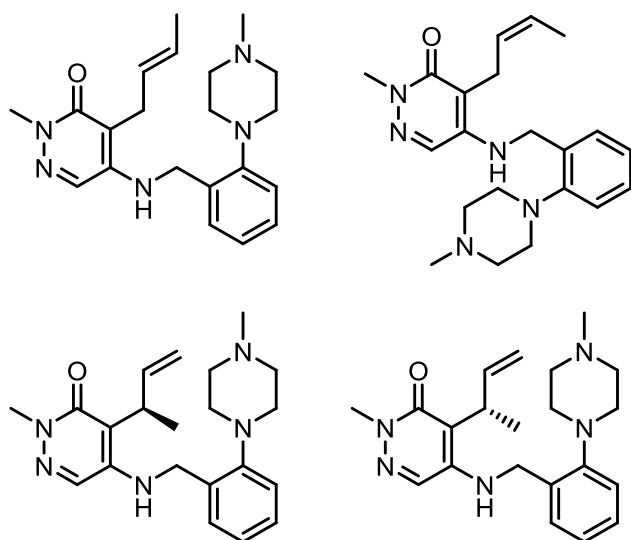
The solvent system was sparged with nitrogen for 2 hours prior to use. (*E*)-2-(But-2-en-1-yl)-4,4,5,5-tetramethyl-1,3,2-dioxaborolane (0.34 mL, 1.7 mmol) was added to a stirred solution of **3.028** (290 mg, 0.834 mmol), potassium carbonate (288 mg, 2.08 mmol), Pd(OAc)$_2$ (37 mg, 0.17 mmol) and butyldi-1-adamantylphosphine (0.060 g, 0.17 mmol) in 1,4-dioxane (1 mL) and water (0.5 mL) under nitrogen at rt. The resultant mixture was heated to 100 °C and stirred for 1.5 hours in a microwave reactor. The resultant solution was diluted with EtOAc (3 mL) and passed through Celite before being concentrated *in vacuo*. The resultant residue was dissolved in EtOAc (3 mL) and washed with water (3 mL) before being concentrated *in vacuo*, dissolved in 1:1 MeOH:DMSO and purified by MDAP (high pH). The desired fractions were combined and concentrated *in vacuo* yielding a mixture of 4-(but-3-en-2-yl)-2-methyl-5-((2-(4-methylpiperazin-1-yl)benzyl)amino)pyridazin-3(2H)-one, **3.024** and **3.030** as a combined off-white gum. The gum was dissolved in EtOH (4.5 mL) and purified *via* chiral chromatography (Chiralpak AD-H column, 10% EtOH (+0.2% isopropylamine)/heptane (+0.2% isopropylamine)). The desired fractions were combined and concentrated *in vacuo* yielding the following four products.

3.024 (26 mg, 0.071 mmol, 8%) as a colourless oil. ^{1}H NMR (700 MHz, METHANOL-d_4) δ ppm 7.58 (s, 1 H), 7.29 (dd, *J*=7.7, 1.2 Hz, 1 H), 7.27-7.23 (m, 1 H), 7.19 (dd, *J*=8.0, 1.0 Hz, 1 H), 7.07 (td, *J*=7.4, 1.1 Hz, 1 H), 5.49 (dqt, *J*=15.3, 6.2, 1.2 Hz, 1 H), 5.44 (dtq, *J*=15.3, 5.5, 1.1 Hz, 1 H), 4.54 (s, 2 H), 3.62 (s, 3 H), 3.23-3.20 (m, 2 H),

2.99 (t, J=4.8 Hz, 4 H), 2.69 (app. br. s, 4 H), 2.38 (s, 3 H), 1.64 (dd, J=6.0, 1.2 Hz, 3 H); ^{13}C NMR (101 MHz, METHANOL-d_4) δ ppm 161.8, 150.6, 145.9, 133.3, 128.4, 128.1, 128.0, 125.6, 125.3, 124.1, 119.6, 110.1, 55.1, 52.1, 44.8, 40.9, 38.9, 25.4, 16.6; HRMS (M+H)$^+$ calculated for $C_{21}H_{30}N_5O$ 368.2450; found 368.2447; LC/MS (high pH): R_t = 0.96 min (100%) [M+H]$^+$ = 368.

3.030 (15 mg, 0.041 mmol, 5%) as a colourless oil. ^{1}H NMR (400 MHz, METHANOL-d_4) δ ppm 7.61 (s, 1 H), 7.37-7.24 (m, 2 H), 7.24-7.19 (m, 1 H), 7.13-7.07 (m, 1 H), 5.59 (dqt, J=10.5, 6.8, 2.0 Hz, 1 H), 5.34 (dtq, J=10.5, 6.8, 1.8 Hz, 1 H), 4.57 (s, 2 H), 3.64 (s, 3 H), 3.04-2.96 (m, 4 H), 2.70 (app. br. s, 4 H), 2.40 (s, 3 H), 1.77-1.73 (m, 3 H); ^{13}C NMR (101 MHz, METHANOL-d_4) δ ppm 161.7, 150.6, 145.8, 133.2, 128.4, 128.2, 128.1, 125.8, 125.3, 124.7, 119.6, 111.1, 55.1, 52.1, 44.7, 41.2, 38.9, 20.7, 11.9; HRMS (M+H)$^+$ calculated for $C_{21}H_{30}N_5O$ 368.2450; found 368.2444; LC/MS (high pH): R_t = 0.97 min (100%) [M+H]$^+$ = 368.

3.031 (27 mg, 0.073 mmol, 9%) as a colourless oil. $[\alpha_D]^{23}$ (c = 10 mg/mL, MeOH): +21°;^{1}H NMR (400 MHz, METHANOL-d_4) δ ppm 7.59 (s, 1 H), 7.35-7.24 (m, 2 H), 7.23-7.18 (m, 1 H), 7.10 (td, J=7.6, 1.2 Hz, 1 H), 6.18 (ddd, J=17.4, 10.5, 5.1 Hz, 1 H), 5.17 (dt, J=17.4, 1.8 Hz, 1 H), 5.13 (dt, J=10.5, 1.8 Hz, 1 H) 4.59-4.49 (m, 2 H), 4.05-3.97 (m, 1 H), 3.62 (s, 3 H), 3.05-2.95 (m, 4 H), 2.80-2.63 (m, 4 H), 2.40 (s, 3 H), 1.38 (d, J=7.3 Hz, 3 H); ^{13}C NMR (101 MHz, METHANOL-d_4) δ ppm 161.3, 150.5, 145.4, 139.8, 133.2, 128.7, 128.2, 128.1, 124.2, 119.6, 113.8, 113.4, 55.1, 52.2, 44.7, 41.0, 38.9, 32.6, 14.1; HRMS (M+H)$^+$ calculated for $C_{21}H_{30}N_5O$ 368.2450; found 368.2444; LC/MS (high pH): R_t = 0.98 min (100%) [M+H]$^+$ = 368; HPLC (Chiralpak AD-H column, 4.6 mm × 25 cm, 10% EtOH(+0.2% isopropylamine)/heptane, 1 mL/min): 10.5 min (major enantiomer) 11.6 (minor enantiomer) 97% ee.

3.032 (23 mg, 0.063 mmol, 8%) as a colourless oil. $[\alpha_D]^{23}$ (c = 10 mg/mL, MeOH): -21°; ^{1}H NMR (400 MHz, METHANOL-d_4) δ ppm 7.59 (s, 1 H), 7.35-7.24 (m, 2 H), 7.23-7.18 (m, 1 H), 7.10 (td, J=7.6, 1.2 Hz, 1 H), 6.18 (ddd, J=17.4, 10.5, 5.1 Hz, 1 H), 5.17 (dt, J=17.4, 1.8 Hz, 1 H), 5.13 (dt, J=10.5, 1.8 Hz, 1 H) 4.59-4.49 (m, 2 H), 4.05-3.97 (m, 1 H), 3.62 (s, 3 H), 3.05-2.95 (m, 4 H), 2.80-2.63 (m, 4 H), 2.40 (s, 3 H), 1.38 (d, J=7.3 Hz, 3 H); ^{13}C NMR (101 MHz, METHANOL-d_4) δ ppm 161.3, 150.5, 145.4, 139.8, 133.2, 128.7, 128.2, 128.1, 124.2, 119.6, 113.8, 113.4, 55.1, 52.2, 44.7, 41.0, 38.9, 32.6, 14.1; HRMS (M+H)$^+$ calculated for $C_{21}H_{30}N_5O$ 368.2450; found 368.2444; LC/MS (high pH): R_t = 0.98 min (100%) [M+H]$^+$ = 368; HPLC (Chiralpak

AD-H column, 4.6 mm × 25 cm, 10% EtOH(+0.2% isopropylamine)/heptane, 1 mL/min): 11.3 (major enantiomer), 10.4 (minor enantiomer) 95% ee.

5-Chloro-4-methylpyridazin-3(2H)-one (3.033)
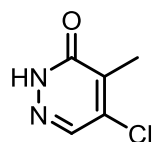
3.4 M Methylmagnesium bromide in THF solution (13.37 mL, 45.56 mmol) was added dropwise to a stirred suspension of 4,5-dichloropyridazin-3(2H)-one (2.500 g, 15.15 mmol) in THF (50 mL) at 0 °C under nitrogen. The resultant solution was stirred at 0 °C for 10 min before being allowed to warm to rt and stirred for 5.5 hours. Saturated aq. NH_4Cl solution (25 mL) was added dropwise. The reaction mixture was diluted with 2 M aq. HCl solution (25 mL) and extracted with EtOAc (25 mL). The aqueous layer was extracted further with EtOAc (25 mL). The organic fractions were combined, washed with brine (25 mL), passed through a hydrophobic frit and concentrated *in vacuo*. The resulting solid was triturated and then sonicated in diethyl ether (75 mL). The solid was removed under reduced pressure and washed with Et_2O. The filtrate was concentrated *in vacuo* yielding **3.033** (1.785 g, 12.35 mmol, 81%) as a yellow solid. m.p. 124–126 °C; v_{max} (solid)/cm^{-1}: 2873, 1634 (C=O), 1376, 1177, 1024, 884, 564; ^{1}H NMR (400 MHz, METHANOL-d_4) δ ppm 7.88 (s, 1 H), 2.24 (s, 3 H); ^{13}C NMR (101 MHz, METHANOL-d_4) δ ppm 161.9, 137.6, 137.5, 136.9, 11.4; HRMS (M+H)$^+$ calculated for $C_5H_6ClN_2O$ 145.0169; found 145.0168; LC/MS (formic): R_t = 0.53 min (98%) [M+H]$^+$ = 145.

5-Chloro-2,4-dimethylpyridazin-3(2H)-one (3.034)
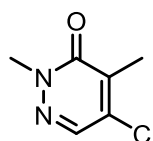
Methyl iodide (1.135 mL, 18.16 mmol) was added to a stirred mixture of tetrabutylammonium bromide (6.63 g, 20.6 mmol), **3.033** (1.750 g, 12.11 mmol) and potassium carbonate (3.35 g, 24.2 mmol) in MeCN (20 mL) at rt under nitrogen. The reaction mixture was stirred for 3 hours at rt before being heated to 60 °C and stirred for 1 hour. The resultant mixture was allowed to cool to rt before being filtered under reduced pressure and the filtrate concentrated *in vacuo*. The resultant solid was dissolved in EtOAc (60 mL) and washed with 2 M aq. HCl solution (40 mL). MeOH was added dropwise to dissolve a white precipitate. The organic layer was then washed with brine (40 mL), passed through a hydrophobic frit, and concentrated *in vacuo*. The resultant solid was dissolved in minimal DCM and

purified by silica chromatography (0-50% EtOAc in cyclohexane). The desired fractions were concentrated *in vacuo* yielding **3.034** (1.062 g, 6.697 mmol, 55%) as a white solid. m.p. 73–74 °C; v_{max} (solid)/cm^{-1}: 3032, 1634 (C=O), 1591, 1016, 887, 501; ^{1}H NMR (400 MHz, METHANOL-d_4) δ ppm 7.89 (s, 1 H), 3.76 (s, 3 H), 2.26 (s, 3 H); ^{13}C NMR (101 MHz, METHANOL-d_4) δ ppm 160.7, 136.6, 136.0, 135.9, 39.4, 12.0; HRMS (M+H)$^+$ calculated for $C_6H_8ClN_2O$ 159.0325; found 159.0325; LC/MS (TFA): R_t = 0.63 min (100%) [M+H]$^+$ = 159.

4-(But-3-en-1-yl)-5-chloro-2-methylpyridazin-3(2H)-one (3.035)
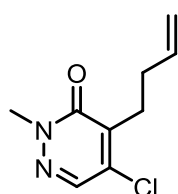
3.034 (0.500 g, 3.15 mmol) was dissolved in THF (10 mL) at rt under nitrogen. The solution was cooled to -78 °C before 1 M LiHMDS in THF solution (4.73 mL, 4.73 mmol) and 3-bromoprop-1-ene (0.355 mL, 4.10 mmol) were added under nitrogen. The resultant solution was stirred at -78 °C under nitrogen for 45 min before being diluted with MeOH (5 mL), allowed to warm to rt, and concentrated *in vacuo*. The resultant residue was dissolved in EtOAc (10 mL) and washed with water. The aqueous layer was separated and extracted further with EtOAc (2 × 10 mL). The organic layers were combined, washed with brine (15 mL), passed through a hydrophobic frit before being concentrated *in vacuo*. The resultant residue was dissolved in minimal DCM and purified by silica chromatography (0-50% EtOAc in cyclohexane). The desired fractions were combined yielding **3.035** (0.150 g, 0.755 mmol, 24%) as a colourless oil. ^{1}H NMR (400 MHz, METHANOL-d_4) δ ppm 7.89 (s, 1 H), 5.89 (ddt, J=17.0, 10.2, 6.8 Hz, 1 H), 5.04 (app. dq, J=17.1, 1.8 Hz, 1 H), 4.98 (ddt, J=10.1, 1.8, 1.1 Hz, 1 H), 3.75 (s, 3 H), 2.84 (t, J=7.3 Hz, 2 H), 2.39-2.30 (m, 2 H); ^{13}C NMR (101 MHz, METHANOL-d_4) δ ppm 160.3, 138.9, 136.7, 136.6, 114.7, 39.4, 30.5, 26.7 (N.B. one carbon signal missing, 136.7 broad and intense possible overlap of two signals); LC/MS (formic): R_t = 0.96 min (91%) [M+H]$^+$ = 199.

4-(But-3-en-1-yl)-2-methyl-5-((2-(4-methylpiperazin-1-yl)benzyl)amino)pyridazin-3(2H)-one (3.026)
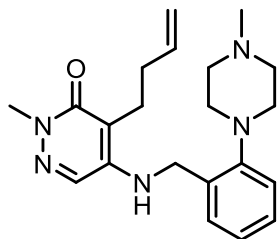
(2-(4-Methylpiperazin-1-yl)phenyl)methanamine (0.169 mL, 0.876 mmol), **3.035** (145 mg, 0.730 mmol), sodium *tert*-butoxide (0.140 g, 1.46 mmol), $Pd_2(dba)_3$ (54 mg, 0.073 mmol) and 2-(dicyclohexylphosphino)3,6-dimethoxy-2′,4′,6′-triisopropyl-1,1′-biphenyl (78 mg, 0.15 mmol) were dissolved in THF (0.5 mL). The resultant solution was stirred at 100 °C for 1 hour in a microwave reactor. The reaction was allowed to cool to rt before being concentrated *in vacuo*. The resultant residue was dissolved in 1:1 MeOH:DMSO and purified by MDAP (high pH). The desired fractions were combined yielding **3.026** (54 mg, 0.15 mmol, 20%) as a white solid. ^1H NMR (400 MHz, METHANOL-d_4) δ ppm 7.56 (s, 1 H), 7.35 (dd, J=7.5, 1.2 Hz, 1 H), 7.30-7.24 (m, 1 H), 7.20 (dd, J=7.5, 1.2 Hz, 1 H), 7.09 (td, J=7.5, 1.2 Hz, 1 H), 5.93 (ddt, J=17.0, 10.2, 6.8 Hz, 1 H), 5.09-5.01 (m, 1 H), 4.99-4.94 (m, 1 H), 4.55 (s, 2 H), 3.62 (s, 3 H), 3.01 (t, J=4.8 Hz, 4 H), 2.78-2.60 (m, 6 H), 2.40 (s, 3 H), 2.27 (app. q, J=7.4 Hz, 2 H) (N.B. exchangeable amine proton not visible); ^{13}C NMR (101 MHz, METHANOL-d_4) δ ppm 161.9, 150.5, 145.9, 137.7, 133.4, 128.4, 128.1, 128.0, 124.1, 119.5, 114.2, 111.6, 55.2, 52.1, 44.8, 40.9, 38.8, 30.6, 22.4; HRMS (M+H)$^+$ calculated for $C_{21}H_{30}N_5O$ 368.2450; found 368.2451; LC/MS (high pH): R_t = 0.93 min (100%) $[M+H]^+$ = 368.

4-Butyl-5-chloropyridazin-3(2H)-one (3.041)
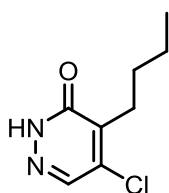
4,5-Dichloropyridazin-3(2H)-one (1.000 g, 6.062 mmol) was dissolved in THF (30 mL) at rt under nitrogen. The solution was allowed to cool to -78 °C before 1.6 M ^nBuLi in hexanes (8.90 mL, 14.2 mmol) was added dropwise over 10 min. The resultant solution was stirred at -78 °C for 15 min. The solution was diluted with IPA (20 mL) and allowed to warm to rt before being concentrated *in vacuo*. The resultant residue was dissolved in EtOAc (40 mL) and washed with water (40 mL). The layers were separated and the aqueous extracted further with EtOAc (30 mL). The combined organic fractions were washed with brine (30 mL) and passed through a hydrophobic frit before being concentrated *in vacuo*. The resultant residue was dissolved in minimal DCM and purified by silica

chromatography (0-30% EtOAc in cyclohexane). The desired fractions were combined yielding **3.041** (0.715 g, 3.83 mmol, 63%) as an off white solid. ^{1}H NMR (400 MHz, CHLOROFORM-*d*) δ ppm 11.88 (br. s, 1 H), 7.76 (s, 1 H), 2.80-2.69 (m, 2 H), 1.64-1.54 (m, 2 H), 1.50-1.38 (m, 2 H), 0.97 (t, *J*=7.2 Hz, 3 H); ^{13}C NMR (101 MHz, CHLOROFORM-*d*) δ ppm 161.8, 141.6, 138.1, 137.3, 28.9, 27.0, 22.8, 13.8; HRMS (M+H)[+] calculated for $C_8H_{12}ClN_2O$ 187.0638; found 187.0644; LC/MS (formic): R_t = 0.90 min (100%) [M+H][+] = 187.

4-Butyl-5-chloro-2-methylpyridazin-3(2H)-one (3.042)
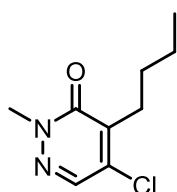
Methyl iodide (0.359 mL, 5.75 mmol) was added to a stirred mixture of tetrabutylammonium bromide (2099 mg, 6.511 mmol), **3.041** (715 mg, 3.83 mmol) and potassium carbonate (1059 mg, 7.663 mmol) in MeCN (8 mL) at rt. The resultant solution was heated to 60 °C and stirred for 5 hours. The resultant mixture was allowed to cool to rt before being filtered under reduced pressure and the filtrate concentrated *in vacuo*. The resultant solid was dissolved in EtOAc (30 mL) and washed with 1 M aq. HCl solution (30 mL). The organic layer was then washed with brine (20 mL), passed through a hydrophobic frit, and concentrated *in vacuo*. The resultant solid was dissolved in minimal DCM and purified by silica chromatography (0-25% EtOAc in cyclohexane). The desired fractions were concentrated *in vacuo* yielding **3.042** (593 mg, 2.96 mmol, 77%) as a yellow oil. ^{1}H NMR (400 MHz, CHLOROFORM-*d*) δ ppm 7.68 (s, 1 H), 3.77 (s, 3 H), 2.79-2.68 (m, 2 H), 1.60-1.52 (m, 2 H), 1.49-1.37 (m, 2 H), 0.97 (t, *J*=7.3 Hz, 3 H); ^{13}C NMR (101 MHz, CHLOROFORM-*d*) δ ppm 160.2, 140.6, 136.3, 135.9, 40.2, 28.9, 27.5, 22.8, 13.8; HRMS (M+H)[+] calculated for $C_9H_{14}ClN_2O$ 201.0795; found 201.0802; LC/MS (formic): R_t = 1.07 min (95%) [M+H][+] = 201.

4-Butyl-2-methyl-5-((2-(4-methylpiperazin-1-yl)benzyl)amino)pyridazin-3(2H)-one (3.039)
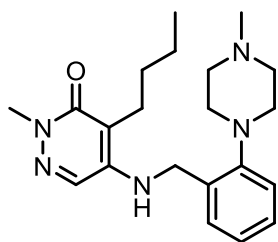
(2-(4-Methylpiperazin-1-yl)phenyl)methanamine (0.06 mL, 0.3 mmol), **3.042** (0.050 g, 0.25 mmol), sodium *tert*-butoxide (48 mg, 0.50 mmol), $Pd_2(dba)_3$ (23 mg, 0.025 mmol) and 2-(dicyclohexylphosphino)3,6-dimethoxy-2′,4′,6′-triisopropyl-1,1′-biphenyl (27 mg, 0.050 mmol) were dissolved in THF (0.5 mL). The reaction mixture was heated to 100 °C in a microwave reactor and stirred for 1 hour. The resultant solution was allowed to cool to rt, diluted with EtOAc (10 mL), filtered through Celite and concentrated *in vacuo*. The resultant residue was dissolved in EtOAc (10 mL) and washed sequentially with water (10 mL) and brine (10 mL). The organic layer was passed through a hydrophobic frit and concentrated *in vacuo*. The resultant residue was dissolved in 1:1 MeOH:DMSO and purified by MDAP (high pH). The desired fractions were combined and concentrated *in vacuo* yielding **3.039** (0.020 g, 0.054 mmol, 22%) as an orange oil. ^1H NMR (400 MHz, METHANOL-d_4) δ ppm 7.55 (s, 1 H), 7.36-7.31 (m, 1 H), 7.30-7.24 (m, 1 H), 7.21 (dd, J=7.3, 1.2 Hz, 1 H), 7.09 (td, J=7.3, 1.2 Hz, 1 H), 4.56 (s, 2 H), 3.62 (s, 3 H), 3.02 (t, J=4.9 Hz, 4 H), 2.73 (app. br. s, 4 H), 2.55 (t, J=7.2 Hz, 2 H), 2.42 (s, 3 H), 1.56-1.38 (m, 4 H), 0.98 (t, J=7.2 Hz, 3 H) (N.B. exchangeable amine proton not visible); ^{13}C NMR (101 MHz, METHANOL-d_4) δ ppm 161.9, 150.5, 145.8, 133.4, 128.4, 128.0, 127.9, 124.1, 119.5, 112.6, 55.2, 52.1, 44.8, 40.9, 38.8, 28.8, 26.6, 22.5, 13.1; HRMS $(M+H)^+$ calculated for $C_{21}H_{32}N_5O$ 370.2607; found 370.2607; LC/MS (high pH): R_t = 1.01 min (100%) $[M+H]^+$ = 370.

5-Chloro-4-ethylpyridazin-3(2H)-one (3.043)
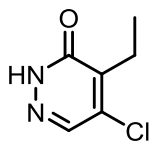
3 M Ethylmagnesium bromide in Et_2O solution (15.15 mL, 45.45 mmol) was added dropwise to a stirred suspension of 4,5-dichloropyridazin-3(2H)-one (2.500 g, 15.15 mmol) in THF (50 mL) at 0 °C under nitrogen. The resultant solution was stirred at 0 °C for 10 min before being allowed to warm to rt and stirred for 3 hours. Saturated aq. NH_4Cl solution (25 mL) was added slowly over 10 min. The reaction mixture was diluted with 2 M aq. HCl solution (50 mL) and extracted with EtOAc (50 mL). The aqueous layer was extracted further with EtOAc

(25 mL). The organic layers were combined, washed with brine (25 mL), passed through a hydrophobic frit and concentrated *in vacuo*. The resultant oil was dissolved in minimal DCM and purified by silica chromatography (0-40% EtOAc in cyclohexane). The desired fractions were combined yielding **3.043** (625 mg, 3.94 mmol, 26%) as a white solid. m.p. 135–138 °C; v_{max} (solid)/cm^{-1}: 2864, 1638 (C=O), 1177, 914, 575; ^{1}H NMR (400 MHz, METHANOL-d_4) δ ppm 7.88 (s, 1 H), 2.75 (q, *J*=7.6 Hz, 2 H), 1.17 (t, *J*=7.6 Hz, 3 H) (N.B. exchangeable lactam proton not visible); ^{13}C NMR (101 MHz, METHANOL-d_4) δ ppm 161.4, 141.7, 137.9, 137.0, 20.0, 10.0; HRMS (M+H)$^+$ calculated for $C_6H_8ClN_2O$ 159.0325; found 159.0325; LC/MS (formic): R_t = 0.66 min (98%) [M+H]$^+$ = 159.

5-Chloro-4-ethyl-2-methylpyridazin-3(2H)-one (3.044)
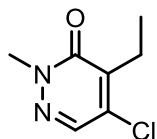
Methyl iodide (0.197 mL, 3.15 mmol) was added to a stirred mixture of tetrabutylammonium bromide (1118 mg, 3.468 mmol), **3.043** (0.250 g, 1.576 mmol) and potassium carbonate (436 mg, 3.15 mmol) in MeCN (5 mL) at rt. The resultant mixture was stirred under nitrogen for 3 hours at rt. The resultant mixture was filtered under reduced pressure and the filtrate concentrated *in vacuo*. The resultant solid was dissolved in EtOAc (50 mL) and washed with 2 M aq. HCl solution (30 mL). MeOH was added dropwise to dissolve a white precipitate. The organic layer was then washed with brine (30 mL), passed through a hydrophobic frit, and concentrated *in vacuo*. The resultant solid was dissolved in minimal DCM and purified by silica chromatography (0-50% EtOAc in cyclohexane). The desired fractions were concentrated *in vacuo* yielding **3.044** (170 mg, 0.985 mmol, 63%) as a colourless oil. ^{1}H NMR (400 MHz, METHANOL-d_4) δ ppm 7.89 (s, 1 H), 3.75 (s, 3 H), 2.76 (q, *J*=7.6 Hz, 2 H), 1.16 (t, *J*=7.6 Hz, 3 H); ^{13}C NMR (101 MHz, METHANOL-d_4) δ ppm 160.2, 140.9, 136.8, 136.0, 39.4, 20.6, 9.9; HRMS (M+H)$^+$ calculated for $C_7H_{10}ClN_2O$ 173.0482; found 173.0478; LC/MS (formic): R_t = 0.80 min (99%) [M+H]$^+$ = 173.

4-Ethyl-2-methyl-5-((2-(4-methylpiperazin-1-yl)benzyl)amino)pyridazin-3(2H)-one (3.036)
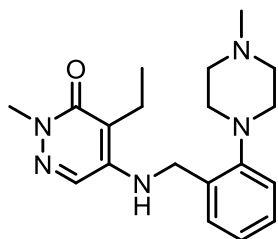
(2-(4-Methylpiperazin-1-yl)phenyl)methanamine (0.134 mL, 0.695 mmol), **3.044** (0.100 g, 0.579 mmol), sodium *tert*-butoxide (111 mg, 1.16 mmol), $Pd_2(dba)_3$ (53 mg, 0.058 mmol) and 2-(dicyclohexylphosphino)3,6-dimethoxy-2′,4′,6′-triisopropyl-1,1′-biphenyl (62 mg, 0.12 mmol) were dissolved in THF (0.5 mL) and heated to 100 °C in a microwave reactor. The reaction mixture was stirred at 100 °C for 1 hour. The resultant solution was allowed to cool to rt, diluted with EtOAc (10 mL), filtered through Celite and concentrated *in vacuo*. The resultant residue was dissolved in EtOAc (10 mL) and washed sequentially with water (10 mL) and brine (10 mL). The organic layer was passed through a hydrophobic frit and concentrated *in vacuo*. The resultant residue was dissolved in 1:1 MeOH:DMSO and purified by MDAP (high pH). The desired fractions were combined and concentrated *in vacuo* yielding **3.036** (91 mg, 0.27 mmol, 46%) as a white solid. m.p. 148–149 °C; v_{max} (solid)/cm^{-1}: 3344, 2796, 1595 (C=O), 1225, 769; ^{1}H NMR (400 MHz, METHANOL-d_4) δ ppm 7.56 (s, 1 H), 7.37-7.31 (m, 1 H), 7.30-7.23 (m, 1 H), 7.21 (dd, J=7.4, 1.3 Hz, 1 H), 7.09 (td, J=7.4, 1.3 Hz, 1 H), 4.56 (s, 2 H), 3.62 (s, 3 H), 3.01 (t, J=4.8 Hz, 4 H), 2.71 (app. br. s, 4 H), 2.57 (q, J=7.5 Hz, 2 H), 2.40 (s, 3 H), 1.10 (t, J=7.5 Hz, 3 H) (N.B. exchangeable amine proton not visible); ^{13}C NMR (101 MHz, METHANOL-d_4) δ ppm 161.7, 150.5, 145.5, 133.4, 128.5, 128.0, 127.9, 124.1, 119.5, 113.8, 55.2, 52.2, 44.8, 40.8, 38.8, 16.0, 10.1; HRMS (M+H)$^+$ calculated for $C_{19}H_{28}N_5O$ 342.2294; found 342.2292; LC/MS (high pH): R_t = 0.84 min (100%) [M+H]$^+$ = 342.

5-Chloro-4-isopropylpyridazin-3(2H)-one (3.045)
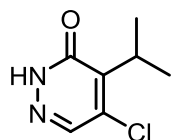
2.9 M Isopropylmagnesium bromide in 2-methyltetrahydrofuran solution (3.14 mL, 9.09 mmol) was added dropwise to a stirred suspension of 4,5-dichloropyridazin-3(2H)-one (0.500 g, 3.03 mmol) in THF (10 mL) at 0 °C under nitrogen. The resultant solution was stirred at 0 °C for 10 min before being allowed to warm to rt and stirred for 1.5 hours. Saturated aq. NH_4Cl solution (5 mL) was added dropwise. EtOAc (5 mL) and 2 M aq. HCl solution (5 mL) were added, the mixture shaken, and the organic layer removed. The aqueous layer was extracted further with EtOAc (25 mL). The organic layers were combined,

washed with brine (25 mL), passed through a hydrophobic frit and concentrated *in vacuo*. The resultant oil was dissolved in minimal DCM and purified by silica chromatography (0-40% EtOAc in cyclohexane). The desired fractions were combined and concentrated *in vacuo* yielding **3.045** (0.140 g, 0.811 mmol, 27%) as an off-white solid. m.p. 98–102 °C; v_{max} (solid)/cm^{-1}: 2966, 2876, 1645 (C=O), 1180, 1055, 918, 593; ^{1}H NMR (400 MHz, METHANOL-d_4) δ ppm 7.84 (s, 1 H), 3.50 (spt, *J*=7.1 Hz, 1 H), 1.36 (d, *J*=7.1 Hz, 6 H); ^{13}C NMR (101 MHz, METHANOL-d_4) δ ppm 160.9, 143.8, 138.0, 136.2, 28.9, 17.4; HRMS (M+H)$^+$ calculated for $C_7H_{10}ClN_2O$ 173.0482; found 173.0477; LC/MS (formic): R_t = 0.81 min (85%) [M+H]$^+$ = 173.

5-Chloro-4-isopropyl-2-methylpyridazin-3(2H)-one (3.046)
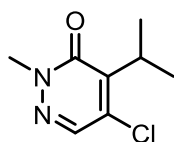
Methyl iodide (0.07 mL, 1 mmol) was added to a stirred mixture of tetrabutylammonium bromide (406 mg, 1.26 mmol), **3.045** (128 mg, 0.742 mmol) and potassium carbonate (205 mg, 1.48 mmol) in MeCN (5 mL) at rt. The resultant mixture was stirred under nitrogen for 2.5 hours at rt. The reaction mixture was filtered under reduced pressure and the filtrate concentrated *in vacuo*. The resultant solid was dissolved in EtOAc (10 mL) and washed with 2 M aq. HCl solution (10 mL). MeOH was added dropwise to the organic layer to dissolve a white precipitate which was then washed with brine (10 mL), passed through a hydrophobic frit, and concentrated *in vacuo*. The resultant solid was dissolved in minimal DCM and purified by silica chromatography (0-50% EtOAc in cyclohexane). The desired fractions were concentrated *in vacuo* yielding **3.046** (26 mg, 0.14 mmol, 19%) as a colourless oil. ^{1}H NMR (400 MHz, DMSO-d_6) δ ppm 7.94 (s, 1 H), 3.63 (s, 3 H), 3.38 (sept., *J*=7.1 Hz, 1 H), 1.28 (d, *J*=7.1 Hz, 6 H); ^{13}C NMR (101 MHz, DMSO-d_6) δ ppm 158.9, 142.8, 136.8, 134.7, 29.3, 18.7 (N.B. one carbon signal obscured by solvent peak at 40.2 ppm); HRMS (M+H)$^+$ calculated for $C_8H_{12}ClN_2O$ 187.0638; found 187.0638 LC/MS (formic): R_t = 0.97 min (100%) [M+H]$^+$ = 187.

4-Isopropyl-2-methyl-5-((2-(4-methylpiperazin-1-yl)benzyl)amino)pyridazin-3(2H)-one (3.038)
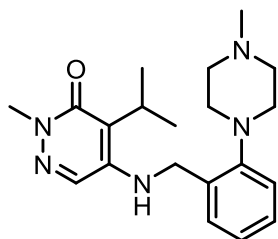
(2-(4-Methylpiperazin-1-yl)phenyl)methanamine (0.09 mL, 0.5 mmol), **3.046** (75 mg, 0.40 mmol), sodium *tert*-butoxide (77 mg, 0.80 mmol), Pd$_2$(dba)$_3$ (37 mg, 0.040 mmol) and 2-(dicyclohexylphosphino)3,6-dimethoxy-2′,4′,6′-triisopropyl-1,1′-biphenyl (43 mg, 0.080 mmol) were dissolved in THF (4 mL). The reaction mixture was stirred at 100 °C for 1 hour in a microwave reactor. The resultant solution was allowed to cool to rt, diluted with EtOAc (10 mL), filtered through Celite and concentrated *in vacuo*. The resultant residue was dissolved in EtOAc (10 mL) and washed sequentially with water (15 mL) and brine (15 mL). The organic layer was passed through a hydrophobic frit and concentrated *in vacuo*. The resultant residue was dissolved in 1:1 MeOH:DMSO and purified by MDAP (high pH). The desired fractions were combined and concentrated *in vacuo* yielding **3.038** (51 mg, 0.14 mmol, 36%) as a white solid. m.p. 163–165 °C; v_{max} (solid) /cm^{-1}: 3308, 2794, 1591 (C=O), 1450, 1141, 772; ^{1}H NMR (400 MHz, METHANOL-d_4) δ ppm 7.52 (s, 1 H), 7.33 (dd, *J*=7.7, 1.1 Hz, 1 H), 7.29-7.23 (m, 1 H), 7.23-7.19 (dd, *J*=7.3, 1.2 Hz, 1 H), 7.10 (td, *J*=7.3, 1.2 Hz, 1 H), 4.55 (s, 2 H), 3.58 (s, 3 H), 3.23-3.14 (m, 1 H), 3.01 (t, *J*=4.8 Hz, 4 H), 2.69 (app. br. s, 4 H), 2.40 (s, 3 H), 1.35 (d, *J*=7.1 Hz, 6 H) (N.B. exchangeable amine proton not visible); ^{13}C NMR (101 MHz, METHANOL-d_4) δ ppm 161.3, 150.5, 145.2, 133.4, 128.6, 128.1, 128.0, 124.2, 119.5, 116.6, 55.1, 52.1, 44.8, 41.1, 38.7, 24.6, 17.8; HRMS (M+H)$^+$ calculated for C$_{20}$H$_{30}$N$_5$O 356.2450; found 356.2449.; LC/MS (high pH): R$_t$ = 0.92 min (98%) [M+H]$^+$ = 356.

2-Methyl-5-((2-(4-methylpiperazin-1-yl)benzyl)amino)-4-propylpyridazin-3(2H)-one (3.037)
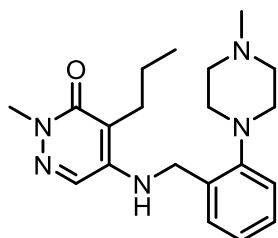
The solvent system was sparged with nitrogen for 1 hour prior to use. **3.028** (0.100 g, 0.287 mmol), propylboronic acid (0.100 g, 1.14 mmol), potassium carbonate (99 mg, 0.72 mmol), Pd(OAc)$_2$ (26 mg, 0.12 mmol) and butyldi-1-adamantylphosphine (52 mg, 0.14 mmol) were dissolved in in 1,4-dioxane (1.65 mL) and water (0.825 mL) under nitrogen at rt. The resultant mixture

240

was heated to 100 °C and stirred for 1 hour in a microwave reactor. The resultant solution was diluted with EtOAc (10 mL) and filtered through Celite before being concentrated *in vacuo*. The resultant residue was dissolved in 1:1 MeOH:DMSO and purified by MDAP (high pH). The desired fractions were combined yielding **3.037** (0.030 g, 0.084 mmol, 29%) as an off white solid. ^{1}H NMR (400 MHz, METHANOL-d_4) δ ppm 7.55 (s, 1 H), 7.37-7.31 (m, 1 H), 7.29-7.24 (m, 1 H), 7.23-7.17 (m, 1 H), 7.09 (td, *J*=7.5, 1.2 Hz, 1 H), 4.55 (s, 2 H), 3.62 (s, 3 H), 3.01 (t, *J*=4.8 Hz, 4 H), 2.71 (app. br. s, 4 H), 2.57-2.48 (m, 2 H), 2.40 (s, 3 H), 1.61-1.46 (m, 2 H), 1.02 (t, *J*=7.3 Hz, 3 H). (N.B. exchangeable amine proton not visible); ^{13}C NMR (101 MHz, METHANOL-d_4) δ ppm 162.0, 150.5, 145.9, 133.4, 128.4, 128.0, 127.9, 124.1, 119.5, 112.4, 55.1, 52.1, 44.8, 40.8, 38.8, 24.8, 19.7, 13.0; HRMS (M+H)$^+$ calculated for $C_{20}H_{30}N_5O$ 356.2450; found 356.2442; LC/MS (high pH): R_t = 0.92 min (100%) [M+H]$^+$ = 356.

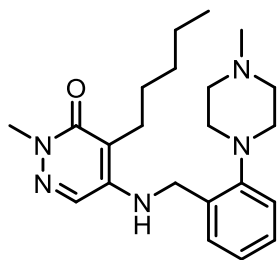### 2-Methyl-5-((2-(4-methylpiperazin-1-yl)benzyl)amino)-4-pentylpyridazin-3(2H)-one (3.040)

The solvent system sparged with nitrogen for 1 hour prior to use. **3.028** (0.100 g, 0.287 mmol), pentylboronic acid (0.100 g, 0.862 mmol), potassium carbonate (99 mg, 0.72 mmol), Pd(OAc)$_2$ (26 mg, 0.12 mmol) and butyldi-1-adamantylphosphine (52 mg, 0.14 mmol) were dissolved in in 1,4-dioxane (1.65 mL) and water (0.83 mL) under nitrogen at rt. The reaction mixture was heated to 100 °C and stirred for 1 hour in a microwave reactor. The resultant solution was diluted with EtOAc (5 mL) and filtered through Celite before being concentrated *in vacuo*. The resultant residue was dissolved in 1:1 MeOH:DMSO and purified by MDAP (high pH). The desired fractions were combined yielding **3.040** (28 mg, 0.073 mmol, 25%) as an off white solid. ^{1}H NMR (400 MHz, METHANOL-d_4) δ ppm 7.56 (s, 1 H), 7.36-7.31 (m, 1 H), 7.30-7.24 (m, 1 H), 7.20 (dd, *J*=7.5, 1.2 Hz, 1 H), 7.09 (td, *J*=7.5, 1.2 Hz, 1 H), 4.55 (s, 2 H), 3.62 (s, 3 H), 3.01 (t, *J*=4.8 Hz, 4 H), 2.71 (app. br. s, 4 H), 2.58-2.49 (m, 2 H), 2.40 (s, 3 H), 1.57-1.46 (m, 2 H), 1.44-1.34 (m, 4 H), 0.97-0.91 (m, 3 H); ^{13}C NMR (101 MHz, METHANOL-d_4) δ ppm 162.0, 150.5, 145.8, 133.4, 128.4, 128.0, 127.9, 124.1, 119.5, 112.7, 55.2, 52.2, 44.8, 40.9, 38.8,

31.6, 26.3, 22.9, 22.4, 13.0; HRMS (M+H)$^+$ calculated for $C_{22}H_{34}N_5O$ 384.2763; found 384.2756; LC/MS (high pH): R_t = 1.08 min (96%) [M+H]$^+$ = 384.

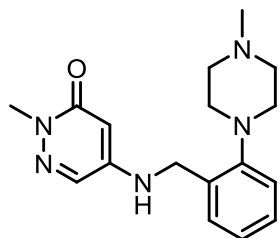**2-Methyl-5-((2-(4-methylpiperazin-1-yl)benzyl)amino)pyridazin-3(2H)-one (3.047)**

The solvent system sparged with nitrogen for 20 min prior to use. **3.028** (0.100 g, 0.287 mmol), potassium butyltrifluoroborate (94 mg, 0.58 mmol), potassium carbonate (99 mg, 0.72 mmol), Pd(OAc)$_2$ (13 mg, 0.057 mmol) and butyldi-1-adamantylphosphine (22 mg, 0.063 mmol) were dissolved in in 1,4-dioxane (3 mL) and water (1.5 mL) under nitrogen at rt. The resultant mixture was heated to 100 °C and stirred for 1 hour in a microwave reactor. The resultant solution was diluted with EtOAc (5 mL) and filtered through Celite before being concentrated *in vacuo*. The resultant residue was dissolved in EtOAc (10 mL) and washed sequentially with water (10 mL) and brine (10 mL). The organic layer was then passed through a hydrophobic frit and concentrated *in vacuo*. The resultant residue was dissolved in 1:1 MeOH:DMSO and purified by MDAP (high pH). The desired fractions were combined yielding **3.047** (39 mg, 0.12 mmol, 43%) as a white solid. m.p. 190–192 °C; ν$_{max}$ (solid) /cm^{-1}: 3245, 2941, 2790, 1591 (C=O), 1450, 761; ^{1}H NMR (400 MHz, METHANOL-d_4) δ ppm 7.57 (d, *J*=2.7 Hz, 1 H), 7.37-7.32 (m, 1 H), 7.31-7.25 (m, 1 H), 7.22 (dd, *J*=7.5, 1.2 Hz, 1 H), 7.11 (td, *J*=7.5, 1.2 Hz, 1 H), 5.62 (d, *J*=2.7 Hz, 1 H), 4.39 (s, 2 H), 3.61 (s, 3 H), 2.99 (t, *J*=4.8 Hz, 4 H), 2.68 (app. br. s, 4 H), 2.38 (s, 3 H); HRMS (M+H)$^+$ calculated for $C_{17}H_{24}N_5O$ 314.1981; found 314.1986; LC/MS (high pH): R_t = 0.76 min (100%) [M+H]$^+$ = 314.

***tert*-Butyl 5-((5-butyl-1-methyl-6-oxo-1,6-dihydropyridazin-4-yl)amino)-3,4-tetrahydroisoquinoline-2(1H)-carboxylate (3.051)**
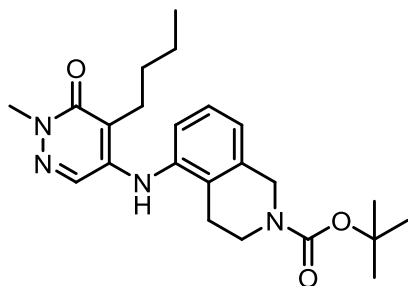
tert-Butyl 5-amino-3,4-tetrahydroisoquinoline-2(1H)-carboxylate (515 mg, 2.07 mmol), **3.042** (0.320 g, 1.60 mmol), sodium *tert*-butoxide (307 mg, 3.19 mmol), Pd$_2$(dba)$_3$ (118 mg, 0.159 mmol) and 2-(dicyclohexylphosphino)3,6-dimethoxy-2′,4′,6′-triisopropyl-1,1′-biphenyl (171 mg, 0.319 mmol) were dissolved in THF (10 mL). The reaction mixture was stirred at 100 °C for 1 hour in a microwave reactor. The resultant solution was allowed to cool to rt, diluted with EtOAc (25 mL), filtered through Celite and concentrated *in vacuo*. The resultant residue was dissolved in EtOAc (30 mL) and washed sequentially with water (30 mL) and brine (20 mL). The organic layer was passed through a hydrophobic frit and concentrated *in vacuo*. The resultant residue was dissolved in minimal DCM and purified by silica chromatography (0-50% EtOAc in cyclohexane). The desired fractions were combined yielding **3.051** (167 mg, 0.405 mmol, 25%) as a pale orange solid. m.p. 60-65 °C; v$_{max}$ (solid)/cm^{-1}: 3295, 2930, 1694 (C=O), 1584 (C=O), 1395, 1163, 769; ^{1}H NMR (400 MHz, METHANOL-d_4) δ ppm 7.29 (t, *J*=7.6 Hz, 1 H), 7.22 (s, 1 H), 7.15 (d, *J*=7.6 Hz, 1 H), 7.09 (d, *J*=7.6 Hz, 1 H), 4.62 (s, 2 H), 3.68 (s, 3 H), 3.64 (t, *J*=5.9 Hz, 2 H), 2.74 (t, *J*=5.9 Hz, 2 H), 2.68-2.61 (m, 2 H), 1.61-1.40 (m, 13 H), 0.98 (t, *J*=7.2 Hz, 3 H) (N.B. exchangeable amine proton not visible); ^{13}C NMR (101 MHz, METHANOL-d_4) δ ppm 162.2, 155.1, 144.6, 137.4, 135.5, 131.9, 129.3, 126.9, 124.9, 124.6, 115.1, 80.1, 38.9, 28.9, 27.3, 26.6, 24.4, 22.9, 22.4, 13.1 (N.B. one carbon missing); HRMS (M+H)$^+$ calculated for C$_{23}$H$_{33}$N$_4$O$_3$ 413.2555; found 413.2557; LC/MS (formic): R$_t$ = 1.24 min (98%) [M+H]$^+$ = 413.

4-Butyl-2-methyl-5-((1,2,3,4-tetrahydroisoquinolin-5-yl)amino)pyridazin-3(2H)-one (3.052)
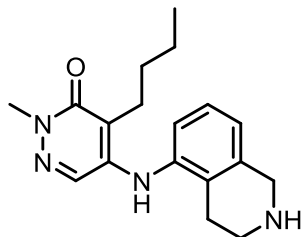
3.051 (150 mg, 0.364 mmol) was dissolved in 4 M HCl in 1,4-dioxane (3 mL) at rt and stirred for 45 min. The reaction mixture was concentrated *in vacuo*. The resultant residue was dissolved in MeOH and passed through a preconditioned (MeOH) aminopropyl column (1 g) and eluted with MeOH (10 mL). The desired fractions were concentrated *in vacuo* yielding **3.052** (114 mg, 0.365 mmol, 100%) as a yellow solid. ^{1}H NMR (400 MHz, METHANOL-d_4) δ ppm 7.28 (t, *J*=7.6 Hz, 1 H), 7.23 (s, 1 H), 7.14-7.08 (m, 2 H), 4.14 (s, 2 H), 3.68 (s, 3 H), 3.22 (t, *J*=6.1 Hz, 2 H), 2.79 (t, *J*=6.1 Hz, 2 H), 2.69-2.61 (m, 2 H), 1.61-1.51 (m, 2 H), 1.51-1.41 (m, 2 H), 0.98 (t, *J*=7.2 Hz, 3 H) (N.B. exchangeable amine protons not visible); ^{13}C NMR (101 MHz, METHANOL-d_4) δ ppm 162.2, 144.6, 137.7, 135.0, 131.2, 129.3, 126.8, 125.3, 124.9, 115.2, 46.4, 42.3, 39.0, 29.0, 23.5, 23.0, 22.4, 13.1; HRMS (M+H)[+] calculated for $C_{18}H_{25}N_4O$ 313.2028; found 313.2033; LC/MS (formic): R_t = 0.48 min (100%) [M+H][+] = 313.

4-Butyl-2-methyl-5-((2-methyl-1,2,3,4-tetrahydroisoquinolin-5-yl)amino)pyridazin-3(2H)-one (3.053)
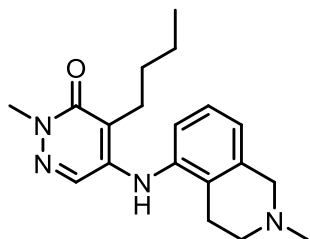
37% Formaldehyde in water with 10-15 % MeOH (0.25 mL, 3.4 mmol) and formic acid (1.00 mL, 26.1 mmol) were added to **3.052** (105 mg, 0.336 mmol) and heated to 80 °C for 6 hours. The reaction mixture was allowed to cool to rt and concentrated *in vacuo*. The resultant residue was dissolved in minimal DCM and purified by silica chromatography (0-10% MeOH in DCM). The desired fractions were combined and concentrated *in vacuo*. The resultant solid was dissolved in MeOH (1.5 mL) and loaded on to an SCX (1 g) column. The column was washed with MeOH (3 mL) before eluting with 2 M ammonia in MeOH solution (4 mL). The desired fractions were combined yielding **3.053** (65 mg, 0.20 mmol, 59%) as a white solid. ^{1}H NMR (400 MHz, CHLOROFORM-*d*) δ ppm 7.44 (s, 1 H), 7.18 (t, *J*=7.8 Hz, 1 H), 7.00 (d, *J*=7.8 Hz, 1 H), 6.95 (d, *J*=7.8 Hz, 1 H), 5.41 (s, 1 H), 3.73 (s, 3 H), 3.62 (s, 2 H), 2.79-2.71 (m, 4 H), 2.66-2.59 (m, 2 H), 2.49 (s, 3 H),

1.63-1.54 (m, 2 H), 1.52-1.45 (m, 2 H), 0.99 (t, J=7.3 Hz, 3 H); ^{13}C NMR (101 MHz, CHLOROFORM-d) δ ppm 161.5, 142.4, 137.2, 137.1, 128.9, 128.7, 126.6, 124.0, 121.9, 117.7, 58.0, 52.5, 45.9, 39.8, 29.2, 25.5, 23.6, 23.0, 14.0; HRMS (M+H)$^+$ calculated for $C_{19}H_{27}N_4O$ 327.2185; found 327.2189; LC/MS (formic): R_t = 0.49 min (100%) [M+H]$^+$ = 327.

2-Bromo-5-butylthieno[3,2-c]pyridin-4(5H)-one (3.055)
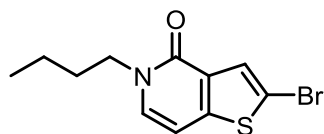
To a solution of 2-bromothieno[3,2-c]pyridin-4(5H)-one (1 g, 4.35 mmol) and cesium carbonate (4.250 g, 13.04 mmol) in THF (25 mL), 1-iodobutane (0.718 mL, 6.52 mmol) was added in a single portion and the mixture heated to 60 °C for 19 hours. The reaction mixture was allowed to cool to rt and concentrated *in vacuo*. The resultant solid was suspended in water (15 mL) and filtered under reduced pressure. The solid was washed with water (10 mL), collected and dried under vacuum at 40 ºC yielding **3.055** (884 mg, 3.09 mmol, 71%) as a brown solid. ^{1}H NMR (400 MHz, CHLOROFORM-d) δ ppm 7.63 (s, 1 H), 7.13 (d, J=7.1 Hz, 1 H), 6.56 (d, J=7.1 Hz, 1 H), 4.01 (t, J=7.4 Hz, 2 H), 1.83-1.70 (m, 2 H), 1.41 (sext., J=7.4 Hz, 2 H), 0.98 (t, J=7.4 Hz, 3 H); ^{13}C NMR (101 MHz, CHLOROFORM-d) δ ppm 157.6, 148.4, 132.6, 131.3, 127.7, 112.2, 100.8, 49.2, 31.6, 19.9, 13.7; HRMS (M+H)$^+$ calculated for $C_{11}H_{13}BrNOS$ 285.9901; found 285.9910; LC/MS (formic): R_t = 1.13 min (97%) [M+H]$^+$ = 286.

5-Butyl-4-oxo-4,5-dihydrothieno[3,2-c]pyridine-2-carbonitrile (3.056)
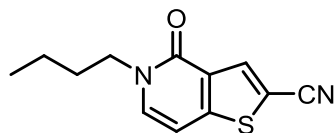
Two batches of **3.055** (2.00 g, 6.99 mmol), dicyanozinc (1.641 g, 13.98 mmol) and Pd(PPh$_3$)$_4$ (0.808 g, 0.699 mmol) in DMF (10 mL) were heated to 115 °C in a microwave reactor for 4.5 hours. The batches were diluted with EtOAc (50 mL each), combined, filtered through Celite and concentrated *in vacuo*. The resulting residue was diluted with DCM, filtered under reduced pressure, and the filtrate concentrated *in vacuo*. The resultant residue was dissolved in minimal DCM and purified by silica

chromatography (0-40% EtOAc in cyclohexane). The desired fractions were combined and concentrated *in vacuo* yielding **3.056** (984 mg, 4.24 mmol, 61%) as a white solid. m.p. 95–99 °C; v_{max} (solid)/cm^{-1}: 3103, 2960, 2871, 2209 (C≡N), 1631 (C=O), 1588, 769; ^{1}H NMR (400 MHz, CHLOROFORM-*d*) δ ppm 8.15 (s, 1 H), 7.32 (d, *J*=7.1 Hz, 1 H), 6.65 (d, *J*=7.1 Hz, 1 H), 4.06-3.99 (m, 2 H), 1.82-1.72 (m, 2 H), 1.41 (sext., *J*=7.3 Hz, 2 H), 0.99 (t, *J*=7.3 Hz, 3 H); ^{13}C NMR (101 MHz, CHLOROFORM-*d*) δ ppm 158.1, 150.6, 136.3, 135.9, 130.0, 113.8, 107.6, 100.6, 49.2, 31.5, 19.9, 13.7; HRMS (M+H)$^+$ calculated for $C_{12}H_{13}N_2OS$ 233.0749; found 233.0754; LC/MS (formic): R_t = 0.98 min (93%) [M+H]$^+$ = 233.

7-Bromo-5-butyl-4-oxo-4,5-dihydrothieno[3,2-c]pyridine-2-carbonitrile (3.057)
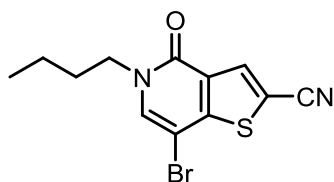
To a stirred solution of **3.056** (984 mg, 4.24 mmol) in THF (20 mL) was added *N*-bromosuccinimide (1131 mg, 6.354 mmol) at rt. The resultant solution was stirred at rt for 65 hours before being concentrated *in vacuo*. The resultant solid was triturated with diethyl ether (15 mL) and filtered under reduced pressure. The collected solid was washed sequentially with diethyl ether (10 mL) and water (20 mL) before being dried yielding **3.057** (816 mg, 2.62 mmol, 62%) as a cream solid. The filtrate was diluted with EtOAc (25 mL) and washed sequentially with water (20 mL) and brine (20 mL). The organic layer was passed through a hydrophobic frit and concentrated *in vacuo*. The resultant solid was dissolved in minimal DCM and purified by silica chromatography (0-30% EtOAc in cyclohexane). The desired fractions were combined and concentrated *in vacuo* yielding **3.057** (313 mg, 1.006 mmol, 24%) as a cream solid. Both solids were combined yielding **3.057** (1129 mg, 3.63 mmol, 86%) as a cream solid. m.p. 115–116 °C; v_{max} (solid)/cm^{-1}: 3043, 2957, 2872, 2212 (C≡N), 1651 (C=O), 1582, 764; ^{1}H NMR (400 MHz, CHLOROFORM-*d*) δ ppm 8.23 (s, 1 H), 7.45 (s, 1 H), 4.02 (t, *J*=7.3 Hz, 2 H), 1.83-1.72 (m, 2 H), 1.42 (sext., *J*=7.3 Hz, 2 H), 1.00 (t, *J*=7.3 Hz, 3 H); ^{13}C NMR (101 MHz, CHLOROFORM-*d*) δ ppm 160.8, 156.3, 140.8, 139.5, 133.2, 117.2, 112.6, 95.6, 53.3, 35.3, 23.6, 17.4; HRMS (M+H)$^+$ calculated for $C_{12}H_{12}BrN_2OS$ 310.9854; found 310.9855; LC/MS (formic): R_t = 1.18 min (95%) [M+H]$^+$ = 311.

Methyl 7-bromo-5-butyl-4-oxo-4,5-dihydrothieno[3,2-c]pyridine-2-carbimidate (3.058)
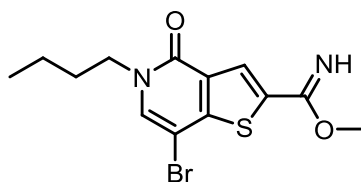
To a suspension of **3.057** (1106 mg, 3.554 mmol) in MeOH (35 mL) was added sodium methoxide (25 wt% solution in MeOH) (0.813 mL, 3.55 mmol). The reaction mixture was heated to 75 ⁰C once dissolution was achieved. After 15 minutes 4-aminotetrahydro-2H-thiopyran 1,1-dioxide (499 mg, 3.34 mmol) was added and the solution was heated for a further 18 hours. A further portion of sodium methoxide (25 wt% solution in MeOH) (0.813 mL, 3.55 mmol) was added at rt before the reaction was heated to 75 ⁰C and stirred for 3 hours. The reaction was cooled to 75 ⁰C and a portion of 4-aminotetrahydro-2H-thiopyran 1,1-dioxide, hydrochloride (125 mg, 0.673 mmol) was added. The reaction was stirred at 75 ⁰C for 5 hours. The solution was allowed to cool to rt before being concentrated *in vacuo*. The resultant residue was dry loaded and purified by silica chromatography (0-75% EtOAc in cyclohexane). The desired fractions were combined yielding **3.058** (326 mg, 0.950 mmol, 27%) as a white solid. m.p. 152-154 °C; v_{max} (solid)/cm^{-1}: 3295, 3077, 2953, 1648 (C=O), 1578, 1314, 1129, 702; ^{1}H NMR (400 MHz, METHANOL-d_4) δ ppm 8.23 (s, 1 H), 7.84 (s, 1 H), 4.07 (t, *J*=7.5 Hz, 2 H), 3.97-3.87 (m, 3 H), 1.82-1.71 (m, 2 H), 1.41 (sext., *J*=7.3 Hz, 2 H), 1.00 (t, *J*=7.3 Hz, 3 H); ^{13}C NMR (176 MHz, METHANOL-d_4) δ ppm 163.4, 159.8, 152.7, 136.5, 136.4, 135.7, 130.9, 128.7, 94.5, 50.6, 32.7, 21.0, 14.2; HRMS (M+H)$^+$ calculated for $C_{13}H_{16}BrN_2O_2S$ 343.0116; found 343.0119; LC/MS (formic): R_t = 0.92 min (97%) [M+H]$^+$ = 343.

7-Bromo-5-butyl-*N*-(1,1-dioxidotetrahydro-2H-thiopyran-4-yl)-4-oxo-4,5-dihydrothieno[3,2-c]pyridine-2-carboximidamide (3.059)
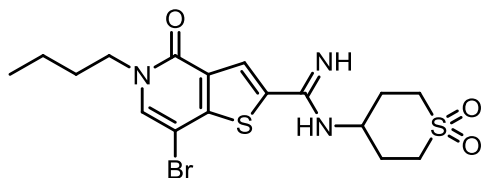
Triethylamine (0.181 mL, 1.30 mmol) was added to a stirred solution 4-aminotetrahydro-2H-thiopyran 1,1-dioxide (168 mg, 1.13 mmol) and **3.058** (297 mg, 0.865 mmol) in DMF (5 mL). The resultant solution was heated to 120 ⁰C and stirred for 17 hours. The resultant solution was allowed to cool to rt before being diluted with water (35 mL). The resultant precipitate was collected under reduced pressure, dissolved in

minimal DCM and purified by silica chromatography (0-50% 25% MeOH in DCM in cyclohexane). The desired fractions were combined and concentrated *in vacuo* yielding **3.059** (83 mg, 0.18 mmol, 21%) as a pale orange solid. ^{1}H NMR (400 MHz, CHLOROFORM-*d*) δ ppm 7.91 (s, 1 H), 7.33 (s, 1 H), 5.01 (br. s, 1 H), 4.01 (t, *J*=7.3 Hz, 2 H), 3.77-3.53 (m, 2 H), 3.05-2.88 (m, 2 H), 2.49-2.33 (m, 2 H), 2.26-2.12 (m, 2 H), 1.80-1.72 (quint., *J*=7.3 Hz, 2 H), 1.49-1.36 (m, 2 H), 0.99 (t, *J*=7.3 Hz, 3 H) (N.B. exchangeable amidine protons not visible); HRMS (M+H)$^+$ calculated for $C_{17}H_{23}BrN_3O_3S_2$ 460.0364; found 460.0368; LC/MS (formic): R_t = 0.56 min (91%) [M+H]$^+$ = 460.

5-Butyl-*N*-(1,1-dioxidotetrahydro-2H-thiopyran-4-yl)-4-oxo-7-(3-(trifluoromethyl)phenyl)-4,5-dihydrothieno[3,2-c]pyridine-2-carboximidamide (3.060)
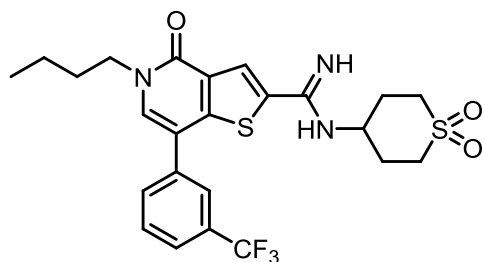
3.059 (73 mg, 0.16 mmol), (3-(trifluoromethyl)phenyl)boronic acid (36 mg, 0.19 mmol), potassium carbonate (53 mg, 0.38 mmol) and PEPPSI-^{i}Pr (10 mg, 0.014 mmol) were dissolved in water (0.13 mL) and IPA (0.38 mL). The resultant mixture was heated to 120 ºC and stirred for 30 minutes in a microwave reactor. The reaction mixture was allowed to cool to rt before being diluted with EtOAc (10 mL), filtered through Celite and concentrated *in vacuo*. The resultant residue was dissolved in 1:1 MeOH:DMSO and purified by MDAP (high pH). The desired fractions were combined yielding **3.060** (43 mg, 0.082 mmol, 52%) as a white solid. m.p. 121-124 °C; v_{max} (solid)/cm^{-1}: 3296, 2957, 1651 (C=O), 1583, 1118; ^{1}H NMR (400 MHz, CHLOROFORM-*d*) δ ppm 7.97 (s, 1 H), 7.88-7.78 (m, 1 H), 7.76-7.60 (m, 3 H), 7.24 (s, 1 H), 4.09 (t, *J*=7.3 Hz, 2 H), 3.76 (br. s, 1 H), 3.57-3.45 (m, 2 H), 3.01-2.86 (m, 2 H), 2.49-2.29 (m, 2 H), 2.26-2.13 (m, 2 H), 1.82 (quin., *J*=7.3 Hz, 2 H), 1.44 (sext., *J*=7.3 Hz, 2 H), 1.00 (t, *J*=7.3 Hz, 3 H) (N.B. exchangeable amidine protons not visible); ^{19}F NMR (376 MHz, CHLOROFORM-*d*) δ ppm -62.64 (s, 3 F); HRMS (M+H)$^+$ calculated for $C_{24}H_{27}F_3N_3O_3S_2$ 526.1446; found 526.1448; LC/MS (high pH): R_t = 1.20 min (100%) [M+H]$^+$ = 526.

3-Butyl-6-chloro-[1,2,4]triazolo[4,3-b]pyridazin-8-amine (3.063b) and 3-butyl-6-chloro-[1,2,4]triazolo[4,3-b]pyridazin-7-amine (3.063a)

3,6-Dichloropyridazin-4-amine (0.3000 g, 18.29 mmol) was dissolved in hydrazine hydrate (22.3 mL, 274 mmol) at rt under nitrogen. The resultant mixture was heated to 135 °C and stirred under nitrogen for 30 min. The solution was allowed to cool to rt before being diluted with crushed ice. The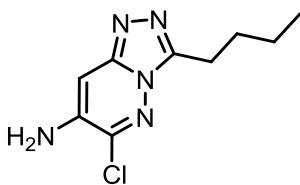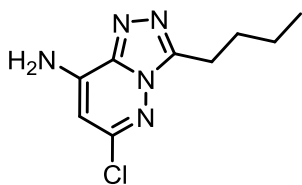 precipitate was collected under reduced pressure, washed with ice-cold water and dried under vacuum at 40 °C yielding a pale brown solid. The solid was dissolved in pentanoic acid (7.85 mL, 71.4 mmol) at rt under nitrogen. The resultant solution was heated to 100 °C and stirred for 3 hours. The resultant solution was allowed to cool to rt before being diluted with water (75 mL) and EtOAc (75 mL). The layers were separated, and the aqueous layer extracted with EtOAc (50 mL). The combined organic fractions were washed with brine (75 mL), passed through a hydrophobic frit, and concentrated *in vacuo*. The resultant residue was loaded on to silica and purified by silica chromatography (0-50% 3:1 EtOAc:EtOH in cyclohexane). The desired fractions were combined yielding **3.063b** (1.754 g, 7.772 mmol, 42%) as a yellow solid. ^{1}H NMR (400 MHz, DMSO-d_6) δ ppm 7.86 (s, 2 H), 6.12 (s, 1 H), 2.99 (t, *J*=7.6 Hz, 2 H), 1.77 (quint., *J*=7.6 Hz, 2 H), 1.38 (sext., *J*=7.6 Hz, 2 H), 0.92 (t, *J*=7.6 Hz, 3 H); ^{13}C NMR (101 MHz, DMSO-d_6) δ ppm 150.3, 149.8, 144.4, 139.8, 94.1, 28.5, 23.7, 22.2, 14.0; HRMS (M+H)$^+$ calculated for $C_9H_{13}ClN_5$ 226.0859; found 226.0866; LC/MS (formic): R_t = 0.89 min (100%) [M+H]$^+$ = 226 and **3.063a** (302 mg, 1.34 mmol, 7%) as a yellow solid. ^{1}H NMR (400 MHz, DMSO-d_6) δ ppm 6.94 (s, 1 H), 6.39 (s, 2 H), 2.95 (t, *J*=7.3 Hz, 2 H), 1.74 (quint., *J*=7.3 Hz, 2 H), 1.37 (sext., *J*=7.3 Hz, 2 H), 0.91 (t, *J*=7.3 Hz, 3 H); ^{13}C NMR (101 MHz, DMSO-d_6) δ ppm 147.2, 145.6, 143.0, 138.9, 95.9, 28.5, 23.4, 22.2, 14.0; HRMS (M+H)$^+$ calculated for $C_9H_{13}ClN_5$ 226.0859; found 226.0867; LC/MS (high pH): R_t = 0.80 min (98%) [M+H]$^+$ = 226.

Ethyl (3-butyl-6-chloro-[1,2,4]triazolo[4,3-b]pyridazin-8-yl)carbamate (3.064)
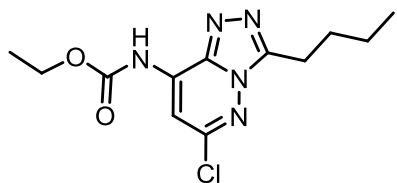
4-Methylmorpholine (3.35 mL, 30.5 mmol) and ethyl chloroformate (1.831 mL, 19.06 mmol) were added to a stirred solution of **3.063b** (1721 mg, 7.626 mmol) in DCM (15 mL) at 0 °C. The resultant solution was allowed to warm to rt and stirred for 5 min. The resultant solution was diluted with DCM (50 mL) and washed with water (2 × 50 mL). The organic layer was separated, washed with brine (50 mL), passed through a hydrophobic frit and concentrated *in vacuo*. The resultant residue was dissolved in minimal DCM and purified by silica chromatography (0-80% EtOAc in cyclohexane). The desired fractions were combined yielding **3.064** (1.523 g, 5.115 mmol, 67%) as an orange oil. ^{1}H NMR (400 MHz, DMSO-d_6) δ ppm 11.17 (br. s, 1 H), 7.64 (s, 1 H), 4.26 (q, J=7.1 Hz, 2 H), 3.05 (t, J=7.3 Hz, 2 H), 1.85-1.75 (m, 2 H), 1.45-1.35 (m, 2 H), 1.29 (t, J=7.1 Hz, 3 H), 0.93 (t, J=7.3 Hz, 3 H); ^{13}C NMR (101 MHz, DMSO-d_6) δ ppm 154.0, 150.8, 149.9, 138.9, 136.7, 103.5, 62.5, 28.4, 23.6, 22.2, 14.7, 14.0; HRMS (M+H)$^+$ calculated for $C_{12}H_{17}ClN_5O_2$ 298.1071; found 298.1076; LC/MS (formic): R_t = 1.14 min (86%) [M+H]$^+$ = 298.

Ethyl (3-butyl-6-(4-methyl-3-nitrophenyl)-[1,2,4]triazolo[4,3-b]pyridazin-8-yl)carbamate (3.065)
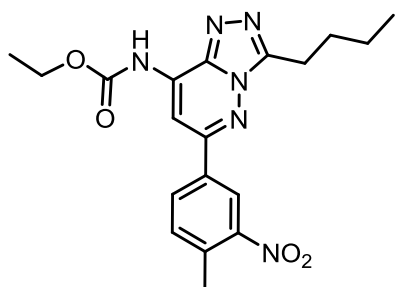
The solvent system was sparged with nitrogen for 1 hour prior to use. **3.064** (0.480 g, 1.61 mmol), (4-methyl-3-nitrophenyl)boronic acid (0.438 g, 2.42 mmol), PdCl$_2$(dppf) (0.590 g, 0.806 mmol) and sodium carbonate (1.709 g, 16.12 mmol) were dissolved in toluene (15 mL) and EtOH (15 mL) under nitrogen at rt. The resultant solution was heated to 100 °C and stirred for 5 hours under nitrogen before being allowed to cool to rt and concentrated *in vacuo*. The resultant residue was dissolved in EtOAc (35 mL) and washed sequentially with water (35 mL) and brine (35 mL). The organic layer was passed through a hydrophobic frit and concentrated *in vacuo*. The resultant residue was dissolved in minimal DCM and purified by silica chromatography (0-100% EtOAc in cyclohexane).

The desired fractions were combined yielding **3.065** (243 mg, 0.610 mmol, 38%) as an orange solid. m.p. 135-140 °C; v_{max} (solid)/cm^{-1}: 3295, 2959, 2211, 1738, 1529 (N-O), 1220; ^{1}H NMR (400 MHz, DMSO-d_6) δ ppm 10.91 (s, 1 H), 8.50 (d, J=2.0 Hz, 1 H), 8.18 (dd, J=8.1, 2.0 Hz, 1 H), 8.13 (s, 1 H), 7.70 (d, J=8.1 Hz, 1 H), 4.28 (q, J=7.1 Hz, 2 H), 3.17 (t, J=7.5 Hz, 2 H), 2.60 (s, 3 H), 1.94-1.81 (m, 2 H), 1.51-1.37 (m, 2 H), 1.32 (t, J=7.1 Hz, 3 H), 0.96 (t, J=7.5 Hz, 3 H); ^{13}C NMR (101 MHz, DMSO-d_6) δ ppm 154.1, 152.4, 149.8, 139.2, 135.9, 135.5, 134.6, 134.3, 131.7, 123.0, 101.0, 62.2, 28.6, 23.7, 22.2, 19.9, 14.7, 14.0 (N.B. one carbon signal not visible); HRMS (M+H)$^+$ calculated for $C_{19}H_{23}N_6O_4$ 399.1781; found 399.1778; LC/MS (formic): R_t = 1.30 min (92%) [M+H]$^+$ = 399.

Ethyl (6-(3-amino-4-methylphenyl)-3-butyl-[1,2,4]triazolo[4,3-b]pyridazin-8-yl)carbamate (3.066)
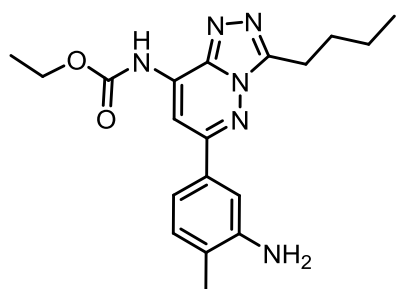
Powdered iron (142 mg, 2.55 mmol) was added to a stirred solution of **3.065** (203 mg, 0.510 mmol) and AcOH (0.175 mL, 3.06 mmol) in EtOH (15 mL) and water (5 mL). The reaction mixture was then heated to 80 °C and stirred for 2 hours. The resultant solution was allowed to cool to rt before being concentrated *in vacuo*. The resultant residue was dissolved in saturated aq. NaHCO$_3$ solution (15 mL) and extracted with EtOAc (3 × 20 mL). The organic fractions were combined, washed with brine (20 mL), passed through a hydrophobic frit and concentrated *in vacuo*. The resultant residue was dissolved in minimal DCM and purified by silica chromatography (30-100% EtOAc in cyclohexane). The desired fractions were combined yielding **3.066** (93 mg, 0.25 mmol, 50%) as a pale brown solid. m.p. 79-83 °C; v_{max} (solid)/cm^{-1}: 2959, 1738, 1561, 1530, 1220; ^{1}H NMR (400 MHz, DMSO-d_6) δ ppm 10.71 (br. s, 1 H), 8.08 (s, 1 H), 7.25 (d, J=1.5 Hz, 1 H), 7.15-7.04 (m, 2 H), 5.16 (br. s, 2 H), 4.26 (q, J=7.1 Hz, 2 H), 3.15 (t, J=7.5 Hz, 2 H), 2.13 (s, 3 H), 1.86 (quint., J=7.5 Hz, 2 H), 1.41 (sext., J=7.5 Hz, 2 H), 1.30 (t, J=7.1 Hz, 3 H), 0.95 (t, J=7.5 Hz, 3 H); ^{13}C NMR (101 MHz, DMSO-d_6) δ ppm 155.2, 154.2, 150.9, 147.7, 139.4, 135.0, 133.8, 131.0, 124.4, 115.2, 112.4, 101.6, 62.1, 28.6, 23.8, 22.2, 17.8, 14.8, 14.0; HRMS (M+H)$^+$ calculated for $C_{19}H_{25}N_6O_2$ 369.2039; found 369.2036; LC/MS (formic): R_t = 1.11 min (94%) [M+H]$^+$ = 369.

Ethyl (3-butyl-6-(4-methyl-3-(methylsulfonamido)phenyl)-[1,2,4]triazolo[4,3-b]pyridazin-8-yl)carbamate (3.067)
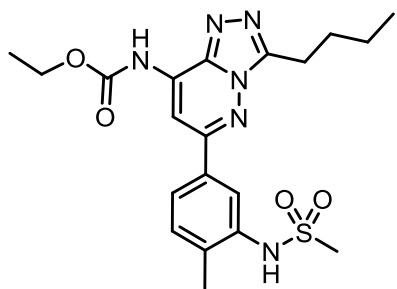
Mesyl chloride (0.169 mL, 2.17 mmol) was added to a stirred solution of **3.066** (0.080 g, 0.22 mmol) and pyridine (0.061 mL, 0.76 mmol) in DCM (3 mL) and the resultant solution stirred at rt for 3 hours before being concentrated *in vacuo*. The resultant residue was dissolved in 1:1 MeOH:DMSO and purified by MDAP (high pH). The desired fractions were concentrated *in vacuo* yielding **3.067** (72 mg, 0.16 mmol, 74%) as a white solid. m.p. 199-204 °C; v_{max} (solid)/cm^{-1}: 3228, 2959, 1727, 1564, 1533, 1223; ^{1}H NMR (400 MHz, DMSO-d_6) δ ppm 8.11 (s, 1 H), 7.91 (d, *J*=1.8 Hz, 1 H), 7.75 (dd, *J*=8.0, 1.8 Hz, 1 H), 7.47 (d, *J*=8.0 Hz, 1 H), 4.27 (q, *J*=7.1 Hz, 2 H), 3.16 (t, *J*=7.5 Hz, 2 H), 3.03 (s, 3 H), 2.40 (s, 3 H), 1.86 (quint., *J*=7.5 Hz, 2 H), 1.42 (sext., *J*=7.5 Hz, 2 H), 1.31 (t, *J*=7.1 Hz, 3 H), 0.95 (t, *J*=7.5 Hz, 3 H) (N.B. exchangeable sulfonamide and carbamate protons not visible); ^{13}C NMR (101 MHz, DMSO-d_6) δ ppm 154.2, 154.0, 151.1, 139.3, 137.1, 136.9, 135.5, 134.0, 132.1, 124.8, 124.7, 101.3, 62.2, 40.6, 28.6, 23.8, 22.2, 18.6, 14.8, 14.0. (N.B. peak at 40.6 is obscured by DMSO solvent peak but clearly visible); HRMS (M+H)$^+$ calculated for $C_{20}H_{27}N_6O_4S$ 447.1814; found 447.1809; LC/MS (formic): R_t = 1.07 min (99%) [M+H]$^+$ = 447.

5. Appendix

5.1 Key for Regression Model Variables

Abbreviation	Variable
aring	Count of aromatic rings
betah	Abrahams descriptors
bonds	Count of bonds
carbons	Count of carbon atoms
cLogP	Calculated LogP (Biobyte)
cmr	Calculated molar refractivity
csp^3	Count of sp^3 carbons
flex	Flexibility (= int(100×rotatable bonds / total bonds)
fsp^3	Fraction of sp^3 carbons (=csp^3/ number of carbons)
HBA	Count of H-bond acceptors (GSK definition)
HBD	Count of H-bond donors (GSK definition)
heavy	Count of Heavy (non-hydrogen) atoms
hetrat	Heteroatom ratio
lipHBA	Lipinski hydrogen bond acceptor count
lipHBD	Lipinski hydrogen bond donor count
LogP	Calculated LogP
LogDph2.0	Calculated LogD at pH 2.0 (Chemaxon)
LogDph5.5	Calculated LogD at pH 5.5 (Chemaxon)
LogDph6.5	Calculated LogD at pH 6.5 (Chemaxon)
LogDph7.4	Calculated LogD at pH 7.4 (Chemaxon)
LogDph11.0	Calculated LogD at pH 11.0 (Chemaxon)
mv	Molar volume (Schroedinger)
mw	Molecular Weight
pK_a_ma	Calculated most acidic pK_a (ChemAxon)
pK_a_mb	Calculated most basic pK_a (Chemaxon)
pos	Count of positively ionisable groups
rb	Count of rotatable bonds
sp^2	Count of sp^2 hybridised atoms
sp^3	Count of sp^3 hybridised atoms
tpsa	Topological polar surface area

Table 5.01: Key for the regression model variables shown in Figure 2.19.

5.2 Cross Screening Panel Data

To investigate the selectivity of compound **2.061·HCl** further, **2.061·HCl** was screened against an internal panel of 18 (**Table 5.02**) pharmacologically relevant assays and a larger panel of 40 (**Table 5.03**) pharmacologically relevant assays. Compound **3.039** was also screened against the larger panel (**Table 5.03**).

Assay	2.061·HCl (pXC$_{50}$)
Cell Health (Mitochondrial Integrity)	3.9
Cell Health (Membrane Permeability)	3.8
Cell Health (Nucleus size)	3.8
Adenosine 2a Ag	<4.0
Adrenergic α2c Ag	<4.0
Dopamine 2 Ag	<4.0
Dopamine 2 Ant	<4.0
Muscarine 2 Ag	<4.3
Muscarine 2 Ant	<4.3
μ Opioid Ag	<4.0
κ Opioid Ag	<4.0
MATE1 Inh	4.2
pI3Kγ Ant	<4.5
LCK Ant	<4.5
Aurora B Ant	<4.5
COX2 Block	<4.0
α1 nicotinic AchR open	<4.2
α1 nicotinic AchR block	<4.2

Table 5.02: Cross screening panel data for 2.061·HCl.

Assay	2.061·HCl (pXC$_{50}$)	3.039 (pXC$_{50}$)
hERG Qube Ant	<4.3	4.7
Phospholipidosis Accum	<4.0	4.0
MrgX2 Ag	<4.0	5.3
Adrenergic α1b Ant	<4.6	4.9
Adrenergic β2 Ag	<4.0	<4.0
Adrenergic β2 Ant	<4.0	<4.0
Dopamine 1 Ant	<4.0	<4.0
Histamine 1Ant	<4.6	<4.6
Muscarine Ag	<4.3	<4.3
Muscarine Ant	<4.3	<4.3
Neurokinin 1 Ant	<4.6	<4.6
Serotonin 1B Ag	4.8	5.7
Serotonin 2A Ag	<4.0	<4.0
Serotonin 2A Ant	<4.0	<4.0
Serotonin 2C Ag	<4.0	4.7
Serotonin 2C Ant	<4.0	4.3
Vasopressin 1a Ant	<4.3	<4.3
Monoamine oxidase A Inh	<4.0	<4.0
PDE4B Ant	4.9	<4.0
PDE3A Inh	<4.0	<4.0
AChEase Inh	<4.0	4.3
KCNQ1/mink Block	<4.6	<4.6
Kv1.5 Block	<4.3	<4.3
Cav1.2 Qube Block	<4.0	<4.0
Nav1.5 Qube Block	<4.3	<4.3
Serotonin 3 Open	<4.3	<4.3
Serotonin 3 Block	<4.3	<4.3
NMDA/NR2B Block	<4.0	<4.0
CYP3A4 Ant	5.5	4.8
Noradrenaline-NET Ant	<4.0	<4.0
OATP1B1 Inh	<4.3	<4.3
Serotonin-SERT Ant	<4.0	4.1
PXR Ag	<4.3	<4.3
AhR Ag	<4.0	<4.0
BSEP Inh	4.3	4.1
Androgen Receptor Ag	-	<4.0
Glucocorticoid Receptor Ag	-	<4.0
Serotonin 2B Ag	<4.0	<4.0
CB1 Ag	4.7	<4.0
CHO null host Calcium Ag	<4.0	<4.0

Table 5.03: Cross screening panel data for 2.061·HCl and 3.039.

5.3 BROMO*scan* Full-Curve Data for Compound 3.039

Compound **3.039** was screened against the DiscoverX BROMO*scan* panel of 40 bromodomains. 11-point dose-response curves were measured up to a maximum concentration of 30 µM. The K_D and corresponding pK_D values calculated are shown in **Table 5.04**.

Bromodomain	K_D (nM)	pK_D
ATAD2A	>30000	<4.5
ATAD2B	>30000	<4.5
BAZ2A	>30000	<4.5
BAZ2B	>30000	<4.5
BRD1	>30000	<4.5
BRD2(1)	>30000	<4.5
BRD2(1,2)	>30000	<4.5
BRD2(2)	>30000	<4.5
BRD3(1)	>30000	<4.5
BRD3(1,2)	>30000	<4.5
BRD3(2)	>30000	<4.5
BRD4(1)	>30000	<4.5
BRD4(1,2)	>30000	<4.5
BRD4(2)	>30000	<4.5
BRD4(full-length,short-iso.)	>30000	<4.5
BRD7	560	6.3
BRD8(1)	>30000	<4.5
BRD8(2)	>30000	<4.5
BRD9	64	7.2
BRDT(1)	>30000	<4.5
BRDT(1,2)	>30000	<4.5
BRDT(2)	>30000	<4.5
BRPF1	>30000	<4.5
BRPF3	>30000	<4.5
CECR2	>30000	<4.5
CREBBP	>30000	<4.5
EP300	>30000	<4.5
FALZ	>30000	<4.5
GCN5L2	>30000	<4.5
PBRM1(2)	>30000	<4.5
PBRM1(5)	>30000	<4.5
PCAF	>30000	<4.5
SMARCA2	>30000	<4.5

SMARCA4	>30000	<4.5
TAF1(2)	>30000	<4.5
TAF1L(2)	>30000	<4.5
TRIM24 (Bromo.)	>30000	<4.5
Trim24 (PHD,Bromo.)	>30000	<4.5
TRIM33 (PHD,Bromo.)	>30000	<4.5
WDR9(2)	18000	4.7

Table 5.04: DiscoverX BROMO*scan* data for compound 3.039.

5.4 Compound 3.028, 3.029, 3.063a and 3.063b NMR Evidence

Rotating-frame nuclear Overhauser effect spectroscopy (ROESY) was used to support the assignment of **3.028** and **3.029** as their respective regioisomers. Unlike many traditional 2D NMR techniques,[228] which show through-bond nuclei-correlation, ROESY identifies correlations between nuclei through space.[229] For regioisomer **3.028**, a strong correlation was observed between the pyridazinone hydrogen (labelled by the number 6) and the benzylic hydrogens (labelled by the number 9) (**Figure 5.01**), suggesting the two proton environments are in close proximity to one another, and the amine is appended to the 5-position. This signal was not observed in the ROESY spectrum for **3.029** (**Figure 5.02**), suggesting the two proton environments are further apart, and the amine was appended at the 4-position.
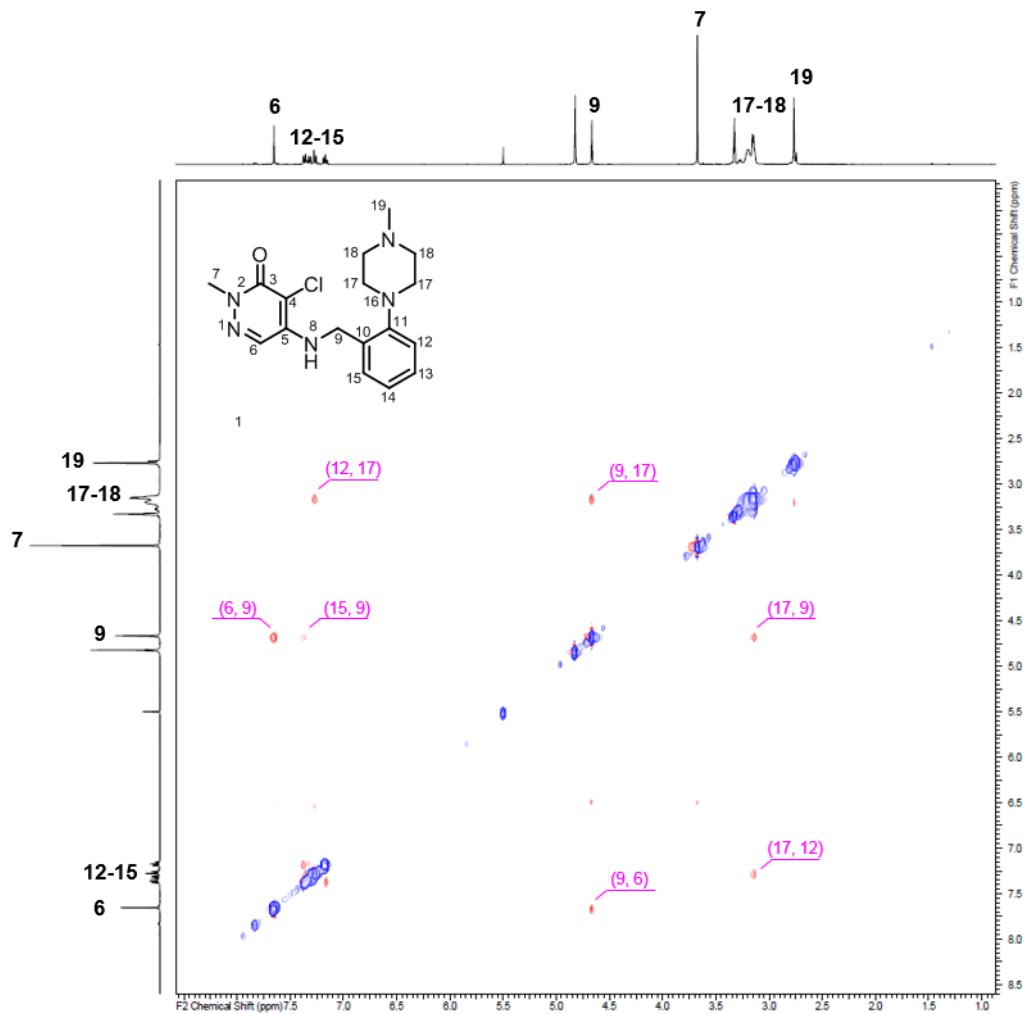
Figure 5.01: Compound 3.028 ROSEY spectrum.
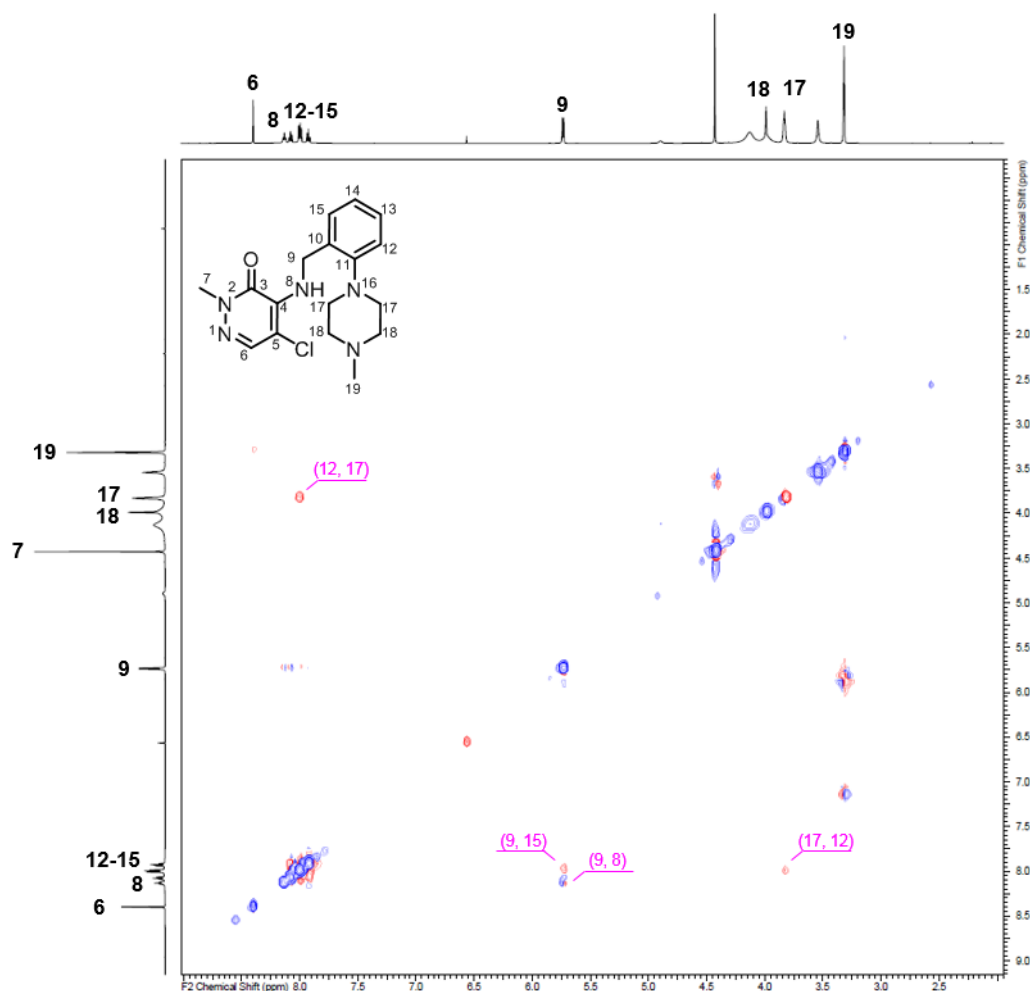
Figure 5.02: Compound 3.029 ROSEY spectrum.

Heteronuclear multiple-bond correlation spectroscopy (HMBC), a 2D NMR technique which shows through-bond correlations (typically 2-4 bonds) between heteronuclei,[230] was used to support the assignment of **3.063b** and **3.063a** as their respective regioisomers. ^{15}NHMBC was utilized to establish the position of the triazolopyridazine hydrogen and the respective nitrogens, starting with compound **3.063a** (**Figure 5.02**). Two strong correlations were observed between the protons labelled 13 and the nitrogen signals at 213.1 and 318.4 ppm, therefore assigned as nitrogens 4 and 2 respectively. Similarly, a strong correlation was also seen from triazolopyridazine proton (12) to nitrogen 4, suggesting proton 12 was three bonds away, and was therefore assigned as **3.063a**.
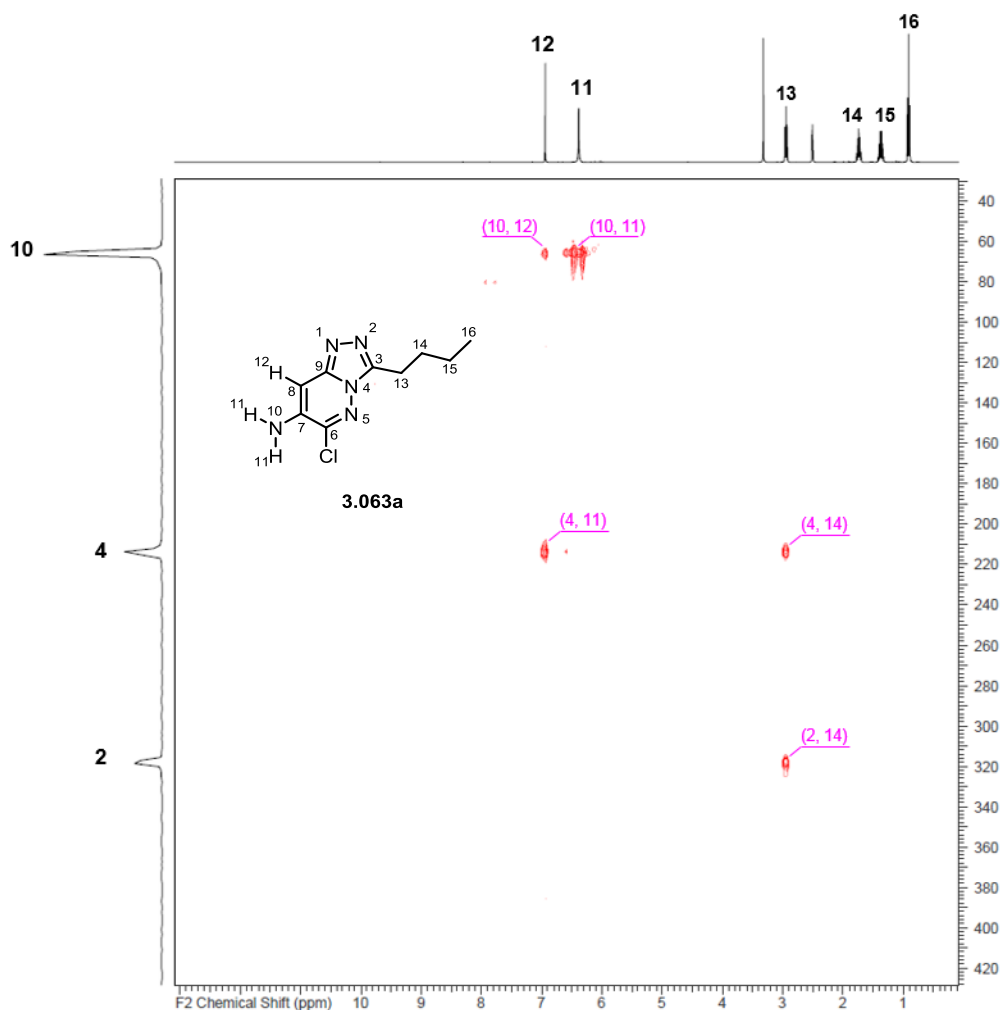
Figure 5.03: Compound 3.063a ^{15}NHMBC spectrum.

The ROESY spectrum of **3.063b** showed the same strong correlation between the protons labelled 13 and nitrogens 4 and 2. The triazolopyridazine proton (12) was shown to be correlating to two different nitrogens at 255.6 and 295.1 ppm, assigned as nitrogens 5 and 1 respectively. The lack of correlation between the triazolopyridazine proton (12) and nitrogen 4 suggested that proton 12 was now further away than in **3.063a** and was therefore assigned as regioisomer **3.063b** where they are separated by four bonds.
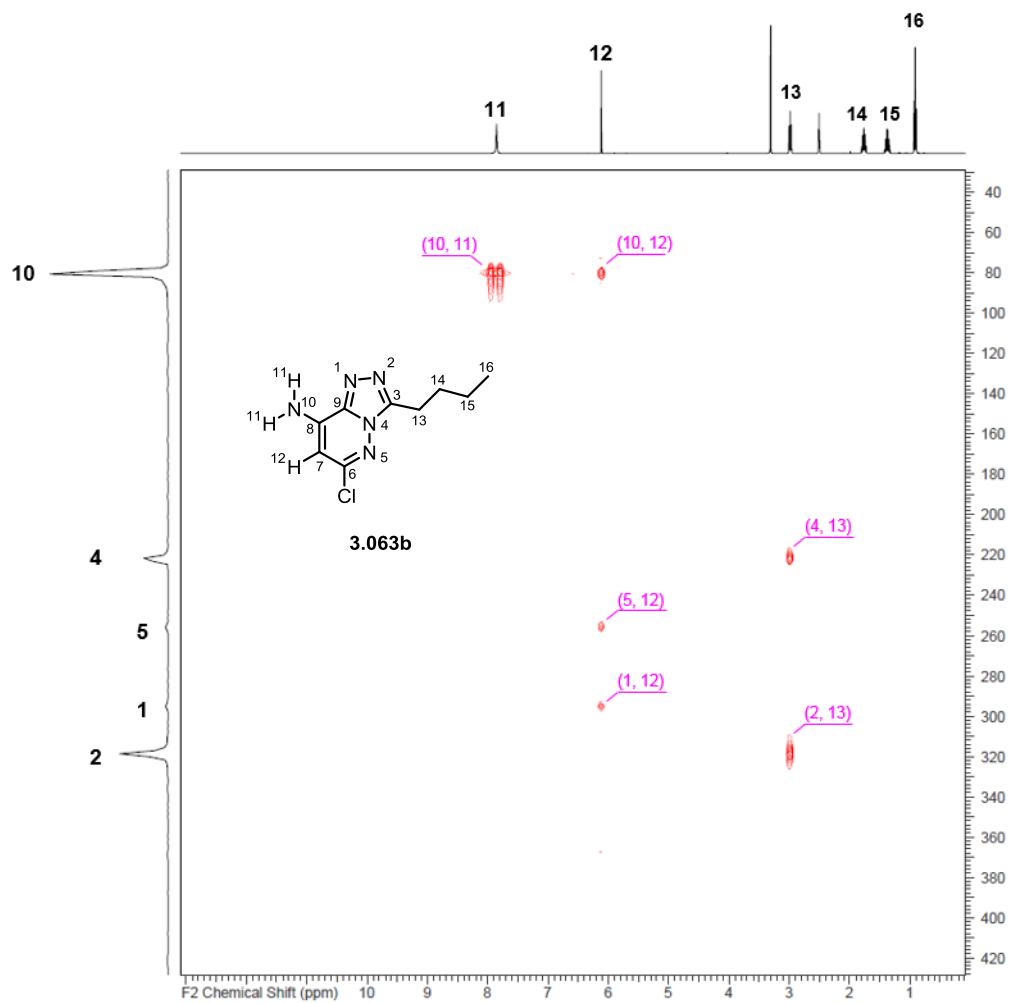
Figure 5.04: Compound 3.063b ^{15}NHMBC spectrum.

6. References

(1)   Dahm, R. *Dev. Biol.* **2005**, *278*, 274–288.

(2)   Franklin, R. E.; Gosling, R. G. *Nature* **1953**, *171*, 740–741.

(3)   Wilkins, M. H. F.; Stokes, A. R.; Wilson, H. R. *Nature* **1953**, *171*, 738–740.

(4)   Watson, J. D.; Crick, F. H. C. *Nature* **1953**, *171*, 737–738.

(5)   Griffiths, A. J.; Miller, J. H.; Suzuki, D. T.; Lewontin, R. C.; Gelbart, W. M. *An Introduction to Genetic Analysis*, 7th ed.; W. H. Freeman: New York, 2000.

(6)   Sinden, R. R. *DNA Structure and Function*; Academic Press: San Diego, 1994.

(7)   Ohyama, T. *DNA Conformation and Transcription*; Springer: New York, 2005.

(8)   Discovery of DNA Double Helix: Watson and Crick. https://www.nature.com/scitable/topicpage/discovery-of-dna-structure-and-function-watson-397/ (accessed Oct 16, 2019).

(9)   Franklin, R. E.; Gosling, R. G. *Acta Crystallogr.* **1953**, *6*, 673–677.

(10)   Taillandier, E.; Liquier, J. *Methods Enzymol.* **1992**, *211*, 307–335.

(11)   Brahms, J.; Pilet, J.; Lan, T.-T. P.; Hill, L. R. *Proc. Natl. Acad. Sci.* **1973**, *70*, 3352–3355.

(12)   Wood, B. R. *Chem. Soc. Rev.* **2016**, *45*, 1980–1998.

(13)   Berg, J. M.; Tymoczko, J. L.; Stryer, L. *Biochemistry*, 5th ed.; W.H. Freeman: New York, 2002.

(14)   Ussery, D. W. DNA Structure: A-, B- and Z-DNA Helix Families. In *Encyclopedia of Life Sciences*; Macmillan Publishers: London, 2002.

(15)   Burge, S.; Parkinson, G. N.; Hazel, P.; Todd, A. K.; Neidle, S. *Nucleic Acids Res.* **2006**, *34*, 5402–5415.

(16)   A-DNA, B-DNA, Z-DNA - Public Domain Image. https://en.wikipedia.org/wiki/DNA#/media/File:A-DNA,_B-DNA_and_Z-DNA.png (accessed Oct 16, 2019).

(17)   Abrahem, A.; Pelchat, M. *Nucleic Acids Res.* **2008**, *36*, 5201–5211.

(18)   Merrick, W. C. *J. Biol. Chem.* **2010**, *285*, 21197–21201.

(19)   Crick, F. *Nature* **1970**, *227*, 561–562.

(20)   International, Human Genome Sequencing Consortium *Nature* **2004**, *431*, 931–945.

(21)   Arrowsmith, C. H.; Bountra, C.; Fish, P. V.; Lee, K.; Schapira, M. *Nat. Rev. Drug Discov.* **2012**, *11*, 384–400.

(22)   Goldberg, A. D.; Allis, C. D.; Bernstein, E. *Cell* **2007**, *128*, 635–638.

(23)   Egger, G.; Liang, G.; Aparicio, A.; Jones, P. A. *Nature* **2004**, *429*, 457–463.

(24)   Kulis, M.; Esteller, M. DNA Methylation and Cancer. In *Advances in Genetics*; Academic Press: San Diego, 2010.

(25)   Martin, C.; Zhang, Y. *Nat. Rev. Mol. Cell Biol.* **2005**, *6*, 838–849.

(26)   Verdone, L.; Caserta, M.; Di Mauro, E. *Biochem. Cell Biol.* **2005**, *83*, 344–353.

(27)   Cao, J.; Yan, Q. *Front. Oncol.* **2012**, *2*, 1–9.

(28)   Rossetto, D.; Avvakumov, N.; Côté, J. *Epigenetics* **2012**, *7*, 1098–1108.

(29)   Shiio, Y.; Eisenman, R. N. *Proc. Natl. Acad. Sci.* **2003**, *100*, 13225–13230.

(30)   Verdone, L.; La Fortezza, M.; Ciccarone, F.; Caiafa, P.; Zampieri, M.; Caserta, M. *PLoS One* **2015**, *10*, 1–14.

(31)   Berg, J. M.; Tymoczko, J. L.; Stryer, L. *Biochemistry*, 5th ed.; W H Freeman: New York, 2002.

(32)   Handy, D. E.; Castro, R.; Loscalzo, J. *Circulation* **2011**, *123*, 2145–2156.

(33)   McGinty, R. K.; Tan, S. Histone, Nucleosome, and Chromatin Structure. In *Fundamentals of Chromatin*; Springer: New York, 2014.

(34)   Venkatesh, S.; Workman, J. L. *Nat. Rev. Mol. Cell Biol.* **2015**, *16*, 178–189.

(35)   Luger, K.; Mäder, A. W.; Richmond, R. K.; Sargent, D. F.; Richmond, T. J. *Nature* **1997**, *389*, 251–260.

(36)   Peterson, C. L.; Laniel, M.-A. *Current Biology*. 2004, pp R546–R551.

(37)   Tarakhovsky, A. *Nat. Immunol.* **2010**, *11*, 565–568.

(38)   Roth, S. Y.; Denu, J. M.; Allis, C. D. *Annu. Rev. Biochem.* **2001**, *70*, 81–120.

(39)   Jain, A. K.; Barton, M. C. *J. Mol. Biol.* **2017**, *429*, 2003–2010.

(40)   Chen, H.; Tini, M.; Evans, R. M. *Curr. Opin. Cell Biol.* **2001**, *13*, 218–224.

(41)   Allis, C. D.; Jenuwein, T. *Nat. Rev. Genet.* **2016**, *17*, 487–500.

(42)   Haynes, S. R.; Dollard, C.; Winston, F.; Beck, S.; Trowsdale, J.; Dawid, I. B. *Nucleic Acids Res.* **1992**, *20*, 2603.

(43)   Elfring, L. K.; Daniel, C.; Papoulas, O.; Deuring, R.; Sarte, M.; Moseley, S.; Beek, S. J.; Waldrip, W. R.; Daubresse, G.; DePace, A.; Kennison, J. A.; Tamkun, J. W. *Genetics* **1998**, *148*, 251–265.

(44)   Dhalluin, C.; Carlson, J. E.; Zeng, L.; He, C.; Aggarwal, A. K.; Zhou, M.-M. *Nature* **1999**, *399*, 491–496.

(45)   Meslamani, J.; Smith, S. G.; Sanchez, R.; Zhou, M.-M. *Bioinformatics* **2014**, *30*, 1481–1483.

(46)   Fish, P. V; Filippakopoulos, P.; Bish, G.; Brennan, P. E.; Bunnage, M. E.; Cook, A. S.; Federov, O.; Gerstenberger, B. S.; Jones, H.; Knapp, S.; Marsden, B.; Nocka, K.; Owen, D. R.; Philpott, M.; Picaud, S.; Primiano, M. J.; Ralph, M. J.; Sciammetta, N.; Trzupek, J. D. *J. Med. Chem.* **2012**, *55*, 9831–9837.

(47)   Unzue, A.; Zhao, H.; Lolli, G.; Dong, J.; Zhu, J.; Zechner, M.; Dolbois, A.; Caflisch, A.; Nevado, C. *J. Med. Chem.* **2016**, *59*, 3087–3097.

(48)   Meslamani, J.; Smith, S. G.; Sanchez, R.; Zhou, M.-M. *Drug Discov. Today Technol.* **2016**, *19*, 3–15.

(49)   Noguchi-Yachide, T. *Chem. Pharm. Bull* **2016**, *540*, 540–547.

(50)   Moustakim, M.; Clark, P. G. K.; Hay, D. A.; Dixon, D. J.; Brennan, P. E. *Medchemcomm* **2016**, *7*, 2246–2264.

(51)   Theodoulou, N. H.; Bamborough, P.; Bannister, A. J.; Becher, I.; Bit, R. A.; Che, K. H.; Chung, C.; Dittmann, A.; Drewes, G.; Drewry, D. H.; Gordon, L.; Grandi, P.; Leveridge, M.; Lindon, M.; Michon, A.-M.; Molnar, J.; Robson, S. C.; Tomkinson, N. C. O.; Kouzarides, T.; Prinjha, R. K.; Humphreys, P. G. *J. Med. Chem.* **2016**, *59*, 1425–1439.

(52)   Fogel, D. B. *Contemp. Clin. trials Commun.* **2018**, *11*, 156–164.

(53)   Jones, L. H. *Expert Opin. Drug Discov.* **2016**, *11*, 623–625.

(54)   Jain, K. K. *Drug Discov. Today* **2004**, *9*, 307–309.

(55)   Smith, C. *Nature* **2003**, *422*, 341–347.

(56) Oprea, T. I.; Bologa, C. G.; Boyer, S.; Curpan, R. F.; Glen, R. C.; Hopkins, A. L.; Lipinski, C. A.; Marshall, G. R.; Martin, Y. C.; Ostopovici-Halip, L.; Rishton, G.; Ursu, O.; Vaz, R. J.; Waller, C.; Waldmann, H.; Sklar, L. A. *Nat. Chem. Biol.* **2009**, *5*, 441–447.

(57) Frye, S. V. *Nat. Chem. Biol.* **2010**, *6*, 159–161.

(58) Theodoulou, N. H.; Tomkinson, N. C. O.; Prinjha, R. K.; Humphreys, P. G. *ChemMedChem* **2016**, *11*, 477–487.

(59) Zheng, J. *Formulation and analytical development for low-dose oral drug products*, 1st ed.; John Wiley & Sons: Hoboken, 2009.

(60) Mirguet, O.; Gosmini, R.; Toum, J.; Clément, C. A.; Barnathan, M.; Brusq, J.-M.; Mordaunt, J. E.; Grimes, R. M.; Crowe, M.; Pineau, O.; Ajakane, M.; Daugan, A.; Jeffrey, P.; Cutler, L.; Haynes, A. C.; Smithers, N. N.; Chung, C.; Bamborough, P.; Uings, I. J.; Lewis, A.; Witherington, J.; Parr, N.; Prinjha, R. K.; Nicodème, E. *J. Med. Chem.* **2013**, *56*, 7501–7515.

(61) Filippakopoulos, P.; Qi, J.; Picaud, S.; Shen, Y.; Smith, W. B.; Fedorov, O.; Morse, E. M.; Keates, T.; Hickman, T. T.; Felletar, I.; Philpott, M.; Munro, S.; McKeown, M. R.; Wang, Y.; Christie, A. L.; West, N.; Cameron, M. J.; Schwartz, B.; Heightman, T. D.; La Thangue, N.; French, C. A.; Wiest, O.; Kung, A. L.; Knapp, S.; Bradner, J. E. *Nature* **2010**, *468*, 1067–1073.

(62) Arrowsmith, C. H.; Audia, J. E.; Austin, C.; Baell, J.; Bennett, J.; Blagg, J.; Bountra, C.; Brennan, P. E.; Brown, P. J.; Bunnage, M. E.; Buser-Doepner, C.; Campbell, R. M.; Carter, A. J.; Cohen, P.; Copeland, R. A.; Cravatt, B.; Dahlin, J. L.; Dhanak, D.; Edwards, A. M.; Frederiksen, M.; Frye, S. V; Gray, N.; Grimshaw, C. E.; Hepworth, D.; Howe, T.; Huber, K. V. M.; Jin, J.; Knapp, S.; Kotz, J. D.; Kruger, R. G.; Lowe, D.; Mader, M. M.; Marsden, B.; Mueller-Fahrnow, A.; Müller, S.; O'Hagan, R. C.; Overington, J. P.; Owen, D. R.; Rosenberg, S. H.; Roth, B.; Ross, R.; Schapira, M.; Schreiber, S. L.; Shoichet, B.; Sundström, M.; Superti-Furga, G.; Taunton, J.; Toledo-Sherman, L.; Walpole, C.; Walters, M. A.; Willson, T. M.; Workman, P.; Young, R. N.; Zuercher, W. J. *Nat. Chem. Biol.* **2015**, *11*, 536–542.

(63) Scott, A. R. *Nature* **2016**, *533*, S60–S61.

(64) Zhang, G.; Smith, S. G.; Zhou, M.-M. *Chem. Rev.* **2015**, *115*, 11625–11668.

(65) Home - ClinicalTrials.gov. https://clinicaltrials.gov/ct2/home (accessed Oct 25, 2019).

(66) Nelson, K. M.; Dahlin, J. L.; Bisson, J.; Graham, J.; Pauli, G. F.; Walters,

M. A. *J. Med. Chem.* **2017**, *60*, 1620–1637.

(67)   Kuttan, R.; Bhanumathy, P.; Nirmala, K.; George, M. C. *Cancer Lett.* **1985**, *29*, 197–202.

(68)   Baell, J. B.; Holloway, G. A. *J. Med. Chem.* **2010**, *53*, 2719–2740.

(69)   Baell, J. B.; Nissink, J. W. M. *ACS Chem. Biol.* **2018**, *13*, 36–44.

(70)   Priyadarsini, K. I. *Curr. Pharm. Des.* **2013**, *19*, 2093–2100.

(71)   Baell, J.; Walters, M. A. *Nature* **2014**, *513*, 481–483.

(72)   Baell, J. B. *J. Nat. Prod.* **2016**, *79*, 616–628.

(73)   Bunnage, M. E.; Piatnitski Chekler, E. L.; Jones, L. H. *Nat. Chem. Biol.* **2013**, *9*, 195–199.

(74)   Ottaviani, G.; Martel, S.; Carrupt, P.-A. *J. Med. Chem.* **2006**, *49*, 3948–3954.

(75)   Volpe, D. A. *Future Med. Chem.* **2011**, *3*, 2063–2077.

(76)   Gordon, L. J.; Allen, M.; Artursson, P.; Hann, M. M.; Leavens, B. J.; Mateus, A.; Readshaw, S.; Valko, K.; Wayne, G. J.; West, A. *J. Biomol. Screen.* **2016**, *21*, 156–164.

(77)   Mateus, A.; Gordon, L. J.; Wayne, G. J.; Almqvist, H.; Axelsson, H.; Seashore-Ludlow, B.; Treyer, A.; Matsson, P.; Lundbäck, T.; West, A.; Hann, M. M.; Artursson, P. *Proc. Natl. Acad. Sci.* **2017**, *114*, E6231–E6239.

(78)   Di, L.; Kerns, E. H. *Drug-like properties : concepts, structure design and methods from ADME to toxicity optimization*, 2nd ed.; Academic Press: Burlington, 2016.

(79)   Young, R. J.; Green, D. V. S.; Luscombe, C. N.; Hill, A. P. *Drug Discov. Today* **2011**, *16*, 822–830.

(80)   Valkó, K.; Bevan, C.; Reynolds, D. *Anal. Chem.* **1997**, *69*, 2022–2029.

(81)   Robinson, M. W.; Hill, A. P.; Readshaw, S. A.; Hollerton, J. C.; Upton, R. J.; Lynn, S. M.; Besley, S. C.; Boughtflower, B. J. *Anal. Chem.* **2017**, *89*, 1772–1777.

(82)   Lin, B.; Pease, J. H. *J. Pharm. Biomed. Anal.* **2016**, *122*, 126–140.

(83)   Lane, S.; Boughtflower, B.; Mutton, I.; Paterson, C.; Farrant, D.; Taylor, N.; Blaxill, Z.; Carmody, C.; Borman, P. *Anal. Chem.* **2005**, *77*, 4354–4365.

(84)   Yan, Y.; Marriott, G. *Curr. Opin. Chem. Biol.* **2003**, *7*, 635–640.

(85) de Jong, L. A. A.; Uges, D. R. A.; Franke, J. P.; Bischoff, R. *J. Chromatogr. B* **2005**, *829*, 1–25.

(86) Yasgar, A.; Jadhav, A.; Simeonov, A.; Coussens, N. P. *Methods Mol. Biol.* **2016**, *1439*, 77–98.

(87) Leavitt, S.; Freire, E. *Curr. Opin. Struct. Biol.* **2001**, *11*, 560–566.

(88) Niesen, F. H.; Berglund, H.; Vedadi, M. *Nat. Protoc.* **2007**, *2*, 2212–2221.

(89) Hopkins, A. L.; Keserü, G. M.; Leeson, P. D.; Rees, D. C.; Reynolds, C. H. *Nat. Rev. Drug Discov.* **2014**, *13*, 105–121.

(90) Johnson, T. W.; Gallego, R. A.; Edwards, M. P. *J. Med. Chem.* **2018**, *61*, 6401–6420.

(91) Machleidt, T.; Woodroofe, C. C.; Schwinn, M. K.; Méndez, J.; Robers, M. B.; Zimmerman, K.; Otto, P.; Daniels, D. L.; Kirkland, T. A.; Wood, K. V. *ACS Chem. Biol.* **2015**, *10*, 1797–1804.

(92) Carisey, A.; Stroud, M.; Tsang, R.; Ballestrem, C. Fluorescence Recovery After Photobleaching. In *Cell Migration Developmental Methods and Protocols*; Humana Press: New Jersey, 2011.

(93) Workman, P.; Collins, I. *Chem. Biol.* **2010**, *17*, 561–577.

(94) NCT03568656 - Study to Evaluate CCS1477 in Advanced Tumours. https://clinicaltrials.gov/ct2/show/NCT03568656?term=CCS1477&rank =1 (accessed Sep 30, 2019).

(95) CCS14 Scientific Posters. https://www.cellcentric.com/ccs1477/Publications/ (accessed Sep 30, 2019).

(96) Clegg, M. A.; Tomkinson, N. C. O.; Prinjha, R. K.; Humphreys, P. G. *ChemMedChem* **2019**, *14*, 362–385.

(97) Modak, R.; Basha, J.; Bharathy, N.; Maity, K.; Mizar, P.; Bhat, A. V.; Vasudevan, M.; Rao, V. K.; Kok, W. K.; Natesh, N.; Taneja, R.; Kundu, T. K. *ACS Chem. Biol.* **2013**, *8*, 1311–1323.

(98) Malatesta, M.; Steinhauer, C.; Mohammad, F.; Pandey, D. P.; Squatrito, M.; Helin, K. *Cancer Res.* **2013**, *73*, 6323–6333.

(99) Stimson, L.; Rowlands, M. G.; Newbatt, Y. M.; Smith, N. F.; Raynaud, F. I.; Rogers, P.; Bavetsias, V.; Gorsuch, S.; Jarman, M.; Bannister, A.; Kouzarides, T.; McDonald, E.; Workman, P.; Aherne, G. W. *Mol. Cancer Ther.* **2005**, *4*, 1521–1532.

(100) Duclot, F.; Meffre, J.; Jacquet, C.; Gongora, C.; Maurice, T. *Neuroscience* **2010**, *167*, 850–863.

(101) Zhou, M. M.; Gerona-Navarro, G.; Rodriguez-Fernandez, Y.; Casaccia, P. Small molecule transcription modulators of bromodomains. WO 2015/184257 A2, 2015.

(102) Mujtaba, S.; He, Y.; Zeng, L.; Farooq, A.; Carlson, J. E.; Ott, M.; Verdin, E.; Zhou, M.-M. *Mol. Cell* **2002**, *9*, 575–586.

(103) Quy, V. C.; Pantano, S.; Rossetti, G.; Giacca, M.; Carloni, P. *Biology (Basel).* **2012**, *1*, 277–296.

(104) Kiernan, R. E.; Vanhulle, C.; Schiltz, L.; Adam, E.; Xiao, H.; Maudoux, F.; Calomme, C.; Burny, A.; Nakatani, Y.; Jeang, K.; Benkirane, M.; Van Lint, C. *EMBO J.* **1999**, *18*, 6106–6118.

(105) Albrecht, B. K.; Burdick, D. J.; Cote, A.; Duplessis, M.; Nasveschuk, C. G.; Taylor, A. M. Pyridazinone Derivatives and their Use in the Treatment of Cancer. WO 2016/112298 A1, 2016.

(106) Albrecht, B. K.; Cote, A.; Crawford, T.; Duplessis, M.; Good, A. C.; Leblanc, Y.; Magnuson, S.; Nasveschuk, C. G.; Pastor, R.; Romero, F. A.; Taylor, A. M. Phthalazine derivatives of formula (1) as PCAF and GCN5 inhibitors for use in the treatment of cancer. WO 2016/036954 A1, 2016.

(107) Albrecht, B. K.; Cote, A.; Crawford, T.; Duplessis, M.; Good, A. C.; Leblanc, Y.; Magnuson, S. R.; Nasveschuk, C. G.; Romero, A. F.; Tang, Y.; Taylor, A. M. Therapeutic pyridazine compounds and uses thereof. WO 2016/138114 A1, 2016.

(108) Humphreys, P. G.; Bamborough, P.; Chung, C.; Craggs, P. D.; Gordon, L.; Grandi, P.; Hayhow, T. G.; Hussain, J.; Jones, K. L.; Lindon, M.; Michon, A.-M.; Renaux, J. F.; Suckling, C. J.; Tough, D. F.; Prinjha, R. K. *J. Med. Chem.* **2017**, *60*, 695–709.

(109) Moustakim, M.; Clark, P. G. K.; Trulli, L.; Fuentes de Arriba, A. L.; Ehebauer, M. T.; Chaikuad, A.; Murphy, E. J.; Mendez-Johnson, J.; Daniels, D.; Hou, C.-F. D.; Lin, Y.-H.; Walker, J. R.; Hui, R.; Yang, H.; Dorrell, L.; Rogers, C. M.; Monteiro, O. P.; Fedorov, O.; Huber, K. V. M.; Knapp, S.; Heer, J.; Dixon, D. J.; Brennan, P. E. *Angew. Chem. Int. Ed.* **2017**, *56*, 827–831.

(110) Caron, C.; Lestrat, C.; Marsal, S.; Escoffier, E.; Curtet, S.; Virolle, V.; Barbry, P.; Debernardi, A.; Brambilla, C.; Brambilla, E.; Rousseaux, S.; Khochbin, S. *Oncogene* **2010**, *29*, 5171–5181.

(111) Chen, X.; Cheung, S. T.; So, S.; Fan, S. T.; Barry, C.; Higgins, J.; Lai, K.-M.; Ji, J.; Dudoit, S.; Ng, I. O. L.; Van De Rijn, M.; Botstein, D.; Brown, P. O. *Mol. Biol. Cell* **2002**, *13*, 1929–1939.

(112) Urbanucci, A.; Barfeld, S.; Kytölä, V.; Itkonen, H. M.; Coleman, I. M.;

Vodák, D.; Sjöblom, L.; Sheng, X.; Tolonen, T.; Minner, S.; Burdelski, C.; Kivinummi, K. K.; Kohvakka, A.; Kregel, S.; Takhar, M.; Alshalalfa, M.; Davicioni, E.; Erho, N.; Lloyd, P.; Karnes, R. J.; Ross, A. E.; Schaeffer, E. M.; Vander Griend, D. J.; Knapp, S.; Corey, E.; Feng, F. Y.; Nelson, P. S.; Saatcioglu, F.; Knudsen, K. E.; Tammela, T. L. J.; Sauter, G.; Schlomm, T.; Nykter, M.; Visakorpi, T.; Mills, I. G. *Cell Rep.* **2017**, *19*, 2045–2059.

(113) Kalashnikova, E. V.; Revenko, A. S.; Gemo, A. T.; Andrews, N. P.; Tepper, C. G.; Zou, J. X.; Cardiff, R. D.; Borowsky, A. D.; Chen, H. W. *Cancer Res.* **2010**, *70*, 9402–9412.

(114) Raeder, M. B.; Birkeland, E.; Trovik, J.; Krakstad, C.; Shehata, S.; Schumacher, S.; Zack, T. I.; Krohn, A.; Werner, H. M.; Moody, S. E.; Wik, E.; Stefansson, I. M.; Holst, F.; Oyan, A. M.; Tamayo, P.; Mesirov, J. P.; Kalland, K. H.; Akslen, L. A.; Simon, R.; Beroukhim, R.; Salvesen, H. B. *PLoS One* **2013**, *8*, e54873.

(115) Ciro, M.; Prosperini, E.; Quarto, M.; Grazini, U.; Walfridsson, J.; McBlane, F.; Nucifero, P.; Pacchiana, G.; Capra, M.; Christensen, J.; Helin, K. *Cancer Res.* **2009**, *69*, 8491–8498.

(116) Bamborough, P.; Chung, C.; Furze, R. C.; Grandi, P.; Michon, A.-M.; Sheppard, R. J.; Barnett, H.; Diallo, H.; Dixon, D. P.; Douault, C.; Jones, E. J.; Karamshi, B.; Mitchell, D. J.; Prinjha, R. K.; Rau, C.; Watson, R. J.; Werner, T.; Demont, E. H. *J. Med. Chem.* **2015**, *58*, 6151–6178.

(117) Bamborough, P.; Chung, C.; Demont, E. H.; Furze, R. C.; Bannister, A. J.; Che, K. H.; Diallo, H.; Douault, C.; Grandi, P.; Kouzarides, T.; Michon, A.-M.; Mitchell, D. J.; Prinjha, R. K.; Rau, C.; Robson, S.; Sheppard, R. J.; Upton, R.; Watson, R. J. *Angew. Chem. Int. Ed.* **2016**, *55*, 11382–11386.

(118) Brown, T.; Swansbury, J.; Taj, M. M. *Leuk. Lymphoma* **2012**, *53*, 338–341.

(119) Carlson, S.; Glass, K. C. *J. Cell. Physiol.* **2014**, *229*, 1571–1574.

(120) Zhu, J.; Zhou, C.; Caflisch, A. *Eur. J. Med. Chem.* **2018**, *155*, 337–352.

(121) Igoe, N.; Bayle, E. D.; Fedorov, O.; Tallant, C.; Savitsky, P.; Rogers, C.; Owen, D. R.; Deb, G.; Somervaille, T. C. P.; Andrews, D. M.; Jones, N.; Cheasty, A.; Ryder, H.; Brennan, P. E.; Müller, S.; Knapp, S.; Fish, P. V. *J. Med. Chem.* **2017**, *60*, 668–680.

(122) Demont, E. H.; Bamborough, P.; Chung, C.; Craggs, P. D.; Fallon, D.; Gordon, L. J.; Grandi, P.; Hobbs, C. I.; Hussain, J.; Jones, E. J.; Le Gall, A.; Michon, A.-M.; Mitchell, D. J.; Prinjha, R. K.; Roberts, A. D.; Sheppard, R. J.; Watson, R. J. *ACS Med. Chem. Lett.* **2014**, *5*, 1190–

1195.

(123) Bamborough, P.; Barnett, H. A.; Becher, I.; Bird, M. J.; Chung, C.; Craggs, P. D.; Demont, E. H.; Diallo, H.; Fallon, D. J.; Gordon, L. J.; Grandi, P.; Hobbs, C. I.; Hooper-Greenhill, E.; Jones, E. J.; Law, R. P.; Le Gall, A.; Lugo, D.; Michon, A.-M.; Mitchell, D. J.; Prinjha, R. K.; Sheppard, R. J.; Watson, A. J. B.; Watson, R. J. *ACS Med. Chem. Lett.* **2016**, *7*, 552–557.

(124) Clegg, M. A.; Tomkinson, N. C.; Prinjha, R. K.; Humphreys, P. G. *Future Med. Chem.* **2017**, *9*, 1579–1582.

(125) Anders, L.; Guenther, M. G.; Qi, J.; Fan, Z. P.; Marineau, J. J.; Rahl, P. B.; Lovén, J.; Sigova, A. A.; Smith, W. B.; Lee, T. I.; Bradner, J. E.; Young, R. A. *Nat. Biotechnol.* **2014**, *32*, 92–96.

(126) Tinworth, C. P.; Lithgow, H.; Churcher, I. *MedChemCommun.* **2016**, *7*, 2206–2216.

(127) Lai, A. C.; Toure, M.; Hellerschmied, D.; Salami, J.; Jaime-Figueroa, S.; Ko, E.; Hines, J.; Crews, C. M. *Angew. Chem. Int. Ed. Engl.* **2016**, *55*, 807–810.

(128) Robb, C. M.; Contreras, J. I.; Kour, S.; Taylor, M. A.; Abid, M.; Sonawane, Y. A.; Zahid, M.; Murry, D. J.; Natarajan, A.; Rana, S. *Chem. Commun. (Camb).* **2017**, *53*, 7577.

(129) Sakamoto, K. M.; Kim, K. B.; Verma, R.; Ransick, A.; Stein, B.; Crews, C. M.; Deshaies, R. J. *Mol. Cell. Proteomics* **2003**, *2*, 1350–1358.

(130) Puppala, D.; Lee, H.; Kim, K. B.; Swanson, H. I. *Mol. Pharmacol.* **2008**, *73*, 1064–1071.

(131) Yang, C.-Y.; Qin, C.; Bai, L.; Wang, S. *Drug Discov. Today Technol.* **2019**, *31*, 43–51.

(132) Gechijian, L. N.; Buckley, D. L.; Lawlor, M. A.; Reyes, J. M.; Paulk, J.; Ott, C. J.; Winter, G. E.; Erb, M. A.; Scott, T. G.; Xu, M.; Seo, H.-S.; Dhe-Paganon, S.; Kwiatkowski, N. P.; Perry, J. A.; Qi, J.; Gray, N. S.; Bradner, J. E. *Nat. Chem. Biol.* **2018**, *14*, 405–412.

(133) Farnaby, W.; Koegl, M.; Roy, M. J.; Whitworth, C.; Diers, E.; Trainor, N.; Zollman, D.; Steurer, S.; Karolyi-Oezguer, J.; Riedmueller, C.; Gmaschitz, T.; Wachter, J.; Dank, C.; Galant, M.; Sharps, B.; Rumpel, K.; Traxler, E.; Gerstberger, T.; Schnitzer, R.; Petermann, O.; Greb, P.; Weinstabl, H.; Bader, G.; Zoephel, A.; Weiss-Puxbaum, A.; Ehrenhöfer-Wölfer, K.; Wöhrle, S.; Boehmelt, G.; Rinnenthal, J.; Arnhof, H.; Wiechens, N.; Wu, M.-Y.; Owen-Hughes, T.; Ettmayer, P.; Pearson, M.; McConnell, D. B.; Ciulli, A. *Nat. Chem. Biol.* **2019**, *15*, 672–680.

(134) Bassi, Z. I.; Fillmore, M. C.; Miah, A. H.; Chapman, T. D.; Maller, C.; Roberts, E. J.; Davis, L. C.; Lewis, D. E.; Galwey, N. W.; Waddington, K. E.; Parravicini, V.; MacMillan-Jones, A. L.; Gongora, C.; Humphreys, P. G.; Churcher, I.; Prinjha, R. K.; Tough, D. F. *ACS Chem. Biol.* **2018**, *13*, 2862–2867.

(135) Robinson, P. J.; Trnka, M. J.; Bushnell, D. A.; Davis, R. E.; Mattei, P.-J.; Burlingame, A. L.; Kornberg, R. D. *Cell* **2016**, *166*, 1411–1422.

(136) TAF1 Human Bromodomain Amino Acid Sequence. https://www.uniprot.org/uniprot/P21675 (accessed Feb 8, 2019).

(137) Chung, C.; Coste, H.; White, J. H.; Mirguet, O.; Wilde, J.; Gosmini, R. L.; Delves, C.; Magny, S. M.; Woodward, R.; Hughes, S. A.; Boursier, E. V.; Flynn, H.; Bouillot, A. M.; Bamborough, P.; Brusq, J.-M. G.; Gellibert, F. J.; Jones, E. J.; Riou, A. M.; Homes, P.; Martin, S. L.; Uings, I. J.; Toum, J.; Clément, C. A.; Boullay, A.-B.; Grimley, R. L.; Blandel, F. M.; Prinjha, R. K.; Lee, K.; Kirilovsky, J.; Nicodeme, E. *J. Med. Chem.* **2011**, *54*, 3827–3838.

(138) Oh, H. R.; An, C. H.; Yoo, N. J.; Lee, S. H. *Pathol. Oncol. Res.* **2017**, *23*, 125–130.

(139) TAF1L TATA-box binding protein associated factor 1 like [Homo sapiens (human)]. https://www.ncbi.nlm.nih.gov/gene/138474 (accessed Oct 21, 2019).

(140) TAF1L Human Bromodomain Amino Acid Sequence. https://www.uniprot.org/uniprot/Q8IZX4 (accessed Feb 8, 2019).

(141) Centeno, F.; Ramírez-Salazar, E.; García-Villa, E.; Gariglio, P.; Garrido, E. *Intervirology* **2008**, *51*, 137–143.

(142) Tavassoli, P.; Wafa, L. A.; Cheng, H.; Zoubeidi, A.; Fazli, L.; Gleave, M.; Snoek, R.; Rennie, P. S. *Mol. Endocrinol.* **2010**, *24*, 696–708.

(143) Patel, A. B.; Louder, R. K.; Greber, B. J.; Grünberg, S.; Luo, J.; Fang, J.; Liu, Y.; Ranish, J.; Hahn, S.; Nogales, E. *Science (80-.).* **2018**, *362*, eaau8872.

(144) O'Rawe, J. A.; Wu, Y.; Dörfel, M. J.; Rope, A. F.; Au, P. Y. B.; Parboosingh, J. S.; Moon, S.; Kousi, M.; Kosma, K.; Smith, C. S.; Tzetis, M.; Schuette, J. L.; Jiménez-Barró, L. T.; Monaghan, K. G.; Wang, K.; Davis, E. E.; Katsanis, N.; Kalscheuer, V. M.; Wang, E. H.; Metcalfe, K.; Kleefstra, T.; Innes, A. M.; Kitsiou-Tzeli, S.; Rosello, M.; Keegan, C. E.; Lyon, G. J. *Am. J. Hum. Genet.* **2015**, *97*, 922–932.

(145) Domingo, A.; Amar, D.; Grütz, K.; Lee, L. V.; Rosales, R.; Brüggemann, N.; Jamora, R. D.; Cutiongco-dela Paz, E.; Rolfs, A.; Dressler, D.; Walter, U.; Krainc, D.; Lohmann, K.; Shamir, R.; Klein, C.;

Westenberger, A. *Cell. Mol. Life Sci.* **2016**, *73*, 3205–3215.

(146) Kawarai, T.; Morigaki, R.; Kaji, R.; Goto, S. *Brain Sci.* **2017**, *7*, 72–84.

(147) Makino, S.; Kaji, R.; Ando, S.; Tomizawa, M.; Yasuno, K.; Goto, S.; Matsumoto, S.; Tabuena, M. D.; Maranon, E.; Dantes, M.; Lee, L. V; Ogasawara, K.; Tooyama, I.; Akatsu, H.; Nishimura, M.; Tamiya, G. *Am. J. Hum. Genet.* **2007**, *80*, 393–406.

(148) Rakovic, A.; Domingo, A.; Grütz, K.; Kulikovskaja, L.; Capetian, P.; Cowley, S. A.; Lenz, I.; Brüggemann, N.; Rosales, R.; Jamora, D.; Rolfs, A.; Seibler, P.; Westenberger, A.; König, I.; Klein, C. *Mov. Disord.* **2018**, *33*, 1108–1118.

(149) Bhattacharya, S.; Lou, X.; Hwang, P.; Rajashankar, K. R.; Wang, X.; Gustafsson, J.-A.; Fletterick, R. J.; Jacobson, R. H.; Webb, P. *Proc. Natl. Acad. Sci.* **2014**, *111*, 9103–9108.

(150) Sdelci, S.; Lardeau, C.-H.; Tallant, C.; Klepsch, F.; Klaiber, B.; Bennett, J.; Rathert, P.; Schuster, M.; Penz, T.; Fedorov, O.; Superti-Furga, G.; Bock, C.; Zuber, J.; Huber, K. V. M.; Knapp, S.; Müller, S.; Kubicek, S. *Nat. Chem. Biol.* **2016**, *12*, 504–510.

(151) Sdelci, S.; Kubicek, S. TAF1 inhibitors for the therapy of cancer. WO 2017/140728 A1, 2017.

(152) Adler, M.; Burdick, D. J.; Crawford, T.; Duplessis, M.; Magnuson, S.; Nasveschuk, C. G.; Romero, F. A.; Tang, Y.; Tsui, V. H. and Wang, S. Therapeutic compounds and uses thereof. WO 2016/123391 A1, 2016.

(153) Bouché, L.; Christ, C. D.; Siegel, S.; Fernández-Montalván, A. E.; Holton, S. J.; Fedorov, O.; ter Laak, A.; Sugawara, T.; Stöckigt, D.; Tallant, C.; Bennett, J.; Monteiro, O.; Díaz-Sáez, L.; Siejka, P.; Meier, J.; Pütter, V.; Weiske, J.; Müller, S.; Huber, K. V. M.; Hartung, I. V.; Haendler, B. *J. Med. Chem.* **2017**, *60*, 4002–4022.

(154) McKeown, M. R.; Shaw, D. L.; Fu, H.; Liu, S.; Xu, X.; Marineau, J. J.; Huang, Y.; Zhang, X.; Buckley, D. L.; Kadam, A.; Zhang, Z.; Blacklow, S. C.; Qi, J.; Zhang, W.; Bradner, J. E. *J. Med. Chem.* **2014**, *57*, 9019–9027.

(155) Suh, J. L.; Watts, B.; Stuckey, J. I.; Norris-Drouin, J. L.; Cholensky, S. H.; Dickson, B. M.; An, Y.; Mathea, S.; Salah, E.; Knapp, S.; Khan, A.; Adams, A. T.; Strahl, B. D.; Sagum, C. A.; Bedford, M. T.; James, L. I.; Kireev, D. B.; Frye, S. V. *Biochemistry* **2018**, *57*, 2140–2149.

(156) Crawford, T. D.; Tsui, V.; Flynn, E. M.; Wang, S.; Taylor, A. M.; Cô, A.; Audia, J. E.; Beresini, M. H.; Burdick, D. J.; Cummings, R.; Dakin, L. A.; Duplessis, M.; Good, A. C.; Hewitt, M. C.; Huang, H.-R.; Jayaram, H.; Kiefer, J. R.; Jiang, Y.; Murray, J.; Nasveschuk, C. G.; Pardo, E.; Poy,

F.; Romero, F. A.; Tang, Y.; Wang, J.; Xu, Z.; Zawadzke, L. E.; Zhu, X.; Albrecht, B. K.; Magnuson, S. R.; Bellon, S.; Cochran, A. G. *J. Med. Chem.* **2016**, *59*, 5391–5402.

(157) Wang, S.; Tsui, V.; Crawford, T. D.; Audia, J. E.; Burdick, D. J.; Beresini, M. H.; Côté, A.; Cummings, R.; Duplessis, M.; Flynn, E. M.; Hewitt, M. C.; Huang, H.-R.; Jayaram, H.; Jiang, Y.; Joshi, S.; Murray, J.; Nasveschuk, C. G.; Pardo, E.; Poy, F.; Romero, F. A.; Tang, Y.; Taylor, A. M.; Wang, J.; Xu, Z.; Zawadzke, L. E.; Zhu, X.; Albrecht, B. K.; Magnuson, S. R.; Bellon, S.; Cochran, A. G. *J. Med. Chem.* **2018**, *61*, 9301–9315.

(158) Remillard, D.; Buckley, D. L.; Seo, H.-S.; Ferguson, F. M.; Dhe-Paganon, S.; Bradner, J. E.; Gray, N. S. *ACS Med. Chem. Lett.* **2019**, *10*, 1443–1449.

(159) Ciceri, P.; Müller, S.; O'Mahony, A.; Fedorov, O.; Filippakopoulos, P.; Hunt, J. P.; Lasater, E. A.; Pallares, G.; Picaud, S.; Wells, C.; Martin, S.; Wodicka, L. M.; Shah, N. P.; Treiber, D. K.; Knapp, S. *Nat. Chem. Biol.* **2014**, *10*, 305–312.

(160) Ember, S. W.; Zhu, J.-Y.; Olesen, S. H.; Martin, M. P.; Becker, A.; Berndt, N.; Georg, G. I.; Schönbrunn, E. *ACS Chem. Biol.* **2014**, *9*, 1160–1171.

(161) Theodoulou, N. Development of Chemical Probes for non-BET Bromodomains, PhD Thesis, University of Strathclyde, 2016.

(162) Demont, E. H.; Chung, C.; Furze, R. C.; Grandi, P.; Michon, A.-M.; Wellaway, C.; Barrett, N.; Bridges, A. M.; Craggs, P. D.; Diallo, H.; Dixon, D. P.; Douault, C.; Emmons, A. J.; Jones, E. J.; Karamshi, B. V.; Locke, K.; Mitchell, D. J.; Mouzon, B. H.; Prinjha, R. K.; Roberts, A. D.; Sheppard, R. J.; Watson, R. J.; Bamborough, P. *J. Med. Chem.* **2015**, *58*, 5649–5673.

(163) Leeson, P. *Nature* **2012**, *481*, 455–456.

(164) Tamaddon, F.; Tayefi, M.; Hosseini, E.; Zare, E. *J. Mol. Catal. A Chem.* **2013**, *366*, 36–42.

(165) ChemAxon - Software Solutions and Services for Chemistry & Biology. https://chemaxon.com/products/instant-jchem (accessed Apr 14, 2019).

(166) Manallack, D. T. *Perspect. Medicin. Chem.* **2007**, *1*, 25–38.

(167) Manallack, D. T.; Prankerd, R. J.; Yuriev, E.; Oprea, T. I.; Chalmers, D. K. *Chem. Soc. Rev.* **2013**, *42*, 485–496.

(168) Tehler, U.; Fagerberg, J. H.; Svensson, R.; Larhed, M.; Artursson, P.; Bergströ, C. A. S. *J. Med. Chem.* **2013**, *56*, 2690–2694.

(169) Di, L.; Kerns, E. H. *Blood-brain barrier in drug discovery : optimizing brain exposure of CNS drugs and minimizing brain side effects for peripheral drugs*; John Wiley & Sons: Hoboken, 2014.

(170) Lerchner, A.; Machauer, R.; Betschart, C.; Veenstra, S.; Rueeger, H.; McCarthy, C.; Tintelnot-Blomley, M.; Jaton, A.-L.; Rabe, S.; Desrayaud, S.; Enz, A.; Staufenbiel, M.; Paganetti, P.; Rondeau, J.-M.; Neumann, U. *Bioorg. Med. Chem. Lett.* **2010**, *20*, 603–607.

(171) Talele, T. T. *J. Med. Chem.* **2016**, *59*, 8712–8756.

(172) Pirrung, M. C. *Handbook of Synthetic Organic Chemistry*.; Academic Press: San Diego, 2016.

(173) Briggs, C. R. S.; O'Hagan, D.; Howard, J. A. K.; Yufit, D. S. *J. Fluor. Chem.* **2003**, *119*, 9–13.

(174) Wolfe, S. *Acc. Chem. Res.* **1972**, *5*, 102–111.

(175) Goodman, L.; Gu, H.; Pophristic, V. *J. Phys. Chem. A* **2005**, *109*, 1223–1229.

(176) Tavasli, M.; O'Hagan, D.; Pearson, C.; Petty, M. C. *Chem. Commun.* **2002**, 1226–1227.

(177) Linclau, B.; Leung, L.; Nonnenmacher, J.; Tizzard, G. *Beilstein J. Org. Chem.* **2010**, *6*, 62.

(178) Hunter, L. *Beilstein J. Org. Chem.* **2010**, *6*, 38.

(179) Sun, A.; Lankin, D. C.; Hardcastle, K.; Snyder, J. P. *Chem. - Eur. J.* **2005**, *11*, 1579–1591.

(180) Snyder, J. P.; Chandrakumar, N. S.; Sato, H.; Lankin, D. C. *J. Am. Chem. Soc.* **2000**, *122*, 544–545.

(181) Pfeifer, N. D.; Harris, K. B.; Yan, G. Z.; Brouwer, K. L. R. *Drug Metab. Dispos.* **2013**, *41*, 1949–1956.

(182) Cruciani, G.; Carosati, E.; De Boeck, B.; Ethirajulu, K.; Mackie, C.; Howe, T.; Vianello, R. *J. Med. Chem.* **2005**, *48*, 6970–6979.

(183) Molecular Discovery: MetaSite. https://www.moldiscovery.com/software/metasite/ (accessed Oct 25, 2019).

(184) Zhang, X.; Chen, K.; Wu, Y.-D.; Wiest, O. *PLoS One* **2017**, *12*, e0186570.

(185) Aldeghi, M.; Ross, G. A.; Bodkin, M. J.; Essex, J. W.; Knapp, S.; Biggin, P. C. *Commun. Chem.* **2018**, *1*, Article 19, 1–12.

(186) Nittinger, E.; Gibbons, P.; Eigenbrot, C.; Davies, D. R.; Maurer, B.; Yu, C. L.; Kiefer, J. R.; Kuglstatter, A.; Murray, J.; Ortwine, D. F.; Tang, Y.; Tsui, V. *J. Comput. Aided. Mol. Des.* **2019**, *33*, 307–330.

(187) Seo, J.; Igarashi, J.; Li, H.; Martasek, P.; Roman, L. J.; Poulos, T. L.; Silverman, R. B. *J. Med. Chem.* **2007**, *50*, 2089–2099.

(188) Robinson, D.; Bertrand, T.; Carry, J.-C.; Halley, F.; Karlsson, A.; Mathieu, M.; Minoux, H.; Perrin, M.-A.; Robert, B.; Schio, L.; Sherman, W. *J. Chem. Inf. Model.* **2016**, *56*, 886–894.

(189) Ladbury, J. E. *Chem. Biol.* **1996**, *3*, 973–980.

(190) Zhang, X.; Chen, K.; Wu, Y.-D.; Wiest, O. *PLoS One* **2017**, *12*, e0186570.

(191) Fedorov, O.; Castex, J.; Tallant, C.; Owen, D. R.; Martin, S.; Aldeghi, M.; Monteiro, O.; Filippakopoulos, P.; Picaud, S.; Trzupek, J. D.; Gerstenberger, B. S.; Bountra, C.; Willmann, D.; Wells, C.; Philpott, M.; Rogers, C.; Biggin, P. C.; Brennan, P. E.; Bunnage, M. E.; Schüle, R.; Günther, T.; Knapp, S.; Müller, S. *Sci. Adv.* **2015**, *1*, e1500723.

(192) Gerstenberger, B. S.; Trzupek, J. D.; Tallant, C.; Fedorov, O.; Filippakopoulos, P.; Brennan, P. E.; Fedele, V.; Martin, S.; Picaud, S.; Rogers, C.; Parikh, M.; Taylor, A.; Samas, B.; O'Mahony, A.; Berg, E.; Pallares, G.; Torrey, A. D.; Treiber, D. K.; Samardjiev, I. J.; Nasipak, B. T.; Padilla-Benavides, T.; Wu, Q.; Imbalzano, A. N.; Nickerson, J. A.; Bunnage, M. E.; Müller, S.; Knapp, S.; Owen, D. R. *J. Med. Chem.* **2016**, *59*, 4800–4811.

(193) Sutherell, C. L.; Tallant, C.; Monteiro, O. P.; Yapp, C.; Fuchs, J. E.; Fedorov, O.; Siejka, P.; Müller, S.; Knapp, S.; Brenton, J. D.; Brennan, P. E.; Ley, S. V. *J. Med. Chem.* **2016**, *59*, 5095–5101.

(194) Crawford, T. D.; Audia, J. E.; Bellon, S.; Burdick, D. J.; Bommi-Reddy, A.; Côté, A.; Cummings, R. T.; Duplessis, M.; Flynn, E. M.; Hewitt, M.; Huang, H.-R.; Jayaram, H.; Jiang, Y.; Joshi, S.; Kiefer, J. R.; Murray, J.; Nasveschuk, C. G.; Neiss, A.; Pardo, E.; Romero, F. A.; Sandy, P.; Sims, R. J.; Tang, Y.; Taylor, A. M.; Tsui, V.; Wang, J.; Wang, S.; Wang, Y.; Xu, Z.; Zawadzke, L.; Zhu, X.; Albrecht, B. K.; Magnuson, S. R.; Cochran, A. G. *ACS Med. Chem. Lett.* **2017**, *8*, 737–741.

(195) Crawford, T. D.; Vartanian, S.; Côté, A.; Bellon, S.; Duplessis, M.; Flynn, E. M.; Hewitt, M.; Huang, H.-R.; Kiefer, J. R.; Murray, J.; Nasveschuk, C. G.; Pardo, E.; Romero, F. A.; Sandy, P.; Tang, Y.; Taylor, A. M.; Tsui, V.; Wang, J.; Wang, S.; Zawadzke, L.; Albrecht, B. K.; Magnuson, S. R.; Cochran, A. G.; Stokoe, D. *Bioorg. Med. Chem. Lett.* **2017**, *27*, 3534–3541.

(196) Harder, E.; Damm, W.; Maple, J.; Wu, C.; Reboul, M.; Xiang, J. Y.; Wang, L.; Lupyan, D.; Dahlgren, M. K.; Knight, J. L.; Kaus, J. W.; Cerutti, D. S.; Krilov, G.; Jorgensen, W. L.; Abel, R.; Friesner, R. A. *J. Chem. Theory Comput.* **2016**, *12*, 281–296.

(197) Becke, A. D. *J. Chem. Phys.* **1993**, *98*, 1372–1377.

(198) Basavaiah, D.; Veeraraghavaiah, G. *Chem. Soc. Rev.* **2012**, *41*, 68–78.

(199) Still, W. C.; Gennari, C. *Tetrahedron Lett.* **1983**, *24*, 4405–4408.

(200) Ando, K. *J. Org. Chem.* **1997**, *62*, 1934–1939.

(201) BRD7 Human Bromodomain Amino Acid Sequence. https://www.uniprot.org/uniprot/Q9NPI1 (accessed Jul 19, 2019).

(202) BRD9 Human Bromodomain Amino Acid Sequence. https://www.uniprot.org/uniprot/Q9H8M2 (accessed Jul 19, 2019).

(203) Shain, A. H.; Pollack, J. R. *PLoS One* **2013**, *8*, e55119.

(204) Kadoch, C.; Hargreaves, D. C.; Hodges, C.; Elias, L.; Ho, L.; Ranish, J.; Crabtree, G. R. *Nat. Genet.* **2013**, *45*, 592–601.

(205) Hodges, C.; Kirkland, J. G.; Crabtree, G. R. *Cold Spring Harb. Perspect. Med.* **2016**, *6*, 1–24.

(206) Cleary, S. P.; Jeck, W. R.; Zhao, X.; Chen, K.; Selitsky, S. R.; Savich, G. L.; Tan, T.-X.; Wu, M. C.; Getz, G.; Lawrence, M. S.; Parker, J. S.; Li, J.; Powers, S.; Kim, H.; Fischer, S.; Guindi, M.; Ghanekar, A.; Chiang, D. Y. *Hepatology* **2013**, *58*, 1693–1702.

(207) Wang, X.; Wang, S.; Troisi, E. C.; Howard, T. P.; Haswell, J. R.; Wolf, B. K.; Hawk, W. H.; Ramos, P.; Oberlick, E. M.; Tzvetkov, E. P.; Vazquez, F.; Hahn, W. C.; Park, P. J.; Roberts, C. W. M. *Nat. Commun.* **2019**, *10*, 1–11.

(208) Drost, J.; Mantovani, F.; Tocco, F.; Elkon, R.; Comel, A.; Holstege, H.; Kerkhoven, R.; Jonkers, J.; Voorhoeve, P. M.; Agami, R.; Del Sal, G. *Nat. Cell Biol.* **2010**, *12*, 380–389.

(209) Harte, M. T.; O'Brien, G. J.; Ryan, N. M.; Gorski, J. J.; Savage, K. I.; Crawford, N. T.; Mullan, P. B.; Harkin, D. P. *Cancer Res.* **2010**, *70*, 2538–2547.

(210) Yu, X.; Li, Z.; Shen, J. *Am. J. Transl. Res.* **2016**, *8*, 742–748.

(211) Liu, Y.; Zhao, R.; Wang, H.; Luo, Y.; Wang, X.; Niu, W.; Zhou, Y.; Wen, Q.; Fan, S.; Li, X.; Xiong, W.; Ma, J.; Li, X.; Tan, M.; Li, G.; Zhou, M. *Cell Death Dis.* **2016**, *7*, e2156.

(212) Wu, W.-J.; Hu, K.-S.; Chen, D.-L.; Zeng, Z.-L.; Luo, H.-Y.; Wang, F.; Wang, D.-S.; Wang, Z.-Q.; He, F.; Xu, R.-H. *Eur. J. Clin. Invest.* **2013**, *43*, 131–140.

(213) Park, Y.-A.; Lee, J.-W.; Choi, J.-J.; Jeon, H.-K.; Cho, Y.; Choi, C.; Kim, T.-J.; Lee, N. W.; Kim, B.-G.; Bae, D.-S. *Gynecol. Oncol.* **2012**, *124*, 125–133.

(214) Pern, F.; Bogdanova, N.; Schürmann, P.; Lin, M.; Ay, A.; Länger, F.; Hillemanns, P.; Christiansen, H.; Park-Simon, T.-W.; Dörk, T. *PLoS One* **2012**, *7*, e47993.

(215) Kikuchi, M.; Okumura, F.; Tsukiyama, T.; Watanabe, M.; Miyajima, N.; Tanaka, J.; Imamura, M.; Hatakeyama, S. *Biochim. Biophys. Acta - Mol. Cell Res.* **2009**, *1793*, 1828–1836.

(216) Kouri, F. M.; Hurley, L. A.; Daniel, W. L.; Day, E. S.; Hua, Y.; Hao, L.; Peng, C.-Y.; Merkel, T. J.; Queisser, M. A.; Ritner, C.; Zhang, H.; James, C. D.; Sznajder, J. I.; Chin, L.; Giljohann, D. A.; Kessler, J. A.; Peter, M. E.; Mirkin, C. A.; Stegh, A. H. *Genes Dev.* **2015**, *29*, 732–745.

(217) Clark, P. G. K.; Vieira, L. C. C.; Tallant, C.; Fedorov, O.; Singleton, D. C.; Rogers, C. M.; Monteiro, O. P.; Bennett, J. M.; Baronio, R.; Müller, S.; Daniels, D. L.; Méndez, J.; Knapp, S.; Brennan, P. E.; Dixon, D. J. *Angew. Chem.* **2015**, *127*, 6315–6319.

(218) Martin, L. J.; Koegl, M.; Bader, G.; Cockcroft, X.-L.; Fedorov, O.; Fiegen, D.; Gerstberger, T.; Hofmann, M. H.; Hohmann, A. F.; Kessler, D.; Knapp, S.; Knesl, P.; Kornigg, S.; Müller, S.; Nar, H.; Rogers, C.; Rumpel, K.; Schaaf, O.; Steurer, S.; Tallant, C.; Vakoc, C. R.; Zeeb, M.; Zoephel, A.; Pearson, M.; Boehmelt, G.; McConnell, D. *J. Med. Chem.* **2016**, *59*, 4462–4475.

(219) BI-9564. https://opnme.com/molecules/brd9-bi9564 (accessed Aug 24, 2018).

(220) SGC | TP-472. http://www.thesgc.org/chemical-probes/TP-472 (accessed Oct 3, 2019).

(221) Raha, D.; Wilson, T. R.; Peng, J.; Peterson, D.; Yue, P.; Evangelista, M.; Wilson, C.; Merchant, M.; Settleman, J. *Cancer Res.* **2014**, *74*, 3579–3590.

(222) Wang, N.; Li, F.; Bao, H.; Li, J.; Wu, J.; Ruan, K. *ChemBioChem* **2016**, *17*, 1456–1463.

(223) Albrecht, B. K.; Cote, A.; Crawford, T.; Fauber, B.; Huang, H.-R.; Lore, J. M.; Magnuson, S.; Nasveschuk, C. G.; Salmeron, A.; Sims, R. J.; Taylor, A. M. Treating TH2-Mediated diseases by inhibition of bromodomains. US 2016/0024504 A1, 2016.

(224) Martin, L.; Steurer, S.; Cockcroft, X.-L. New pyridinones and isoquinolinones as inhibitors of the bromodomain BRD9. WO 2016/139361 A1, 2016.

(225) Remillard, D.; Buckley, D. L.; Paulk, J.; Brien, G. L.; Sonnett, M.; Seo, H.-S.; Dastjerdi, S.; Wühr, M.; Dhe-Paganon, S.; Armstrong, S. A.; Bradner, J. E. *Angew. Chem. Int. Ed.* **2017**, *56*, 5738–5743.

(226) Picaud, S.; Leonards, K.; Lambert, J. P.; Dovey, O.; Wells, C.; Fedorov, O.; Monteiro, O.; Fujisawa, T.; Wang, C. Y.; Lingard, H.; Tallant, C.; Nikbin, N.; Guetzoyan, L.; Ingham, R.; Ley, S. V.; Brennan, P.; Muller, S.; Samsonova, A.; Gingras, A. C.; Schwaller, J.; Vassiliou, G.; Knapp, S.; Filippakopoulos, P. *Sci. Adv.* **2016**, *2*, e1600760.

(227) BROMOscan Technology Platform https://www.discoverx.com/technologies-platforms/competitive-binding-technology/bromoscan-technology-platform (accessed Sep 30, 2019).

(228) Claridge, T. D. W. *Tetrahedron Org. Chem. Ser.* **1999**, *19*, 221–257.

(229) Claridge, T. D. W. *Tetrahedron Org. Chem. Ser.* **2009**, *27*, 247–302.

(230) Schoefberger, W.; Schlagnitweit, J.; Müller, N. *Annu. Reports NMR Spectrosc.* **2011**, *72*, 1–60.